



**NAVAL
POSTGRADUATE
SCHOOL**

MONTEREY, CALIFORNIA

DISSERTATION

**WESTERN NORTH PACIFIC MONSOON DEPRESSIONS:
FORMATION, STRUCTURE, AND TRANSITION TO
TROPICAL CYCLONES**

by

Jodi C. Beattie

September 2015

Dissertation Supervisor:

Russell Elsberry

Approved for public release; distribution is unlimited

THIS PAGE INTENTIONALLY LEFT BLANK

REPORT DOCUMENTATION PAGE

Form Approved OMB No. 0704-0188

Public reporting burden for this collection of information is estimated to average 1 hour per response, including the time for reviewing instruction, searching existing data sources, gathering and maintaining the data needed, and completing and reviewing the collection of information. Send comments regarding this burden estimate or any other aspect of this collection of information, including suggestions for reducing this burden, to Washington headquarters Services, Directorate for Information Operations and Reports, 1215 Jefferson Davis Highway, Suite 1204, Arlington, VA 22202-4302, and to the Office of Management and Budget, Paperwork Reduction Project (0704-0188) Washington DC 20503.

1. AGENCY USE ONLY (Leave blank)	2. REPORT DATE September 2015	3. REPORT TYPE AND DATES COVERED Dissertation
4. TITLE AND SUBTITLE WESTERN NORTH PACIFIC MONSOON DEPRESSIONS: FORMATION, STRUCTURE, AND TRANSITION TO TROPICAL CYCLONES		5. FUNDING NUMBERS
6. AUTHOR(S) Beattie, Jodi C.		
7. PERFORMING ORGANIZATION NAME(S) AND ADDRESS(ES) Naval Postgraduate School Monterey, CA 93943-5000		8. PERFORMING ORGANIZATION REPORT NUMBER
9. SPONSORING /MONITORING AGENCY NAME(S) AND ADDRESS(ES) N/A		10. SPONSORING/MONITORING AGENCY REPORT NUMBER

11. SUPPLEMENTARY NOTES The views expressed in this dissertation are those of the author and do not reflect the official policy or position of the Department of Defense or the U.S. Government. IRB Protocol number N/A.

12a. DISTRIBUTION / AVAILABILITY STATEMENT Approved for public release; distribution is unlimited	12b. DISTRIBUTION CODE
---	-------------------------------

13. ABSTRACT (maximum 200 words)

Even though monsoon depressions are the synoptic precursors for a substantial fraction of the western North Pacific tropical cyclones, little is known about how they form. High resolution reanalyses, satellite imagery and precipitation estimates are used to examine the physical mechanisms for monsoon depression formation in all 44 cases during 2009. An interaction of at least one cross-equatorial airstream from the Southern Hemisphere with the monsoon trough or confluent zone preceded all 44 monsoon depression formations. Four types of cross-equatorial airstreams provide wave-activity flux that contributes to the formations. At the formation time, the elliptical monsoon depressions on average are 1098 km east-west and 812 km north-south, and have vorticity maxima on either end. Wave-activity flux convergence over a vorticity maximum within the monsoon depression was analyzed in all transitions to tropical cyclones during 2009. In about half of these transitions, the inward-directed wave-activity flux was associated with the same primary airstream as during the monsoon depression formation. In the other half, another airstream or the trade easterlies was the source of the wave-activity flux. Persistent wave-activity flux convergence was not analyzed in any of the 25 monsoon depressions that failed to transition to a tropical cyclone.

14. SUBJECT TERMS monsoon depression, formation, structure, transition, tropical cyclone, pre-tropical cyclone seedling		15. NUMBER OF PAGES 199	
16. PRICE CODE			
17. SECURITY CLASSIFICATION OF REPORT Unclassified	18. SECURITY CLASSIFICATION OF THIS PAGE Unclassified	19. SECURITY CLASSIFICATION OF ABSTRACT Unclassified	20. LIMITATION OF ABSTRACT UU

NSN 7540-01-280-5500

Standard Form 298 (Rev. 2-89)
Prescribed by ANSI Std. Z39-18

THIS PAGE INTENTIONALLY LEFT BLANK

Approved for public release; distribution is unlimited

**WESTERN NORTH PACIFIC MONSOON DEPRESSIONS: FORMATION,
STRUCTURE, AND TRANSITION TO TROPICAL CYCLONES**

Jodi C. Beattie
Lieutenant Commander, United States Navy
B.S., U.S. Naval Academy, 1999
M.S., Naval Postgraduate School, 2003

Submitted in partial fulfillment of the
requirements for the degree of

DOCTOR OF PHILOSOPHY IN METEOROLOGY

from the

NAVAL POSTGRADUATE SCHOOL
September 2015

Author: Jodi C. Beattie

Approved by:	Russell Elsberry Professor of Meteorology Dissertation Supervisor	Wendell A. Nuss Professor of Meteorology Dissertation Committee Chair
	Eric A. Hendricks Professor of Meteorology	Qing Wang Professor of Meteorology
	Jamie H. MacMahan Professor of Oceanography	Karl D. Pfeiffer, PhD Principle Engineer, Atmospheric and Environmental Research

Approved by: Wendell A. Nuss, Chair, Department of Meteorology

Approved by: Douglas Moses, Vice Provost for Academic Affairs

THIS PAGE INTENTIONALLY LEFT BLANK

ABSTRACT

Even though monsoon depressions are the synoptic precursors for a substantial fraction of the western North Pacific tropical cyclones, little is known about how they form. High resolution reanalyses, satellite imagery and precipitation estimates are used to examine the physical mechanisms for monsoon depression formation in all 44 cases during 2009. An interaction of at least one cross-equatorial airstream from the Southern Hemisphere with the monsoon trough or confluent zone preceded all 44 monsoon depression formations. Four types of cross-equatorial airstreams provide wave-activity flux that contributes to the formations. At the formation time, the elliptical monsoon depressions on average are 1098 km east-west and 812 km north-south, and have vorticity maxima on either end. Wave-activity flux convergence over a vorticity maximum within the monsoon depression was analyzed in all transitions to tropical cyclones during 2009. In about half of these transitions, the inward-directed wave-activity flux was associated with the same primary airstream as during the monsoon depression formation. In the other half, another airstream or the trade easterlies was the source of the wave-activity flux. Persistent wave-activity flux convergence was not analyzed in any of the 25 monsoon depressions that failed to transition to a tropical cyclone.

THIS PAGE INTENTIONALLY LEFT BLANK

TABLE OF CONTENTS

I.	INTRODUCTION	1
A.	SYNOPTIC-SCALE FEATURES OF THE WESTERN NORTH PACIFIC	1
1.	Monsoon Trough	1
2.	Intertropical Convergence Zone	2
3.	Monsoon Depression	2
4.	Monsoon Gyre.....	3
B.	MONSOON DEPRESSION FORMATION	3
C.	MONSOON DEPRESSION STRUCTURE.....	4
D.	THE TRANSITION OF A MONSOON DEPRESSION TO A PRE-TROPICAL CYCLONE SEEDLING	6
II.	MONSOON DEPRESSION FORMATION	9
A.	BACKGROUND.....	9
B.	SYNOPTIC ANALYSIS OF THE JULY 2007 MONSOON DEPRESSION FORMATIONS	11
1.	Monsoon Depression MD ₁	13
2.	Monsoon Depression MD ₂	15
C.	EXAMINATION OF PHYSICAL MECHANISMS FOR MONSOON DEPRESSION FORMATION	18
1.	Rossby Wave Dispersion	18
2.	Waves in the Easterlies	21
3.	Cross-Equatorial Flow	22
D.	CONCEPTUAL MODEL OF MONSOON DEPRESSION FORMATION.....	23
E.	APPLICABILITY OF THE CONCEPTUAL MODEL OF MONSOON DEPRESSION FORMATION	32
1.	Methodology.....	33
2.	Analysis of Airstreams	34
F.	SUMMARY AND CONCLUSIONS FOR MONSOON DEPRESSION FORMATION.....	45
III.	STRUCTURE OF MONSOON DEPRESSIONS AT FORMATION TIME	49
A.	INTRODUCTION	49
B.	METHODOLOGY	50
C.	STRUCTURAL CHARACTERISTICS.....	53
1.	Horizontal Structure	53
2.	Vertical Structure.....	55
D.	DISCUSSION OF MONSOON DEPRESSION STRUCTURE.....	58
IV.	MONSOON DEPRESSIONS AS PRE-TROPICAL CYCLONE SEEDLINGS	61
A.	INTRODUCTION	61
B.	METHODOLOGY	62

C.	SYNOPTIC ANALYSIS OF THE JULY 2007 MONSOON DEPRESSIONS	63
1.	Transition of MD ₂ to a Pre-tropical Cyclone Seedling.....	65
2.	Non-transition of MD ₁ to a Tropical Cyclone	75
D.	ANALYSIS OF THE 2009 MONSOON DEPRESSIONS	79
1.	Methodology.....	79
2.	Analysis of Transitioning Monsoon Depressions from 2009	80
3.	Analysis of Non-transitioning Monsoon Depressions during 2009	150
V.	SUMMARY	157
A.	MONSOON DEPRESSION FORMATION	157
B.	MONSOON DEPRESSION STRUCTURE.....	158
C.	TRANSITION TO PRE-TROPICAL CYCLONE SEEDLING	159
D.	RELEVANCE TO THE DEPARTMENT OF DEFENSE (DOD).....	160
E.	FUTURE WORK.....	162
APPENDIX. WAVE-ACTIVITY FLUX.....		165
LIST OF REFERENCES.....		171
INITIAL DISTRIBUTION LIST.....		175

LIST OF FIGURES

- Figure 1. MTSAT-1R infrared image at 1800 UTC 6 July 2007 illustrating the two monsoon depressions described in Chapter II.B. The meridional and zonal lines indicate the horizontal extent of each monsoon depression based on the infrared imagery; grid spacing is 15-degrees in latitude and longitude.....13
- Figure 2. Streamlines and relative vorticity (shading scale at bottom in units of 10^{-4} s^{-1}) at 850 hPa from the 1-degree ECMWF analysis at 1200 UTC 1 July 2007. The box labeled MT₁ depicts the east–west oriented monsoon trough that lead to the first, long-lasting monsoon depression east of the Philippines. The box in the Southern Hemisphere labeled AC indicates an anticyclone that is contributing to a southerly flow that enhances the cross-equatorial flow into MT₁.14
- Figure 3. Streamlines and relative vorticity as in Figure 2 except at 1800 UTC 4 July 2007 and includes a chain of cyclonic circulations that extend southeastward from TY Toraji in the South China Sea. Following the formation of MD₁, MD₂ will form in association with the traditionally oriented MT₂. A Southern Hemisphere anticyclone (AC) in conjunction with the midlatitude westerly trough contributes to sustained cross-equatorial flow. A near-equatorial cyclone (C_{SH}) in the Southern Hemisphere also facilitates cross-equatorial flow.....15
- Figure 4. Streamlines at 850 hPa from the 1-degree ECMWF analysis at 1800 UTC 5 July 2007 and TRMM precipitation. The large box highlights the southerly flow that wrapped around the end of the monsoon trough and into the monsoon depression circulation. The small box shows the wave in the easterly flow approaching the formation region.....17
- Figure 5. 850 hPa wave-activity flux vectors (units of m^2s^{-2}), the streamfunction anomaly (contours), and wave-activity flux convergence (shaded) that are labeled corresponding to the cyclonic circulations for (a) 0600 UTC 4 July 2007; (b) 0000 UTC 5 July 2007; (c) 1800 UTC 5 July 2007 and (d) 0600 UTC 6 July 2007.20
- Figure 6. Idealized representation of the three cross-equatorial airstreams (A, B, and C) in the conceptual model of monsoon depression formation. Horizontal arrows in the Northern Hemisphere represent the equatorial westerlies and trade easterlies.24
- Figure 7. Ensembles of 120 hour HYSPLIT backward trajectories at 850 hPa originating in the region of the first monsoon depression (MD₁). The star represents the point at which the trajectories ended, open ends are the 120 h prior to the ending times-locations of (a) 0000 UTC 1 July 2007, 0°, 125°E; and (b) 1800 UTC 3 July 2007, 6°N, 127°E.26
- Figure 8. Ensembles of 120 hour HYSPLIT backward trajectories as in Figure 7, except for the pre-TY Man-Yi monsoon depression (MD₂) and ending times-

locations of (a) 0000 UTC 6 July 2007, 3°N, 153°E; (b) 0000 UTC 4 July 2007, 3°S, 135°N; (c) 0000 UTC 4July 2007, 5°S, 150°E; and (d) 0000 UTC 6 July 2007, 2°N, 158°E.	27
Figure 9. Center locations of all 2009 monsoon depressions. The filled circle (●) highlights those that formed from airstream A; the filled triangle (▲) highlights those that formed from airstream B; the filled diamond (◆) highlights those that formed from airstream C; the asterisk (*) highlights those that formed from airstream C _□ ; and the plus sign (+) highlights those that are undefined as they formed east of 180°E.....	32
Figure 10. Streamlines and relative vorticity as in Figure 2, except from the 0.25-degree ECMWF analysis at 1200 UTC 2 July 2009. The large southern box highlights the center of the Southern Hemisphere anticyclone; the small northern box highlights the forming monsoon depression; the solid arrows highlight the three cross-equatorial airstreams A, B, and C of the conceptual model.....	36
Figure 11. Streamlines and relative vorticity as in Figure 10, except at times of (a) 0000 UTC 22 October 2009, for airstreams B and C with the Southern Hemisphere cyclone; (b) 0600 UTC 29 September 2009, for airstream C with the Southern Hemisphere cyclone; (c) 0600 UTC 11 September 2009, for airstream C _□ without the Southern Hemisphere cyclone; and (d) 0000 UTC 25 July 2009, for airstream A. The southern box highlights the Southern Hemisphere anticyclone centers; the northern box highlights the developing monsoon depression; and the arrows highlight the cross-equatorial airstream that is dominant in the formation of that monsoon depression.	38
Figure 12. Ensembles of 120 hour HYSPLIT backward trajectories as in Figure 7, except for ending times-locations of (a) 0600 UTC 29 September 2009, 14°N, 161°E; (b) 0000 UTC 28 September 2009, 0°, 160°E; and (c) 0000 UTC 27 September 2009, 5°S, 65°E.	39
Figure 13. Wave-activity flux vectors ($m^2 s^{-2}$) as in Figure 5, but at (a) 1200 UTC 9 Sep and (b) 0000 UTC 10 Sep 2009, and the boxes highlight the cross-equatorial wave-activity fluxes at two times prior to the formation of the pre-TY Choi-Wan monsoon depression at 14°N, 155°E.....	43
Figure 14. Streamlines and isotachs (shading scale to the right in units of $m s^{-1}$) at 850 hPa from the 0.25-degree ECMWF analysis at (a) 1800 UTC 22 August 2009 and (b) 1800 UTC 22 September 2009. The TRMM precipitation products with inset infrared satellite images that correspond to (c) Figure 14a and (d) Figure 14b. The solid lines represent the locations for the vertical cross sections in Figures 16 and 17.	52
Figure 15. Box plots of precipitation, winds, vorticity, pressure and cloud diameters (degrees) in latitude (left five boxes) and longitude (right five boxes) for the 44 monsoon depressions during 2009. The horizontal line in the narrow portion of each box is the median value, the top and bottom of	

each box are the upper and lower quartile values (75 th and 25 th percentile, respectively), the whiskers extend to the most extreme data points not considered outliers, and outliers are plotted individually as crosses.....	54
Figure 16. Vertical cross-sections along (a) 16.5°N and (b) 141°E of meridional and zonal winds (contours, m s ⁻¹) and relative vorticity (shaded, 10 ⁻⁴ s ⁻¹) from the 0.25-degree ECMWF analysis at 1800 UTC 22 August 2009. Arrowhead represents the center of the monsoon depression.	56
Figure 17. Winds and relative vorticity as in Figure 16, except at 1800 UTC 22 September 2009 along (a) 15°N and (b) 134°E.....	57
Figure 18. ECMWF 850 hPa streamlines and wind speed (shaded contours > 8 m s ⁻¹ ; scale at bottom) at (a) 0600 UTC 6 July; (b) 1200 UTC 6 July; (c) 1800 UTC 6 July; (d) 0000 UTC 7 July; (e) 0600 UTC 7 July; and (f) 1200 UTC 7 July (time of the first JTWC warning). The small boxes highlight MD ₁ and the large boxes highlight MD ₂ . The region of increased westerlies along airstream B into the southwestern quadrant of MD ₂ and the easterlies into the northeastern quadrant of MD ₂ are included in the large boxes.....	65
Figure 19. (a) MTSAT-1R infrared image at 1200 UTC 6 July 2007 illustrating the pre-TY Man-Yi monsoon depression MD ₂ with western and eastern convective regions relative to a convection-free center near 5°N, 150°E. (b) Corresponding TRMM 3B42 precipitation (mm/hour; shading scale on right) with two regions of precipitation corresponding to the western and eastern convective regions in panel (a). The letter C corresponds to the estimated center of the cyclonic circulation.	67
Figure 20. (a) Streamlines and relative vorticity as in Figure 2, except at 1200 UTC 6 July 2007. Note the cyclonic circulation and relative vorticity maximum are associated with the MD ₂ western convective region and precipitation region in Figure 19. (b) Corresponding 850 hPa wave-activity flux vectors (units of m ² s ⁻²), the streamfunction anomaly (contours), and wave-activity flux divergence (shading scale at the bottom; units of m s ⁻²) as in Figure 5...68	68
Figure 21. As in Figure 19 except at 0000 UTC 7 July with (a) MTSAT-1R IR image of MD ₂ indicating continued convective organization in the western portion of the circulation. (b) TRMM 3B42 precipitation (mm/hour) with two regions of precipitation corresponding to the western and eastern convective regions in panel (a).....	70
Figure 22. As in Figure 20 except at 0000 UTC 7 July 2007 with (a) streamlines and relative vorticity with a broad cyclonic circulation related to the western convective region of MD ₂ in Figure 21a. (b) Wave-activity flux convergence continues in the region of the MD ₂ cyclonic vorticity maximum.....	71
Figure 23. As in Figure 19 except at 1200 UTC 7 July with (a) MTSAT-1R infrared image indicating continued convective organization associated with the TD 04W that developed from the western convective region of MD ₂ . (b)	

Corresponding TRMM 3B42 precipitation (mm/hour) in association with TD 04W.....	72
Figure 24. As in Figure 20 except for 1200 UTC 7 July with (a) streamlines and relative vorticity with a broad cyclonic circulation related to the dissipating MD ₁ and the new TD 04W. (b) Wave-activity flux convergence continues in the region of the cyclonic vorticity maximum corresponding to TD 04W that will later become TY Man-Yi and over the center of MD ₁	73
Figure 25. An idealized representation of MD ₂ (dashed ellipse), the trade easterlies (horizontal arrows), trough of the wave in the easterlies (dashed lines), the cross-equatorial airstreams B and C (curved arrows as in Figure 6), the western vorticity maximum (circle) and the primary inward-directed wave-activity flux (thick arrows).	75
Figure 26. (a) MTSAT-1R infrared image at 1200 UTC 6 July 2007 illustrating the monsoon depression MD ₁ near 10°N, 125°E. (b) Corresponding TRMM 3B42 precipitation (mm/hour; shading scale on right) with precipitation maxima to the northwest of center. The letter C corresponds to the estimated center of the cyclonic circulation.	76
Figure 27. As in Figure 26 except at 0000 UTC 7 July with (a) MTSAT-1R IR image of MD ₁ and the southern convective maximum. (b) TRMM 3B42 precipitation (mm/hour) with regions of precipitation corresponding to the southern convective regions in panel (a).	77
Figure 28. As in Figure 26 except at 1200 UTC 7 July with (a) MTSAT-1R infrared image indicating persistent convection associated with MD ₁ . (b) Corresponding TRMM 3B42 precipitation (mm/hour) in association with the dissipating MD ₁	78
Figure 29. As in Figure 20 except at 1200 UTC 27 September with (a) streamlines and relative vorticity for the pre-Super TY Melor monsoon depression. (b) Wave-activity flux vectors entering the box from the south result in two regions of convergence corresponding to the areas of the vorticity maxima.	82
Figure 30. As in Figure 20 except at 0000 UTC 28 September with (a) streamlines and relative vorticity indicating the pre-Super TY Melor monsoon depression is now circular. (b) Wave-activity flux vectors continue to enter the box from the south, and outward wave-activity flux is beginning to the north.....	84
Figure 31. As in Figure 20 except at 1200 UTC 28 September with (a) streamlines and relative vorticity with two cyclonic relative vorticity maxima and (b) corresponding wave-activity flux convergence distribution.	86
Figure 32. As in Figure 20 except at 0000 UTC 29 September with (a) streamlines and relative vorticity showing the elliptically shaped cyclonic circulation at the time of pre-tropical cyclone seedling, and (b) corresponding wave-activity flux convergence distribution.	88

Figure 33.	As in Figure 20 except for 0600 UTC 11 September with (a) streamlines and relative vorticity with a broad cyclonic circulation related the pre-TD 15W monsoon depression. (b) Wave-activity flux convergence continues in the region of the cyclonic vorticity maximum from the south and east corresponding to the circulation that will later become TY Choi-Wan.	91
Figure 34.	As in Figure 19 except at 0600 UTC 11 September with (a) MTSAT-1R infrared image indicating continued convective organization associated with the pre-TD 15W that developed from the eastern convective region and (b) TRMM 3B42 precipitation (mm/hour) in association with the pre-TD 15W.....	92
Figure 35.	As in Figure 20 except for 1200 UTC 11 September with (a) streamlines and relative vorticity just prior to the JTWC TCFA (2230 UTC 11 September). (b) Wave-activity flux convergence continues in the region of the cyclonic vorticity maximum from the south and east corresponding to the circulation that will later become TY Choi-Wan.	93
Figure 36.	As in Figure 19 except at 1200 UTC 11 September with (a) MTSAT-1R infrared image indicating continued convective organization associated with the pre-TD 14W that developed from the eastern convective region and (b) TRMM 3B42 precipitation (mm/hour) in association with the pre-TD 14W.....	94
Figure 37.	As in Figure 20 except for 1200 UTC 6 October 2009 with (a) streamlines and relative vorticity with airstream B. (b) Outward-directed wave-activity flux is to the north and east with a small amount of inward-directed wave-activity flux from the west.....	96
Figure 38.	As in Figure 20 except for 0000 UTC 7 October with (a) streamlines and relative vorticity showing airstreams B and C and a more circular monsoon depression. (b) Outward-directed wave-activity flux continues to the north and east, and the inward-directed wave-activity flux from the west has increased.....	98
Figure 39.	As in Figure 20 except for 1200 UTC 7 October with (a) streamlines and relative vorticity showing airstreams B and C have merged. (b) Inward-directed wave-activity flux from the northeast is the predominant flux, and has replaced the outward-directed wave-activity flux to the north. Large outward-directed flux to the east continues, but it is shifted to the south away from the central region.....	100
Figure 40.	As in Figure 20 except for 0000 UTC 8 October with (a) streamlines and relative vorticity maxima only 2.5 hours prior to TCFA. (b) Inward-directed wave-activity flux from the northeast has become a primary factor.....	102
Figure 41.	As in Figure 20 except for 1200 UTC 23 September with (a) streamlines and relative vorticity for the pre-TY Ketsana (17W) case with an interaction of airstream A and the trade easterlies. (b) Inward-directed wave-activity flux	

from the south-southwest leading to wave-activity flux convergence over the southern portion of the circulation.....	105
Figure 42. As in Figure 20 except for 0000 UTC 24 September with (a) streamlines and relative vorticity just 4.5 hours prior to JTWC issuing a TCFA for pre-TY Ketsana. (b) Inward-directed wave-activity flux vectors are found on the northern and southern sides of the maximum vorticity band and are favorable for spin-up	107
Figure 43. As in Figure 20 except at 1200 UTC 14 July with (a) streamlines and relative vorticity for a circular pre-TY Molave monsoon depression. (b) Corresponding wave-activity flux distribution.....	110
Figure 44. As in Figure 20 except at 1800 UTC 14 July with (a) streamlines and relative vorticity for the pre-TY Molave monsoon depression. C indicates the center based on the JTWC TCFA issued at this time. (b) Corresponding wave-activity flux distribution and IR satellite image annotated with the center as defined by the TCFA.	112
Figure 45. As in Figure 20 except at 0000 UTC 15 July with (a) streamlines and relative vorticity for the pre-TY Molave pre-tropical cyclone seedling. (b) Corresponding wave-activity flux distribution and IR satellite image.....	114
Figure 46. As in Figure 20 except at 0600 UTC 15 July with (a) streamlines and relative vorticity for the pre-TY Molave TD 07W. (b) Corresponding wave-activity flux distribution.	116
Figure 47. As in Figure 20 except at 1200 UTC 7 July with (a) streamlines and relative vorticity for the pre-TS Soudelor monsoon depression. (b) Corresponding wave-activity flux shows inward-directed flux vectors from the northeast and southeast.	119
Figure 48. As in Figure 20 except at 0000 UTC 8 July with (a) streamlines and relative vorticity for the pre-TS Soudelor monsoon depression. (b) Corresponding wave-activity flux distribution.	121
Figure 49. As in Figure 20 except at 1200 UTC 8 July with (a) streamlines and relative vorticity for the pre-TS Soudelor monsoon depression. (b) Corresponding wave-activity flux distribution.	123
Figure 50. As in Figure 20 except at 0000 UTC 9 July with (a) streamlines and relative vorticity for the pre-TS Soudelor. (b) Corresponding wave-activity flux distribution.....	125
Figure 51. As in Figure 20 except at 0000 UTC 11 September with (a) streamlines and relative vorticity for the pre-TY Koppu monsoon depression. (b) Corresponding wave-activity flux distribution.....	128
Figure 52. As in Figure 20 except at 1200 UTC 11 September with (a) streamlines and relative vorticity for the pre-TY Koppu monsoon depression. (b) Corresponding wave-activity flux distribution.....	130

Figure 53.	As in Figure 20 except at 0000 UTC 12 September with (a) streamlines and relative vorticity for the pre-TY Koppu monsoon depression. (b) Corresponding wave-activity flux distribution.....	132
Figure 54.	As in Figure 20 except at 1200 UTC 25 September with (a) streamlines and relative vorticity for the pre-Super TY Parma monsoon depression. (b) Corresponding wave-activity flux distribution.....	134
Figure 55.	As in Figure 20 except at 0000 UTC 26 September with (a) streamlines and relative vorticity for the pre-Super TY Parma monsoon depression. (b) Corresponding wave-activity flux distribution.....	136
Figure 56.	As in Figure 20 except at 1200 UTC 26 September with (a) streamlines and relative vorticity for the pre-Super TY Parma monsoon depression. (b) Corresponding wave-activity flux distribution.....	138
Figure 57.	As in Figure 20 except at 0000 UTC 27 September with (a) streamlines and relative vorticity for the pre-Super TY Parma circulation. (b) Corresponding wave-activity flux distribution. Note that the scale for the wave-activity flux convergence is changed by a factor of three compared to Figures 55–56.	140
Figure 58.	As in Figure 20 except at 1200 UTC 24 October with (a) streamlines and relative vorticity for the pre-TY Mirinae monsoon depression. (b) Corresponding wave-activity flux distribution.....	142
Figure 59.	As in Figure 20 except at 0000 UTC 25 October with (a) streamlines and relative vorticity for the pre-TY Mirinae monsoon depression. (b) Corresponding wave-activity flux distribution.....	144
Figure 60.	As in Figure 20 except at 1200 UTC 25 October with (a) streamlines and relative vorticity for the pre-TY Mirinae monsoon depression. (b) Corresponding wave-activity flux distribution.....	146
Figure 61.	Idealized representations of transitioning monsoon depressions (dashed ellipse), trade easterlies (horizontal arrows), cross-equatorial airstreams (curved arrows as in Figure 6), and the primary inward-directed wave-activity flux (thick arrows) for (a) when the airstream responsible for the formation of the monsoon depression does not continue to contribute to a transition to pre-tropical cyclone seedling (e.g., airstream A as in the pre-Super TY Parma) and (b) when the airstream responsible for the formation of the monsoon depression continues (e.g., airstream B indicated by the hashed lines as in pre-TY Koppu), but it is not the primary airstream responsible for transition to pre-tropical seedling.	149

THIS PAGE INTENTIONALLY LEFT BLANK

LIST OF TABLES

Table 1.	List of monsoon depressions that form from airstream C. The first column is the time and date the circulation had all characteristics of a monsoon depression; the next two columns list the latitude and longitude of the circulation center; the last four columns are the latitude and longitude of the Southern Hemisphere anticyclone and Southern Hemisphere cyclone center from which the airstreams originate. With the exception of the 0600 UTC 06 June 2009, 0000 UTC 11 Jul 2009, and 0000 UTC 11 July 2009 monsoon depressions that had a circular shape, all of these monsoon depressions had an elliptical shape with major axis generally oriented east-west.....	35
Table 2.	As in Table 1, except for monsoon depressions that formed from airstream C_{\square} , and there is no column for Southern Hemisphere cyclone. Either an elliptical (E) or circular (C) shape of the monsoon depression is listed in the last column.....	40
Table 3.	As in Table 2, except for monsoon depressions that formed from airstream B.....	42
Table 4.	As in Table 2, except for monsoon depressions that formed from airstream A.....	44
Table 5.	Summary of the 10 non-transitioning monsoon depressions during 2009 in which the inward-directed wave-activity flux (WAF) was absent or small. The first column is the time and date that the circulation had all characteristics of a monsoon depression. The next three columns list the monsoon depression shape, the original airstream at formation, and any additional airstream that may have interacted with the monsoon depression. In column 5, the presence (Y-yes; N-no) of inward-directed wave-activity flux is indicated, and whether or not it resulted in wave-activity flux convergence is indicated in column 6. Presence of outward-directed wave-activity flux is listed in column 7. The last column is the duration (d-days) of the monsoon depression. PHI in column 6 is wave-activity flux convergence due to the interaction with the Philippines.....	153
Table 6.	As in Table 5, but for MD ₁ during 2007 and 11 during 2009 that were non-transitioning monsoon depressions that had persistent wave-activity flux but did not result in transition to a pre-tropical cyclone seedling.	155

THIS PAGE INTENTIONALLY LEFT BLANK

LIST OF ACRONYMS AND ABBREVIATIONS

AC	Anticyclone
ARL	Air Resources Laboratory
C/C _{SH}	Cyclone/ Southern Hemisphere Cyclone
ECMWF	European Centre for Medium-Range Weather Forecasts
GDAS	Global Data Assimilation System
h	Hour
hPa	Hectopascal
HYSPPLIT	Hybrid Single Particles Lagrangian Integrated Trajectory
IR	Infrared
ITCZ	Intertropical Convergence Zone
JTWC	Joint Typhoon Warning Center
K	Kelvin
km	kilometer
MCS	Mesoscale Convective System
MCV	Mesoscale Convective Vortex
MD	Monsoon Depression
MG	Monsoon Gyre
m	meters
MT	Monsoon Trough
MTSAT	Multifunctional Transport Satellite
NCAR	National Center for Atmospheric Research
NCEP	National Centers for Environmental Prediction
PV	Potential Vorticity
QuikSCAT	Quick Scatterometer
s	second
TC	Tropical Cyclone
TCFA	Tropical Cyclone Formation Alert
TCM	Tropical Cyclone Motion
TCS	Tropical Cyclone Structure
TD	Tropical Depression

TRMM	Tropical Rainfall Measuring Mission
TS	Tropical Storm
TY	Typhoon
UTC	Coordinated Universal Time
YOTC	Year of Coordinated Observing Modeling and Forecasting Tropical Convection

ACKNOWLEDGMENTS

To the members of my PhD Committee, Professors Elsberry, Nuss, Hendricks, Wang, MacMahan, and Dr. Pfeiffer, thank you for taking the time to serve on my committee as well as for your insight, experience and perspective.

Support for Prof R. L. Elsberry was provided by the Office of Naval Research Marine Meteorology section and the National Science Foundation.

TRMM precipitation analyses and visualizations used in this study were produced with the Giovanni online data system, developed and maintained by the NASA GES DISC.

Anonymous reviewers during the publication process of Chapters II and III made suggestions and comments that benefited the study.

Prof. R. Elsberry, thank you for providing mentorship and guidance through the many, many years.

To Lt Col (Ret.) Pfeiffer, PhD, a.k.a. “the hero”: Thank you for getting me through the programing, all the assists, support, transition advice, and the cheerleading through the years. You and Karen are a wonderful support system—thank you both for integrating me into your family every summer.

To Mr. R. Creasey and Ms. M. Jordan, thanks to you both for your friendship, guidance, encouragement and assistance along the way.

To Dr. Z. Wang, my thanks for all of your help in the initial stages in obtaining the data sets, analysis and programs; especially your recommendation to use the wave-activity flux for the primary analysis.

To Prof. W. Nuss, thank you for your continued support and mentorship.

Thanks to Mrs. P. Jones, for your assistance through the years in preparing manuscripts and for the storage, enabling me to travel light.

To Mr. B. Strahl, thank you for the continued friendship, the random answer for the random question, all the TCFAs, the encouragement and, of course, the travel tips through the years.

Thank you to the Neus, for your support and for always welcoming me with open arms every summer; you provided a little bit of home that made life normal.

Finally, thank you, Mom, for puppy sitting while I was “summering” in Monterey and for the assist through the struggles that the whole part-time, long-distance scenario brought.

I. INTRODUCTION

This research is driven by the need for a more timely and effective means of identifying regions of convection that could lead to tropical cyclone formation, as only a small fraction of such convective areas in the tropics actually become tropical cyclones (Elsberry 2002). The focus of this research is the western North Pacific, which is an area of frequent tropical cyclone formation. Currently, the Joint Typhoon Warning Center (JTWC) labels each area of convection that may develop into a tropical cyclone within the next 24 h as an invest area. The rate of false alarms is quite high with the existing method of classification in the western North Pacific (Harr and Elsberry 2007). If the mechanisms of tropical cyclone formation in the western North Pacific can be better defined and numerically predicted, it would significantly improve identification of those regions of deep convection that are most likely to lead to a formation, and thus decrease the false alarm rate. More accurately identifying regions of potential monsoon depression and tropical cyclone development will also assist Department of Defense and civilian decision makers in determining whether to sortie ships, evacuate coastal regions, or other expensive and time-consuming preparations.

A. SYNOPTIC-SCALE FEATURES OF THE WESTERN NORTH PACIFIC

During the Northern Hemisphere summer, a monsoonal environment dominates the western North Pacific, which creates a large region favorable for tropical cyclone formation. Within this monsoonal environment, several synoptic-scale circulations such as the monsoon trough, monsoon depression, and monsoon gyre, may serve as the precursors to tropical cyclone formation.

1. Monsoon Trough

The western North Pacific monsoon trough (MT) is a generally northwest-southeast oriented region of low pressure that may extend from the northern Philippines to near 8–10°N, 150°E. However, the western end can vary from 5°N to 25°N due to seasonal migration (Lander 1994). This migration corresponds to the onset (poleward displacement) and retreat (equatorward displacement) of the summer monsoon. The

eastern portion of the monsoon trough may also migrate poleward to establish a southwest-northeast orientation, which is known as a reverse-oriented monsoon trough, but this configuration tends to be less favorable to tropical cyclone formation (Elsberry 2002).

The MT is characterized by a moist southwesterly flow to its south (equatorial westerlies) and easterly flow to its north (tradewind easterlies), which provides a favorable region of cyclonic horizontal wind shear (Lander 1994, Elsberry 2002). Tropical cyclone formation in the western North Pacific monsoon trough is favored because enhancement of the low-level flow on either side of the region near the monsoon trough increases the relative vorticity, convergence, and moisture flux convergence, which are three environmental conditions favorable for tropical cyclone formation (Elsberry 2002).

2. Intertropical Convergence Zone

The monsoon trough as defined above is contrasted with the Intertropical Convergence Zone (ITCZ), which is defined here to be a low-pressure trough closer to the equator that does not have equatorial westerlies to its south. In the ITCZ, the cross-equatorial flow is still from the east, as the low-pressure trough is not displaced far enough from the equator for the Coriolis force to turn the flow to westerlies. However, a region of convergence exists between the tradewind lows of both hemispheres (Elsberry 2002). In summary, the ITCZ has less convergence, less deep convection, and less latent heat release than the monsoon trough (Elsberry 2002).

3. Monsoon Depression

Although some authors (e.g., Chen et al. 1998, 2004) used the term monsoon gyre and monsoon depression (MD) interchangeably, the JTWC defined these to be different circulations. In this study, the monsoon depression is defined as a large cyclonic vortex with a diameter on the order of 1000 km, which has a light-wind core surrounded by a band of stronger winds at large radii containing a loosely organized clusters of deep convection (JTWC 1994, Lander 2004). Harr et al. (1996a) suggested that a monsoon depression might form in the convergent flow between the equatorial westerlies to the

south and trade wind easterlies to the north of the MT. The monsoon depression is the focus of this study because it provides a favorable cyclonic vorticity environment in which mesoscale convective systems (MCSs) and their associated mesoscale convective vortices (MCVs) can develop, persist, and lead to tropical cyclone formation.

4. Monsoon Gyre

The monsoon gyre (MG) is an even larger (diameter on the order of 2500 km) low-level cyclonic vortex in the tropical western North Pacific, which is often located 1000 km or more to the north of the mean monsoon trough axis (JTWC 1994; Lander 1994, 1996). Another feature of this circulation is the existence of deep convection along its southern and eastern periphery. Small tropical cyclones tend to form on the inside of the stronger winds at large radii (Lander 1994). The monsoon gyre may very rarely become a very large tropical cyclone (Lander 1996). Monsoon gyres occur about once every two years between July and September (Lander 1994). This large-scale circulation may persist two to three weeks and may be separated from the Asian continent by a north-south ridge of high pressure (Lander 1994).

B. MONSOON DEPRESSION FORMATION

The western North Pacific monsoon depression is the focus of this study as it is one of leading synoptic-scale circulations that provide favorable conditions for tropical cyclone formation in the region. The three goals of this research are to provide a conceptual model of monsoon depression formation, refine the structural definition of the monsoon depression and provide a conceptual model of monsoon depression transition to a pre-tropical cyclone seedling. This dissertation will examine these processes through case studies using satellite imagery and reanalyses of many cases to explore the physical mechanisms for monsoon depression formation and structure, and then transition to a pre-tropical cyclone seedling. The overall intention is to contribute to a better understanding of the monsoon depression leading to a more accurate identification of suspect regions of deep convection. A better understanding of the formation of the monsoon depression is expected to improve the forecast skill in identifying the regions of deep convection that would be most likely to lead to the formation of a tropical cyclone.

Little is known about the processes that influence the formation, structure, and development of the monsoon depression in the western North Pacific. Therefore, another objective of this portion of the research is to develop a new conceptual model of monsoon depression formation in the western North Pacific based on high resolution European Center for Medium-range Weather Forecasts (ECMWF) analyses and various satellite observations. A third objective is to examine the possible physical mechanisms of formation based on the new conceptual model. A comprehensive conceptual model and working definition of monsoon depression formation should assist forecasters in identifying deep convection regions that will first lead to monsoon depression formation and possibly tropical cyclone formation.

The monsoon depression formation study in Chapter II will begin with a synoptic analysis of the formations of two monsoon depressions in the western North Pacific that occurred within three days in early July 2007. Then, some possible physical mechanisms for monsoon depression formation will be explored based on the July 2007 cases. A conceptual model of monsoon depression formation will be proposed that is an extension of the Harr and Elsberry (1996) description of the 1993 pre-Typhoon Robyn monsoon depression. Finally, the applicability of the conceptual model is examined through an observational study of the 44 cases during April–December 2009 using satellite imagery and analyses.

C. MONSOON DEPRESSION STRUCTURE

The JTWC (1994) and Lander (2004) definitions of a monsoon depression emphasize that the deep convection associated with this circulation is primarily along the perimeter rather than in the central core, as it is in a tropical cyclone. The JTWC (1994) and Lander (1994, 1996) also distinguish a monsoon depression from a monsoon gyre, which they define as a large cyclonic vortex on the order of 2500 km in diameter with a persistent band of deep convective clouds along the southern and eastern peripheries of the circulation. Based on the Lander (1994, 1996) definition, monsoon gyres occur about once every two years between July and September and may persist for two to three weeks. Small tropical cyclones tend to form in a monsoon gyre on the inside of the

stronger winds at large radii, and the monsoon gyre circulation may very rarely become a very large tropical cyclone.

As indicated above, Lander (2004) suggested that two-thirds of western North Pacific monsoon depressions may transition to become a tropical cyclone. Therefore, the structure of the monsoon depression is an important consideration because the large vortex structure of the monsoon depression must somehow be transformed to have a small inner core of intense winds and precipitation. By contrast, Chen et al. (1998, 2004) suggested that 70% of the western North Pacific tropical cyclones form in association with monsoon gyres.

Typhoon (TY) Morakot (08W) moved slowly by Taiwan during 7–9 August 2009 and produced total rainfall accumulations approaching 3,000 mm in the Central Mountain Range. This record-breaking rainfall caused landslides over the mountains, including one landslide that destroyed the entire Shiao-Lin village, resulting in more than 650 deaths and causing severe flooding over most of the southwest plains in Taiwan. Hong et al. (2010), Ge et al. (2010), and Nguyen and Chen (2011) attributed the formation of TY Morakot (2009) to a monsoon gyre. However, Beattie and Elsberry (2012) examined the 25 km ECMWF analyses plus satellite observations during 2009 and found no circulations that met the JTWC (1994) or Lander (1994, 1996) definition of a monsoon gyre. Specifically, the TY Morakot period did not have the fishhook satellite cloud distribution or the kind of small tropical cyclone formations described by Lander. Rather TY Morakot formed from one of 17 monsoon depressions that did spawn a tropical cyclone during 2009 (Beattie and Elsberry 2013).

Thus, distinctly different opinions exist in the literature about monsoon depressions and monsoon gyres in relation to tropical cyclone formation, and also as to the outer wind structure (or size) of the tropical cyclone that might result. Monsoon troughs and/or monsoon depressions are also considered to contribute to tropical cyclone formations in all other basins, so it is important to better understand the monsoon depression structure.

The objective in Chapter III will be to provide quantitative values for the horizontal structure of western North Pacific monsoon depression, which will refine the definition in JTWC (1994) and Lander (1994, 1996) and help to distinguish the monsoon depression from the monsoon gyre.

D. THE TRANSITION OF A MONSOON DEPRESSION TO A PRE-TROPICAL CYCLONE SEEDLING

Seventeen of the 44 monsoon depressions that formed during 2009 transitioned to a pre-tropical cyclone seedling. The focus of this study is how a monsoon depression, with an elliptical horizontal structure that contains a loosely organized cluster of deep convection and a light wind core surrounded by a band of stronger winds at large radii, may be transitioned into a pre-tropical cyclone seedling where the circulation characteristics are more like a tropical cyclone, with a core that continues to decrease in diameter with increasing winds and precipitation. Since such a transition of a monsoon depression into a tropical cyclone will already have gale-force winds at a large radius, the tropical cyclone size (defined by the radius of gale-force winds) will be larger than for tropical cyclones formed from other pre-tropical cyclone circulations (e.g., equatorial waves). The larger monsoon depression-related tropical cyclones thus have a large beta-effect propagation (e.g., Fiorino and Elsberry 1989) toward the north that can be a major contribution to the total motion if the steering flow is relatively small. The larger size is also an important consideration for warnings of when gale-force winds will arrive.

While a number of studies, such as Ritchie and Holland (1999), Chen et al. (1998, 2004), Lander (2004), have made estimates of the numbers of western North Pacific tropical cyclones formed from monsoon depressions, very few case studies (e.g., Lander 1994; Harr et al. 1996) have addressed the physical processes that lead to a transition from a monsoon depression to a tropical cyclone, due in part to the confusion about the distinction between a monsoon gyre and monsoon depression. The monsoon depression has several characteristics that may make it a favorable environment for a tropical cyclone to develop (Gray 1968, 1975). That is, they occur in regions of sufficiently high sea-surface temperatures that provide a moist environment, the vertical wind shear is

generally small, and the broad region of cyclonic vorticity is sufficient so that even the low-latitude circulations may transition to a tropical cyclone.

Harr et al. (1996) described the transitional processes with the pre-TY Robyn monsoon depression during TCM-93. Their analysis indicated that when deep convection occurred near the circulation center the associated vorticity at 850 hPa became more concentrated and the convection in the outer regions became organized as a principle band, which quickly transitioned the pre-TY Robyn circulation into a tropical storm. Chang et al. (2010) observed surges (greater than 8.5 m s^{-1}) in the easterly trades and/or equatorial westerlies, which contributed to 7% of tropical cyclone formations in the western North Pacific over a 20-year period. Although these studies did not explicitly discuss the monsoon depression, similar favorable low-level influences in a monsoon environment (e.g., monsoon trough, monsoon gyre) that may lead to tropical cyclone formation were discussed. It is hypothesized that continued forcing, which is represented in this study by the wave-activity flux, is an important element in the transition of this pre-tropical seedling circulation as the wave-activity flux convergence aids in the scale constriction of the monsoon depression vorticity maximum and its associated convection to a pre-tropical cyclone seedling.

THIS PAGE INTENTIONALLY LEFT BLANK

II. MONSOON DEPRESSION FORMATION

A. BACKGROUND

One mode of monsoon depression formation occurs in the convergence zone between the tradewind easterlies to the north and the equatorial westerlies to the south, as was observed during the Tropical Cyclone Motion (TCM–93) field experiment during 1993 (Harr et al. 1996a). This monsoon depression that developed during TCM–93 eventually intensified to a tropical depression that later became Typhoon (TY) Robyn. The enhanced wind flows in the tradewind easterlies and the equatorial westerlies contributed to the environmental cyclonic vorticity, as the shear vorticity of the two flows was converted to the curvature vorticity of the circulation. The associated surface pressure falls were presumably due to the forced subsidence between the respective regions of convection and led to flow enhancement. This evolution led to a large, closed circulation with weak winds at the center and stronger winds along the perimeter, which satisfies the JTWC definition of a monsoon depression.

Another mode of monsoon depression formation involves the influence of a winter hemisphere circulation as in Love (1985a, 1985b). In this case, a cross-equatorial flow (which Love refers to as a southerly surge; in this study it is referred to as cross-equatorial or southerly flow) penetrates into the summer hemisphere and enhances the equatorial westerlies. This mode was observed during the formation of the pre-TY Man-Yi monsoon depression (July 2007) and, upon re-investigation, in the pre-TY Robyn monsoon depression as well (Beattie and Elsberry 2012). As will be described in a case study in Chapter II.B, cross-equatorial flow in the pre-TY Man-Yi monsoon depression case enhanced the horizontal shear and curvature vorticity of the region by enhancing the westerlies and turning the southern-most end of the monsoon trough northward to form a cyclonic vorticity lobe. This lobe later combined with a weaker lobe of cyclonic vorticity that already existed in the monsoon trough to form the monsoon depression.

Another possible explanation for the development of a monsoon depression may be barotropic instability of the monsoon trough as suggested by Guinn and Schubert

(1993). In their idealized simulation, the monsoon trough (which they labeled as the ITCZ) was represented as a zonal strip of maximum potential vorticity (PV), with a sharp positive (negative) gradient equatorward (poleward) of the PV maximum. Barotropic instability resulted in an eastward-propagating Rossby wave relative to the tradewind easterlies, and a westward propagating Rossby wave relative to the equatorial westerlies. These waves that are travelling in opposite directions have the same phase speed and may favorably phase lock in a configuration that results in wave growth via kinetic energy of the mean flow being transferred to the waves (i.e., the barotropic conversion of kinetic energy). Guinn and Schubert (1993) state that it is this breakdown of the monsoon trough that leads to the collection of cyclonic PV anomalies that may become potential tropical cyclone seedlings. Ferreira and Schubert (1997) extended the Guinn and Schubert (1993) study by incorporating a mass sink as a highly idealized representation of convection. They noted the formations of the most intense cyclonic PV anomalies were biased to the poleward side of the mass sink, which corresponds to the observations of tropical cyclone formations just to the north of the monsoon trough.

Another possible explanation for monsoon depression formation is wave-activity flux convergence. Sobel and Bretherton (1999) observed the reverse case of the Ferreira and Schubert (1997) PV maximum scenario. They suggest that when a strip of maximum PV is observed in the western North Pacific, it forms as a result of the merger of several vortices. Specifically, Sobel and Bretherton suggest that a wave-activity convergence (or wave accumulation) due to the convergence of the low-level mean flow is the mechanism for disturbance formation and growth. This linear wave accumulation mechanism had previously been proposed by Holland (1995).

Kuo et al. (2001) extended the ideas of Holland (1995) and Sobel and Bretherton (1999) by examining the nonlinear interactions between the monsoon circulations of the western North Pacific and equatorial wave disturbances. In particular, Kuo et al. (2001) used a barotropic, nondivergent vorticity model to examine the energy dispersion and wave accumulation in a zonally-opposed confluent flow, which is a scenario designed to represent the eastern end of the western North Pacific monsoon trough. In agreement with the theory of Holland (1995) and Sobel and Bretherton (1999), wave energy

accumulation did occur in the convergence zone. Without considering diabatic processes in this simulation, the wave contraction that occurred would extract energy from the wave versus supplying it. In the Kuo et al. (2001) simulations, a mean flow to wave energy transport could still occur if the vorticity gradient was sharpened by the background flow. Thus, without the diabatic effects, nonlinear energy processes must dominate (via vortex axisymmetrization).

Molinari et al. (2007) also found that a confluent flow contracted and amplified the waves approaching the western North Pacific from the central Pacific and noted that when this process occurred in a region of persistent convective heating, such as in the monsoon trough, the disturbances amplified. Molinari et al. (2007) observed the greatest wave amplification in the monsoon trough region at 850 hPa. This study also supports the wave-activity flux convergence hypothesis of Holland (1995), Sobel and Bretherton (1999), and Kuo et al. (2001).

Molinari et al. (2007) also examined cross-equatorial effects of a wave train (if any) in the Southern (winter) Hemisphere. They found that the only regions in the Southern Hemisphere that had equatorial Rossby waves of significant amplitude were in the regions of background convergence, which is consistent with the Northern Hemisphere studies described above. Molinari et al. (2007) considered the effects of easterly vertical wind shear in wave amplification. Since the vertical shear is also a maximum at 850 hPa, it may help to trap the energy at low levels, where the waves could continue to amplify via disturbance-scale effects (i.e., friction and diabatic effects). Although Molinari et al. (2007) tried to simulate wave growth in the absence of low-level convergence and easterly vertical wind shear, no waves were amplified.

B. SYNOPTIC ANALYSIS OF THE JULY 2007 MONSOON DEPRESSION FORMATIONS

As indicated above, the monsoon depression that transitioned into TY Robyn during early August 1993 (Harr and Elsberry 1996) was the initial prototype of monsoon depression formation for this study. Two monsoon depressions from July 2007 that formed during the dry run for the 2008 Tropical Cyclone Structure (TCS–08) field

experiment (Elsberry and Harr 2008) have been examined. The study period for these July 2007 cases started at 0000 UTC 29 June and ended on 0600 UTC 6 July 2007. This period included the formation of the pre-TY Man-Yi monsoon depression, but did not include its transition to a tropical cyclone late on 7 July, which was a major feature of the TCS-08 dry run. For the 2007 study, 1-degree latitude/longitude ECMWF analyses of wind and vorticity over the domain of 15°S–25°N, 100°E–180°E at 850 hPa were used. The Tropical Rainfall Measuring Mission (TRMM) three-hourly precipitation product (2007; 3B42 V6 derived), Multifunctional Transport Satellite (MTSAT) infrared (IR) imagery (for overall cloud distributions), and Quick Scatterometer (QuikSCAT) surface winds were also examined for these monsoon depression formations.

These two monsoon depressions that formed within three days in early July 2007 in the western North Pacific (Figure 1) became the basis of the new conceptual model of monsoon depression formation (Beattie and Elsberry 2012). The first monsoon depression formed at 7°N in the northwest portion of the domain near the Philippines, and was a long-lasting feature that did not transition to a tropical cyclone. The second, larger monsoon depression closer to the equator (4°N) was short-lived, less than three days, as it transitioned into the tropical cyclone that became TY Man-Yi.

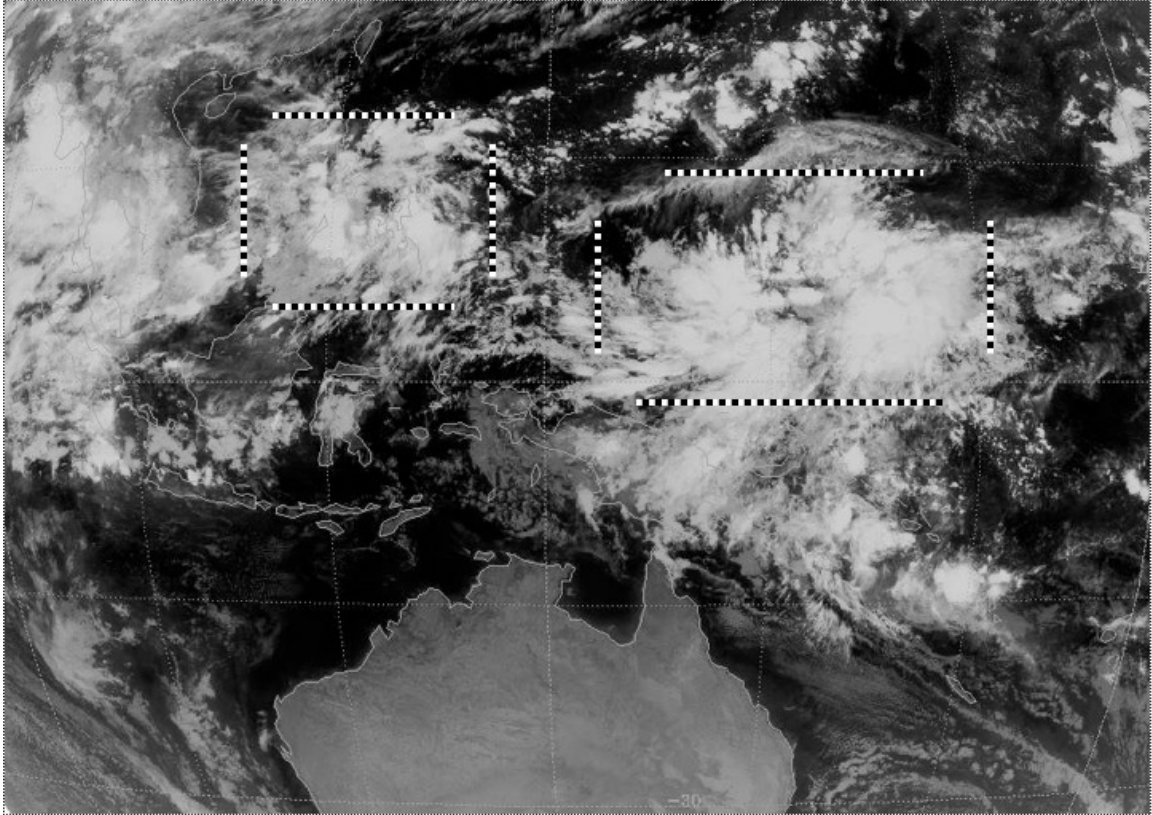


Figure 1. MTSAT-1R infrared image at 1800 UTC 6 July 2007 illustrating the two monsoon depressions described in Chapter II.B. The meridional and zonal lines indicate the horizontal extent of each monsoon depression based on the infrared imagery; grid spacing is 15-degrees in latitude and longitude.

1. Monsoon Depression MD₁

An east-west oriented monsoon trough MT₁, anchored east of the southern Philippines near 9°N, 125°E had become established by 1 July (Figure 2) that would on 3 July become the source region for monsoon depression MD₁ (Figure 3). Cross-equatorial flow in the western portion of the domain (from over Malaysia and western New Guinea; 115°E–135°E) increased, and due to the Coriolis effect the flow became westerlies that established the southern portion of the MT₁ (Figure 2). A cyclonic vorticity lobe then developed along the confluent region at the western end of the monsoon trough. Although the cross-equatorial flow diminished after this time, it strengthened again on 1200 UTC 2 July (not shown) and further enhanced the Northern Hemisphere westerly flow. As the enhanced equatorial westerlies became more southerly

and approached the eastern end of the established east-west MT₁ along 5°N, they resulted in the development of a separate eastern lobe of cyclonic vorticity. By 0000 UTC 3 July, the eastern vorticity lobe combined with the pre-existing vorticity lobe and resulted in a large cyclonic circulation (not shown). This circulation, which was near 7°N, 131°E at 1200 UTC 3 July (Figure 3; MD₁), developed from the cross-equatorial flow and fit all characteristics of a monsoon depression as defined by Lander (2004) and the JTWC (1994).

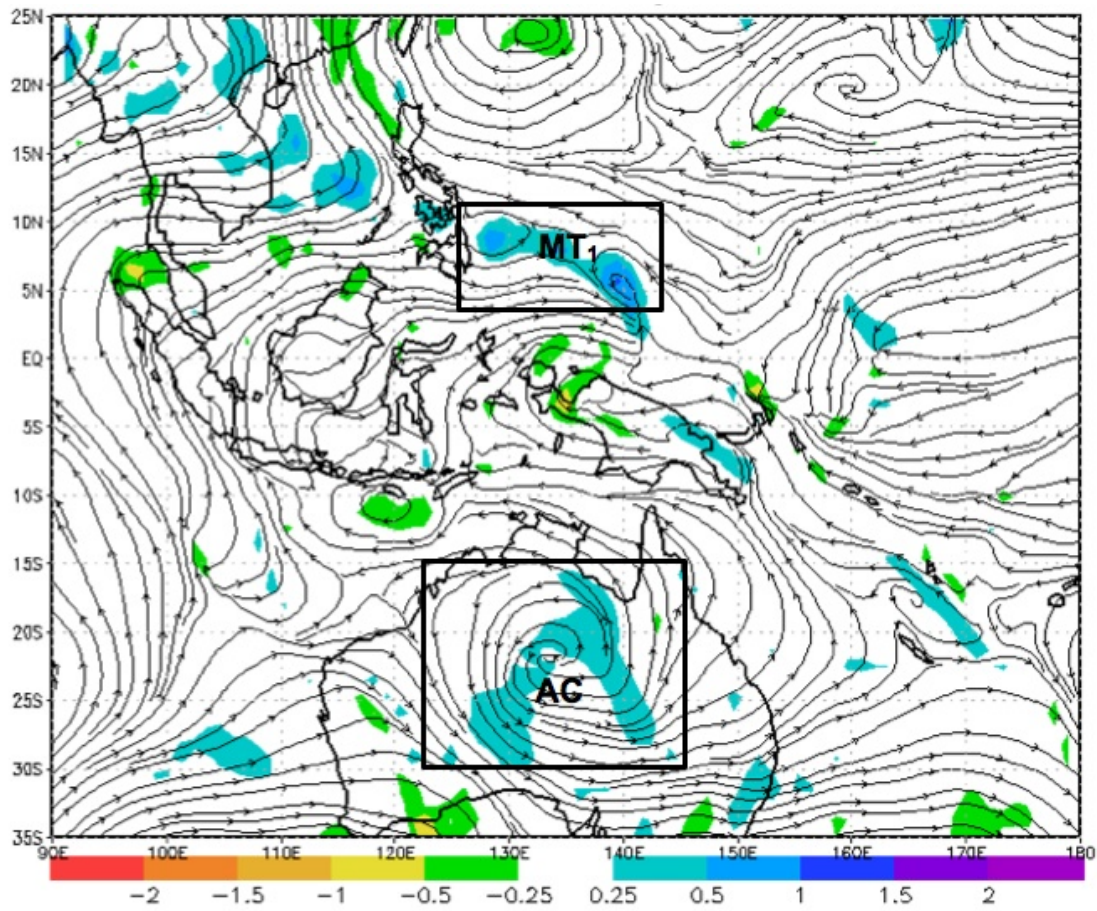


Figure 2. Streamlines and relative vorticity (shading scale at bottom in units of 10^{-4} s^{-1}) at 850 hPa from the 1-degree ECMWF analysis at 1200 UTC 1 July 2007. The box labeled MT₁ depicts the east–west oriented monsoon trough that lead to the first, long-lasting monsoon depression east of the Philippines. The box in the Southern Hemisphere labeled AC indicates an anticyclone that is contributing to a southerly flow that enhances the cross-equatorial flow into MT₁.

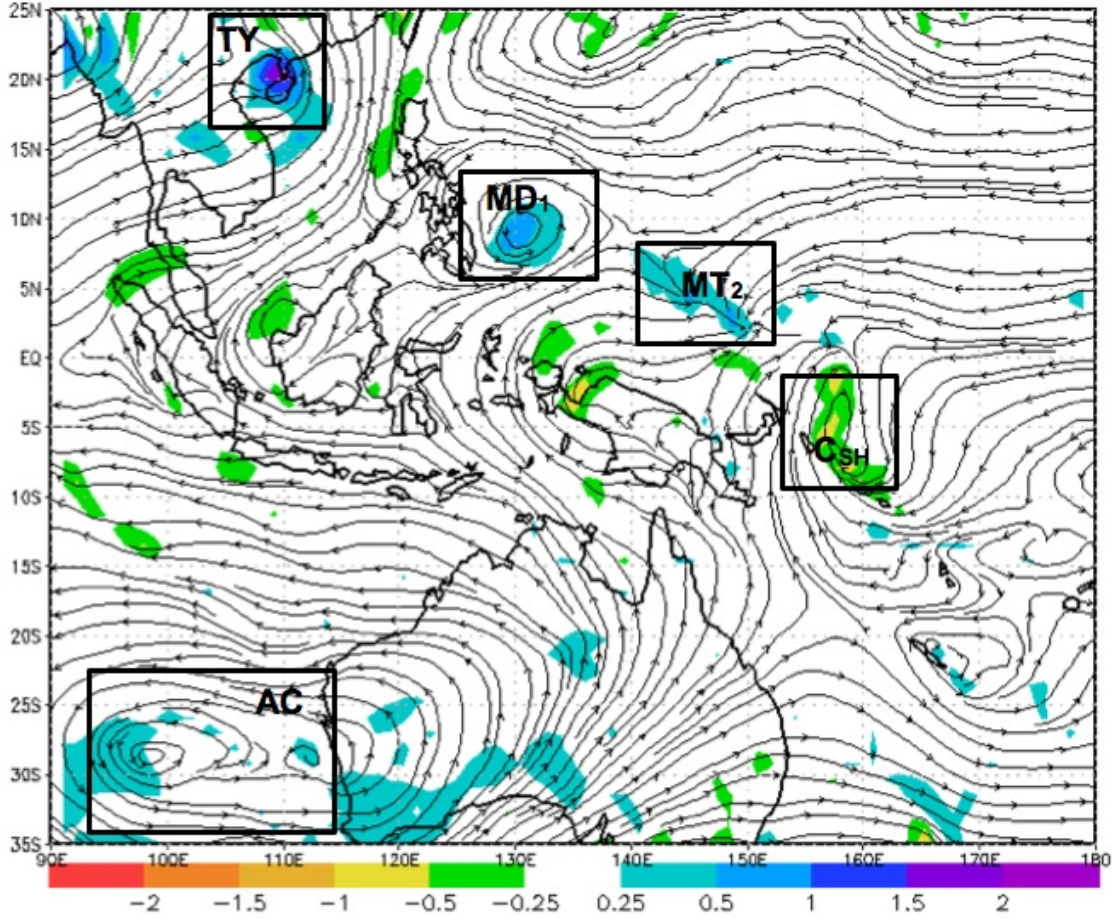


Figure 3. Streamlines and relative vorticity as in Figure 2 except at 1800 UTC 4 July 2007 and includes a chain of cyclonic circulations that extend southeastward from TY Toraji in the South China Sea. Following the formation of MD₁, MD₂ will form in association with the traditionally oriented MT₂. A Southern Hemisphere anticyclone (AC) in conjunction with the midlatitude westerly trough contributes to sustained cross-equatorial flow. A near-equatorial cyclone (CSH) in the Southern Hemisphere also facilitates cross-equatorial flow.

2. Monsoon Depression MD₂

By 1200 UTC 3 July (Figure 3), a chain of cyclonic circulations extended southeastward from Typhoon Toraji that had formed in the South China Sea. Monsoon depression MD₁ was the second cyclonic circulation in the chain, and was followed by a southeast-to-northwest oriented monsoon trough (labeled MT₂ in Figure 3) that formed on 3 July to the southeast of MD₁. This monsoon trough (MT₂) was well established by 1800 UTC 4 July with a maximum vorticity lobe at 850 hPa near 4°N, 150°E. The

formation of this MT₂ occurred as TY Toraji continued to move toward the northwest and MD₁ moved slowly westward. During this period, persistent cross-equatorial flow had turned clockwise to form westerlies equatorward of both monsoon troughs, and persistent tradewind easterly flow existed throughout the eastern portion of the domain. A branch of cross-equatorial flow in the central domain (125°E–135°E) contributed to the enhancement of the westerlies flowing into MT₂. These enhanced equatorial westerlies formed a confluent region with the trade easterlies that then contributed to enhanced regions of cyclonic vorticity along the monsoon trough. As described by Kuo et al. (2001), it is not enough to have a region of confluence to yield a cyclonic circulation, convergence is also needed. In these monsoon depression formations, it is hypothesized that the cross-equatorial flow leads to enhanced westerlies and convergence with the trade easterlies in the confluent region of the monsoon trough.

A separate branch of cross-equatorial flow in the eastern domain (east of New Guinea; 145°E–160°E) was part of a near-equatorial cyclonic circulation in the Southern Hemisphere (labeled C_{SH} in Figure 3) near 5°S, 158°E. By 1800 UTC 5 July (Figure 4), this eastern cross-equatorial flow had penetrated far enough northward to combine with the trade easterlies, which created a region of convergence within the eastern end of the monsoon trough and formed an eastern lobe of cyclonic vorticity. Early stages of this sequence can be observed in Figure 3. In addition to the typical cloudiness in the warm and moist equatorial westerlies in the southwest quadrant of the cyclonic vorticity lobe, the convergent region on the southeastern end of the circulation resulted in a cloud band wrapping around the eastern side of the MT (Figure 4). The associated precipitation band and 850 hPa winds on the southeastern and eastern end of the monsoon trough contributed to a broad elliptical circulation with a west-southwest to east-northeast orientation that fulfilled the criteria for a monsoon depression (Lander 2004; JTWC 1994).

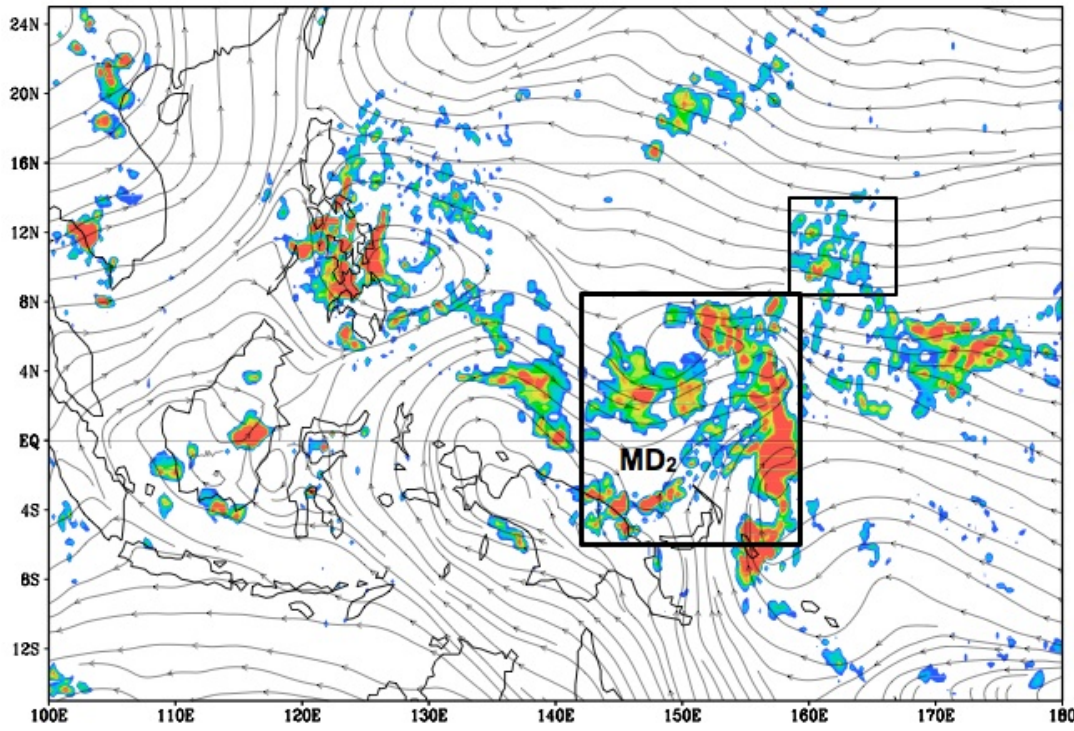


Figure 4. Streamlines at 850 hPa from the 1-degree ECMWF analysis at 1800 UTC 5 July 2007 and TRMM precipitation. The large box highlights the southerly flow that wrapped around the end of the monsoon trough and into the monsoon depression circulation. The small box shows the wave in the easterly flow approaching the formation region.

As in MD₁, the combination of the two cyclonic vorticity lobes at the eastern and western ends of the monsoon trough formed a large cyclonic circulation with outer wind maxima that were well aligned with TRMM precipitation. The merger of these vorticity lobes resulted in the formation of MD₂. Once MD₂ formed, the cross-equatorial flow continued in response to lower pressure in the depression.

In summary, cross-equatorial flows in the western and central regions of the domain enhanced the equatorial westerlies flowing into the monsoon trough, which are hypothesized to increase the horizontal shear and curvature vorticity in the region. Another cross-equatorial flow in the eastern portion of the domain interacted with the southeastern end of the monsoon trough to form a cyclonic vorticity lobe that then began to wrap the monsoon trough into a cyclonic circulation. Each of these cross equatorial

flows was accompanied by regions of deep convection and cirrus-level outflows that then wrapped around an inner region of minimal deep convection as observed in Figure 1. Because the deep convection tended to be concentrated in the confluent regions between the trade easterlies and equatorial westerlies, convection during the monsoon depression formation stage was associated with the eastern and western cyclonic vorticity lobes. Furthermore, the maximum winds were found along the circulation periphery, which was of order of 1000 km in diameter and had a cloud and precipitation-free center.

C. EXAMINATION OF PHYSICAL MECHANISMS FOR MONSOON DEPRESSION FORMATION

Based on these analyses of the two July 2007 monsoon depression formations, three physical mechanisms are examined that may have contributed to their formation. The first is Rossby wave dispersion along a chain of cyclonic circulations as in Figure 3; the second is energy flux associated with easterly waves; and the third is energy flux associated with a cross-equatorial (southerly) flow. Each mechanism was investigated by means of a wave-activity flux calculation to determine the primary mechanism for formation. Takaya and Nakamura (2001) used the wave-activity flux to identify wave propagation and understand the atmospheric dynamics of stationary and propagating small-scale anomalies.

1. Rossby Wave Dispersion

Rossby wave dispersion was considered as a possible contributor to the monsoon depression formation following several wave-activity flux convergence studies (e.g., Sobel and Bretherton 1999; Molinari et al. 2007) in which disturbance formation occurred to the southeast of an already mature cyclonic system. As indicated in Figure 3, TY Toraji was located in the South China Sea to the northwest of MD₁ that formed to the east of the Philippines. Both circulations were to the northwest of the MT₂ region where the second monsoon depression (MD₂) would form. Thus, one interpretation from this analysis was that a wave train from TY Toraji to MD₁ would continue to create a wave-activity flux from the northwest that would contribute to the developing MT₂ (Figure 3) and eventually lead to the formation of MD₂.

The hypothesis is then that a cascade of wave-activity flux to the southeast of each feature would result in an increase of cyclonic vorticity in the regions of each developing monsoon depression. The wave-activity flux was calculated using streamfunctions (Ψ) derived from the ECMWF 1-degree analysis of zonal (u) and meridional (v) wind components at 850 hPa. Following the Takaya and Nakamura (2001) study, the zonal (x) and meridional (y) components of wave-activity flux are:

$$WF_x = \frac{1}{2} \frac{\left[u_b \left(v^2 - \Psi \frac{\partial v}{\partial x} \right) + v_b \left(\Psi \frac{\partial u}{\partial x} - uv \right) \right]}{|\mathbf{U}|} \quad \text{and} \quad (1)$$

$$WF_y = \frac{1}{2} \frac{\left[u_b \left(\Psi \frac{\partial u}{\partial x} - uv \right) + v_b \left(u^2 - \Psi \frac{\partial u}{\partial y} \right) \right]}{|\mathbf{U}|} \quad (2)$$

where $|\mathbf{U}| = \sqrt{u_b^2 + v_b^2}$ and u_b and v_b are the mean zonal and meridional wind components at 850 hPa. Although these wave-activity fluxes (units of $m^2 s^{-2}$) were calculated globally, they have been re-scaled for display in the region of interest ($35^\circ S$ – $25^\circ N$, $90^\circ E$ – $180^\circ E$). A running one-day mean of the 6 h wave-activity fluxes was performed to eliminate some small-scale variability. See the Appendix for further discussion of these equations.

Wave-activity fluxes for the domain are shown in Figures 5a–d from 0600 UTC 4 July to 0600 UTC 6 July. Note that the regions of maximum wave-activity flux (vectors) divergence (shaded) coincide with the cyclonic systems as depicted in Figure 3. If Rossby wave dispersion was contributing to the monsoon depression formations during this period, the expectation would be that the wave-activity flux vectors point toward the southeast. Whereas wave-activity flux emanating from TY Toraji (Figure 5a) was toward the southeast into the trailing anticyclone, the flux from the trailing anticyclone was small and did not reach the region where MD₁ formed (not shown). The flux vectors from the trailing anticyclone remained small and did not have a preferred direction through the time period shown. Wave-activity flux also emanated from MD₁ (Figures 5 a–d), but did not extend to the region where MD₂ would form (labeled MT₂ in Figures 5a and 5b), as the flux vectors were also pointing southward. Therefore, this mechanism was not

considered to be a contributing factor to monsoon depression formation as TY Toraji, MD₁, and MD₂ evolved independently without a direct connection via the wave-activity flux convergence to the subsequent cyclonic circulations in the apparent wave train (Figures 3 and 5a–d).

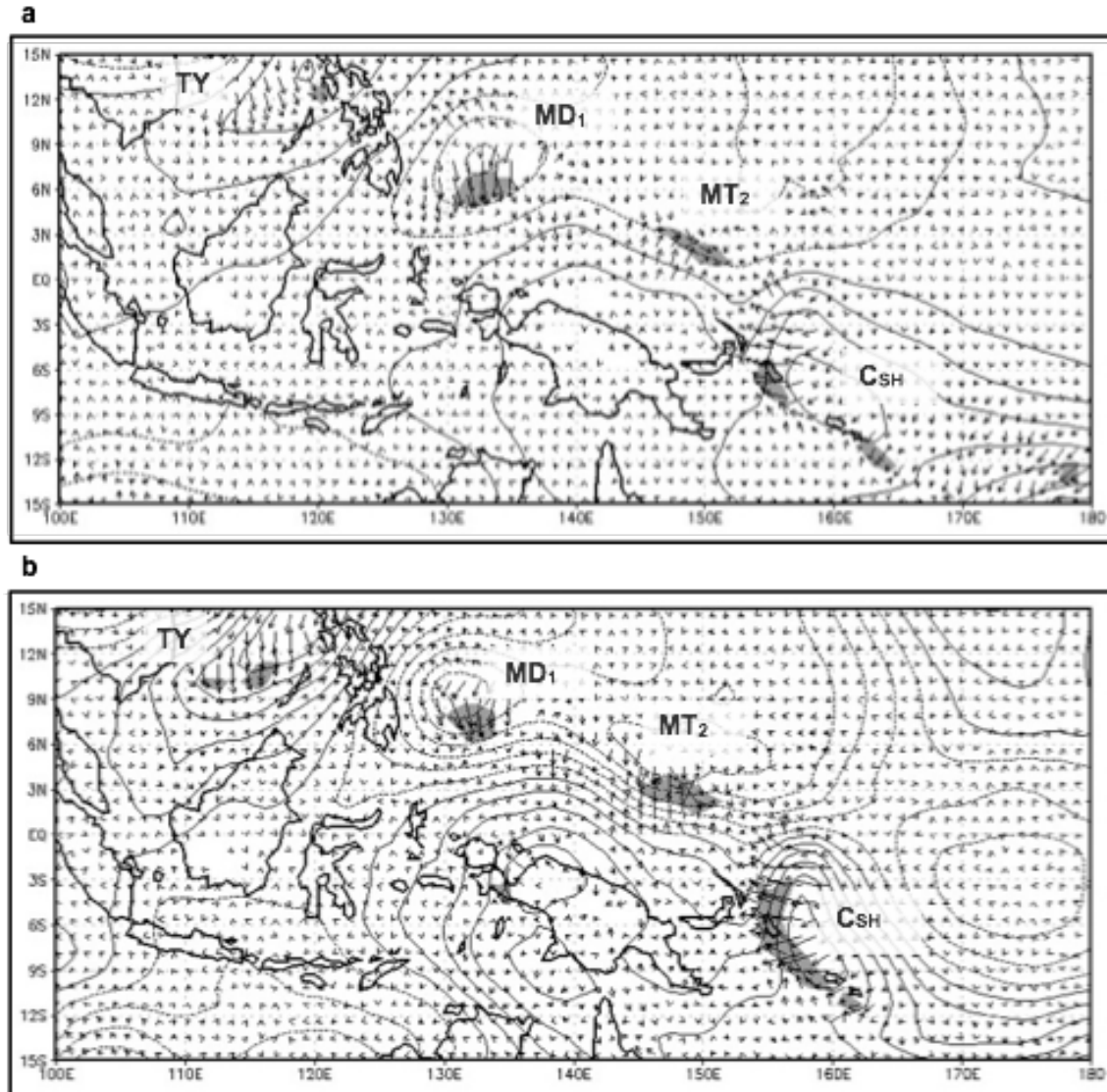


Figure 5. 850 hPa wave-activity flux vectors (units of m^2s^{-2}), the streamfunction anomaly (contours), and wave-activity flux convergence (shaded) that are labeled corresponding to the cyclonic circulations for (a) 0600 UTC 4 July 2007; (b) 0000 UTC 5 July 2007; (c) 1800 UTC 5 July 2007 and (d) 0600 UTC 6 July 2007.

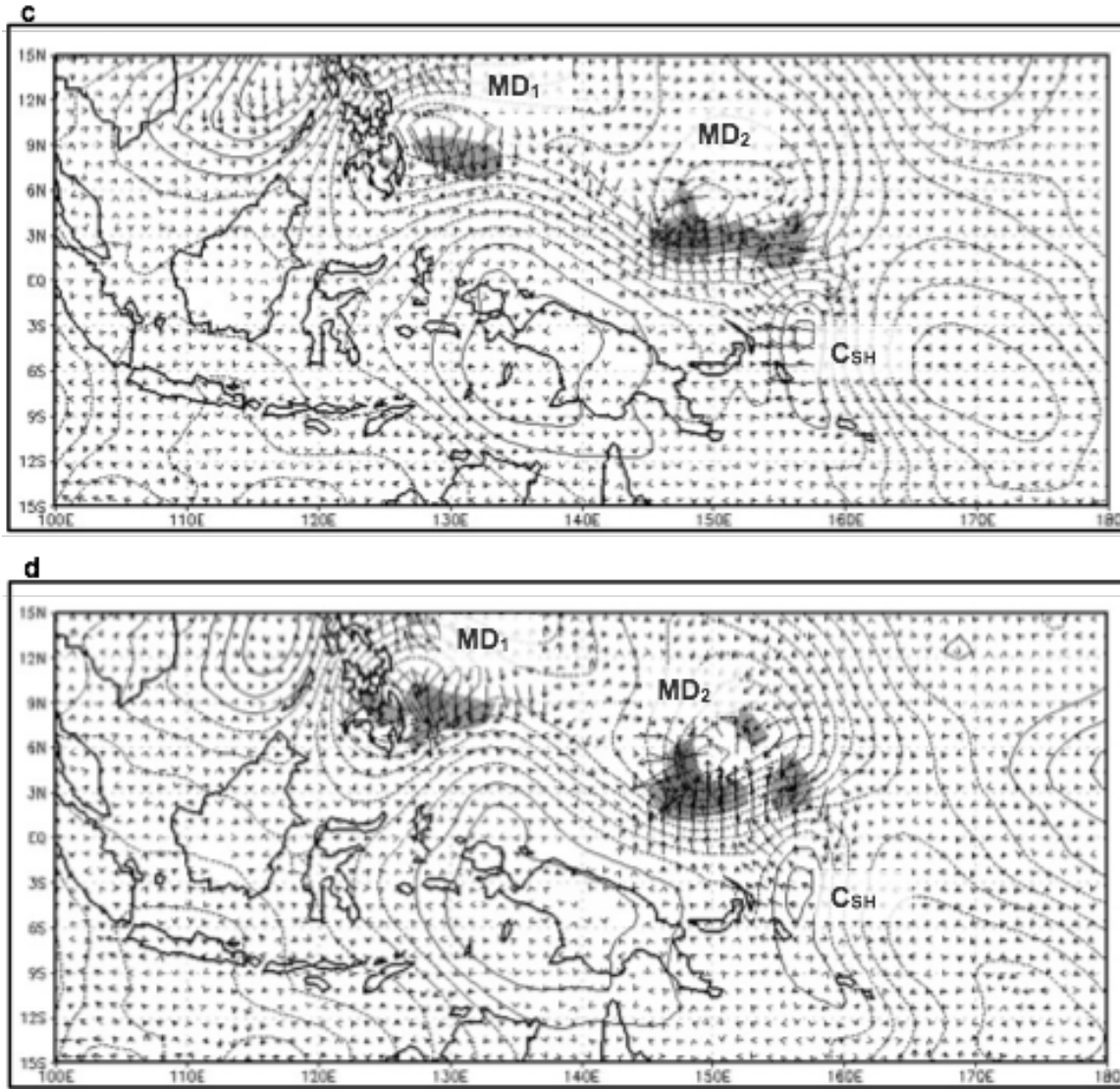


Figure 5, continued.

2. Waves in the Easterlies

As indicated in Chapter II.A, various researchers (e.g., Briegel and Frank 1997; Ritchie and Holland 1999; Sobel and Bretherton 1999; Kuo et al. 2001; Frank and Roundy 2006) have concluded that wave growth in a convergent background flow with positive vorticity provides an environment favorable for tropical cyclone formation. Dickenson and Molinari (2002) documented easterly waves that transitioned to tropical disturbances from which tropical cyclones would later form. Thus, a second hypothesis (as similarly proposed by Molinari et al. 2007) is that monsoon depression formation is

due to the interaction of a wave in the easterlies with the eastern end of a monsoon trough. Molinari et al. (2007) also emphasized the importance of horizontal variations in the background flow and therefore their role in contributing to synoptic-scale disturbance growth.

The hypothesized physical mechanism here is that a wave in the easterly flow is dispersive so the associated wave-activity flux would contribute to monsoon depression formation as it approaches the formation region from the east. No evidence was found that a wave in the easterlies approached the formation region of MD₁ (not shown). A wave in the easterlies (Figure 4, small box) did approach the formation region of MD₂ before formation. However, the wave-activity flux vectors in Figures 5a and 5b in the region of the wave in the easterlies are not directed toward the region where the MD₂ formed (i.e., MT₂). It was only after MD₂ formed that a connection in the wave-activity flux existed between the wave and the northeastern quadrant of MD₂ (Figures 5c and 5d). Even though this mechanism was not considered to be significant for this case of monsoon depression formation, the wave in the easterlies is hypothesized to have contributed to the transition of this MD₂ to a tropical cyclone (Chapter IV).

3. Cross-Equatorial Flow

The synoptic analysis in Chapter II.B suggests a connection between the cross equatorial flow from the Southern (winter) Hemisphere that provides enhanced westerly flow into a confluent region between the trade easterlies and equatorial westerlies. In addition, southerly flow into the eastern end of the monsoon trough appeared to increase the horizontal shear and cyclonic vorticity in the region of monsoon depression formation.

Love (1985a,b) demonstrated that winter hemisphere events could influence tropical cyclone formation in the summer hemisphere equatorial trough (monsoon trough). Love (1985a) suggested that the onset of cross-equatorial flow would be initiated when a rise in subtropical pressure propagated equatorward. If an associated cold surge in the lower troposphere raised the pressure along the Equator west of the genesis region, a west-to-east pressure gradient would lead to enhanced monsoon westerlies from the

surface to 500 hPa (Love 1985a). Love (1985b) also discussed the large-scale transition from equatorial trough (MT) to tropical cyclone via a pre-genesis cluster. Love (1985b) provides enough information to conclude that the pre-genesis cluster has similar characteristics to what Lander (2004) and the JTWC (1994) define as a monsoon depression.

Southerly wave-activity flux vectors also occurred in the same location as the cross-equatorial airstreams originating from the Southern Hemisphere prior to the formation of both MD₁ and MD₂ (Figure 5). These northward-pointing flux vectors were particularly well-defined moving into the formation region of MD₂ (Figures 5a and 5b). Note especially the wave-activity flux vectors associated with the Southern Hemisphere cyclone, C_{SH}, in Figures 5a–d that then resulted in flux convergence in the formation region of MD₂. Thus, these wave-activity flux vectors are consistent with the hypothesis that a primary physical mechanism for monsoon depression formation in the western North Pacific is cross-equatorial flow from the Southern Hemisphere.

D. CONCEPTUAL MODEL OF MONSOON DEPRESSION FORMATION

Based on the synoptic analysis and wave-activity fluxes for the two July 2007 monsoon depressions, a new conceptual model of monsoon depression formation in the western North Pacific was proposed by Beattie and Elsberry (2012) that involves three types of cross-equatorial flows (Figure 6) that tend to be in the western (airstream A), central (airstream B), and eastern (airstream C) regions of the domain as they cross the Equator through well defined channels in the geography (over western Indonesia, across eastern Indonesia and east of New Guinea). Each of these airstreams may interact with the Northern Hemisphere trade easterlies in a confluent environment to create the broad cyclonic circulation of a monsoon depression. It is these cross-equatorial flows that distinguish the new conceptual model from that of Harr and Elsberry (1996), who only considered the Northern Hemisphere aspects. The hypothesis that these cross-equatorial flows are a primary mechanism for monsoon depression formation is somewhat similar to the influence of the winter hemisphere on tropical cyclone formation in the summer hemisphere proposed by Love (1985a,b) as discussed in Chapter II.A.

Although their focus was on convective clusters developing in the Southern Hemisphere (15°S – 0° , 85°E – 100°E), Fukutomi and Yasunari (2005) documented southerly surges during June through August that penetrated to the Equator and interacted with the Northern Hemisphere equatorial westerlies. They defined a surge index based on the 850 hPa meridional winds for a specific box in the eastern South Indian Ocean. Composites (their Figure 3) of the 850 hPa winds during 63 strong southerly surge events that occurred between 1979 and 2001 resemble the evolution in Figure 4 leading to the MD₂ formation. Even though Fukutomi and Yasunari (2005) define these southerly surges as “submonthly,” their case studies indicate a time scale of about four days, and they associate the southerly surge with an amplifying midlatitude wave train.

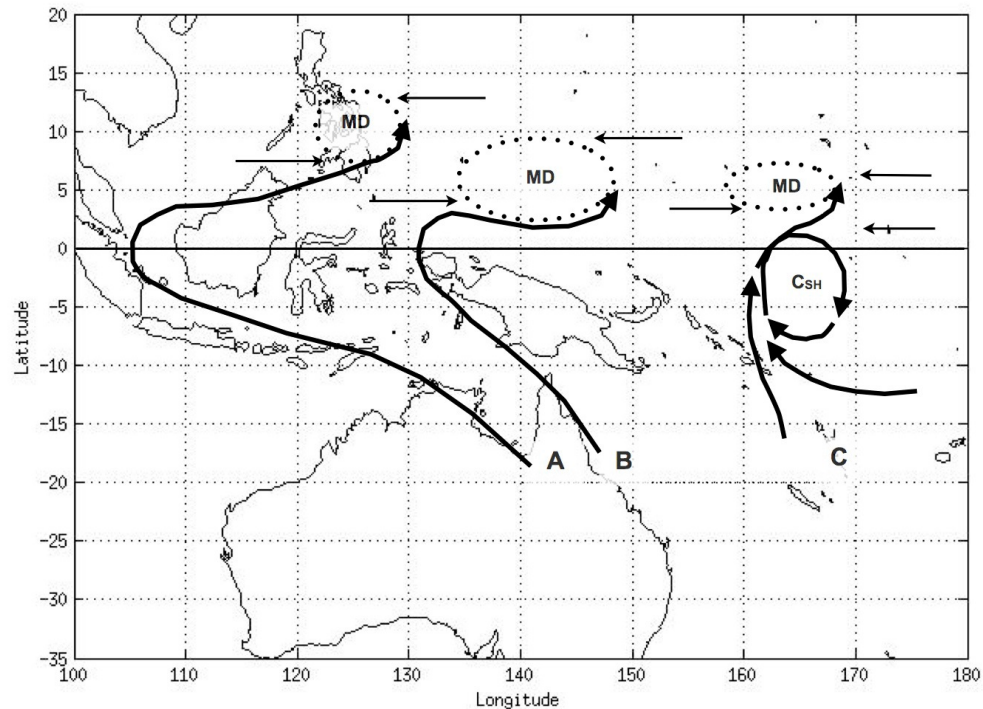


Figure 6. Idealized representation of the three cross-equatorial airstreams (A, B, and C) in the conceptual model of monsoon depression formation. Horizontal arrows in the Northern Hemisphere represent the equatorial westerlies and trade easterlies.

Large-scale circulations such as the Southern Hemisphere cross-equatorial flows, trade easterlies, and equatorial westerlies that establish the monsoon trough in the Northern Hemisphere may be somewhat quasi-stationary on the time scales leading up to a monsoon depression formation. However, the eastward-translating anticyclonic cells that trail the midlatitude troughs in the Southern Hemisphere that are proposed to contribute to the monsoon depression formations are more transient and dictate that trajectories would be more illustrative than streamlines. Therefore, backward trajectories from the monsoon depression formation locations were calculated using the Air Resources Laboratory (ARL) Hybrid Single Particles Lagrangian Integrated Trajectory (HYSPLIT) Model (Draxler and Rolph 2011). Analyses from the NCEP Global Data Assimilation System (GDAS) were the input to the HYSPLIT model.

Using the ARL HYSPLIT web interface, 120 h backward trajectories were plotted for both July 2007 monsoon depression formations. In order to trace the trajectories to a Southern Hemisphere midlatitude source region, a compilation of 120 h analyses was examined (Figures 7 and 8). The first backward trajectory ensemble originates at the edge of each monsoon depression (star), and the second originates from a point (star) within the first set of trajectories that crossed the Equator, which then shows where the trajectories originate in the Southern Hemisphere. As did the wave-activity flux calculations, these backward trajectories show that flow begins in the Southern Hemisphere midlatitudes, crosses the Equator, and continues into the region of monsoon depression formation.

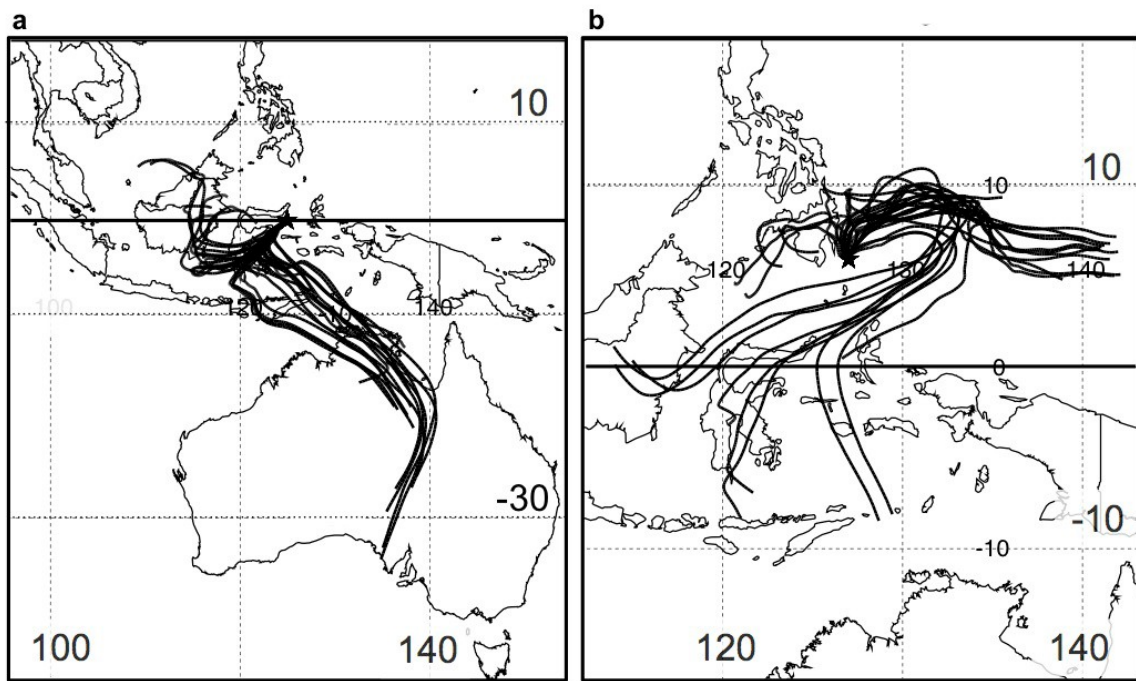


Figure 7. Ensembles of 120 hour HYSPLIT backward trajectories at 850 hPa originating in the region of the first monsoon depression (MD_1). The star represents the point at which the trajectories ended, open ends are the 120 h prior to the ending times-locations of (a) 0000 UTC 1 July 2007, 0° , 125°E ; and (b) 1800 UTC 3 July 2007, 6°N , 127°E .

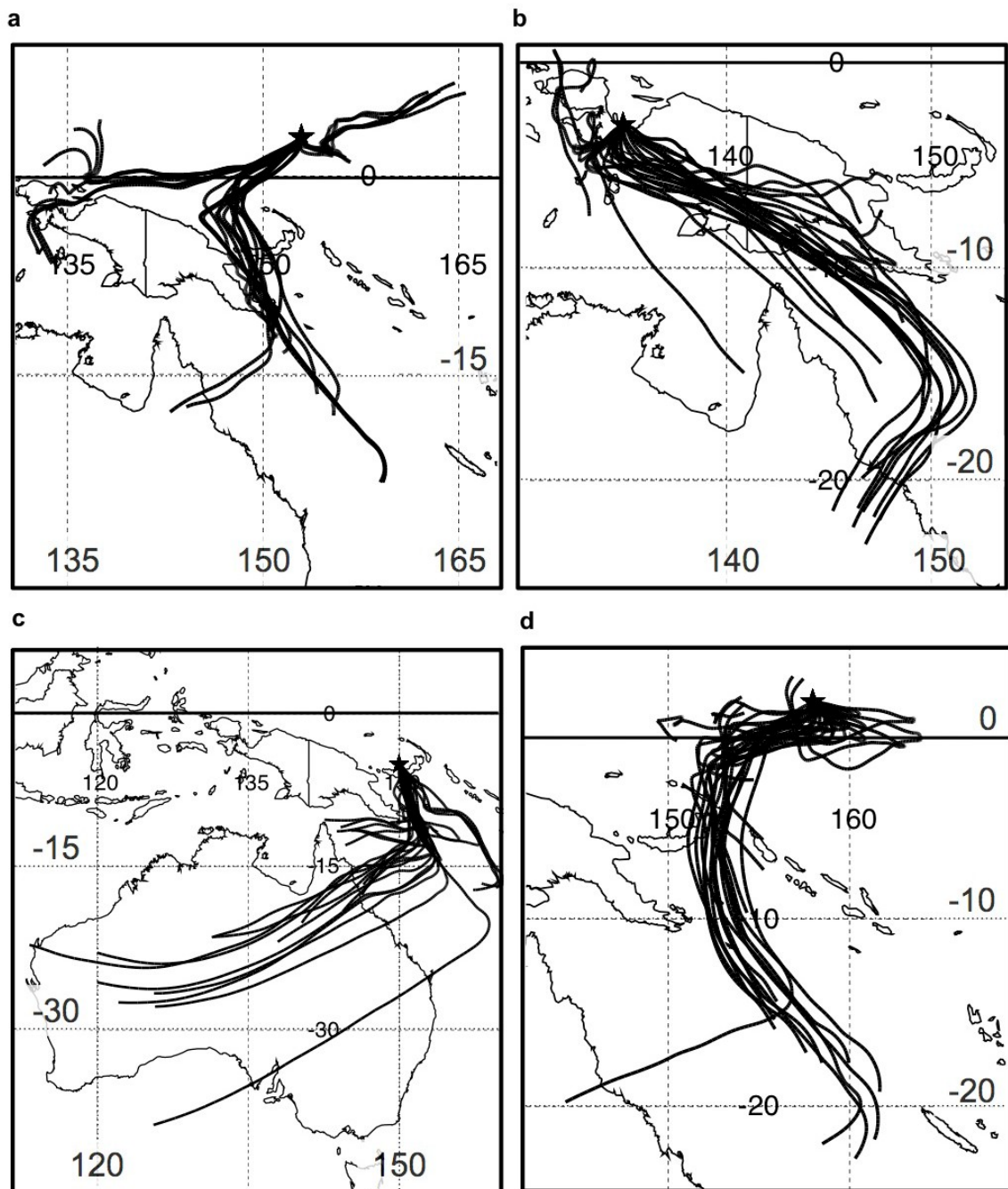


Figure 8. Ensembles of 120 hour HYSPLIT backward trajectories as in Figure 7, except for the pre-TY Man-Yi monsoon depression (MD_2) and ending times- locations of (a) 0000 UTC 6 July 2007, 3°N , 153°E ; (b) 0000 UTC 4 July 2007, 3°S , 135°N ; (c) 0000 UTC 4July 2007, 5°S , 150°E ; and (d) 0000 UTC 6 July 2007, 2°N , 158°E .

Airstream A (Figure 6) in the conceptual model corresponds to the cross-equatorial flow in the western-most portion of the domain as seen in the formations of MD₁ and MD₂ in July 2007. This airstream originates from the eastern side of a Southern Hemisphere midlatitude anticyclone and then becomes part of the southeasterly tradewind flow. After a long west-northwestward pathway, this flow is drawn across the Equator due to the lower pressure in the summer hemisphere. Once airstream A crosses the Equator, it gains a more westerly component due to the Coriolis effect. If airstream A has a large southerly cross-equatorial component, it can penetrate far into the Northern Hemisphere and then interact with the eastern end of a confluent region and wrap it into a cyclonic circulation (dashed portion of Figure 6, airstream A), which was observed in the formation of MD₁. Airstream A has the longest Southern Hemisphere path of any of the airstreams and is also the most western (100°E to 125°E) airstream when crossing the Equator.

Backward trajectories in Figure 7a illustrate an airstream A that originated from the Southern Hemisphere midlatitudes (near 30°S, 140°E) and followed a path toward the northwest before crossing the Equator between 120°E and 130°E (Figure 7b) where the flow began to turn east due to the Coriolis effect. Subsequently, these trajectories began to turn cyclonically between 5°N and 10°N near 130°E, as airstream A entered the confluent region of trade easterlies and equatorial westerlies (MT₁) in which MD₁ formed.

The second cross-equatorial flow labeled as airstream B (Figure 6) also originates from the eastern portion of a Southern Hemisphere midlatitude anticyclone, but has a more direct southerly pathway into the Northern Hemisphere where the Coriolis effect turns the flow to the east. This airstream crosses the Equator in the middle of the domain between 125°E and 150°E. Airstream B enhances the equatorial westerlies and interacts with the trade easterlies in association with a pre-existing confluent region to change the horizontal shear vorticity of the confluent region (or monsoon trough) into curvature vorticity (dashed portion of Figure 6, airstream B).

An excellent example of a more direct southerly airstream turning sharply to enhance the equatorial westerlies and interact with the trade easterlies is shown in Figure

8a. The Southern Hemisphere origin of the cross-equatorial branch at 135°E (western branch) in Figure 8a is illustrated by the backward trajectories in Figure 8b. The origin of the cross-equatorial flow at 150°E (eastern branch) in Figure 8a is indicated by the backward trajectories in Figure 8c. Both Figures 8b and 8c show that the airstreams originated from the Southern Hemisphere. These trajectories may represent the “southerly surge” as described by Love (1985a,b), and may be attributed to the Southern Hemisphere cyclogenesis (and anticyclogenesis) events that generate southerly flows that extend toward the Equator.

A third cross-equatorial flow airstream C (Figure 6) originates from the merger of airstream B and the Southern Hemisphere trade easterlies. That is, the eastern side of airstream B deflects the Southern Hemisphere easterlies equatorward, which results in airstream C. In the pre-TY Man-Yi (MD_2) formation, this southerly flow was then deflected back into the Southern Hemisphere after crossing the Equator and converging with the Northern Hemisphere trade easterlies. This process helped create a near-equatorial Southern Hemisphere cyclone labeled C_{SH} in Figure 6, as the northerly flow was deflected westward after converging with the Southern Hemisphere trade easterlies. The western branch of this clockwise circulation enhances the cross-equatorial flow of airstream C and enables the flow to penetrate farther into the Northern Hemisphere where it is able to interact with the confluent region (or monsoon trough) to form an eastern vorticity lobe.

In the MD_2 formation (Figures 3 and 4), airstream C contributed to confluence at the eastern end of the monsoon trough and thereby enhanced the convergence and increased the cyclonic vorticity of the region that contributed to the development of the circulation. Backward trajectories in Figure 8d indicate that this flow also originated in the Southern Hemisphere and flowed around the cyclone that was centered near 4°S, 158°E. In the conceptual model, as airstream C interacts with the eastern end of the monsoon trough and is wrapped into a broad cyclonic circulation, it creates an elliptically shaped monsoon depression circulation with two cyclonic vorticity lobes as illustrated in Figure 6. This airstream is a second mode of monsoon depression formation.

Compared to the Harr and Elsberry (1996) conceptual model, the new conceptual model attributes a critical role to cross-equatorial flow (airstream A or B) that penetrates into the Northern Hemisphere and enhances the strength of the equatorial westerlies. Subsequent confluence with the trade easterlies leads to convergence and contributes to a region of cyclonic vorticity. Another cross-equatorial flow (airstream A, B, or C) then interacts with the eastern end of the confluent region to create a convergent region that leads to an eastern cyclonic vorticity lobe. This second, more southerly, cross-equatorial flow then helps to combine the two vorticity lobes to form an elliptical monsoon depression circulation.

While these trajectories are useful to indicate the source regions for the airstreams entering the regions of the western or eastern vorticity maxima at the time of monsoon depression formation, they are not sufficient for describing the vorticity dynamics of the spin-up of the monsoon depression. Recall that a characteristic of the monsoon depression is light winds in the interior of the circulation with outer wind maxima that are associated with the deep convective bands that wrap around the circulation. On the inside (outside) of the outer wind maxima will be cyclonic (anticyclonic) relative vorticity.

Consider the vorticity equation in the form:

$$\frac{\partial \zeta}{\partial t} = -\mathbf{v} \cdot \nabla_z \zeta - (f + \zeta) \nabla \cdot \mathbf{V} + \beta \mathbf{v} - \frac{\partial w}{\partial x} \frac{\partial v}{\partial z} + \frac{\partial w}{\partial y} \frac{\partial u}{\partial z} \quad (3)$$

as derived from the Cartesian horizontal equations of motion where frictional effects are ignored. Scale analysis of the first advective term on the right side indicates that the term on the scale of the monsoon depression will be smaller than the second convergence term, even though many of the monsoon depressions form near the Equator where the Coriolis parameter, f , is small. The beta effect term will contribute to spin-up with the enhanced southerly flow on the eastern side of the monsoon depression. The tilting terms may contribute on the cloud scale, but not have an important contribution on the monsoon depression scale.

The large-scale convergence that would be consistent with the 12 h increases in relative vorticity approaching the ending point of the backward trajectories could be inferred as a residual in the conservation of the vorticity equation. A complete

convergence field inferred from such a calculation would require a large number of backward trajectories with ending points uniformly distributed over the area of maximum vorticity at the time of formation of the monsoon depression.

Vorticity fields calculated from the ECMWF analyses and forecasts are rather granular with positive and negative values oriented along bands, which must be associated with alternating values of convergence and divergence. Recall that the wave-activity fluxes in Equations (1) and (2) include divergence-type terms that lead to noisy fluxes that then had to be smoothed using an east-west mean of latitudinal bands to calculate the perturbation fields. Whereas these local maxima in convergence and divergence in the ECMWF analyses and forecasts might be aligned with the cloud bands in the monsoon depression, it cannot be assumed that such coarse resolution analyses are properly representing the cloud-band-scale processes that are occurring in nature. That is, a full understanding of the formation and evolution to maximum intensity of the monsoon depression would require a vorticity budget analysis based on observations on convective scales as well as the large scales. Such an analysis is beyond the scope of this study.

The composite of 63 southerly surges from Fukutomi and Yasunari (2005) also supports the potential role of cross-equatorial flow. As the southerly flow crosses into the southern Bay of Bengal, a band of enhanced equatorial westerlies is created between 5°N and 15°N in the Northern Hemisphere between 80°E and 120°E (their Figure 4b) as implied in the conceptual model in Figure 6. Convergence of the cross-equatorial flow with northerlies also leads to an east-west band of negative Outgoing Longwave Radiation (implying enhanced deep convection) over the same longitudinal interval. A significant difference in the Fukutomi and Yasumari (2005) study is that these enhanced equatorial westerlies do not interact with a confluent or convergent region of easterlies in the Northern Hemisphere as in the conceptual model in Figure 6.

The primary role of airstreams A and B from the Southern Hemisphere is to accelerate the equatorial westerlies that feed into the confluent region of the monsoon depression formation area and appear to have an important role in the spin-up of the western vorticity maximum. Although not observed in the 44 monsoon depression formations during 2009, a westerly wind burst as defined by Sheu and Liu (1995) may

play a similar role is accelerating the equatorial westerlies and contributing to a monsoon depression, or even twin monsoon depressions in both hemispheres.

E. APPLICABILITY OF THE CONCEPTUAL MODEL OF MONSOON DEPRESSION FORMATION

The applicability of this conceptual model of monsoon depression formation was examined from 1 April through 31 December 2009 utilizing high-resolution ECMWF analyses (0.25-degree) from the Year of Coordinated Observing Modeling and Forecasting Tropical Convection (YOTC), which extended from May 2008 through April 2010. This period was chosen for the analysis because 44 monsoon depressions were detected between 110°E and 180°E (Figure 9). By contrast, very few monsoon depressions formed during the La Niña-type conditions that existed during the May–December 2008 and January–March 2010 periods of the YOTC archive.

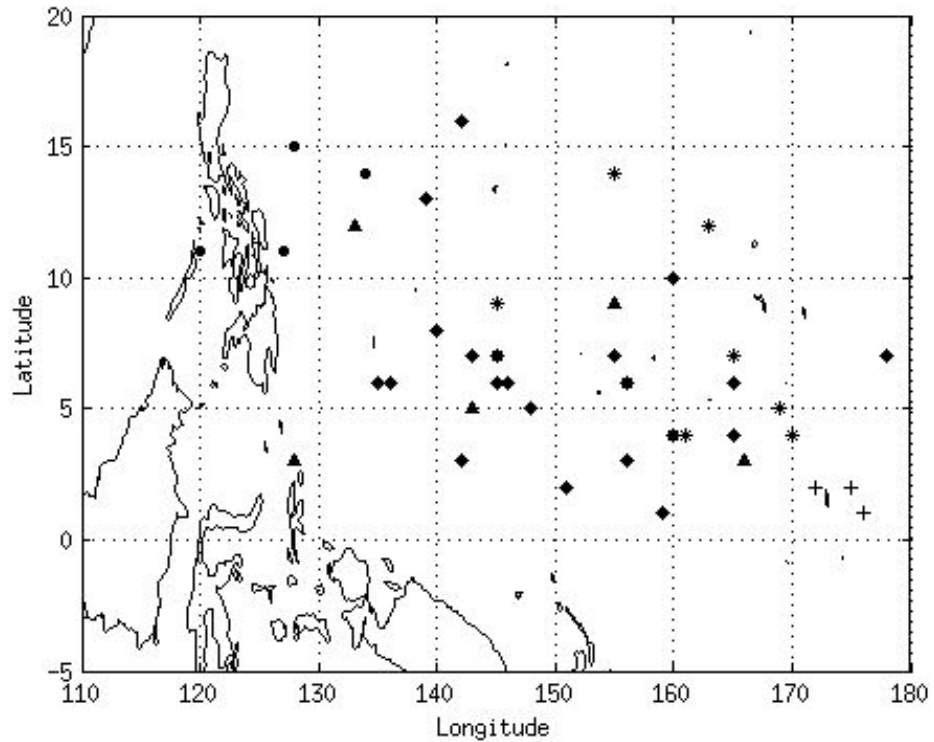


Figure 9. Center locations of all 2009 monsoon depressions. The filled circle (●) highlights those that formed from airstream A; the filled triangle (▲) highlights those that formed from airstream B; the filled diamond (◆) highlights those that formed from airstream C; the asterisk (*) highlights those that formed from airstream C*; and the plus sign (+) highlights those that are undefined as they formed east of 180°E .

1. Methodology

The first step in the observational study was to examine the high-resolution ECMWF analyses of 850 hPa vorticity and streamlines at six-hour intervals. These analysis fields were simultaneously compared with infrared satellite imagery from the MTSAT-1R (through 15 November 2009; <http://www.ncdc.noaa.gov/gibbs>) to confirm that the cyclonic circulations in the analysis were monsoon depressions according to the JTWC (1994) and Lander (2004) definition. That is, each circulation with an associated vorticity maximum in the YOTC analyses was required to have widespread, deep convection around the periphery of the circulation (typically with two regions of concentrated convection in opposite quadrants) with little to no convection in the interior. Furthermore, the surface cyclonic circulation (through 23 November 2009) was validated using QuikSCAT fields from <http://manati.orbit.nesdis.noaa.gov/datasets/QuikSCATData.php>. These fields were also used to confirm that the monsoon depressions had light winds near the circulation center and stronger winds around the circulation periphery. Finally, the three-hourly 0.25-degree TRMM precipitation (3B42 V6 derived) rates were obtained from: http://gdata1.sci.gsfc.nasa.gov/daacbin/G3/gui.cgi?instance_id=TRMM_3-Hourly. Each monsoon depression was required to have minimum precipitation near the circulation center. Thus, a ring-like pattern of precipitation in the TRMM product with a diameter similar to the cloud band in the infrared satellite imagery was used to confirm the circulation was a monsoon depression. The ring-like pattern of precipitation was not required to be continuous, and most of the cases had two precipitation maxima on opposite sides of the circulation center.

For a cyclonic circulation to be classified as a monsoon depression, three of the four data sets had to meet the criteria of a monsoon depression. If a monsoon depression formation was suspected in the YOTC analysis based on the circulation, but could not be conclusively confirmed in the satellite imagery, QuickSCAT and TRMM analyses were still checked. This procedure was necessary since the cloudiness associated with an adjacent circulation may have obscured the characteristic cloud pattern of the monsoon depression. After the mid-November 2009 termination of QuikSCAT, the primary cross-checking tool became the TRMM precipitation.

2. Analysis of Airstreams

Analysis of the 44 monsoon depression formations in Figure 9 indicated 18 (43%) formed in a similar way as the pre-TY Man-Yi monsoon depression (Table 1, ♦ symbols in Figure 9). These monsoon depressions form in the central and eastern portion of the domain (130°E – 180°E). Except for the 1800 UTC 31 Jul and the 0600 UTC 6 August 2009 cases, these monsoon depression formations formed quite close to the Equator, especially during the early or late season (Table 1); these outliers occurred at 18°N and 18.5°N respectively. The later formed when two tropical cyclones were in the western region of the domain, at a similar latitude as the monsoon depression, were influencing the cross-equatorial flow. Notice in Table 1 that the cross-equatorial flows could originate from the region between Southern Hemisphere midlatitude cyclones and anticyclones located across the domain (90°E to 180°E).

Table 1. List of monsoon depressions that form from airstream C. The first column is the time and date the circulation had all characteristics of a monsoon depression; the next two columns list the latitude and longitude of the circulation center; the last four columns are the latitude and longitude of the Southern Hemisphere anticyclone and Southern Hemisphere cyclone center from which the airstreams originate. With the exception of the 0600 UTC 06 June 2009, 0000 UTC 11 Jul 2009, and 0000 UTC 11 July 2009 monsoon depressions that had a circular shape, all of these monsoon depressions had an elliptical shape with major axis generally oriented east-west.

Airstream C	MD Center		Southern Hemisphere			
	Time (UTC)	Lat	Lon	Anticyclone Center	Cyclone Center (C_{SH})	Lat
1800 05 JUL 07	4°N	150°E	29°S	115°E	5°S	158°E
1200 21 APR 09	3°N	142°E	35°S	144°E	5°S	133°E
0600 06 JUN 09	5°N	154°E	26°S	170°E	5°S	150°E
0000 15 JUN 09	2°N	153°E	25°S	160°E	3°S	138°E
1200 21 JUN 09	7°N	136°E	35°S	165°E	3°S	141°E
0000 04 JUL 09	6°N	145°E	31°S	131°E	3°S	152°E
0000 11 JUL 09	7°N	143°E	35°S	151°E	2°S	139°E
1800 16 JUL 09	8°N	140°E	35°S	140°E	0°	132°E
1800 31 JUL 09	18°N	144°E	32°S	138°E	2°S	156°E
0600 06 AUG 09	18.5°N	139°E	29°S	152°E	4°N	142°E
0000 02 SEP 09	6°N	157°E	35°S	155°E	3°S	158°E
0600 21 SEP 09	6°N	146°E	24°S	155°E	3°S	147°E
0600 29 SEP 09	10°N	159°E	29°S	145°E	4°S	165°E
1200 05 OCT 09	7°N	178°E	33°S	130°E	4°S	171°E
1200 13 OCT 09	6°N	154.5°E	24°S	170°E	3°S	145°E
0600 21 OCT 09	4°N	163°E	27°S	148°E	8°S	168°E
0600 17 NOV 09	5°N	143°E	25°S	180°E	4°S	138°E
1200 19 NOV 09	5°N	148°E	33°S	165°E	0°	154°E
1200 27 NOV 09	1°N	159°E	UNDEF	UNDEF	6°S	172°E

This most frequent mode of monsoon depression formation emphasizes the importance of airstream C, which occurs in the eastern domain between 150°E to 180°E (Table 1). In the case shown in Figure 10, the eastern portion of airstream B, which originated from a Southern Hemisphere anticyclone, merges with the Southern Hemisphere trade easterlies, and enhances the southerly flow around the Southern Hemisphere cyclone near 5°S, 160°E. Note the similar role of the Southern Hemisphere cyclone as observed in the July 2007 MD₂ formation (Figure 3).

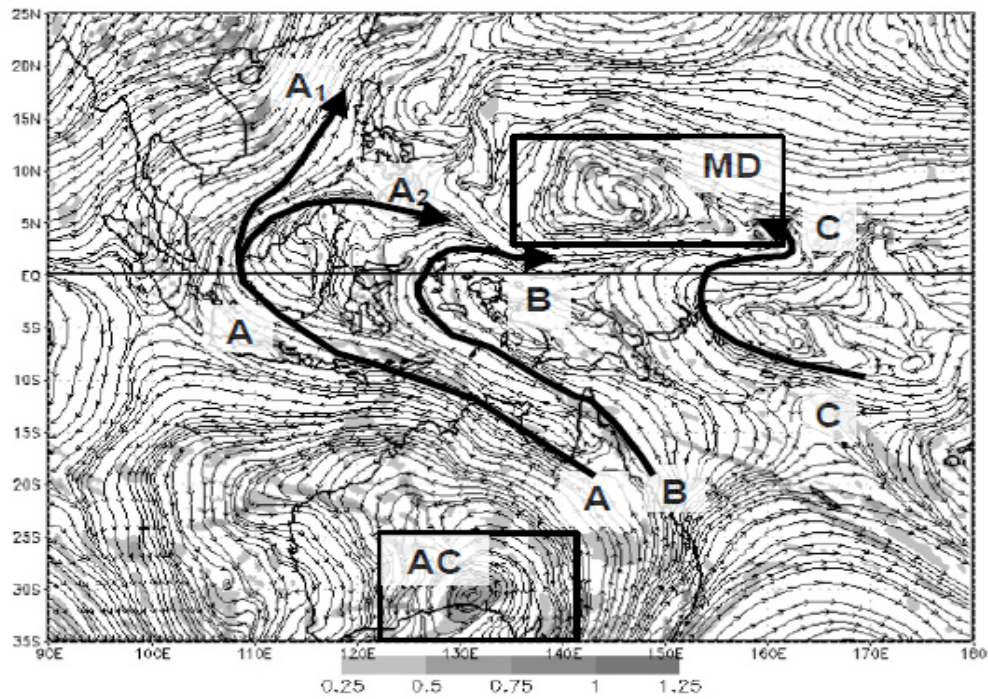


Figure 10. Streamlines and relative vorticity as in Figure 2, except from the 0.25-degree ECMWF analysis at 1200 UTC 2 July 2009. The large southern box highlights the center of the Southern Hemisphere anticyclone; the small northern box highlights the forming monsoon depression; the solid arrows highlight the three cross-equatorial airstreams A, B, and C of the conceptual model.

Two other examples in which airstream C played an important role in the formation of the eastern vorticity lobe are shown in Figures 11a and 11b. The monsoon depression in Figure 11b formed on 0600 UTC 29 September 2009 in association with the cross-equatorial flow from the Southern Hemisphere cyclone. This monsoon depression later transitioned into TY Melor (0000 UTC 30 September 2009). As indicated by the 120 h backward trajectories for this monsoon depression (Figure 12a), the primary sources were from the south and east. The backward trajectory ensemble in Figure 12b ends near the Equator (southern branch of Figure 12a) and highlights airstream C, which is evident from the clockwise flow around the Southern Hemisphere cyclone. The final backward trajectory in Figure 12c was from the edge of this Southern Hemisphere cyclone and highlights that the flow into the Southern Hemisphere cyclone was predominantly from the Southern Hemisphere easterlies.

In 12 of the 44 cases during 2009 (* symbols in Figure 9), airstream C did not have an associated Southern Hemisphere cyclone (Table 2). This variant of airstream C is hereafter referred to as the airstream C_* mode of monsoon depression formation and occurs in the eastern portion of the domain (170°E to 180°E). In this new scenario, a cross-equatorial flow interacts with the Northern Hemisphere trade easterly flow. Southeasterlies begin to develop as the cross-equatorial flow begins to be deflected to the east due to the Coriolis effect, but the strength of the trade easterlies in the Northern Hemisphere is an important factor in preventing the formation of westerlies. When southeasterly flow is established in both hemispheres, a confluent region develops that leads to a small cyclonic vorticity maximum. As the initial cross-equatorial flow ceases, the Northern Hemisphere trade easterlies are re-established and the new cyclonic vorticity maximum may be characterized as a wave in the easterlies. It is this cyclonic vorticity maximum that subsequently develops into a monsoon depression when a second cross-equatorial flow interacts with it. This second cross-equatorial flow event is then labeled as airstream C_* .

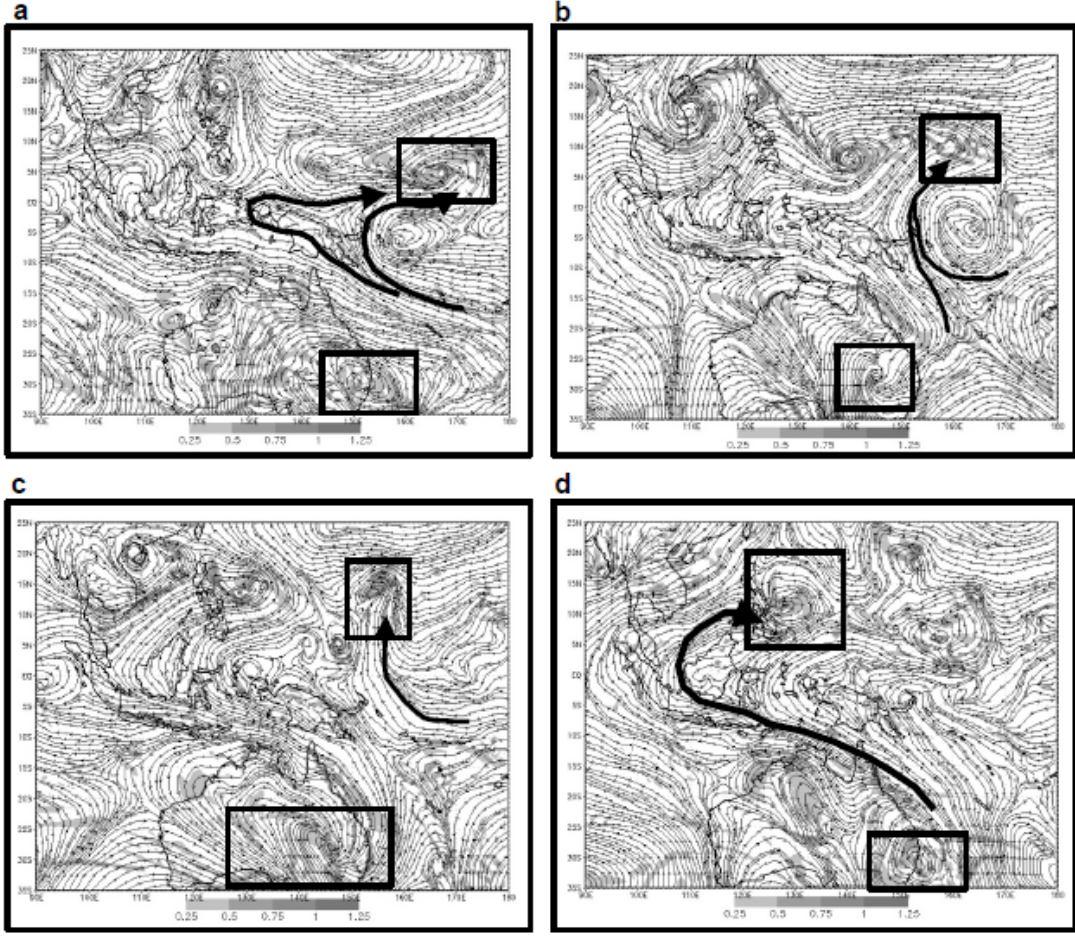


Figure 11. Streamlines and relative vorticity as in Figure 10, except at times of (a) 0000 UTC 22 October 2009, for airstreams B and C with the Southern Hemisphere cyclone; (b) 0600 UTC 29 September 2009, for airstream C with the Southern Hemisphere cyclone; (c) 0600 UTC 11 September 2009, for airstream C_{*} without the Southern Hemisphere cyclone; and (d) 0000 UTC 25 July 2009, for airstream A. The southern box highlights the Southern Hemisphere anticyclone centers; the northern box highlights the developing monsoon depression; and the arrows highlight the cross-equatorial airstream that is dominant in the formation of that monsoon depression.

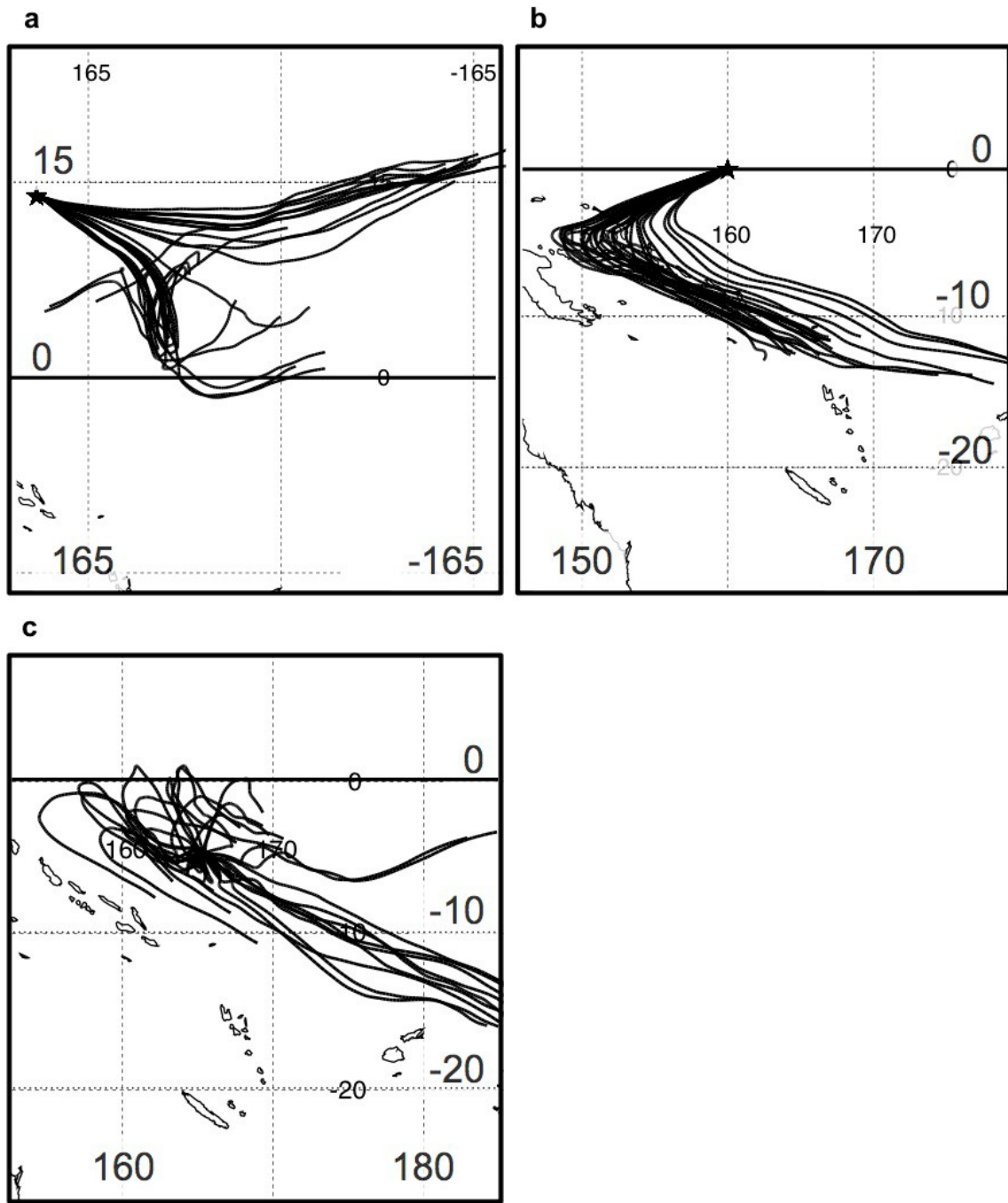


Figure 12. Ensembles of 120 hour HYSPLIT backward trajectories as in Figure 7, except for ending times-locations of (a) 0600 UTC 29 September 2009, 14°N, 161°E; (b) 0000 UTC 28 September 2009, 0°, 160°E; and (c) 0000 UTC 27 September 2009, 5°S, 65°E.

Table 2. As in Table 1, except for monsoon depressions that formed from airstream C_* , and there is no column for Southern Hemisphere cyclone. Either an elliptical (E) or circular (C) shape of the monsoon depression is listed in the last column.

Airstream C_*		Southern Hemisphere			
Time (UTC)	MD Center		Anticyclone Center		
	Lat	Lon	Lat	Lon	Shape
1800 7 MAY 09	3.5°N	145°E	>35°S	125°E	E
1800 22 MAY 09	3°N	150°E	17°S	126°E	E
0000 07 JUL 09	4°N	161°E	26°S	170°E	C
1800 18 JUL 09	4°N	169°E	26°S	156°E	E
0600 13 AUG 09	9°N	145°E	21°S	145°E	E
0000 15 AUG 09	12°N	163°E	23°S	142°E	E
0000 28 AUG 09	7°N	165°E	26°S	178°E	C
0600 11 SEP 09	14°N	155°E	27°S	148°E	E
1200 24 SEP 09	6°N	156°E	25°S	150°E	E
1800 03 NOV 09	4°N	161°E	31°S	123°E	E
1200 21 DEC 09	4°N	170°E	30°S	160°E	E
0600 27 DEC 09	4°N	145°E	34°S	171°E	C

The monsoon depressions that formed from airstream C_* occurred mainly between 145°E–170°E (Table 2). An exception was the first monsoon depression that formed by airstream C_* in 2009, which was early in the season (26 May) and formed farther west as trade easterlies existed in both hemispheres over the majority of the domain. These monsoon depressions also tend to form at latitudes below 10°N, with the exceptions of the 0000 UTC 15 August and 1200 UTC 11 September monsoon depressions, which formed at 12°N and 14°N, respectively. Although the majority of the monsoon depressions that form from this airstream have an elliptical shape, three from 2009 were more circular in shape.

The monsoon depression (Figure 11c) that formed at 0600 UTC 11 September 2009 from the interaction of a wave in the easterlies and airstream C_* , transitioned into TY Choi-Wan (1800 UTC 12 September 2009). In this case, no Southern Hemisphere cyclone was present (compare with Figure 11a and 11b), and the flow across the Equator penetrated far enough north to interact with the wave in the easterlies. Note that the Southern Hemisphere easterlies were first deflected northward by airstream B as in the original airstream C discussion. However, airstream C_* differs from the original airstream C because it penetrates far enough into the Northern Hemisphere such that the flow is not deflected back across the Equator by the trade easterlies, and a Southern Hemisphere cyclone does not form. Two examples of the wave-activity flux for this monsoon depression are shown in Figure 13. At 1200 UTC 9 September 2009 (Figure 13a), which is two days before the monsoon depression formed, the wave in the easterly flow was developing. Note the large wave-activity flux vectors crossing the Equator from the Southern Hemisphere in that region. By 0000 UTC 10 September 2009 (Figure 13b), the wave in the easterlies had propagated westward and the wave-activity flux from the Southern Hemisphere continued into the region of the wave. As the cross-equatorial flux continued, all of the characteristics of a monsoon depression were satisfied by 0600 UTC 11 September (Table 2).

The eight (18%) monsoon depression formations during 2009 in which airstream B had a dominant contribution are listed in Table 3 and are indicated by a \blacktriangle in Figure 9. The formations related to airstream B occur across the entire domain from 3°N – 16°N and 125°E – 170°E (Table 3). As in the earlier modes, these monsoon depressions tend to have an elliptical shape. A characteristic of airstream B in the conceptual model (Figure 6) was that it has a more direct southerly path to the Northern Hemisphere. In the examples of Figures 10 and 11a (western arrow, airstream B), this cross-equatorial flow enhanced the equatorial westerlies after it crossed the Equator. If a confluent region existed downstream of where this flow crosses the Equator, airstream B was considered to increase the convergence needed to transition the confluent region into an elliptical

cyclonic circulation that is a monsoon depression (Figure 6). The monsoon depression that formed on 0000 UTC 22 October 2009 (Figure 11a) was comparable to the July 2007 MD₂ case. The backward trajectory ensemble and wave-activity flux progressed in the same fashion as the pre-TY Man-Yi case (Figures 5 and 8) and, therefore, are not shown.

Table 3. As in Table 2, except for monsoon depressions that formed from airstream B.

Airstream B		Southern Hemisphere			
Time (UTC)	MD Center		Anticyclone Center		
	Lat	Lon	Lat	Lon	Shape
0000 14 APR 09	6°N	128°E	35°S	170°E	E
0000 17 MAY 09	4°N	123°E	34°S	135°E	E
1800 22 JUL 09	4°N	165°E	25°S	174°E	E
1200 09 AUG 09	6°N	144°E	26°S	178°E	E
1800 22 AUG 09	16°N	142°E	23°S	149°E	E
0600 10 SEP 09	12°N	134°E	24°S	140°E	E
1800 04 OCT 09	9°N	154.5°E	30°S	129°E	E
0000 29 OCT 09	3°N	166°E	33°S	151°E	E

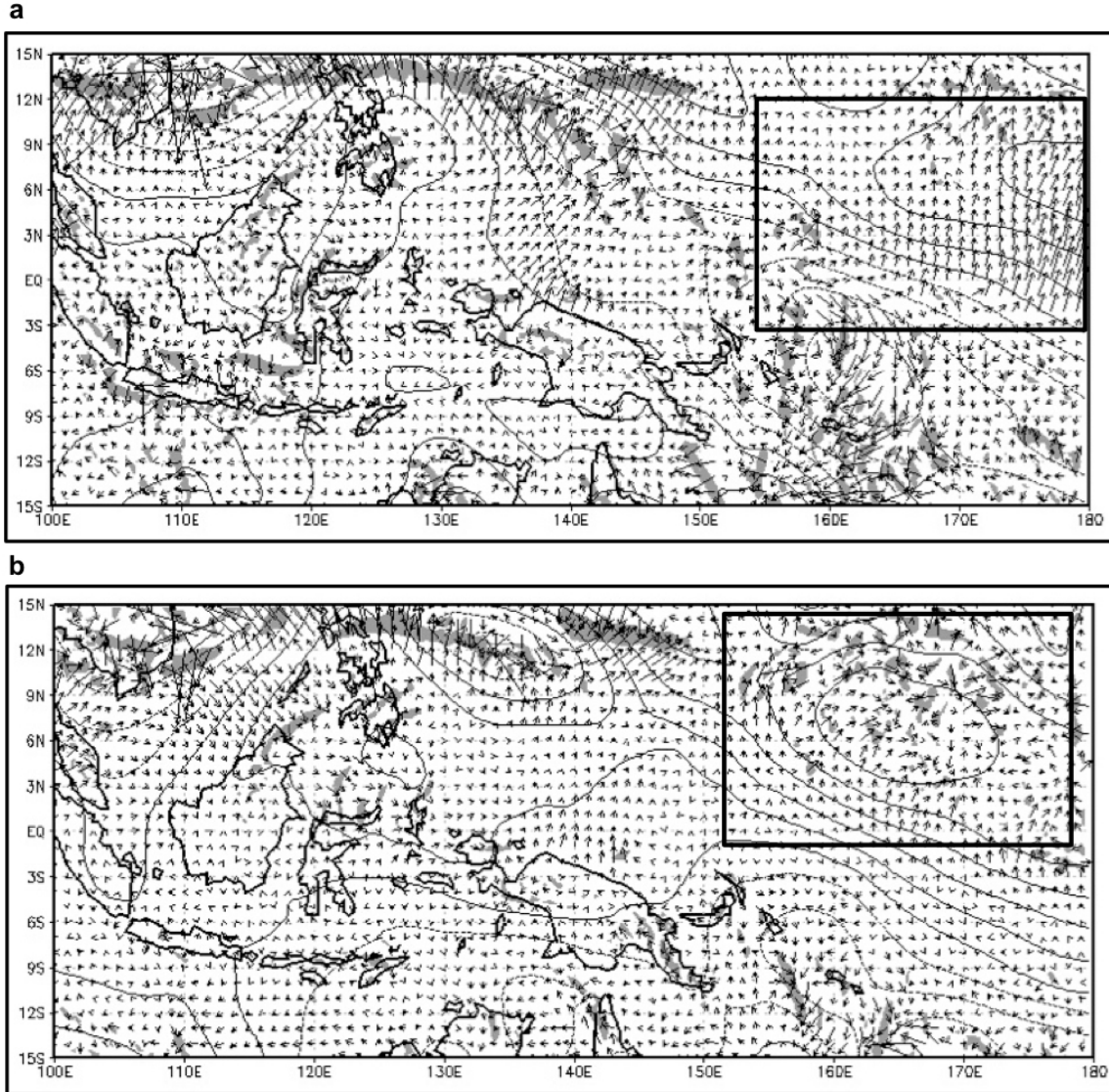


Figure 13. Wave-activity flux vectors ($\text{m}^2 \text{s}^{-2}$) as in Figure 5, but at (a) 1200 UTC 9 Sep and (b) 0000 UTC 10 Sep 2009, and the boxes highlight the cross-equatorial wave-activity fluxes at two times prior to the formation of the pre-TY Choi-Wan monsoon depression at $14^\circ\text{N}, 155^\circ\text{E}$.

Finally, cases in which airstream A had a primary role, the formation of MD₁ from July 2007 and four 2009 monsoon depressions, are listed in Table 4 and indicated in Figure 9 with a ● symbol. In general, these monsoon depressions formed in the western portion of the domain near the Philippines and tended to have a more circular shape (Table 4) rather than the preference for an elliptical shape as in the other scenarios. The example of airstream A from the 2009 data set (Figure 10) had a more northward path

(A₁) and a path that quickly turned to become equatorial westerlies (A₂). It was this airstream A₂, which was also joined by an airstream B, that provided the confluence with the trade easterlies and eventually the convergence that contributed to the spin-up of a western vorticity lobe and ultimately transitioned the confluent region into a cyclonic circulation.

Table 4. As in Table 2, except for monsoon depressions that formed from airstream A.

Airstream A			Southern Hemisphere		
Time (UTC)	MD Center		Anticyclone Center		Shape
	Lat	Lon	Lat	Lon	
1200 03 JUL 07	7°N	131°E	27°S	91°E	C
0000 11 JUL 09	16°N	128°E	28°S	90°E	E
0000 25 JUL 09	11°N	127°E	30°S	155°E	C
1200 24 AUG 09	11.5°N	121°E	25°S	161°E	C
1200 22 SEP 09	14°N	134°E	30°S	90°E	C

Monsoon depression formations from airstream A may also occur as in the July 2007 MD₁ case (Figure 3) in which the cross-equatorial flow penetrates to higher latitudes (around 10°N) (Figure 11d and Table 4). How far north the formation occurs depends on the strength of the cross-equatorial flow relative to the strength of pre-existing westerlies (Figure 11d) in the Northern Hemisphere (path A₁ in Figure 10). The monsoon depressions in Figure 11d formed from airstream A on 0000 UTC 25 July 2009 in a manner similar to the July 2007 MD₁ (Figures 5 and 7). The Southern Hemisphere anticyclone was centered at 30°S, 150°E at the time of formation (Table 4), with a cross-equatorial flow that still extended from the anticyclone to the monsoon depressions at 11°N. The backward trajectory ensemble and wave-activity flux convergence pattern for this case were comparable to the first July 2007 monsoon depressions (Figures 7 and 5), so they are not shown.

Two of the 44 monsoon depressions (5%) could not be categorized by the airstream from which they formed because they were already monsoon depressions when they entered the study domain (+ symbols in Figure 9). Since the formation of these circulations occurred east of 180°E, these monsoon depressions could not be classified as having originated from a particular airstream.

Of the 44 monsoon depressions during 2009 for which the conditions during formation could be established, 41 had cross-equatorial flow from the Southern Hemisphere with an airstream that could be matched with the new conceptual model in Figure 6. As demonstrated in Figure 10, more than one airstream may be present during formation. However, the airstream that was the primary contributor to the formation of each monsoon depression during 2009 has been summarized in Tables 1–4. The most common of these airstreams was airstream C, which appeared to be associated with the formation of the broad, elliptically shaped cyclonic circulations. In many of those cases, airstreams A and B were also present and contributed to the enhancement of the equatorial westerlies that subsequently interacted with a confluent region and thus contributed to monsoon depression formation.

F. SUMMARY AND CONCLUSIONS FOR MONSOON DEPRESSION FORMATION

In summary, the new conceptual model (Figure 6) of monsoon depression formation in the western North Pacific assigns a critical role to cross-equatorial flows that penetrate into the Northern (summer) Hemisphere. One type of cross-equatorial flow enhances the equatorial westerlies that become part of a confluent region with the trade easterlies and is hypothesized to increase the horizontal shear and curvature vorticity of the region. A second type of cross-equatorial flow more directly interacts with the eastern end of the confluent region to form an eastern cyclonic vorticity lobe and contributes to wrapping the flow into a broad cyclonic circulation.

Examination of a sample of 44 monsoon depression formations from April to December 2009 confirmed the role of these cross-equatorial flows in the new conceptual model of monsoon depression formation. However, another scenario of monsoon depression formation that involved airstream C_{*} was detected in the analysis of the 2009 sample. The fundamentals of the conceptual model still apply in this scenario, with the primary difference being that the confluent region is a wave in the easterly flow that appears to have been generated from an earlier cross-equatorial flow farther to the east. These cases have shown that the combination of a confluent region (or monsoon trough) and a southerly flow are frequently associated with monsoon depression formation. That is, all of the monsoon depressions for which formation conditions could be established in the 2009 sample had at least one of the airstreams A, B, or C (C_{*}) interacting with a confluent region. This qualitative analysis of the high-resolution ECMWF analyses was further confirmed by means of wave-activity flux calculations and backward trajectory ensembles.

Another inference from the 2009 cases is that the location of the Southern Hemisphere midlatitude anticyclones and cyclones dictate the cross-equatorial airstream that is involved in the formation of the observed western North Pacific monsoon depressions. An examination of how the amplitude and strength of these Southern Hemisphere anticyclones and cyclones changes the character of the cross-equatorial airstream is beyond the scope of this study. However, the backward trajectories from the two 2007 and the 2009 monsoon depression formations do establish the linkages to the cross-equatorial flows and the Southern Hemisphere anticyclone. Furthermore, Fukutomi and Yasunari (2005) form composites of the 200 hPa wind anomalies and use potential vorticity anomalies on the 315 K potential temperature surface to establish the connection between the amplifying midlatitude wave train and the 850 hPa southerly surges. Thus, the primary contribution for the operational forecasters from this study is that they should also monitor the Southern Hemisphere for evidence of southerly flow of the three types described, as previous guidance had only been to monitor the Northern Hemisphere easterlies and westerlies.

Wave-activity flux calculations indicate that kinetic energy is being propagated from the cross-equatorial flow initiated in the Southern Hemisphere and across the Equator into the region of the monsoon depression formation. Whether or not the cross-equatorial airstream then interacts with a Northern Hemisphere confluent region, which is the second necessary condition for this conceptual model, determines if a monsoon depression will form.

THIS PAGE INTENTIONALLY LEFT BLANK

III. STRUCTURE OF MONSOON DEPRESSIONS AT FORMATION TIME

A. INTRODUCTION

As used at the Joint Typhoon Warning Center (JTWC 1994; Lander 2004), a monsoon depression is a large cyclonic vortex with a diameter on the order of 1000 km that contains a loosely organized cluster of deep convection and has a light wind core surrounded by a band of stronger winds at large radii. Since deep convection associated with a monsoon depression is primarily along the perimeter of the circulation, a central core of convection as in a tropical cyclone is not present.

By contrast, the JTWC (1994) and Lander (1994, 1996) define a monsoon gyre to be a large cyclonic vortex on the order of 2500 km in diameter with a persistent band of deep convective clouds along the southern and eastern periphery of the circulation. Monsoon gyres occur about once every two years between July and September and may persist for two to three weeks (Lander 1994, 1996). Small tropical cyclones tend to form on the inside of the stronger winds at large radii in an monsoon gyre, and the monsoon gyre circulation may very rarely becomes a very large tropical cyclone.

Lander (2004) suggested two-thirds of western North Pacific monsoon depressions may transition to become a tropical cyclone. Therefore, the size of the monsoon depression is an important consideration because the large vortex structure of the monsoon depression must somehow be transformed to have a small inner core of intense winds and precipitation of a large tropical cyclone. By contrast, Chen et al. (1998, 2004) suggested that 70% of the western North Pacific tropical cyclones form in association with monsoon gyres.

As indicated in Chapter I.A., Typhoon Morakot (08W) moved slowly by Taiwan during 7–9 August 2009 and produced total rainfall accumulations approaching 3000 mm in the Central Mountain Range. Hong et al. (2010), Ge et al. (2010), and Nguyen and Chen (2011) attributed the formation of TY Morakot (2009) to a monsoon gyre. However, Beattie and Elsberry (2013) examined the 25 km European Center for

Medium-range Weather Forecasts (ECMWF) analyses plus satellite observations during 2009 and found no monsoon gyres that met the JTWC or Lander (1994, 1996) definition above. Specifically, the TY Morakot period did not have the fish-hook satellite cloud distribution or the kind of small tropical cyclone formations described by Lander. According to Beattie and Elsberry (2013) TY Morakot formed from one of 17 monsoon depressions that did spawn a tropical cyclone during 2009.

Thus, there are some differences of opinion about monsoon depressions and monsoon gyres in relation to tropical cyclone formation and as to the outer wind structure (or size) of the tropical cyclone that might result. Monsoon troughs and/or monsoon depressions are also considered to contribute to tropical cyclone formations in all other basins except the Atlantic, so it is important to better understand the horizontal structure of monsoon depressions. Therefore, the primary objective of this Chapter is to provide quantitative values for the structure of western North Pacific monsoon depressions, and thereby distinguish these monsoon depressions from monsoon gyres.

B. METHODOLOGY

This study of monsoon depression structure was conducted using the 44 monsoon depressions that formed between April and December 2009 (Beattie and Elsberry 2010, 2012). Two factors motivated the selection of the 2009 season. The most important factor was the availability of the high-resolution (0.25-degree latitude/longitude) ECMWF analyses as part of the YOTC archive. The ECMWF data assimilation system is considered to be the most advanced in the world and utilized a wide range of convectional and remote sensing observations. Note that Chen et al. (2004) utilized 2.5-degree latitude/longitude National Centers for Environmental Prediction (NCEP)/National Center for Atmospheric Research (NCAR) reanalyses that may only marginally resolve monsoon depression circulations of 1000 km diameter. The second motivating factor was the large number of monsoon depressions that formed during 2009. By contrast, very few monsoon depressions formed during the La Niña-type conditions that occurred during the 2008 and 2010 periods with ECMWF analyses.

Beattie and Elsberry (2012) describe the procedures for identifying the circulation as a monsoon depression at the time of formation. The monsoon depressions in this study formed between 110°E and 180° with the majority forming between 130°E and 170°E. The formation latitudes ranged from near the Equator to 19°N with some tendency for higher (lower) latitude formations to the west (east).

Circulation diameters at the time of monsoon depression formation, as defined earlier and in Beattie and Elsberry (2012), were first estimated using the 850 hPa wind, 850 hPa vorticity, and sea-level pressure fields from the ECMWF analyses. The wind diameter was defined using the centers of the wind maxima (e.g., Figure 14a and b), which was a minimum of 10 m s^{-1} in the meridional direction and $4\text{--}8 \text{ m s}^{-1}$ in the zonal direction. The reason for this asymmetry is that the trade easterlies and equatorial westerlies act to enhance the zonal flows on the northern and southern sides of the circulation. The uncertainty in estimating these 850 hPa wind diameters is $\pm 0.5^\circ$ latitude and longitude. The diameter based on vorticity was obtained by the horizontal extent of the 850 hPa vorticity maxima at the center of the circulation (not shown). The outermost closed isobar in sea-level pressure (not shown) was also used to define the diameter, except in four cases in which no closed isobars existed because the low pressure was aligned with the southerly flow into the monsoon depression.

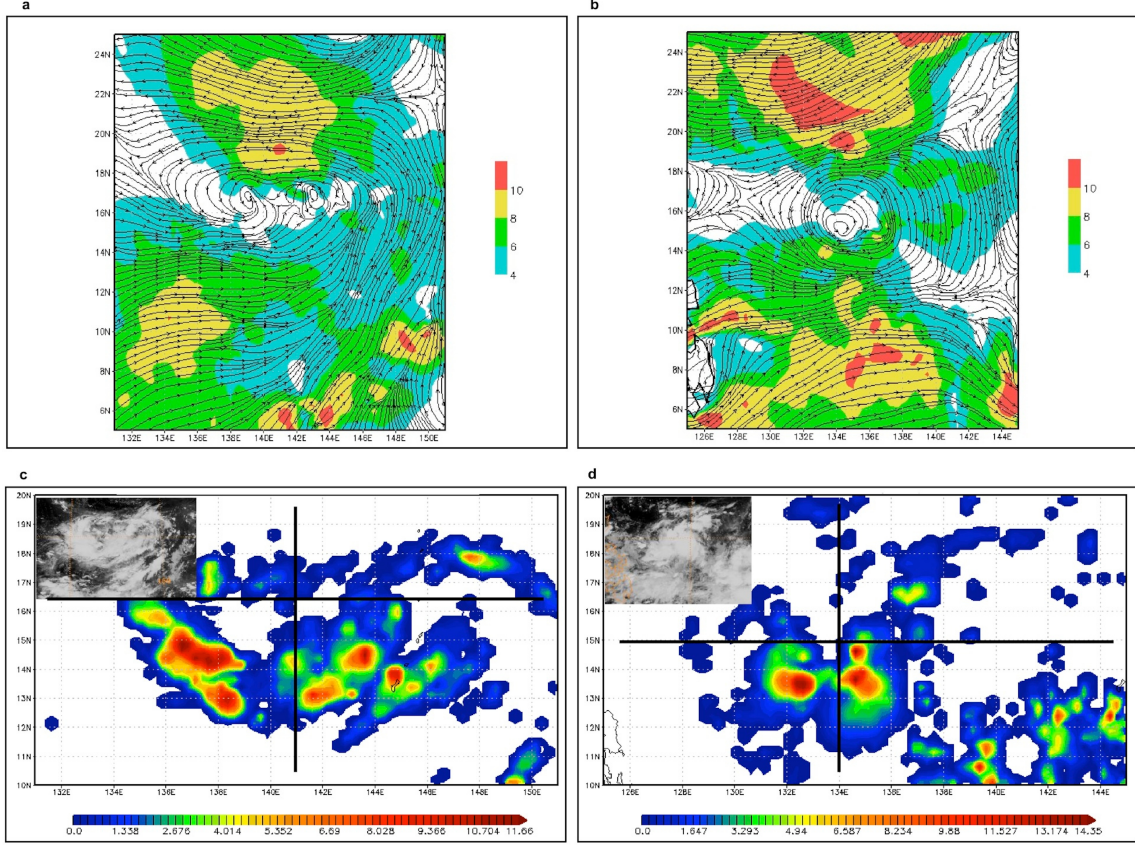


Figure 14. Streamlines and isotachs (shading scale to the right in units of m s^{-1}) at 850 hPa from the 0.25-degree ECMWF analysis at (a) 1800 UTC 22 August 2009 and (b) 1800 UTC 22 September 2009. The TRMM precipitation products with inset infrared satellite images that correspond to (c) Figure 14a and (d) Figure 14b. The solid lines represent the locations for the vertical cross sections in Figures 16 and 17.

Each monsoon depression had deep convection along the periphery with minimal deep convection at the center. It was also observed that the ring of convection was broader in the southwest and northeast quadrants of the circulation, especially when those regions of convection were embedded in the leading edge of the equatorial westerly flow converging with the trade easterlies prior to monsoon depression formation (Beattie and Elsberry 2012). The least reliable diameters ($\pm 1^\circ$ latitude and longitude) were estimated from infrared and water vapor satellite imagery (from MTSAT 1R, except for 16–26 November 2009 when Fen-Yung 2C was used). A more reliable diameter based on the outer edge of the precipitation maximum was estimated from the three-hourly 0.25-

degree TRMM precipitation rates (Figures 14c and d). Finally, QuikSCAT surface winds were examined when available at the appropriate times.

C. STRUCTURAL CHARACTERISTICS

1. Horizontal Structure

The special characteristics of the monsoon depression are the higher winds and deep convection that are wrapped around a broad region of minimum pressure and minimum cloudiness. Harr and Elsberry (1996) described the onset of the monsoon depression as equatorial westerlies extending eastward on the southern side and trade easterlies extending westward on the northern side. Beattie and Elsberry (2012) have expanded that description by adding any combination of three airstreams from the Southern Hemisphere that contributed to the two monsoon depression in early July 2007 and the 44 monsoon depression formations in the western North Pacific during 2009 by either enhancing the equatorial westerlies or by a more direct cross-equatorial flow on the eastern side that enhanced the convergence with the trade easterlies. Harr and Elsberry (1996) also described MCSs that developed and decayed within the equatorial westerlies and within the trade easterlies, which may be analogous to the individual TRMM precipitation maxima in Figures 14c and d.

A simple conceptual model of early stage monsoon depression structure is that the net latent heating in the columns containing the deep convection and stratiform clouds of the MCSs leads to an enhancement of the radial pressure gradient, which leads to a local maximum in tangential winds outside of the region of maximum precipitation. In both the latitudinal and longitudinal directions for the monsoon depressions in the 2009 season (Figure 15), the pressure diameters are among the smallest, while the wind diameters are slightly larger, which is consistent with the conceptual model of Harr and Elsberry (1996). The vorticity diameters are consistently smaller than the wind diameters, which is expected as the vorticity is calculated from the ECMWF wind analyses.

The outliers in Figure 15 are the cloud diameters estimated from the satellite imagery. These diameters are approximately 3–4 degrees larger than the TRMM precipitation diameters. Although the insets in Figure 14c and d are not of the same scale

as the TRMM product, in these and other cases the cirrus outflows from the deep convection lead to larger cloud diameters than the precipitation diameters. To make the measurement of diameters presented below more objective, a well-defined process to first determine the monsoon depression centers and then a method to manage the asymmetries in each circulation would need to be developed. Once this process is established, there would be across the board standardization in determining the diameters of monsoon depressions.

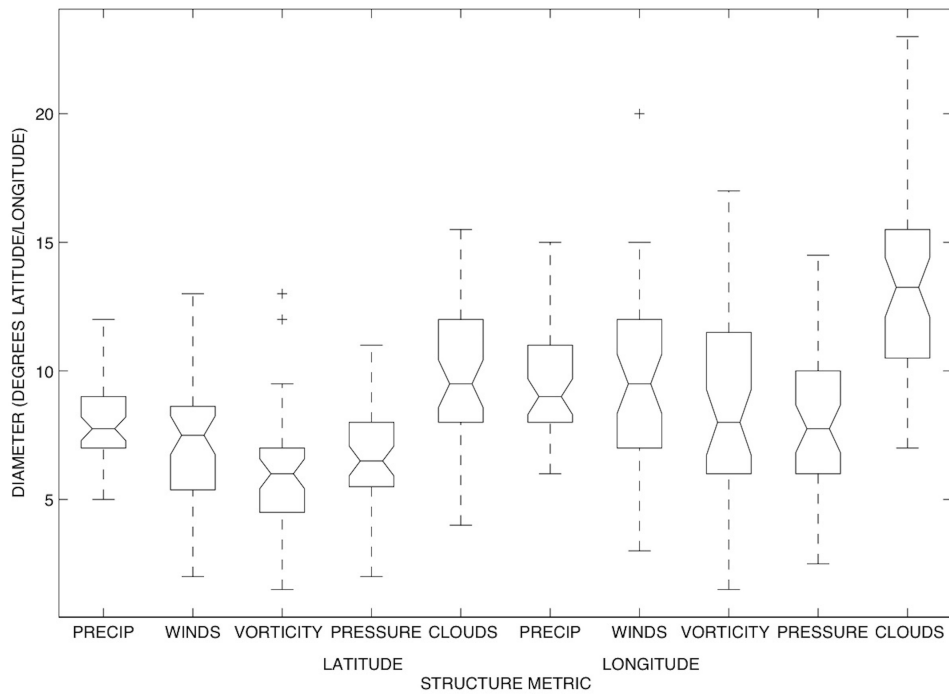


Figure 15. Box plots of precipitation, winds, vorticity, pressure and cloud diameters (degrees) in latitude (left five boxes) and longitude (right five boxes) for the 44 monsoon depressions during 2009. The horizontal line in the narrow portion of each box is the median value, the top and bottom of each box are the upper and lower quartile values (75^{th} and 25^{th} percentile, respectively), the whiskers extend to the most extreme data points not considered outliers, and outliers are plotted individually as crosses.

The majority (80%) of the monsoon depressions were elliptical (e.g., Figure 14a) rather than circular (e.g., Figure 14b) for all variables. The average diameters of the

monsoon depressions based on the most reliable 850 hPa winds for the elliptical monsoon depressions were 7.3 degrees latitude (812 km) and 9.9 degrees longitude (1098 km). The corresponding standard deviations were of the order of 2.6 degrees latitude (288 km) and 3.5 degrees longitude (387 km). Thus, the latitudinal diameters are considerably smaller than the approximate 1000 km in the JTWC definition, and the longitudinal diameters are slightly larger. Incidentally, the circular monsoon depressions had diameters of approximately 750 km.

Another measure demonstrating the ellipticity for the 850 hPa winds is the ratio of the latitudinal to the longitudinal diameter. Including only those monsoon depression classified as non-circular, the mean and standard deviation are 0.69 and 0.14, respectively. The importance of these large diameters and ellipticity for tropical cyclone formation is to determine where within such large monsoon depressions the tropical cyclone inner core of, say, 100 km diameter will form, and how the monsoon depression structure then contributes to the outer vortex wind structure of the new tropical cyclone.

2. Vertical Structure

The primary purpose of illustrating the vertical structure is to emphasize the warm-core structure of monsoon depressions rather than the cold-core structure of a wave in the easterlies, a subtropical cyclone, or other initial baroclinic pre-tropical cyclone seedlings. Although a composite of multiple monsoon depressions would demonstrate this warm-core structure, the two cases in Figure 14 of elliptically and circularly shaped monsoon depressions at the time of formation were selected to illustrate the spatial variability that would be obscured by compositing.

Zonal and meridional cross sections of wind and relative vorticity (10^{-4} s^{-1}) of the large elliptically shaped monsoon depression in Figure 14a are given in Figure 16. In the zonal cross section (Figure 16a), a narrow and vertically oriented tower of maximum southerly winds near 145°E extends above 300 hPa, which may be associated with the eastern circulation center near 143°E in Figure 14a. About two-thirds of the monsoon depressions had similar vorticity maxima that extended above 300 hPa, and the remaining cases did not extend above 450 hPa. A weaker northerly wind maximum between 136°E

and 138°E is primarily confined to the mid-troposphere and may be associated with the western circulation center near 140°E in Figure 14a. In the meridional cross section (Figure 16b), equatorial westerlies near 12°N in the lower troposphere reverse to become easterlies aloft. In this relatively high-latitude monsoon depression, the easterly trade wind maximum exceeds 10 m s^{-1} and has a westerly wind maximum of 5 m s^{-1} at 200 hPa . Therefore, a cyclonic vorticity band is analyzed on the equatorward side of the easterlies centered near 19°N (Figure 16b). Note that although the strongest lower troposphere winds are on the northern side, the maximum cloudiness is on the southern side (Figure 14c) associated with the warm, moist air of the equatorial westerlies.

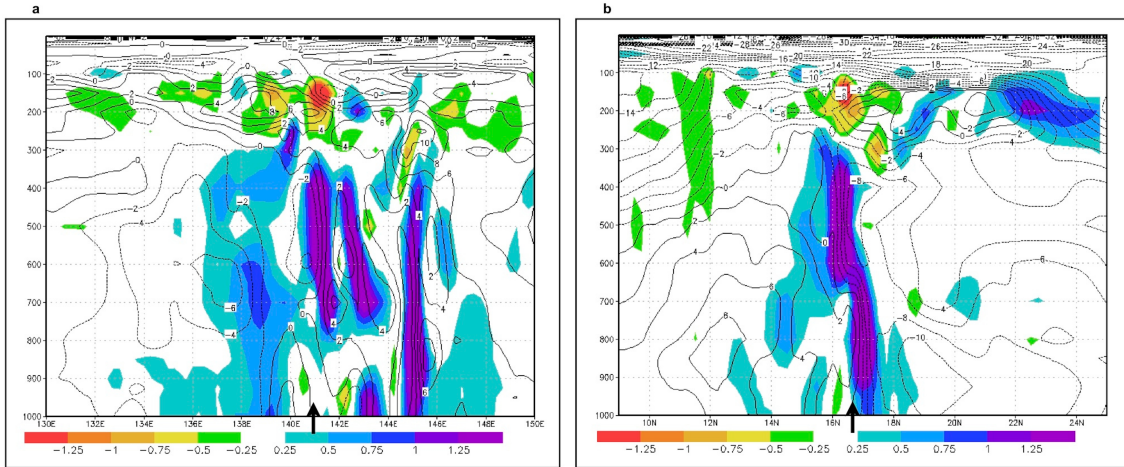


Figure 16. Vertical cross-sections along (a) 16.5°N and (b) 141°E of meridional and zonal winds (contours, m s^{-1}) and relative vorticity (shaded, 10^{-4} s^{-1}) from the 0.25-degree ECMWF analysis at 1800 UTC 22 August 2009. Arrowhead represents the center of the monsoon depression.

Similar cross-sections for the smaller, more circular monsoon depression in Figure 14b are given in Figure 17. In the meridional cross section (Figure 17b), the equatorial westerlies have maximum speeds exceeding 14 m s^{-1} in the middle to the lower troposphere that extend above 200 hPa before reversing to become strong easterlies. A broad equatorward-tilted region of cyclonic vorticity that extends from the surface to 200 hPa exists on the equatorward side. While the easterlies also extend to 300 hPa before reversing to westerlies, only a shallow layer of cyclonic vorticity is analyzed in connection with the easterlies. At least in that northern quadrant, it appears that the vortex

is only defined to be about 500 hPa. As in the elliptical case, the deep convection (Figure 14d) was associated with the equatorial westerlies and not with the trade easterlies.

At least as illustrated in these high-resolution ECMWF analyses, the expected background warm-core monsoon flow of equatorial westerlies (trade easterlies) reversing to become easterlies (westerlies) aloft was generally present in each of the 44 cases. However, lower tropospheric circulations appeared to be extended vertically in association with locally tall and narrow vorticity maxima. Important variability also existed in the level at which the maximum winds were located. Northerly and southerly wind maxima with an average magnitude of 6 m s^{-1} on the western and eastern sides of the monsoon depression were typically in the mid-troposphere and did not always extend down to 850 hPa. The easterly and westerly maxima, with average values of 10.8 m s^{-1} and 8.5 m s^{-1} , respectively, were distributed over a range of levels but always had a relative maximum at 850 hPa.

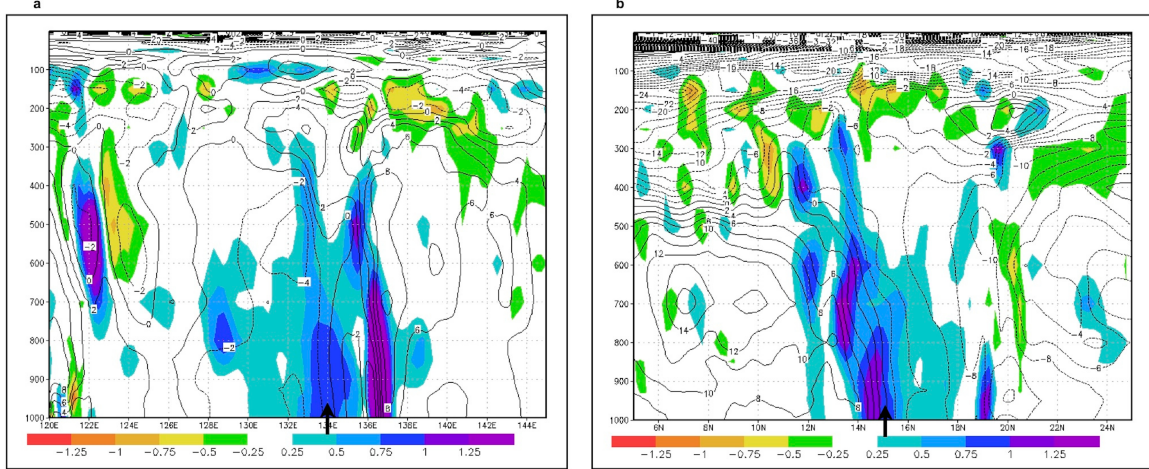


Figure 17. Winds and relative vorticity as in Figure 16, except at 1800 UTC 22 September 2009 along (a) 15°N and (b) 134°E .

Similar horizontal and vertical variability on sub-synoptic scales were present in the wind and vorticity fields for each of the 44 cases. While this variability may exist due to transient convective structures related to the ECMWF physics, it is also plausible that similar variability may be associated with the TRMM precipitation maxima as in Figures

14c and d. If real, the locations and magnitudes of those sub-synoptic features will be important for forecasting “weather” associated with monsoon depressions and may play a role in determining whether and how a tropical cyclone may be spawned.

D. DISCUSSION OF MONSOON DEPRESSION STRUCTURE

The primary objective of this portion of the study has been to provide a more quantitative description of the structure of monsoon depressions in the western North Pacific based on high-resolution ECMWF analyses, satellite imagery, TRMM precipitation product, and QuikSCAT surface winds. The ECMWF analyses provided a consistent depiction of a large majority of these monsoon depressions as elongated, elliptical, 850 hPa wind circulations with maximum winds at outer radii. When available, the QuikSCAT surface wind observations confirmed this elongated structure of stronger winds at larger radii and weak surface winds near the center.

Based on the 850 hPa winds, the average latitudinal and longitudinal diameters of the elliptical (80% of the 44) monsoon depressions were 812 and 1098 km, respectively, with standard deviations of 288 and 387 km. The latitudinal-to-longitudinal ellipticity factor of $0.69 \pm 0.14^\circ$ emphasizes the noncircular structure of these cases. This quantitative structure information augments the less specific definitions of “on the order of 1000 km” by the JTWC (1994) and Lander (2004). Furthermore, these frequently occurring monsoon depressions during 2009 are distinctly different from monsoon gyres that have diameters near 2500 km.

As expected for a warm-core circulation, the vertical structure of the monsoon depressions in the ECMWF analyses had equatorial westerlies and trade easterlies in the lower troposphere reversing to become easterlies and westerlies, respectively, in the upper troposphere. However, considerable variability existed in the azimuthal direction as to the level at which the maximum winds were analyzed and in the vertical extent of associated vorticity features.

The circular monsoon depressions, which have an average diameter of 750 km, are smaller than the elliptical monsoon depressions and contain only one vorticity maximum. Therefore, with persistent inward-directed wave-activity flux, as will be

discussed in Chapter IV, the circular monsoon depressions should more easily transition to a pre-tropical cyclone seedling.

Seventeen monsoon depressions during 2009 spawned a tropical cyclone, including TY Katsana (16W) from the second, circular monsoon depression in Figures 14b and d. Whereas Chen et al. (1998, 2004) had concluded that monsoon gyres have a substantial role in western North Pacific tropical cyclone formation, no monsoon gyres as defined by JTWC (1994) and Lander (1994, 1996, 2004) were observed during this period. Specifically, the large-scale circulation in conjunction with TY Morakot as described by Hong et al. (2010), Ge et al. (2010), and Nguyen and Chen (2011) did not meet those monsoon gyre conditions. A possible explanation for the Chen et al. (2004) conclusion was that they used coarse-resolution (2.5-degree latitude/longitude) reanalyses and evidently had not confirmed the structure based on satellite imagery and specifically with the TRMM precipitation product that was an essential data source for this study. Furthermore, they included some early cases before extensive satellite-based infrared and water vapor atmospheric motion vectors were available for use in advanced data assimilation systems that have greatly improved tropical analyses. How these 17 tropical cyclones formed within the 44 monsoon depressions during 2009 will be examined in Chapter IV.

THIS PAGE INTENTIONALLY LEFT BLANK

IV. MONSOON DEPRESSIONS AS PRE-TROPICAL CYCLONE SEEDLINGS

A. INTRODUCTION

As documented in Chapter III, the average latitudinal and longitudinal diameters of the elliptical monsoon depressions during 2009 were 812 km and 1098 km, respectively. During 2009, 17 of the 44 monsoon depressions transitioned to a tropical cyclone. The focus in this chapter is on how a monsoon depression, with such an elliptical horizontal structure that contains a loosely organized cluster of deep convection and a light wind core surrounded by a band of stronger winds at large radii, may be transitioned into a pre-tropical cyclone seedling and eventually a tropical cyclone with a small inner core of intense winds and heavy precipitation. Since such a transition of a monsoon depression into a tropical cyclone will already have gale-force winds at a large radius, the tropical cyclone size (defined by the radius of gale-force winds) will be larger than for tropical cyclones formed from other pre-tropical cyclone seedlings (e.g., equatorial waves). The larger MD-related tropical cyclones thus have a large beta-effect propagation (e.g., Fiorino and Elsberry 1989) toward the north that can be a major contribution to the total motion if the steering flow is relatively small. The larger size is also an important consideration for warnings of when gale-force winds will arrive.

While a number of studies (e.g., Lander 2004; Chen et al. 1998, 2004; Ritchie and Holland 1999) have made estimates of the numbers of western North Pacific tropical cyclones formed from monsoon depressions, very few case studies (e.g., Lander 1994; Harr et al. 1996) have addressed the physical processes that lead to a transition from a monsoon depression to a tropical cyclone, in part due to the confusion about the distinction between a monsoon gyre and monsoon depression. The monsoon depression has several characteristics that may make it a favorable environment for a tropical cyclone to develop. That is, they are located in regions of sufficiently high sea-surface temperatures that provide a moist environment, the vertical wind shear is generally small, and the broad region of cyclonic vorticity is sufficient so that even the low-latitude circulations may transition to a tropical cyclone (Gray 1968, 1975).

Harr et al. (1996) described the transitional processes with the pre-TY Robyn monsoon depression during TCM-93. Their analysis indicated that when deep convection occurred near the circulation center the associated vorticity at 850 hPa became more concentrated and the convection in the outer regions became organized as a principle band, which quickly transitioned the pre-TY Robyn circulation into a tropical storm. Chang et al. (2010) observed surges (greater than 8.5 m s^{-1}) in the easterly trades and/or equatorial westerlies, which contributed to 7% of tropical cyclone formations in the western North Pacific over a 20-year period. Although these studies did not explicitly discuss the monsoon depression, similar favorable low-level influences in a monsoon environment (e.g., monsoon trough, monsoon gyre) that may lead to tropical cyclone formation were discussed. It is hypothesized that continued forcing, which is represented in this study by the wave-activity flux, is an important element in the transition to a pre-tropical seedling circulation as the wave-activity flux convergence aids in the scale constriction of the monsoon depression vorticity maximum and its associated convection to a tropical cyclone.

As was the approach in Chapter II, the two July 2007 monsoon depression formation cases will first be examined to explore the various external factors that may have contributed to the transition of MD₂ to a tropical cyclone. The MD₁ case will also be examined to determine if these various external factors may explain why MD₁ did not become a pre-tropical cyclone seedling and thus not transition to a tropical cyclone. The external forcing hypothesis will then be the basis for examining the 44 monsoon depressions that occurred during the 2009 study period—for both those that became pre-tropical cyclone seedlings and those that did not.

B. METHODOLOGY

The same data sources used to examine the formation of monsoon depressions in Chapter II will be used for the study of monsoon depressions transition to pre-tropical cyclone seedlings. The primary data sources are the ECMWF 1-degree analyses (2007 cases), ECMWF high-resolution (0.25-degree) YOTC analyses (2009 cases), the MTSAT-1R infrared satellite imagery, and the TRMM precipitation product. The

ECMWF wind analyses will be used to determine wind maxima as well as to calculate the vorticity fields and wave-activity fluxes. Further discussion of the wave-activity flux is in the Appendix.

The study period of the monsoon depressions analyzed for transition is from the time of monsoon depression formation, as defined in Chapter II, to the issuance of the last Tropical Cyclone Formation Alert (TCFA; likelihood of tropical cyclone formation within 24 hours). The monsoon depression circulation should be considered a pre-tropical cyclone seedling at the time of the TCFA, as this is considered to be the time at which the internal processes begin to dominate completing the transition to tropical cyclone, especially since all transitioning monsoon depressions have convection at, or near, the center by the time of the TCFA. If a TCFA was not issued, the discussion will be continued through the time of tropical cyclone formation, which for this study is considered to be the time of the first JTWC warning.

The methodology for the study of the 17 tropical cyclones that formed from monsoon depressions during 2009 will be similar. However, the high-resolution (0.25-degreee latitude/longitude) ECMWF 2009 YOTC analyses will be used as in Chapters II and III.

C. SYNOPTIC ANALYSIS OF THE JULY 2007 MONSOON DEPRESSIONS

As described in Chapter II, two monsoon depressions, labeled as MD₁ and MD₂, formed in the observation area during early July 2007. Although these two monsoon depressions formed in a similar fashion, only MD₂ transitioned to a tropical cyclone, while MD₁ remained a monsoon depression and began to dissipate as the circulation began to interact with the Philippines. The objective of the synoptic analysis in this section is to examine the evolution in the low-level circulation of monsoon depression MD₂ as transitional to a pre-tropical cyclone circulation (subsection 1) and then compare the evolution of the low-level circulation in monsoon depression MD₁ to describe the differences that might explain the lack of transition (subsection 2).

Since MD₁ formed at 1200 UTC 3 July, the study period is narrowed from just after the formation and transition times of MD₂ (0600 UTC 6 July to 1200 UTC 7 July,

respectively; Figures 18a-f). Specifically, this period will be used to examine the differences between a transitioning and non-transitioning monsoon depression as MD₁ began to dissipate midway through this period. Recall from Chapter II that MD₁ was a circular monsoon depression that formed in the western portion of the domain from airstream A, which tends to lead to high latitude monsoon depression formation (Table 4). By contrast, MD₂ was an elliptical monsoon depression that formed in the central portion of the domain from airstream C, which tends to lead to a low latitude monsoon depression formation (Table 1).

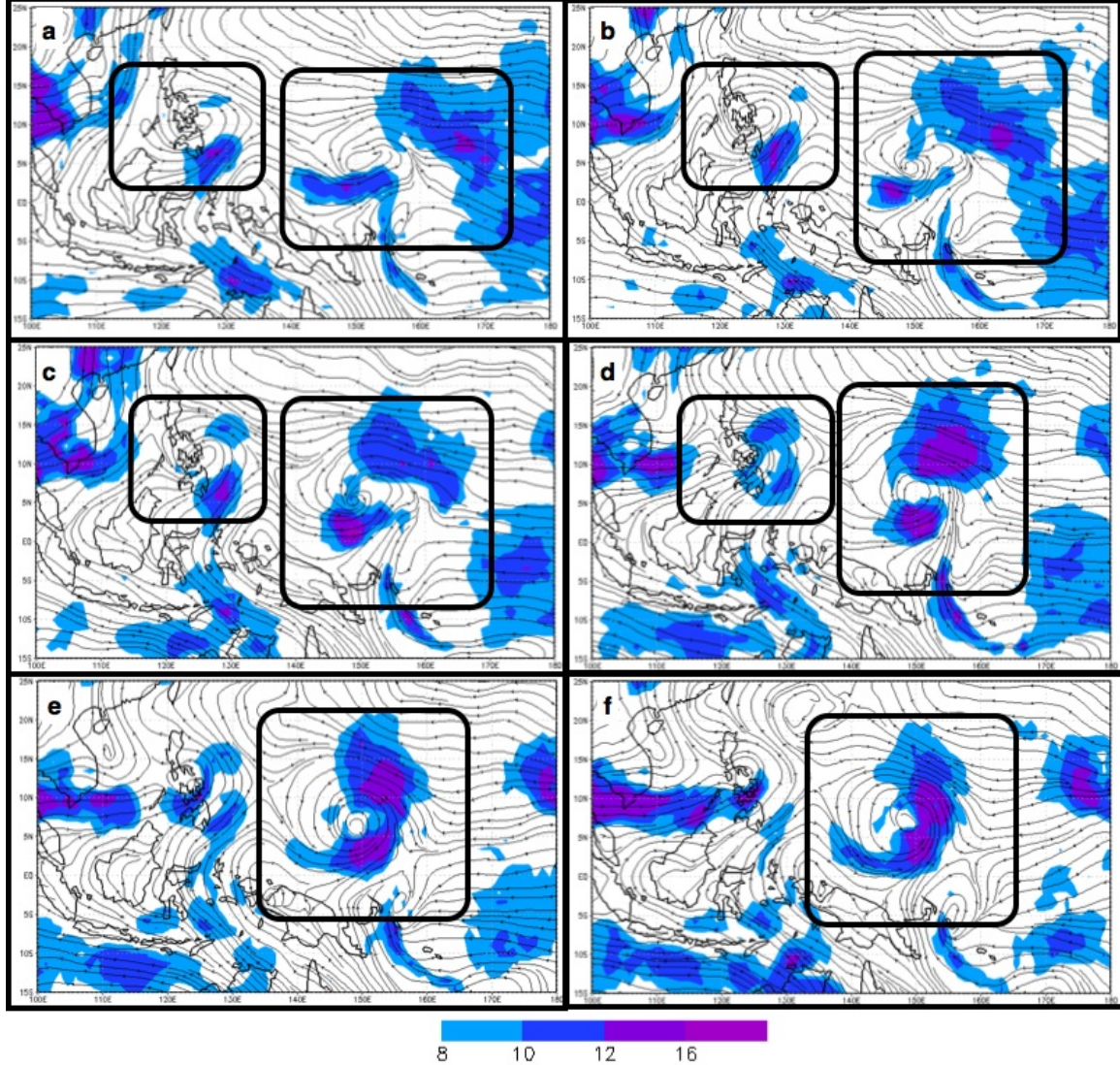


Figure 18. ECMWF 850 hPa streamlines and wind speed (shaded contours $> 8 \text{ m s}^{-1}$; scale at bottom) at (a) 0600 UTC 6 July; (b) 1200 UTC 6 July; (c) 1800 UTC 6 July; (d) 0000 UTC 7 July; (e) 0600 UTC 7 July; and (f) 1200 UTC 7 July (time of the first JTWC warning). The small boxes highlight MD₁ and the large boxes highlight MD₂. The region of increased westerlies along airstream B into the southwestern quadrant of MD₂ and the easterlies into the northeastern quadrant of MD₂ are included in the large boxes.

1. Transition of MD₂ to a Pre-tropical Cyclone Seedling

This observational study begins at 0600 UTC 6 July (Figure 18a), which is 12 hours after the formation of MD₂. The characteristics of the circulation still closely

resembled those of a monsoon depression (see Chapter II.B) as it was still an elliptical circulation that had two distinct vorticity maxima at the eastern and western ends of the circulation with approximately equal magnitude (not shown). The key factor in the formation of MD₂ was the primary wave-activity flux from the Southern Hemisphere, which was directed toward the entire southern portion of the MD₂ circulation (Figure 5d) and this wave-activity flux continues at 0600 UTC 6 July (not shown).

By 1200 UTC 6 July (approximate time of tropical oceanic convective maximum at this longitude), the wind maxima in the trade easterlies and equatorial westerlies approaching the MD₂ circulation have increased to over 12 m s^{-1} (Figure 18b). The convection (Figure 19a) is stronger near the western vorticity maximum (Figure 20a) than the eastern vorticity maximum, and the TRMM 3-h precipitation maximum (Figure 19b) is also associated with the western vorticity maximum. While this western vorticity maximum in MD₂ has an associated closed circulation at 850 hPa, the eastern vorticity maximum is associated with an open-wave circulation (Figure 20a) with a maximum of easterlies approaching from the east. Note that the cross-equatorial flow appears to be strongly interacting with a westerly monsoon flow (airstream B) in the southern region of MD₂, but less strongly with a tradewind easterly flow in the region of the eastern vorticity maximum. This strong interaction between the cross-equatorial flow and westerly wind maximum is confirmed by the wave-activity flux (Figure 20b). Note the broad region of northward-directed flux vectors along the Equator between 143°E and 155°E , which contributes to the convergence of wave-activity flux in the region of the western vorticity maximum. By contrast, the wave-activity flux convergence in the region of the eastern vorticity maximum is relatively small at this time.

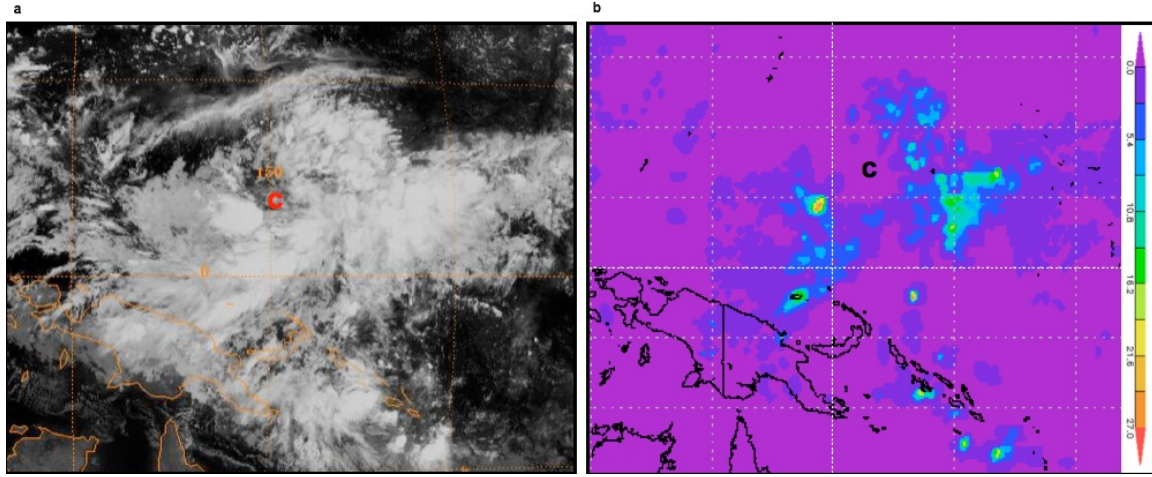


Figure 19. (a) MTSAT-1R infrared image at 1200 UTC 6 July 2007 illustrating the pre-TY Man-Yi monsoon depression MD₂ with western and eastern convective regions relative to a convection-free center near 5°N, 150°E. (b) Corresponding TRMM 3B42 precipitation (mm/hour; shading scale on right) with two regions of precipitation corresponding to the western and eastern convective regions in panel (a). The letter C corresponds to the estimated center of the cyclonic circulation.

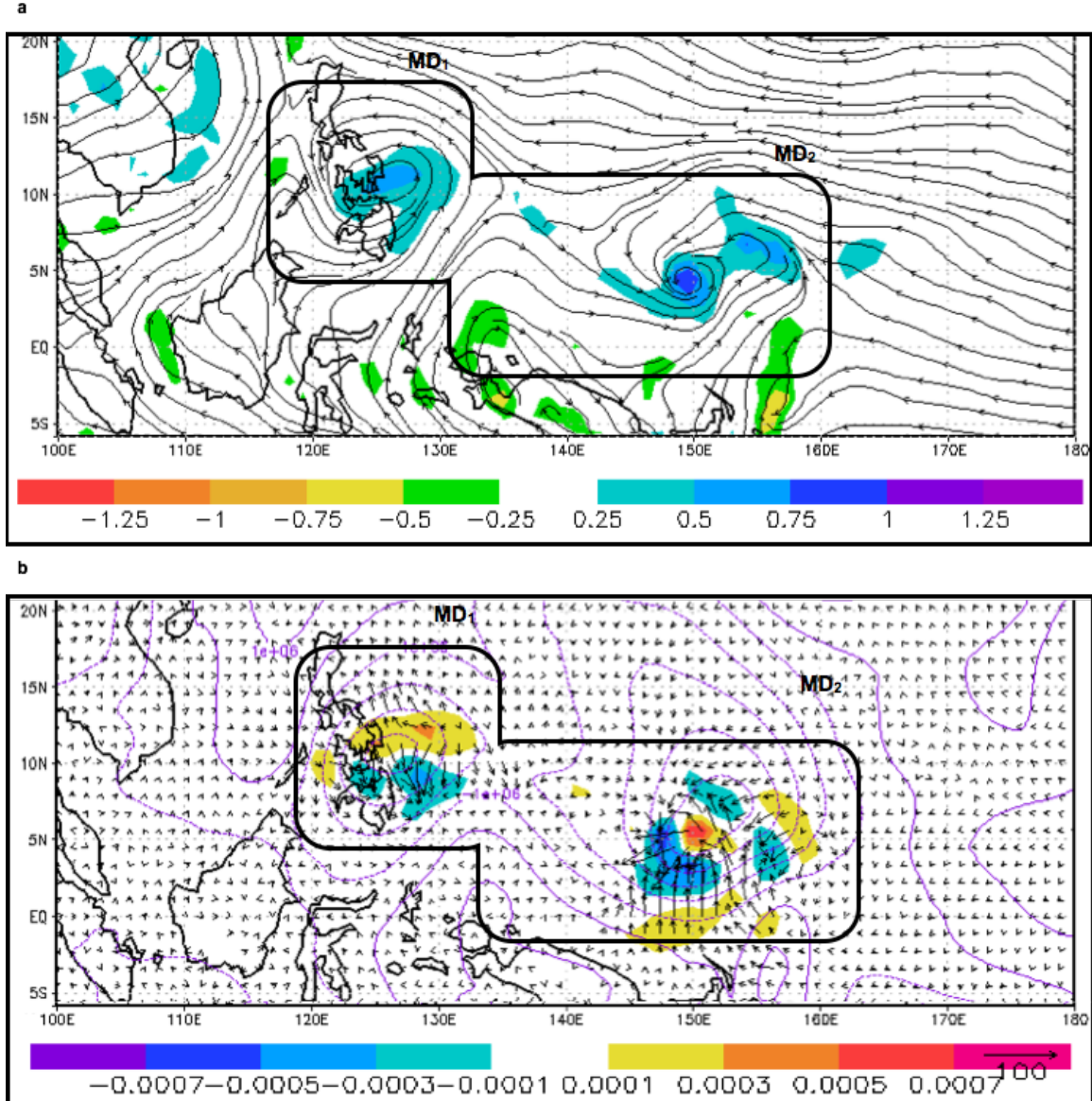


Figure 20. (a) Streamlines and relative vorticity as in Figure 2, except at 1200 UTC 6 July 2007. Note the cyclonic circulation and relative vorticity maximum are associated with the MD₂ western convective region and precipitation region in Figure 19. (b) Corresponding 850 hPa wave-activity flux vectors (units of $\text{m}^2 \text{s}^{-2}$), the streamfunction anomaly (contours), and wave-activity flux divergence (shading scale at the bottom; units of m s^{-2}) as in Figure 5.

The 0000 UTC 7 July IR image of MD₂ (Figure 21a) has an overall convective pattern that is still representative of a monsoon depression with a width of 10 degrees longitude and a relatively cloud-free center between the two organized convective regions. The western convective region has more evidence of cyclonic spin-up, and the

magnitude of the westerly wind maximum has increased with a region of winds higher than 16 m s^{-1} (Figure 18d). However, the circulation is now more circular than elliptical (Figure 22a). Only two hours later the JTWC issued a TCFA as the circulation characteristics in the region of the MD₂ western vorticity maximum have become more like a pre-tropical cyclone seedling. The TRMM 3 h precipitation at 0000 UTC 7 July (Figure 21b) also indicated two separate precipitation regions with the western region having more evidence of an organized circulation. Note also that the ECMWF 850 hPa wind analysis (Figure 22a) has little remaining evidence of the eastern vorticity maximum.

The easterly wind maximum noted in Figure 18d also has a wave-activity flux associated with it (Figure 22b) that is contributing to the wave-activity flux convergence near the western vorticity maximum. This wave-activity flux is downstream (to the west) of the easterly wave axis, and thus reflects the easterly wave is dispersive. Although this wave-activity flux convergence associated with the wave in the easterly flow is secondary to the wave-activity flux convergence associated with the cross-equatorial airstream C, both sets of wave-activity flux vectors are contributing to an amplification of the vorticity maximum that two hours later becomes the pre-tropical cyclone seedling. Indeed, the development of the large 850 hPa cyclonic circulation in Figure 22a is consistent with the presence of this inward-directed wave-activity flux vectors on the northern side (5°N – 10°N , 145°E – 155°E) in addition to the cross-equatorial wave-activity flux vectors on the southern side. While it is important that this circulation was in a monsoon environment that had other favorable factors for tropical cyclone formation, it is asserted that the wave-activity flux convergence was the critical factor that led to the spin-up of cyclonic vorticity in the pre-TY Man-Yi circulation, which the JTWC indicated in the TCFA at 0200 UTC 7 July to be at 4.5°N , 148.1°E .

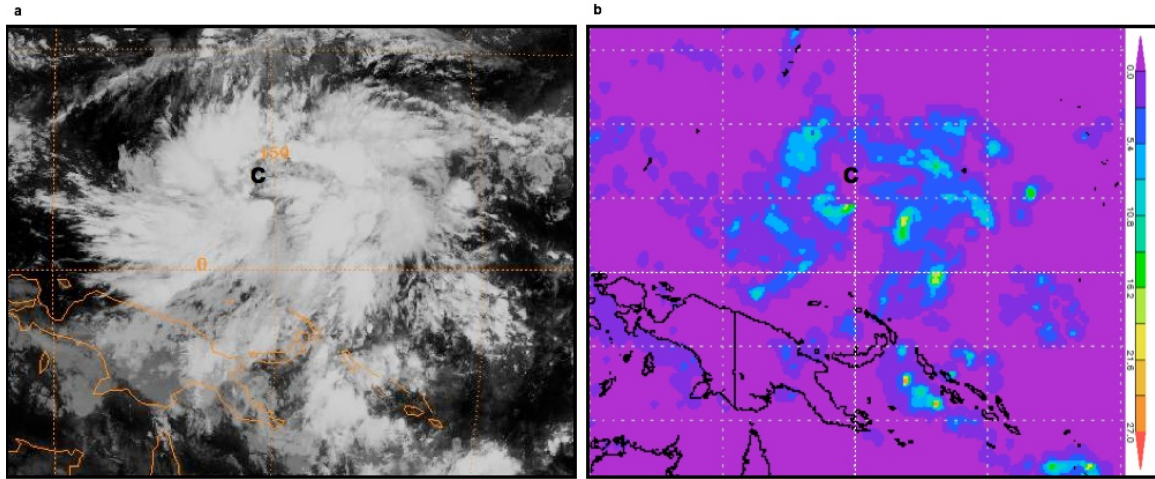


Figure 21. As in Figure 19 except at 0000 UTC 7 July with (a) MTSAT-1R IR image of MD₂ indicating continued convective organization in the western portion of the circulation. (b) TRMM 3B42 precipitation (mm/hour) with two regions of precipitation corresponding to the western and eastern convective regions in panel (a).

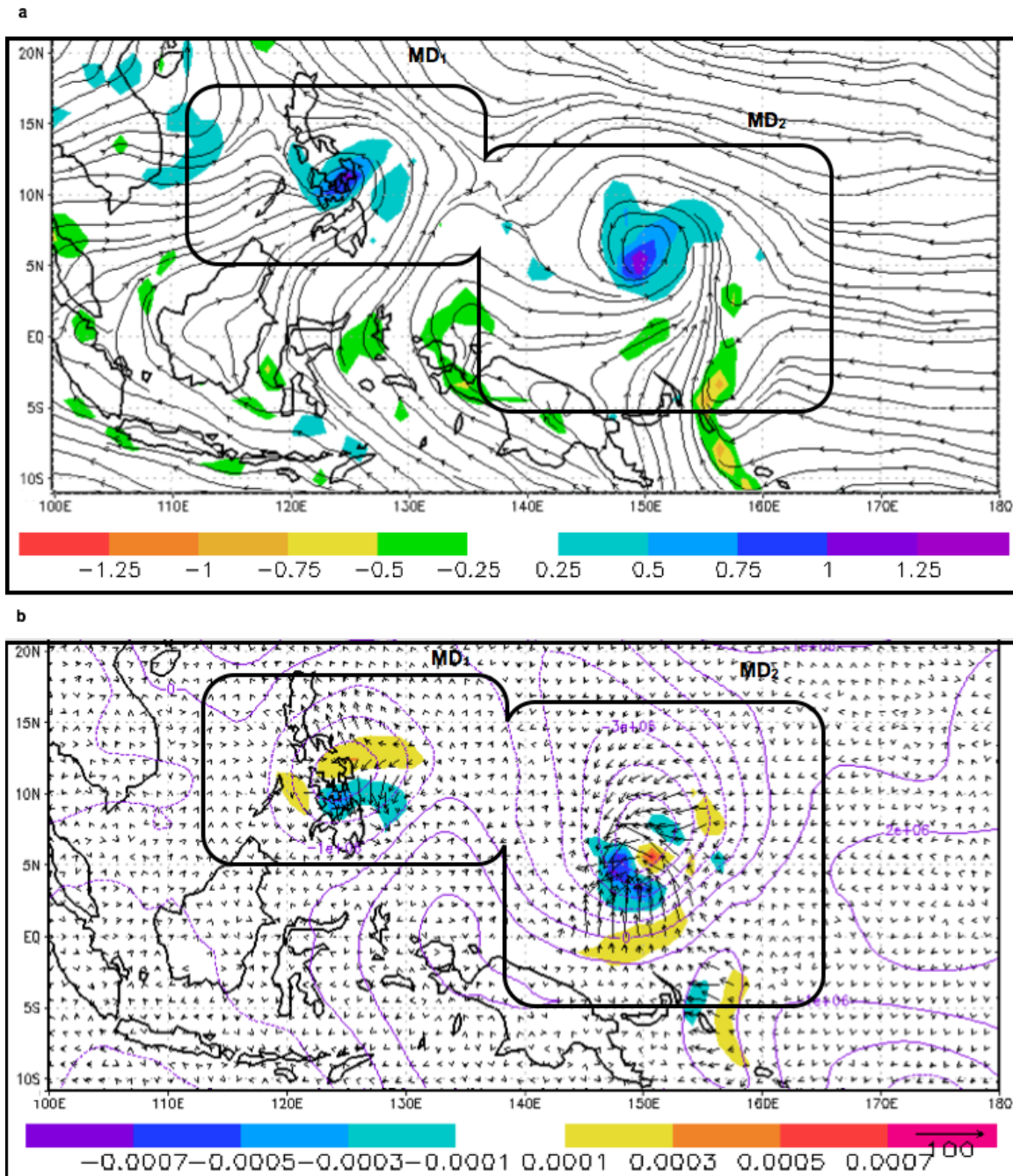


Figure 22. As in Figure 20 except at 0000 UTC 7 July 2007 with (a) streamlines and relative vorticity with a broad cyclonic circulation related to the western convective region of MD₂ in Figure 21a. (b) Wave-activity flux convergence continues in the region of the MD₂ cyclonic vorticity maximum.

At 1200 UTC 7 July the JTWC issued its first warning of a Tropical Depression (TD 04W) since a central convective region had developed within the broad region of convection (Figure 23a) that had evolved from the western vorticity maximum region of MD₂. The central convective region has a corresponding TRMM 3 h precipitation maximum (Figure 23b) in addition to the surrounding precipitation maxima within the outer convective bands in the infrared satellite image (Figure 23a). The ECMWF 850 hPa vorticity maximum was displaced to the east of the center of the overall circulation due to the stronger winds on the eastern side (Figure 18f). The corresponding wave-activity flux at 1200 UTC 7 July (Figure 24b) from the south and east continued to result in a wave-activity flux convergence in the central region of the TD 04W circulation that may be expected to contribute to development of Tropical Storm (TS) Man-Yi.

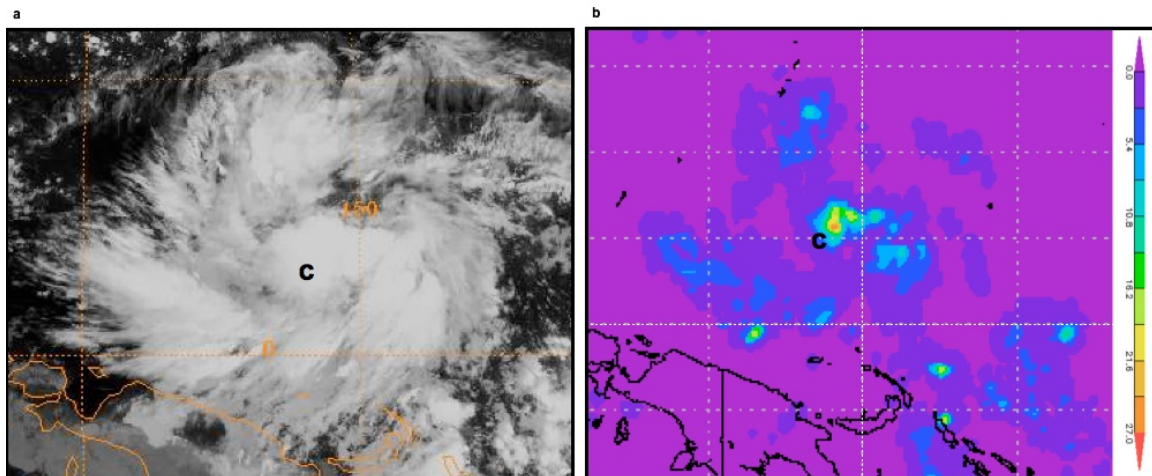


Figure 23. As in Figure 19 except at 1200 UTC 7 July with (a) MTSAT-1R infrared image indicating continued convective organization associated with the TD 04W that developed from the western convective region of MD₂. (b) Corresponding TRMM 3B42 precipitation (mm/hour) in association with TD 04W.

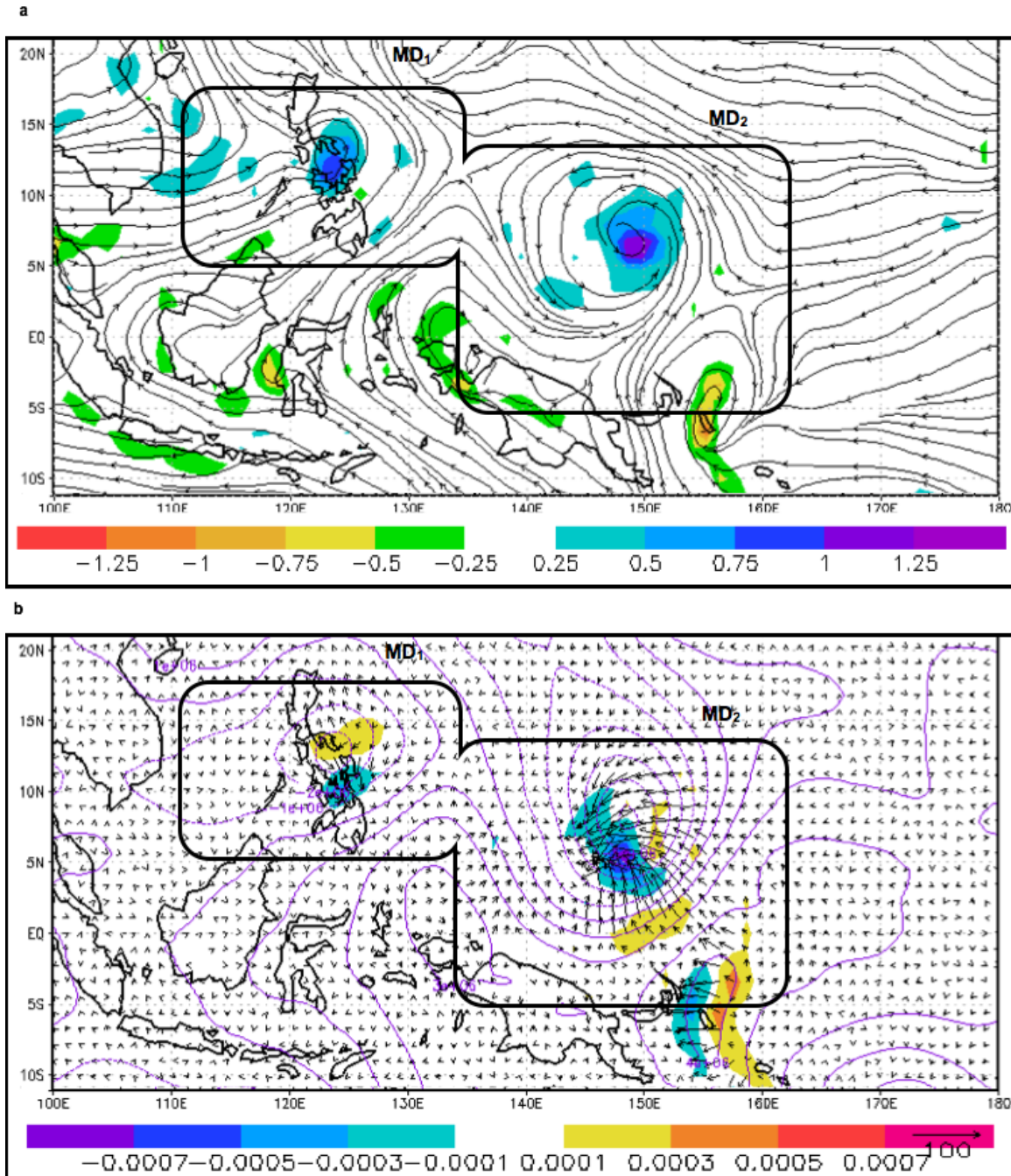


Figure 24. As in Figure 20 except for 1200 UTC 7 July with (a) streamlines and relative vorticity with a broad cyclonic circulation related to the dissipating MD₁ and the new TD 04W. (b) Wave-activity flux convergence continues in the region of the cyclonic vorticity maximum corresponding to TD 04W that will later become TY Man-Yi and over the center of MD₁.

Harr et al. (1996) analyzed the structure of the pre-TY Robyn monsoon depression during TCM-93 through the combination of satellite and aircraft observations during the transition of the circulation to a tropical cyclone. They observed confluence between the circulation and the cross-equatorial flow along the southwestern edge of the monsoon depression, and between the circulation and the easterlies along the northeastern portion of the circulation. A combination of two such external mechanisms was also observed in the MD₂ transition with two regions of wave-activity flux associated with enhanced easterlies and westerlies that were inward-directed and thus produced enhanced wave-activity flux convergence (e.g., Figures 20a and b). Harr et al. (1996) noted that once deep convection developed near the circulation center the associated vorticity at 850 hPa became more concentrated. Similarly, the organization of convection in MD₂ resulted in a more concentrated vorticity maximum and was quickly followed by transition to a pre-tropical cyclone seedling (e.g., Figure 21a, which was 12 hours prior to the first warning).

In summary, two external influences led to a pre-tropical cyclone seedling formation within a specific region of a monsoon depression owing to the persistent inward-directed wave-activity flux leading to the convergence of wave-activity flux over a vorticity maximum within the monsoon depression circulation. As in Figure 25, the MD₂ case featured a continued inward-directed wave-activity flux associated with the same airstream C that initially led to the formation of MD₂. It also had inward-directed flux from a wind maximum within airstream B, which was associated with the maximum of westerlies on the southern side of the MD₂ circulation (Figure 18a-f). As the wave in the easterlies approached shortly after monsoon depression formation, inward-directed wave-activity flux also began from the northeast that converged with the wave-activity flux from the south in the region of the MD₂ western vorticity maximum (Figure 25). This wave-activity flux convergence over the MD₂ western vorticity maximum is considered to have concentrated the circulation and resulted in a spin-up of the vorticity, more organized outer convection, and finally transition to a tropical cyclone.

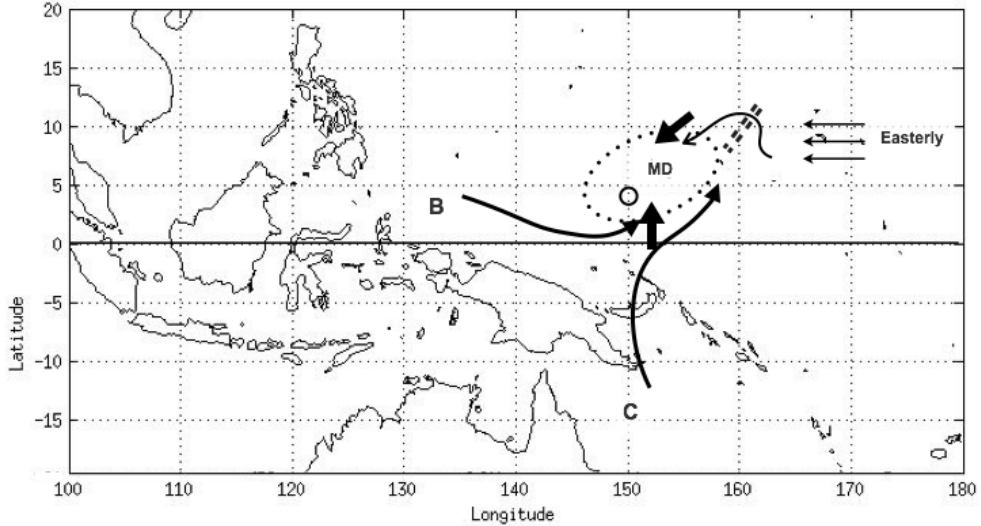


Figure 25. An idealized representation of MD₂ (dashed ellipse), the trade easterlies (horizontal arrows), trough of the wave in the easterlies (dashed lines), the cross-equatorial airstreams B and C (curved arrows as in Figure 6), the western vorticity maximum (circle) and the primary inward-directed wave-activity flux (thick arrows).

2. Non-transition of MD₁ to a Tropical Cyclone

This portion of the observational study also began at 0600 UTC 6 July 2007 (Figure 18a) almost three days after the formation of MD₁. The characteristics of the circulation still closely resembled that of a monsoon depression that had developed in association with airstream A (see Chapter II.B). In contrast to MD₂ at this time, the inward-directed wave-activity flux from the Southern Hemisphere did not continue for MD₁ after formation (Figures 5b-d). Rather, the wave-activity flux convergence was some distance (average of 250 km) southeast of the circulation center, although the convergence did correspond to a region of maximum convective activity (not shown).

By 1200 UTC 6 July, the region of maximum winds in airstream A to the southeast of MD₁ remains as part of the overall circulation rather than a wind maximum moving into the circulation as in MD₂ (Figures 18a and b). Although the IR image (Figure 26a) indicates the convection in MD₁ is more active on the eastern side, the TRMM 3 h precipitation maximum (Figure 26b) is some distance to the northwest of the

circulation center. Since the broad vorticity maximum associated with MD₁ (Figure 20a) corresponds to both the precipitation and convective maxima, with a short vorticity tail that extends into the region of maximum winds to the south of the circulation it might have been expected that MD₁ would transition to a tropical cyclone. However, the wave-activity flux remains directed outward from the center of the MD₁ circulation center and thus away from the vorticity maximum. Some weak wave-activity flux convergence is noted near the wind maximum just to the southeast of the circulation center, but there is no inward directed wave-activity flux that would contribute to a spin-up of the MD₁ circulation (Figure 20b).

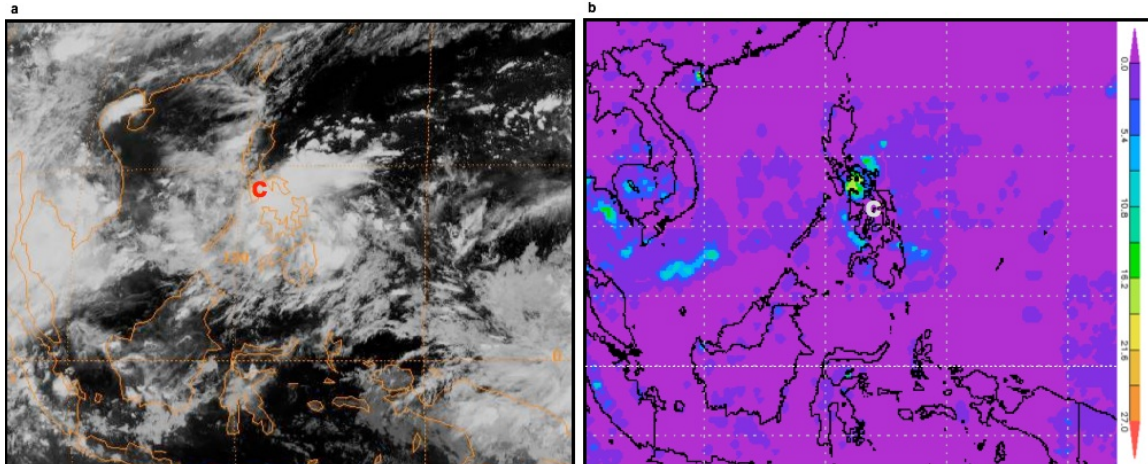


Figure 26. (a) MTSAT-1R infrared image at 1200 UTC 6 July 2007 illustrating the monsoon depression MD₁ near 10°N, 125°E. (b) Corresponding TRMM 3B42 precipitation (mm/hour; shading scale on right) with precipitation maxima to the northwest of center. The letter C corresponds to the estimated center of the cyclonic circulation.

At 0000 UTC 7 July, MD₁ remains over the central portion of the Philippines and still retains the characteristics of a monsoon depression. It is still circular, with a convection-free center (Figure 27a and b). While a broad wind maximum exists along the eastern portion of the circulation, the wind maxima have decreased in magnitude (Figure 18d). Even though airstreams A and B are flowing into the MD₁ monsoon depression circulation (Figure 22a), all of the wave-activity flux is still directed outward and thus is not inward-directed following the airstreams as it was during the formation of MD₂. The

wave-activity flux convergence is noted just to the south of center (Figure 22b), which corresponds to the region of stronger convection (Figures 27a).

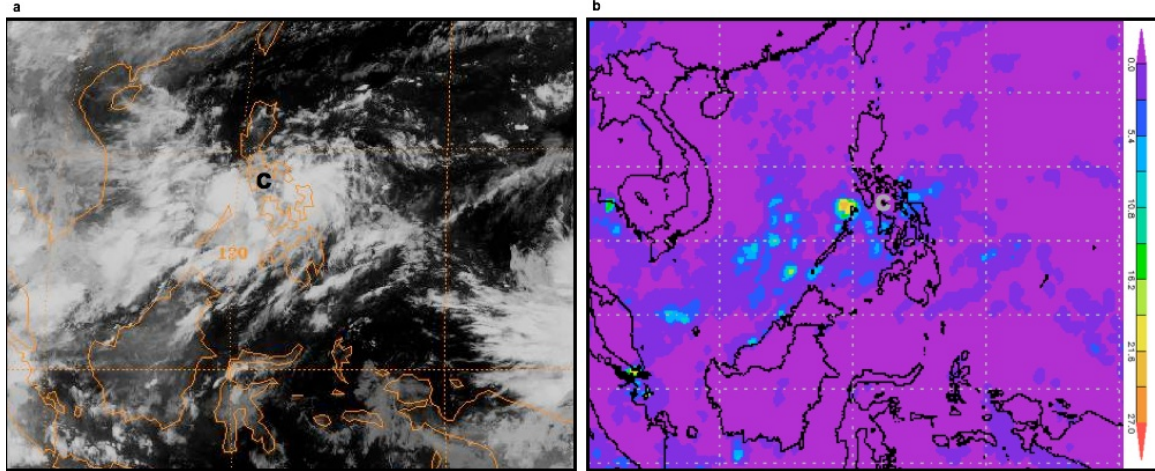


Figure 27. As in Figure 26 except at 0000 UTC 7 July with (a) MTSAT-1R IR image of MD₁ and the southern convective maximum. (b) TRMM 3B42 precipitation (mm/hour) with regions of precipitation corresponding to the southern convective regions in panel (a).

At 1200 UTC 7 July, MD₁ was still over the Philippines and the IR image (Figure 28a) indicated more widespread convection. In addition, the TRMM precipitation has a small rainfall maximum in each quadrant of the circulation (Figure 28b). As indicated by the streamlines in Figure 24a, the MD₁ circulation is no longer closed although there is still a broad vorticity maximum near the center. The wave-activity flux continues to be directed outward from MD₁, but the noticeably smaller region of flux convergence is now co-located with the vorticity maximum. This flux convergence is different from what was observed in MD₂ because it is not originating from an outside source. Indeed, no inward-directed wave-activity flux vectors were observed throughout the period. Consequently, MD₁ continues to weaken over the next 24 hours as it moves northward and becomes an open wave. By 1200 UTC 9 July (not shown), all signs of the MD₁ vorticity maximum and convection had disappeared.

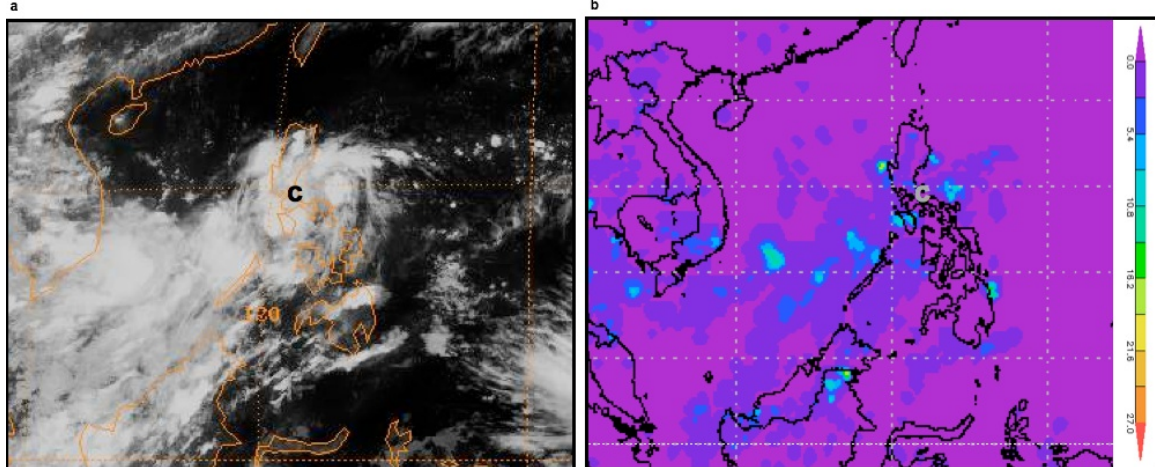


Figure 28. As in Figure 26 except at 1200 UTC 7 July with (a) MTSAT-1R infrared image indicating persistent convection associated with MD₁. (b) Corresponding TRMM 3B42 precipitation (mm/hour) in association with the dissipating MD₁.

In summary, the external influences that led to the transition of MD₂ to become a pre-tropical cyclone seedling did not occur in the long-lasting MD₁ circulation. Specifically, MD₁ did not have the persistent inward-directed wave-activity flux that led to flux convergence over the vorticity maximum, and thus concentration of the circulation with a spin-up of the vorticity maximum. In addition, organization of outer convection did not occur and the transition to a pre-tropical cyclone seedling did not occur. While this lack of a transition of MD₁ to a pre-tropical cyclone seedling may have been due to some other inhibiting factor, the key point is the absence of a similar external forcing as in the MD₂ case that might have contributed to the spin-up of the 850 hPa vorticity for MD₁. This case study of MD₁ serves as motivation for also examining the sample of monsoon depressions during 2009 that did not transition to a tropical cyclone to see if this lack of external forcing was a contributing factor to these non-developments.

D. ANALYSIS OF THE 2009 MONSOON DEPRESSIONS

The applicability of this conceptual model (Figure 25) of monsoon depression transition to tropical cyclone was also examined from 1 April through 31 December 2009 utilizing high-resolution ECMWF analyses (0.25-degree) from the YOTC archive. Of the 44 monsoon depressions that formed during this period, 17 (38.6%) transitioned to a tropical cyclone.

Nine of the 17 transitioning monsoon depressions from 2009 will be examined in Section 2 to describe their transitions from monsoon depressions to pre-tropical cyclone seedlings. The first group consists of four examples in which the primary airstream during the formations of the monsoon depressions persisted and was also the primary airstream in the transition to a pre-tropical cyclone seedling. The second group discussed in Section 2 consists of five examples in which the primary airstream during the monsoon depression formation was only a secondary factor and another airstream was the primary contributing factor in the transition to a pre-tropical cyclone seedling. In Section 3, the 25 monsoon depressions during 2009 that did not transition to a pre-tropical cyclone seedling will be analyzed.

1. Methodology

The methodology used in this chapter is very similar to that used in Chapter II.E. The high-resolution ECMWF analyses of 850 hPa vorticity and streamlines at six-hour intervals were examined in conjunction with the IR satellite imagery from the MTSAT-1R. The three-hourly 0.25-degree TRMM precipitation product was also used.

Since wave-activity flux convergence was a key component in concentrating the vorticity maximum and reducing the scale from a monsoon depression to a pre-tropical cyclone seedling, the wave-activity flux as presented in Chapter II.C.1 remained an essential analysis tool. The necessary, but not sufficient conditions for tropical cyclone formation, as outlined by Gray (1968, 1975) are met in the monsoon depression environment. The sea-surface temperature was greater than 26.5°C across the domain for the period, the monsoon depression is a moist environment of low vertical wind shear,

and provides a background cyclonic vorticity environment so that even the low-latitude circulations have the ability to transition.

It is hypothesized that in the monsoon depression environment (in addition to the Gray (1975) necessary but not sufficient conditions for formation) the convergence of wave-activity flux in one of the monsoon depression vorticity maxima leads to the constriction of scale and thereby creates the pre-tropical cyclone seedling that subsequently intensifies the circulation into a tropical cyclone.

2. Analysis of Transitioning Monsoon Depressions from 2009

a. *Transition to a pre-tropical cyclone seedling with the same primary airstream as during the monsoon depression formation*

(1) Pre-Super TY Melor (20W)

The pre-Super TY Melor case is considered to be a transitioning monsoon depression that involves the persistence of the same airstream that led to the original monsoon depression. The pre-Super TY Melor (20W) monsoon depression during 2009 was used in Chapter II as an example of an airstream C monsoon depression in which there was a characteristic Southern Hemisphere cyclone (C_{SH} ; compare Figure 11b with Figures 11c and 11d). Based on all of the characteristics of monsoon depression formation as defined in Chapter II.E.1, this monsoon depression did not form until after the JTWC had already issued a TCFA at 2330 UTC 28 September. This unusual situation is attributed to the pre-Super TY Melor monsoon depression having a central vorticity maximum rather than an elliptical circulation with separate eastern and western vorticity maxima. Thus except for the size of the circulation, this monsoon depression had a central core that is also a characteristic of a pre-tropical cyclone seedling. For the purposes of this study, the formation time of the monsoon depression will be taken as 1800 UTC 27 September.

Similar to the monsoon depression MD₂ transition that occurred between 5°N and 10°N, the 850 hPa vorticity maximum for the pre-Super TY Melor monsoon depression was also between 5°N and 10°N (see Figure 11b in Chapter II). A long, narrow airstream enhanced by the C_{SH} extends from the Southern Hemisphere to this vorticity maximum.

A confluence line between the monsoon depression and the easterly flow also exists along the northeastern edge of the monsoon depression. These features persisted from formation through transition to a pre-tropical cyclone seedling.

At 1200 UTC 27 September (Figure 29a), the pre-Super TY Melor monsoon depression was elliptically shaped with a northwest-southeast orientation. Note that this pre-Super TY Melor monsoon depression was the trailing circulation among three circulations along the monsoon trough, and thus the airstream C fed directly into this monsoon depression. Consequently, the corresponding wave-activity flux (Figure 29b) is oriented across this cross-equatorial airstream and thus is directed inward toward the vorticity maxima in Figure 29a. These wave-activity flux vectors lead to wave-activity flux convergence along a north-south band corresponding to the confluence between the equatorial westerlies and the easterly trades. However, regions of wave-activity flux divergence are also interspersed among the convergence regions. Consequently, an organized spin-up of cyclonic vorticity is not yet evident at this time.

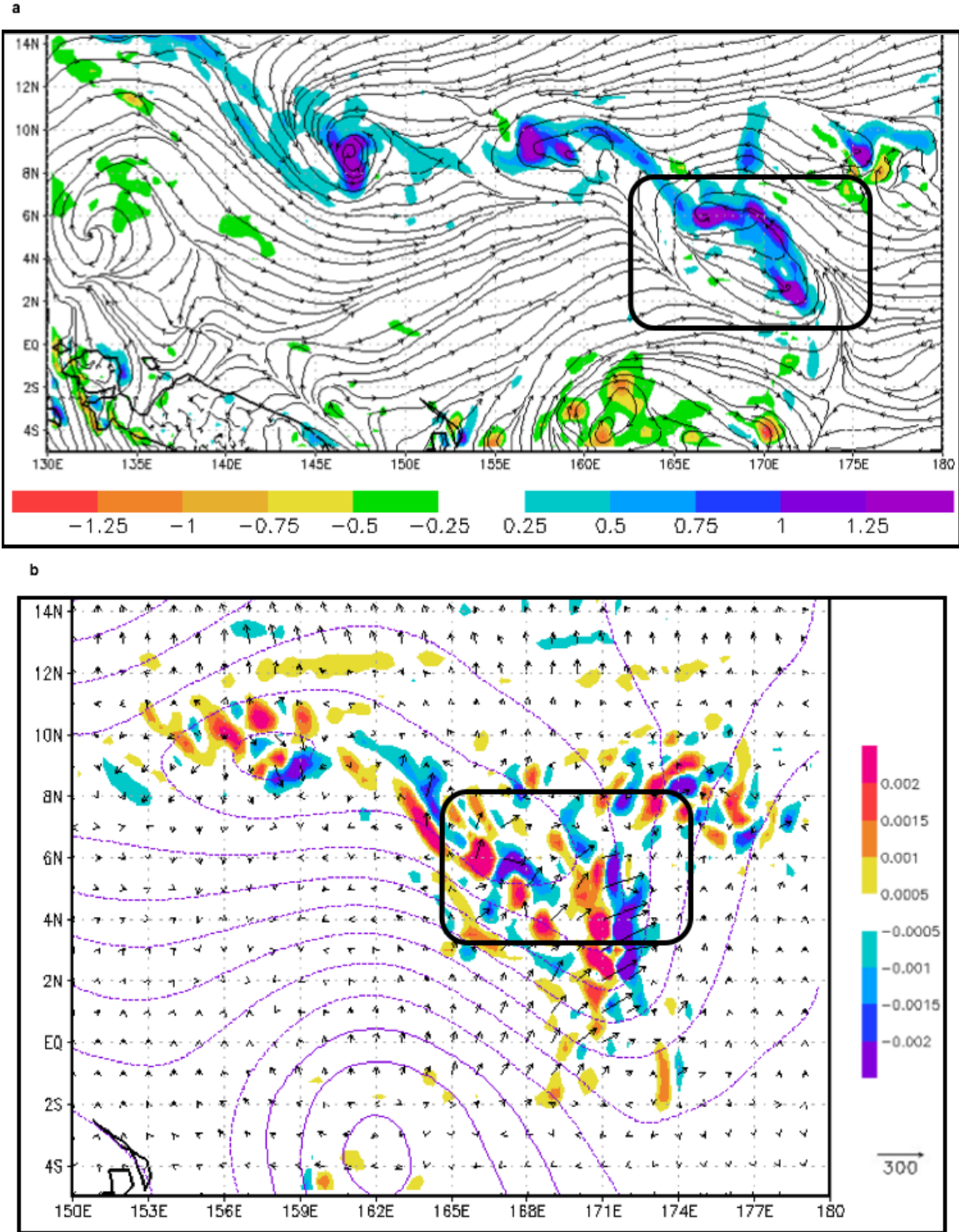


Figure 29. As in Figure 20 except at 1200 UTC 27 September with (a) streamlines and relative vorticity for the pre-Super TY Melor monsoon depression. (b) Wave-activity flux vectors entering the box from the south result in two regions of convergence corresponding to the areas of the vorticity maxima.

At 0000 UTC 28 September (Figure 30a), the 850 hPa circulation center is near 6°N, 167°E, and is coincident with a single vorticity center. While this circulation is beginning to take on the character of a pre-tropical cyclone seedling, it still has an elliptical shape in the IR satellite imagery (not shown). Furthermore, the wave-activity flux convergence at this time is still representative of two vorticity maxima (Figure 30b), with separate areas of wave-activity flux convergence and adjacent wave-activity flux divergence. While inward-directed wave-activity flux persists from the south in conjunction with the Southern Hemisphere cyclone (C_{SH}), outward-directed wave-activity flux is beginning from the northern portion of the monsoon depression, which is a feature not observed in the MD₂ case.

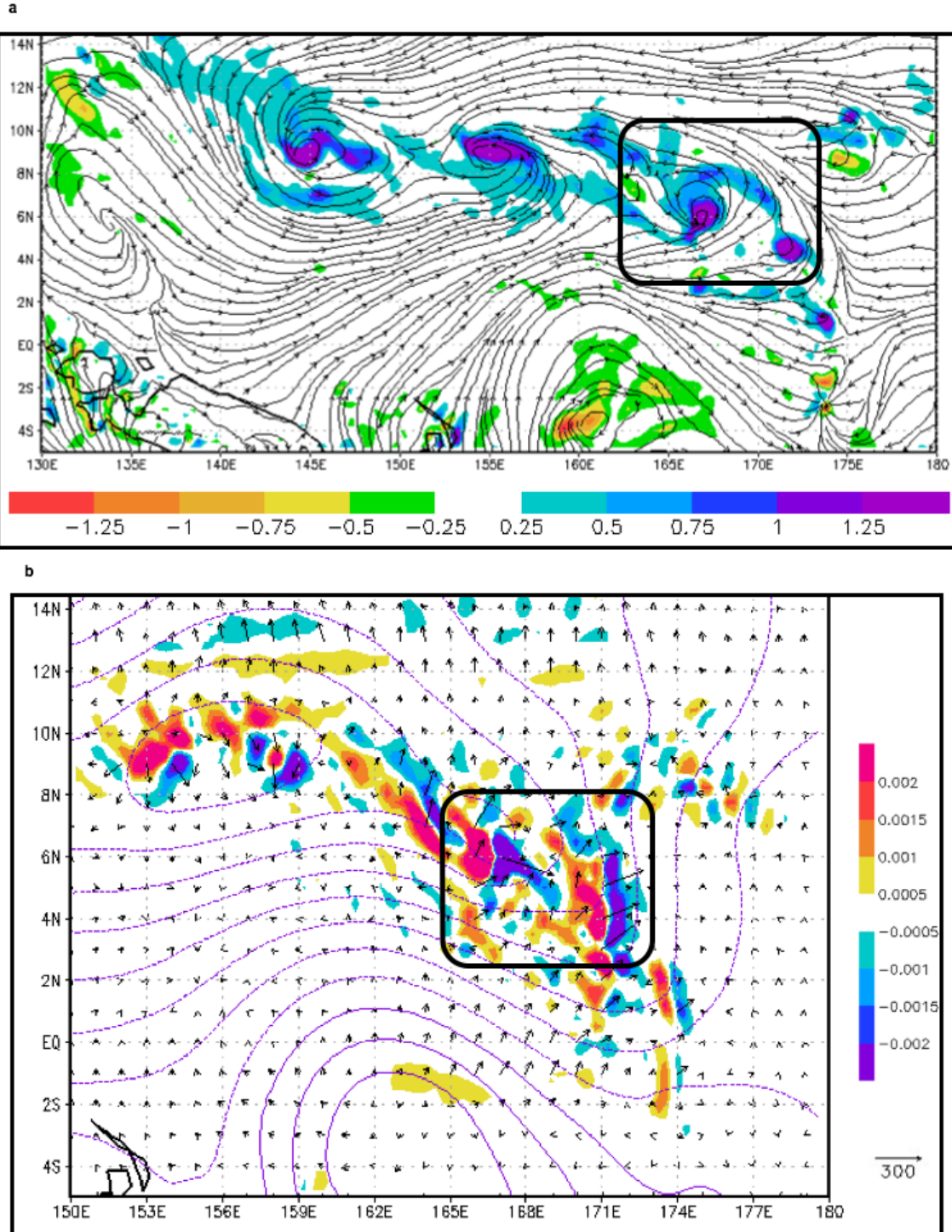


Figure 30. As in Figure 20 except at 0000 UTC 28 September with (a) streamlines and relative vorticity indicating the pre-Super TY Melor monsoon depression is now circular. (b) Wave-activity flux vectors continue to enter the box from the south, and outward wave-activity flux is beginning to the north.

At 1200 UTC 28 September, the ECMWF streamline and vorticity analysis (Figure 31a) clearly depicts a less well-organized circulation with two vorticity maxima. While the region of southerly wave-activity flux vectors (Figure 31b) in conjunction with the cross-equatorial airstream C still exists at this time, it is no longer directed into the entire southern portion of the monsoon depression. Although regions of wave-activity flux convergence exist in the central area of the monsoon depression, these regions are also not well organized in this ECMWF analysis. A region of outward-directed wave-activity flux vectors is analyzed in the western portion of the monsoon depression and farther north along 12°N, which would be expected to hinder the development of a central vorticity maximum as expected with a pre-tropical cyclone seedling. Note that the large region of wave-activity flux convergence to the north of the eastern vorticity maximum has decreased significantly since the cross-equatorial wave-activity flux is not converging over the whole circulation, but rather just over a smaller portion as the monsoon depression moves away from the Southern Hemisphere cyclone.

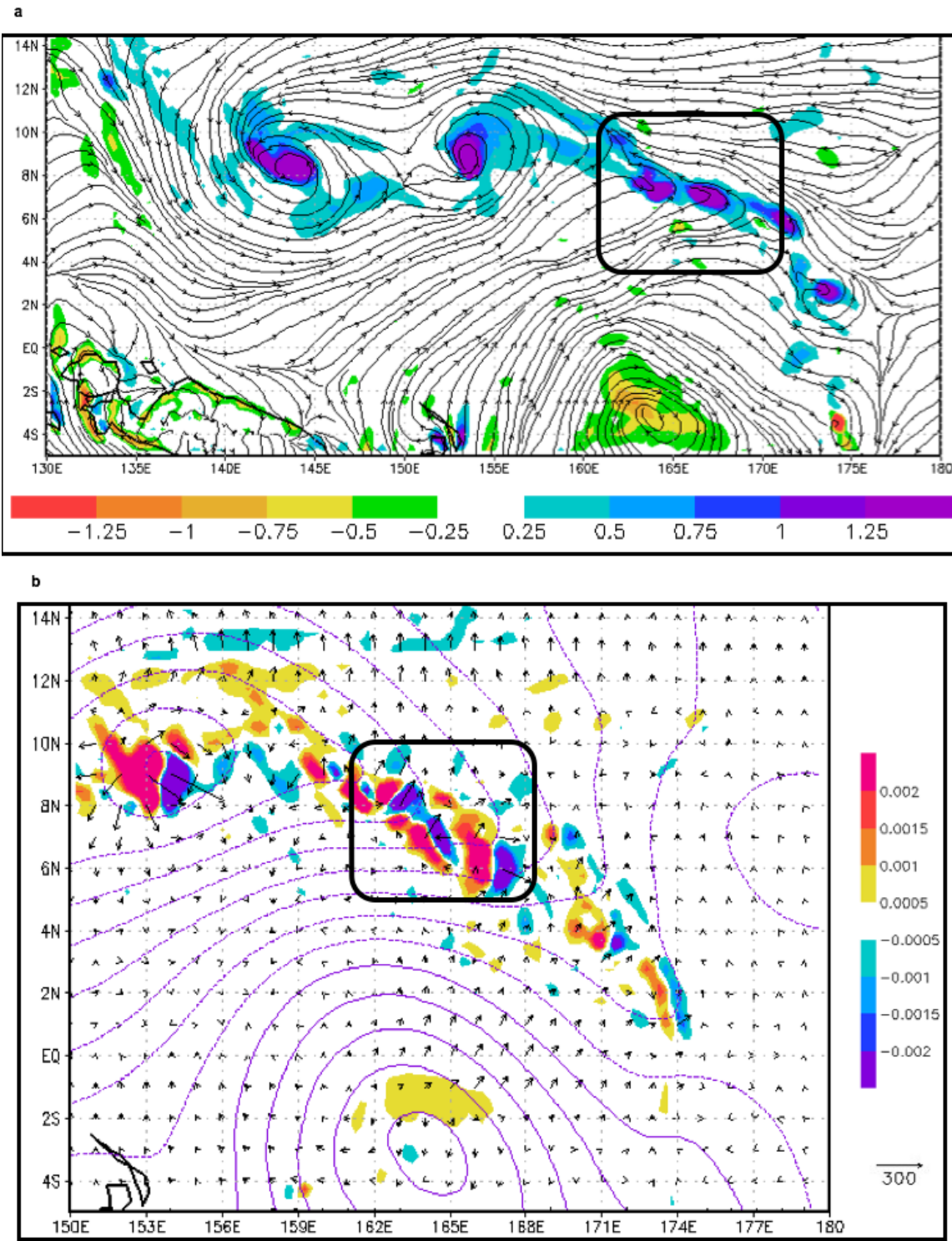


Figure 31. As in Figure 20 except at 1200 UTC 28 September with (a) streamlines and relative vorticity with two cyclonic relative vorticity maxima and (b) corresponding wave-activity flux convergence distribution.

At 0000 29 September, which is only 30 minutes after the JTWC issued the TCFA at 2330 UTC 28 September, the ECMWF analysis (Figure 32a) has a better defined circulation that is associated with the eastern vorticity maximum in the previous analysis in Figure 31a. However, this analysis also retained additional vorticity maxima to the west and east of the primary vorticity maximum. Consequently, the wave-activity flux vectors are somewhat irregular, although a larger region of wave-activity flux convergence (Figure 32b) is associated with the primary vorticity maximum that becomes the pre-tropical cyclone seedling. Some outward-directed wave-activity flux is analyzed to the west, but this is likely related to the western vorticity maximum in Figure 32a. If that wave-activity flux is related to TD 18W, which is immediately to the west in Figure 32a, it is not contributing to the wave-activity flux convergence over this pre-tropical cyclone seedling. The inward-directed wave activity flux from the south associated with airstream C is diminished as the circulation has moved northward and westward. The JTWC issued the first warning as TD 20W at 0900 UTC 29 September, but this warning was valid at 0600 UTC, which is only 6.5 hours after the TCFA.

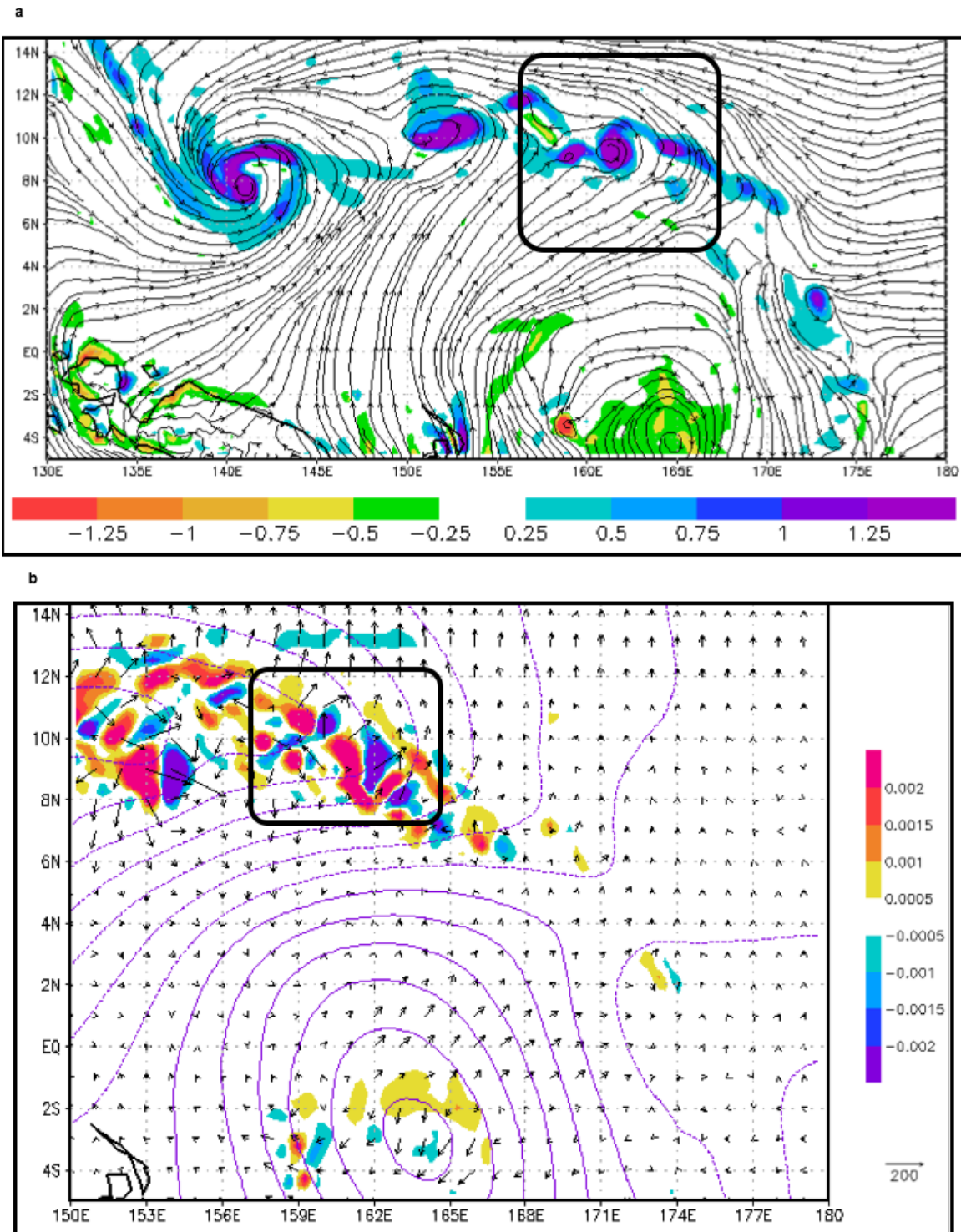


Figure 32. As in Figure 20 except at 0000 UTC 29 September with (a) streamlines and relative vorticity showing the elliptically shaped cyclonic circulation at the time of pre-tropical cyclone seedling, and (b) corresponding wave-activity flux convergence distribution.

As in the conceptual model in Figure 25 based on the pre-TY Man-Yi monsoon depression transition, the transition of the pre-Super TY Melor monsoon depression to a tropical cyclone was due to the primary wave-activity flux associated with the same cross-equatorial airstream C that had led to the formation of the monsoon depression. As in the pre-TY Man-Yi conceptual model, there was a selection of one of the monsoon depression vorticity maxima to be the center of the pre-tropical cyclone circulation. In this case, it was the eastern vorticity maximum rather than the western as in the pre-TY Man-Yi case. This eastern vorticity maximum was exposed to more of the C_{SH} wave-activity flux, as it remained near the central airstream C even as the monsoon depression began to move to the north and west. By contrast, some outward-directed wave-activity flux relative to the western vorticity maximum contributed to wave-activity flux divergence that was unfavorable for amplification of that western vorticity maximum.

(2) Pre-Super TY Choi-Wan (15W)

The pre-TY Choi-Wan (15W) monsoon depression was used in Chapter II as an example of an airstream C_* monsoon depression, in which the airstream does not have the Southern Hemisphere cyclone (C_{SH}) that is characteristic of airstream C monsoon depression formations (compare Figure 11c with Figures 11a and 11b). Even without the Southern Hemisphere cyclone that contributes a strong and persistent cross-equatorial airstream to wrap-up around the developing monsoon depression circulation, airstream C_* is strong enough to cross the Equator and not be turned back toward the Southern Hemisphere cyclone (which forms the C_{SH}).

In contrast to the MD_2 transition that occurred between $5^{\circ}N$ and $10^{\circ}N$, the 850 hPa vorticity maximum for the pre-TY Choi-Wan monsoon depression was near $14.5^{\circ}N$, $155^{\circ}E$ at 0600 UTC 11 September (see Figure 11c and discussion in Chapter II). Note the long, narrow airstream (annotated in Figure 11c) that extends from the Southern Hemisphere to this vorticity maximum, and a long confluence line between this southerly airstream and the easterly flow is analyzed along the eastern edge of the airstream. This was the most northern airstream C_* monsoon depression that transitioned to a pre-tropical cyclone seedling from this category.

The pre-TY Choi-Wan monsoon depression was elliptically shaped as in the 2007 MD₂ case. The northeast-southwest orientation (rather than the more typical east-west orientation) for this monsoon depression was because it was embedded in a high amplitude wave in the easterly flow (Figure 33a). The corresponding wave-activity flux (Figure 33b) is oriented along the cross-equatorial airstream. A region of wave-activity flux convergence also exists along the long confluence line along the eastern edge of the airstream. Notice also that outward-directed wave-activity flux vectors are analyzed to the northwest of the vorticity maximum, which is unfavorable for amplifying the vorticity in that quadrant of the pre-TY Choi-Wan monsoon depression. These wave-activity flux trends persist throughout the 18 hour transition period, whereas the southern and eastern inward-directed areas of wave-activity flux result in flux convergence as in the pre-TY Man-Yi case. Again, the western outward-directed flux is a feature that the pre-TY Man-Yi case did not have.

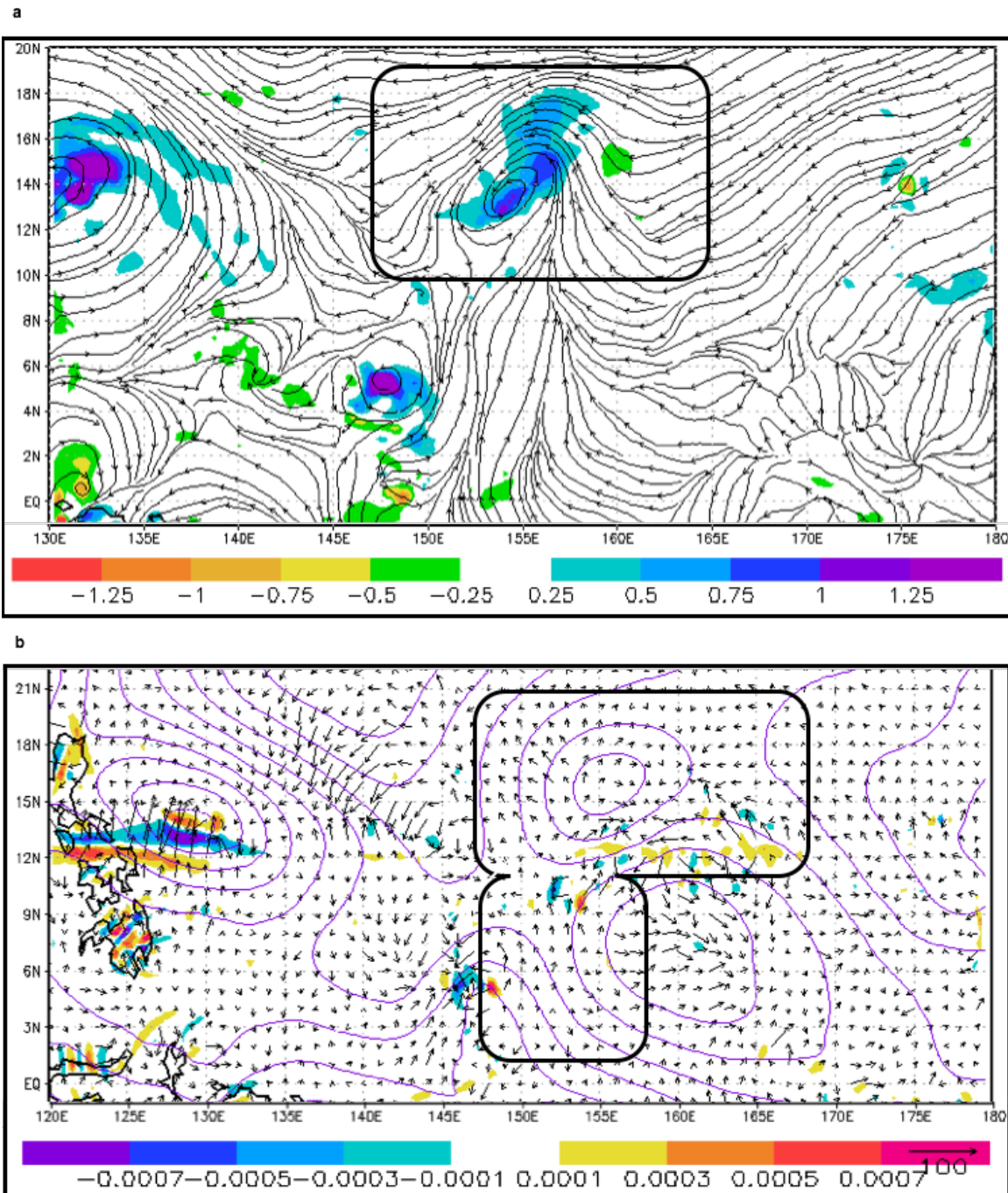


Figure 33. As in Figure 20 except for 0600 UTC 11 September with (a) streamlines and relative vorticity with a broad cyclonic circulation related the pre-TD 15W monsoon depression. (b) Wave-activity flux convergence continues in the region of the cyclonic vorticity maximum from the south and east corresponding to the circulation that will later become TY Choi-Wan.

The infrared satellite imagery (Figure 34a) indicates a relatively elliptical deep convective area in the region of the vorticity maximum and shallow, cyclonically-curved bands of convection in the outer region that may be attributed to the wave in the easterlies. Similarly, the TRMM 3 h precipitation (Figure 34b) has a maximum in the region of the vorticity maximum, but has an extensive outer precipitation region along the southern portion of the circulation with smaller precipitation rates in the northern and western quadrants.

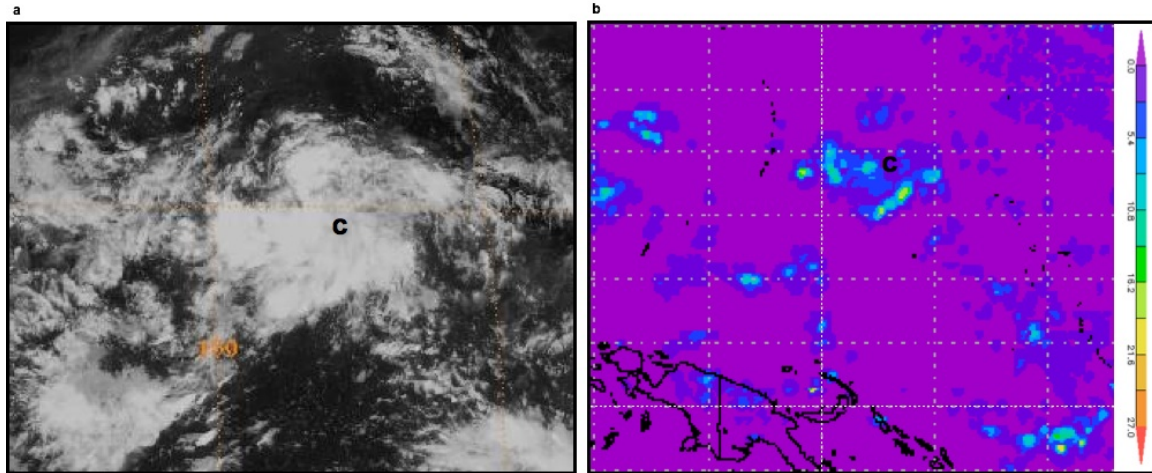


Figure 34. As in Figure 19 except at 0600 UTC 11 September with (a) MTSAT-1R infrared image indicating continued convective organization associated with the pre-TD 15W that developed from the eastern convective region and (b) TRMM 3B42 precipitation (mm/hour) in association with the pre-TD 15W.

At 1200 UTC 11 September (Figure 35a), the 850 hPa circulation center is near 15°N , 154°E , but the vorticity maximum is to the east-northeast near 15.5°N , 157°E . The previous northern vorticity lobe has wrapped around to the northwest of the circulation center, and thus the circulation has become more elliptical in shape. This elliptical shape is quite evident in the IR imagery (Figure 36a) with western and eastern convective regions with a relatively cloud-free region near 15°N , 156°E . The maximum in the TRMM 3 h precipitation (Figure 36b) is near the circulation center, but a cyclonically curved precipitation band extends from south of the center to east of the center where the

vorticity maximum exists. A small precipitation maximum also exists to the west of the circulation center in association with the western convective maximum in Figure 36a.

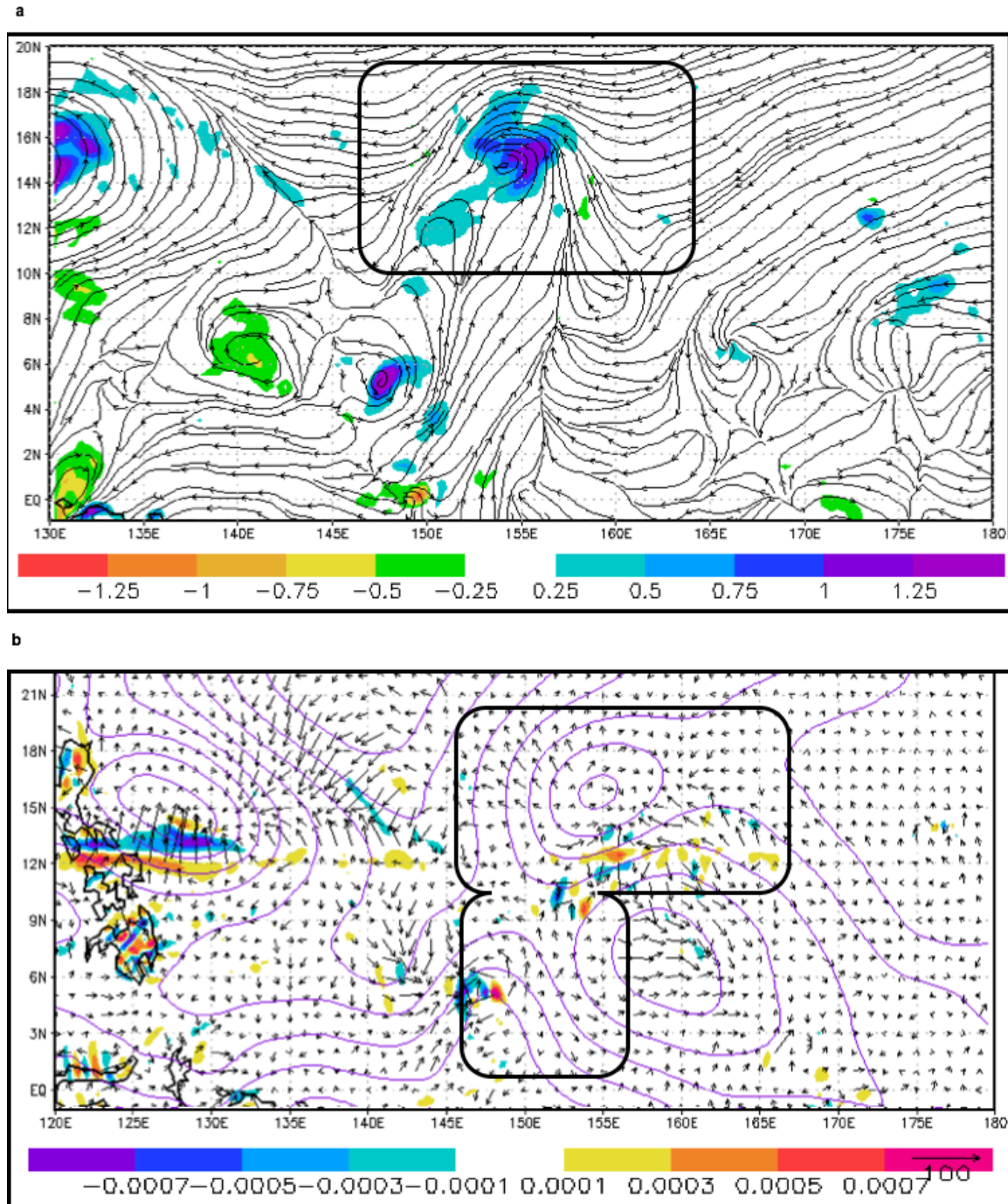


Figure 35. As in Figure 20 except for 1200 UTC 11 September with (a) streamlines and relative vorticity just prior to the JTWC TCFA (2230 UTC 11 September). (b) Wave-activity flux convergence continues in the region of the cyclonic vorticity maximum from the south and east corresponding to the circulation that will later become TY Choi-Wan.

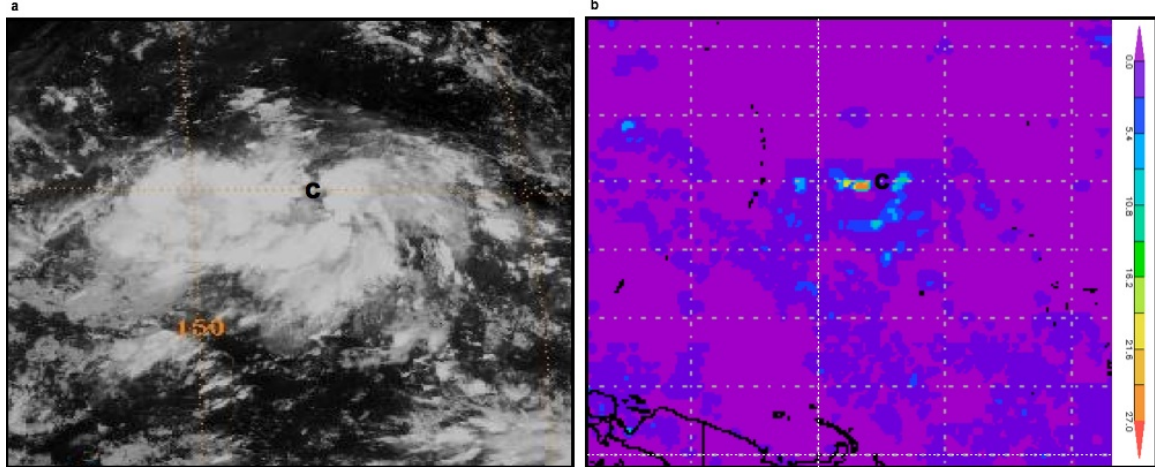


Figure 36. As in Figure 19 except at 1200 UTC 11 September with (a) MTSAT-1R infrared image indicating continued convective organization associated with the pre-TD 14W that developed from the eastern convective region and (b) TRMM 3B42 precipitation (mm/hour) in association with the pre-TD 14W.

While the long region of southerly wave-activity flux vectors (Figure 35b) still exists at 1200 UTC 11 September as in Figure 33b, the much larger, inward-directed wave-activity flux vectors to the southeast of the vorticity maximum are clearly contributing more to the wave-activity flux convergence, and thus vorticity amplification, than those from the south. That is, interaction of the monsoon depression with the easterly flow for this higher-latitude transition appears to be the more important factor to the amplification of the eastern vorticity maximum. Just 10.5 hours later (2230 UTC 11 September), the monsoon depression was a pre-tropical cyclone seedling and the JTWC issued a TCFA at 13.4°N , 154.4°E , which was to the southeast of the 1800 UTC 11 September circulation. The JTWC issued the first warning as TD 15W with a valid time of 0000 UTC 12 September.

Compared to the conceptual model in Chapter IV.C.1 based on the pre-TY Man-Yi monsoon depression transition, the wave-activity flux associated with the cross-equatorial flow extends to a much higher latitude. As in the pre-TY Man-Yi conceptual model, the transition to a tropical cyclone is not solely due to the primary wave-activity flux that is associated with the cross-equatorial airstream on the south side of MD₂ that contributed to amplification of the western vorticity maximum, as it was when the flux

from the interaction of the circulation with the easterly flow began that the circulation transitioned. In this pre-TY Choi-Wan case, the outward-directed wave-activity flux vectors to the northwest of the monsoon depression circulation center were unfavorable for amplification of a vorticity maximum in that quadrant. Thus, pre-TY Choi-Wan (TD 14W) developed to the southeast of the monsoon depression circulation center where the maximum of wave-activity flux convergence was occurring (from the south and east; Figures 33b and 35b).

(3) Pre-TS Nepartak (21W)

The pre-TS Nepartak (2009) monsoon depression was an example of an elliptically shaped airstream B monsoon depression (see discussion on airstream B monsoon depressions in Chapter II.D). The transition to a pre-tropical cyclone seedling took almost four days after the formation. Although there was continuous airstream B interaction, the transition to a pre-tropical cyclone seedling occurred following an eventual interaction with the trade easterlies. In contrast to the MD₂ transition that occurred between 5°N and 10°N, the transition to a tropical cyclone in the pre-TS Nepartak case occurred between 10°N and 15°N.

At 1200 UTC 6 October, airstream B from the west is evident in the streamlines along most of the southern portion of the monsoon depression (Figure 37a), while the trade easterlies comprise the northern part of the circulation. Note also the two maxima of relative vorticity in the broader region of cyclonic vorticity on the eastern side of the circulation. Large wave-activity flux is present at this time, but it is outward to the north and east (Figure 37b) and thus is not contributing to amplification of the vortex. While only a very small inward-directed wave-activity flux from the west is present, this flux associated with airstream B will persist.

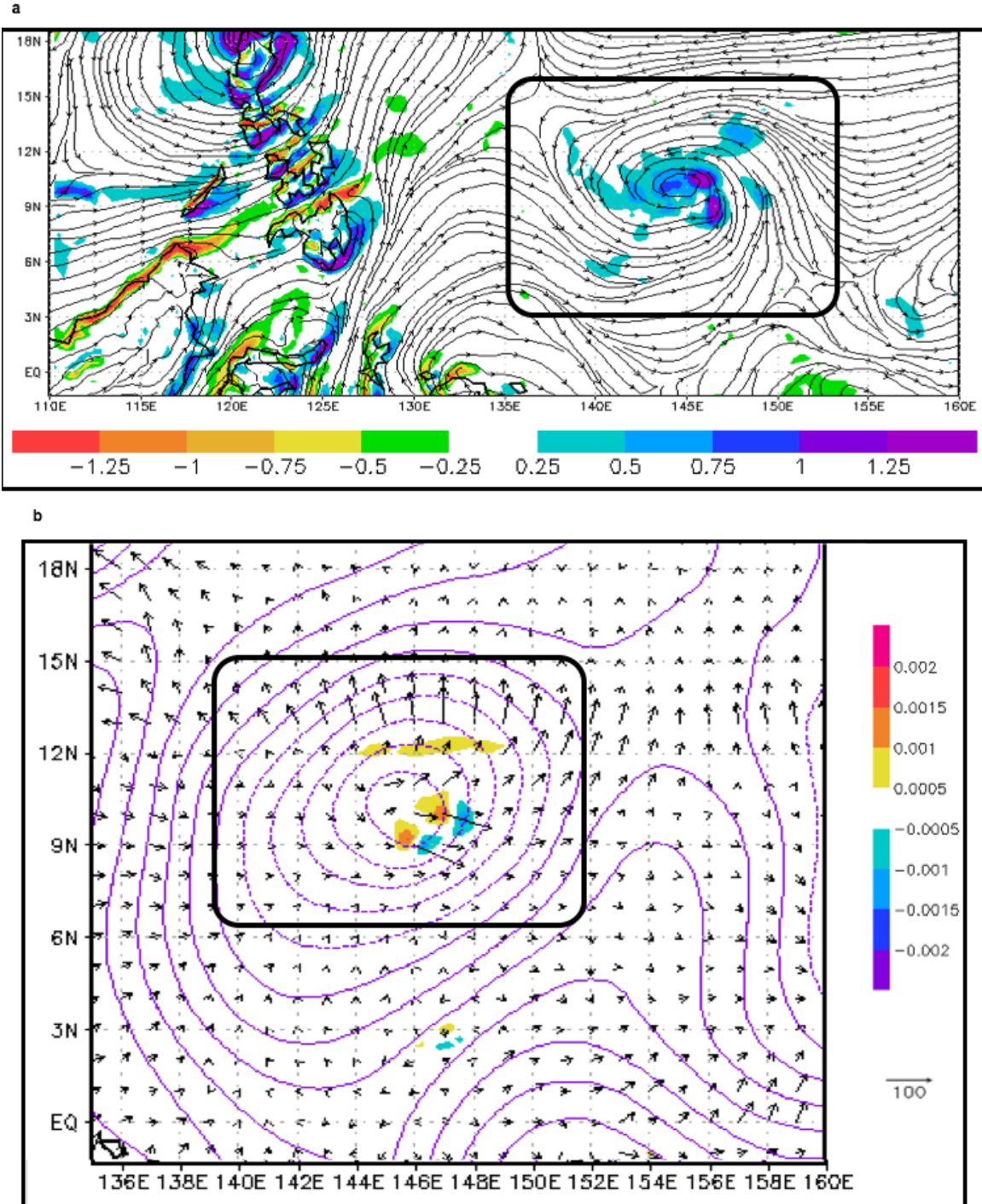


Figure 37. As in Figure 20 except for 1200 UTC 6 October 2009 with (a) streamlines and relative vorticity with airstream B. (b) Outward-directed wave-activity flux is to the north and east with a small amount of inward-directed wave-activity flux from the west.

While airstream B persists at 0000 UTC 7 October (Figure 38a), a narrow band of airstream C is also present. However, the circulation and central vorticity maximum have constricted and now have a more circular circulation. An increase in the outward-directed wave-activity flux to the east is analyzed while the flux to the north has been reduced (Figure 38b). The inward-directed wave-activity flux from the west has increased. Note the wave-activity flux vectors to the northeast of the circulation are beginning to point inward toward the circulation center, which will contribute to vortex spin-up. By contrast, the flux-divergent region over the western portion of the monsoon depression will make that area unfavorable for spin-up to a pre-tropical cyclone seedling.

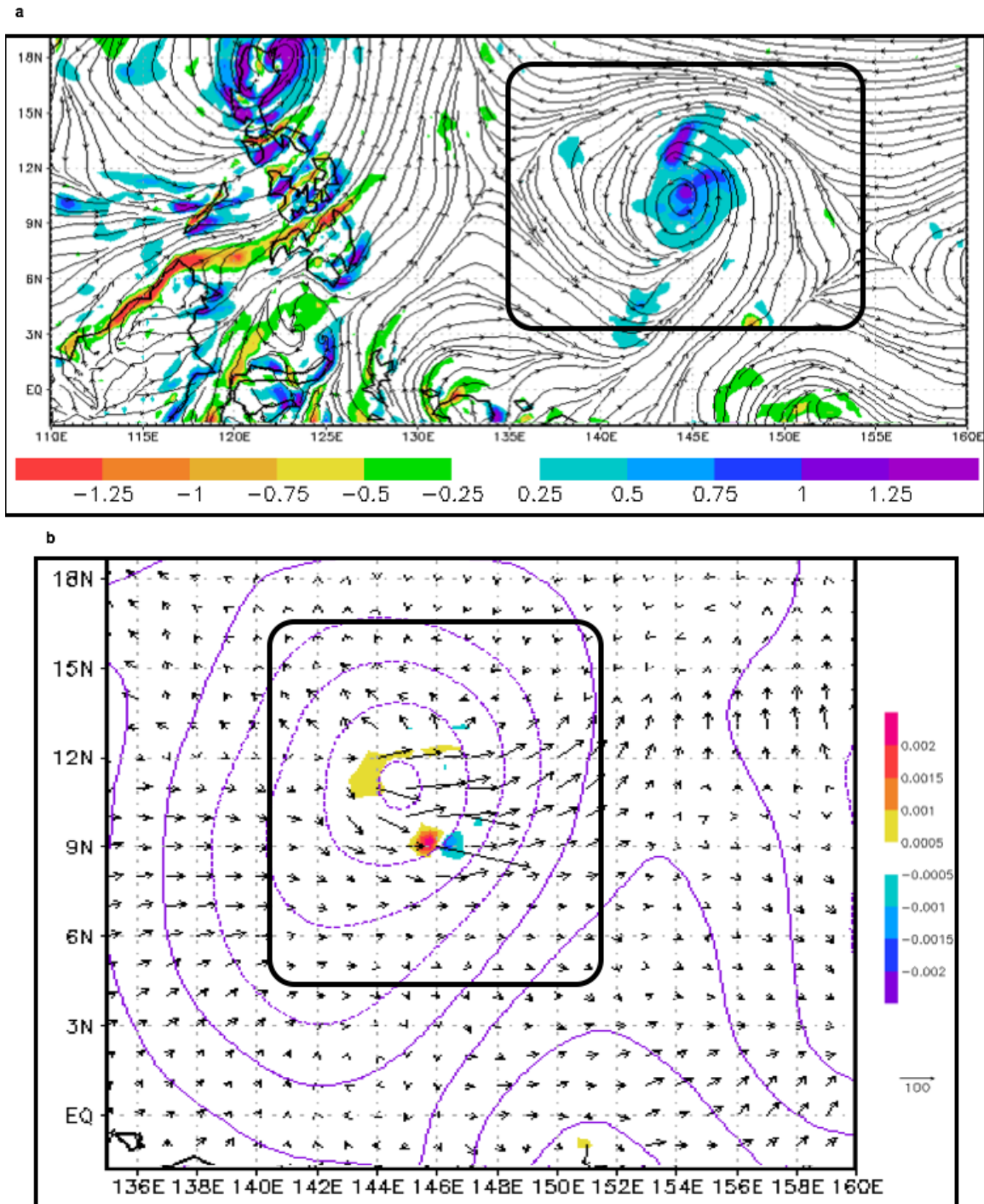


Figure 38. As in Figure 20 except for 0000 UTC 7 October with (a) streamlines and relative vorticity showing airstreams B and C and a more circular monsoon depression. (b) Outward-directed wave-activity flux continues to the north and east, and the inward-directed wave-activity flux from the west has increased.

At 1200 UTC 7 October 2009 (Figure 39a), there is still a broad region of relative vorticity. Since the location of the vorticity maximum corresponds to the region of wave-activity flux divergence at the earlier time, the maximum has decreased in magnitude. The wave-activity flux (Figure 39b) from the northeast has increased significantly and is reaching the central portion of the monsoon depression. While no convergence shading is indicated in Figure 39b, wave-activity flux convergence can be inferred from the magnitude and direction of the vectors. Another positive factor is the outward-directed wave-activity flux to the east is still present, but has shifted to the south. Consequently, the region of wave-activity flux divergence has moved away from the vorticity maximum, which should make it more favorable to spin-up to a pre-tropical cyclone seedling.

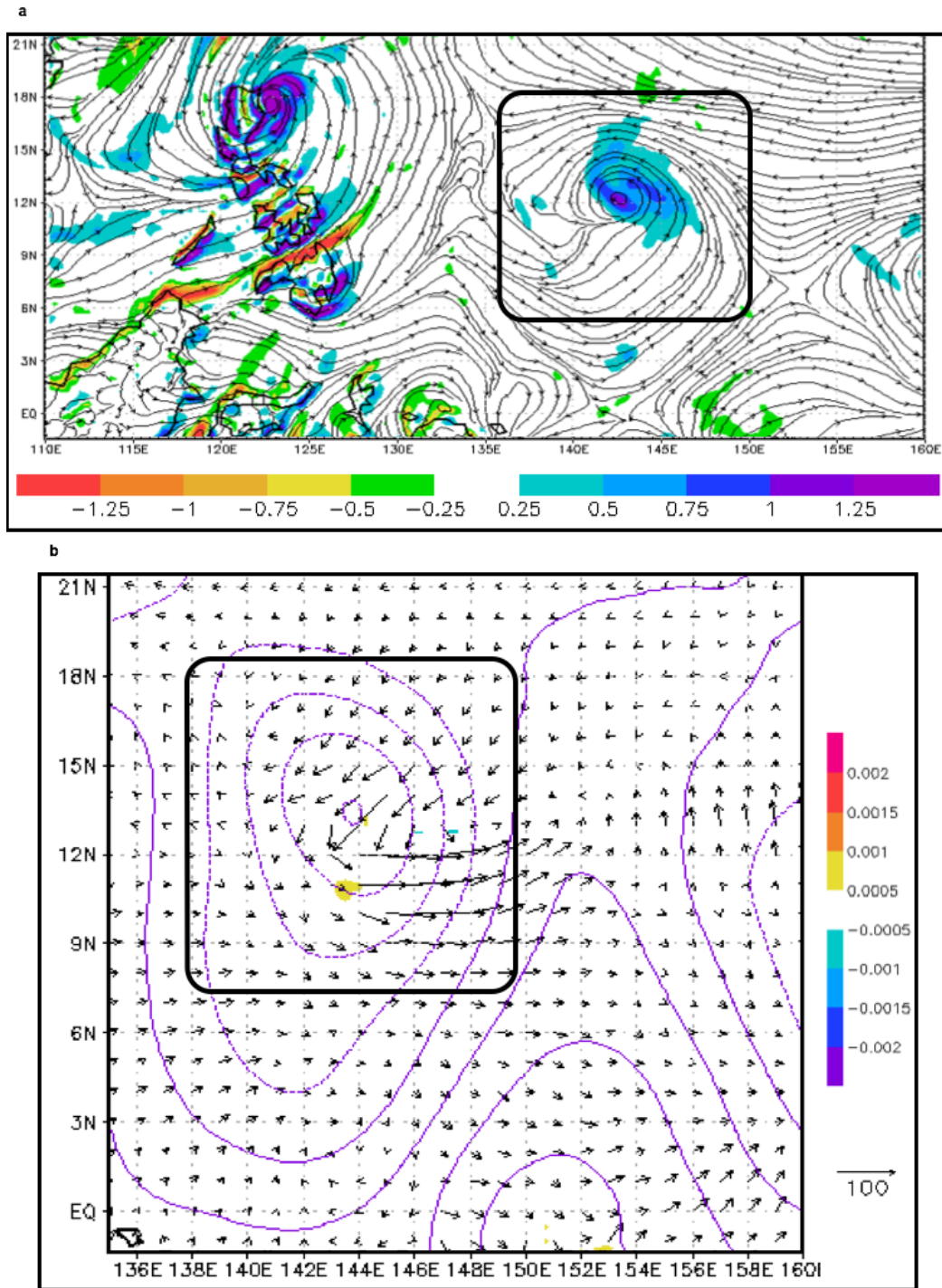


Figure 39. As in Figure 20 except for 1200 UTC 7 October with (a) streamlines and relative vorticity showing airstreams B and C have merged. (b) Inward-directed wave-activity flux from the northeast is the predominant flux, and has replaced the outward-directed wave-activity flux to the north. Large outward-directed flux to the east continues, but it is shifted to the south away from the central region.

At 0000 UTC 8 October (Figure 40a), the overall circulation has spun-up with well-defined airstreams B and C on the southern side interacting strongly with the easterly trades to the northeast of the center. Multiple vorticity maximum are analyzed that are consistent with the intensification of the circulation. Inward-directed wave-activity flux from the northeast is resulting in a large wave-activity flux convergence over the eastern portion of the monsoon depression (Figure 40b), and thus is considered to be the primary factor in the amplification of the vorticity in the northeast quadrant. Although the outward-directed wave-activity flux to the east continues, it is now displaced to the southeast and thus is not inhibiting the spin-up of the vorticity maximum. The circulation will be considered a pre-tropical cyclone seedling at 0230 UTC 8 October with the issuance of a TCFA by the JTWC, and the valid time of the first JTWC warning was 12 hours later at 1200 UTC 8 October.

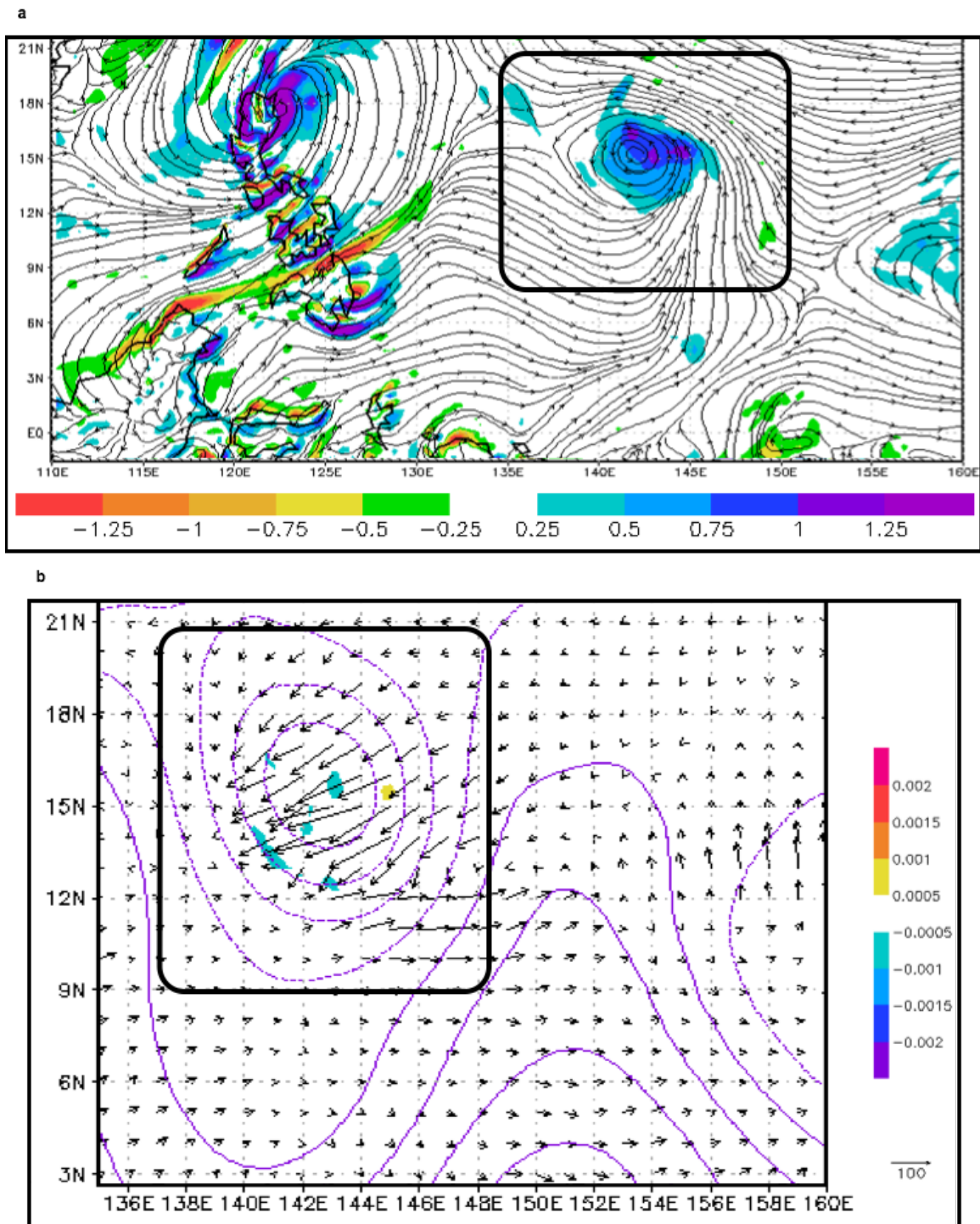


Figure 40. As in Figure 20 except for 0000 UTC 8 October with (a) streamlines and relative vorticity maxima only 2.5 hours prior to TCFA. (b) Inward-directed wave-activity flux from the northeast has become a primary factor.

Compared to the conceptual model based on the pre-TY Man-Yi monsoon depression transition (Chapter IV.C.1), the wave-activity flux associated with the cross-equatorial airstream B was not solely responsible for the transition of this monsoon depression. Prior to the transition, only a small amount of inward-directed flux from the west associated with airstream B could not offset the large outward wave-activity flux toward the east and the northeast leading to the region of wave-activity flux divergence and preventing the spin-up of the circulation to a pre-tropical cyclone seedling (Figure 38). As indicated in Figure 39 and 40, a key factor in the transition of this pre-TS Nepartak case to a pre-tropical cyclone seedling was thus the inward-directed wave-activity flux from the northeast.

In summary, pre-TS Nepartak developed in the northeast quadrant of the monsoon depression circulation when a maximum of wave-activity flux convergence developed in response to the interaction of airstreams B and C with the easterly trades such that the wave-activity flux reversed from being outward (indicating wave dispersion) to being inward-directed. Consequently, this pre-TS Nepartak was more like the pre-TY Choi-Wan case in that an interaction at higher latitudes with an easterly flow had a crucial role in the formation of the pre-tropical cyclone seedling from a monsoon depression.

(4) Pre-TY Ketsana (17W)

The pre-TY Ketsana monsoon depression is an example of a circular monsoon depression that formed from airstream A (see Chapter II.D for a description of airstream A). The transition to a pre-tropical cyclone seedling occurs almost three days after becoming a monsoon depression and occurs at a higher latitude after airstream A interacts with the easterly trades.

One day after the formation of the pre-TY Ketsana monsoon depression, airstream A continues to flow into the southern quadrant of the monsoon depression near 14°N, 133°E (Figure 41a). Incidentally, the northern portion of airstream B is also flowing into the southeastern quadrant of the monsoon depression. Note also the trade easterlies to the north of the circulation wrap around the western quadrant of the circulation to then merge with airstream A. This is in contrast to the monsoon depression transitions described

above in which the trade easterlies interacted with the monsoon depression circulation to create a confluent region on the eastern side. In addition to the central vorticity maximum, multiple vorticity maxima are imbedded in the easterlies that contribute to a broad region of cyclonic relative vorticity with a northwest to southeast orientation. The wave-activity flux convergence at this time is along the southern and western quadrants of the monsoon depression where the largest inward-directed wave-activity flux from the south and southwest are found (Figure 41b). Smaller regions of both wave-activity flux convergence and divergence are found in the northeastern quadrant where airstream A is interacting with the easterly trades.

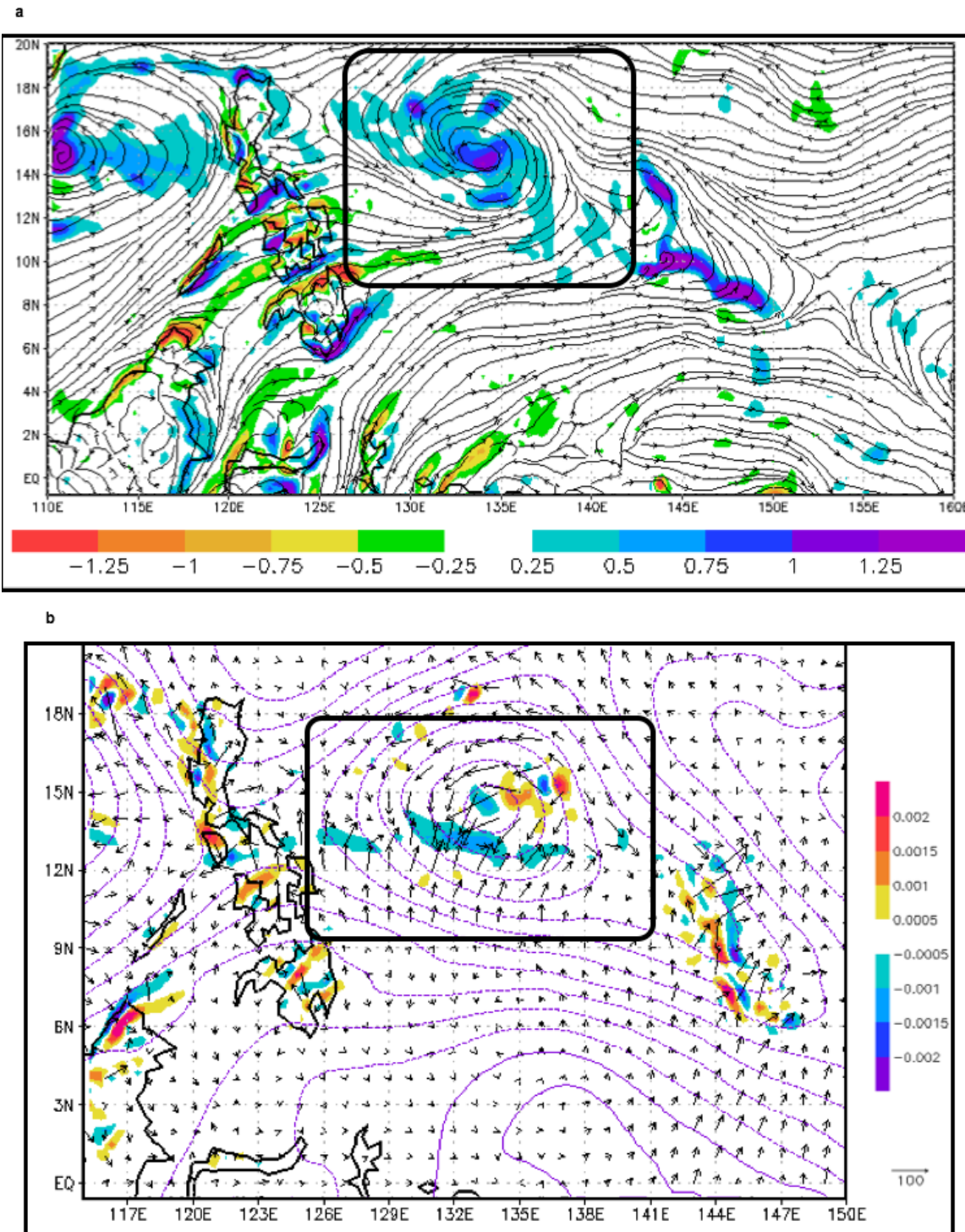


Figure 41. As in Figure 20 except for 1200 UTC 23 September with (a) streamlines and relative vorticity for the pre-TY Ketsana (17W) case with an interaction of airstream A and the trade easterlies. (b) Inward-directed wave-activity flux from the south-southwest leading to wave-activity flux convergence over the southern portion of the circulation.

At 0000 UTC 24 September (Figure 42a), an elongated band of cyclonic vorticity has developed on the southwestern and southern quadrants of the monsoon depression that correspond to the region of wave-activity flux convergence from a day earlier (Figure 41a). This vorticity band now extends to just south of the circulation center, which is elongated to the southeast where another vorticity maximum is analyzed. Inward-directed wave-activity flux has continued along the southern and southwestern quadrants, and now inward-directed wave-activity flux has developed in the northern quadrant (Figure 42b). Thus, the region of wave-activity flux convergence corresponds well with the region of maximum vorticity in Figure 42a, which enhances the western and southern portions of the circulation. Consequently, the elongated vorticity maximum constricted and became the center of the pre-tropical cyclone seedling, and the JTWC issued a TCFA at 0430 UTC 24 September. This trend in wave-activity flux, convergence from the south and southwest and from the north continues through tropical cyclone formation with the first JTWC warning valid at 0000 UTC 25 September.

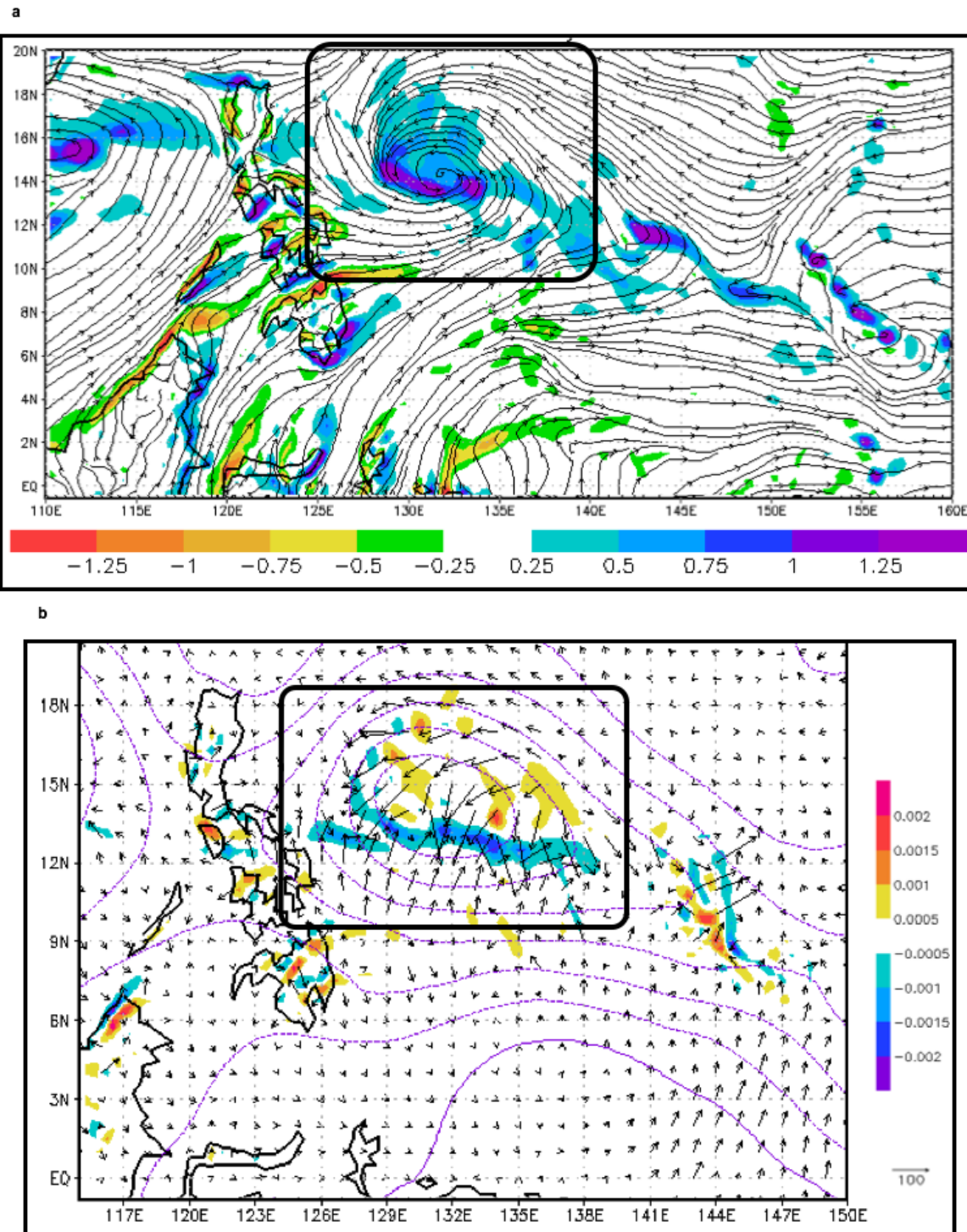


Figure 42. As in Figure 20 except for 0000 UTC 24 September with (a) streamlines and relative vorticity just 4.5 hours prior to JTWC issuing a TCFA for pre-TY Ketsana. (b) Inward-directed wave-activity flux vectors are found on the northern and southern sides of the maximum vorticity band and are favorable for spin-up.

Compared to the conceptual model in Chapter IV.C.1, based on the pre-TY Man-Yi monsoon depression transition, the wave-activity flux associated with the principle airstream A occurs at a higher latitude. As in the pre-TY Man-Yi conceptual model, the pre-TY Ketsana transition from a monsoon depression to a tropical cyclone was not solely due to the primary wave-activity flux that was associated with the cross-equatorial airstream A. Indeed, the wave-activity flux from the interaction with the trade easterlies played a large role as it contributed to amplification of the western vorticity maximum. Thus, pre-TY Ketsana developed in the western quadrant of the monsoon depression circulation where the maximum of wave-activity flux convergence was occurring (Figures 41b and 42b).

b. *Transition to a pre-tropical cyclone seedling with a primary airstream different from that during the monsoon depression formation*

(5) Pre-TY Molave (07W)

The pre-TY Molave (07W) monsoon depression is another example of an airstream C monsoon depression, but this monsoon depression transition differs from the MD₂ case in that the trade easterlies have a larger role.

As with the MD₂ transition that occurred between 5° and 10°N, the 850 hPa vorticity maximum for the pre-TY Molave monsoon depression was near 10°N. In contrast to the elliptical-shaped MD₂ the pre-TY Molave monsoon depression was circular, but several vorticity maxima interacted with the monsoon depression as it transitioned. The analysis of this transitioning monsoon depression will extend through the first warning as a tropical cyclone by the JTWC due to the interaction of another vorticity maximum, which will shift the center of the tropical cyclone northward away from the original monsoon depression vorticity maximum.

At 1200 UTC 14 July (Figure 43a), which is 84 hours after monsoon depression formation, a single, more circular vorticity maximum is analyzed at the center of the pre-TY Molave circulation. In addition to the cross-equatorial airstream B approaching from the south-southwest, airstream A approaches from the west. Note two regions of confluence, one with airstream B and the trade easterlies to the northeast of the

circulation center and the second to the northwest of center comprised of airstream A and the trade easterlies. Only a small region with inward-directed wave-activity flux vectors exists to the west of the monsoon depression, which may be attributed to the confluence of airstream A with the trade easterlies (Figure 43b). The more important factor at this time is the substantial outward-directed wave-activity flux toward the northeast on the eastern side of the monsoon depression, which indicates wave dispersion in association with the strong southeasterly trades rather than monsoon depression vorticity amplification. There is also some weak outward-directed wave-activity flux to the north (Figure 43b) toward the region of vorticity maxima along the northern periphery of the monsoon depression circulation (Figure 43a) that will result in vortex amplification of these northern vorticity maxima.

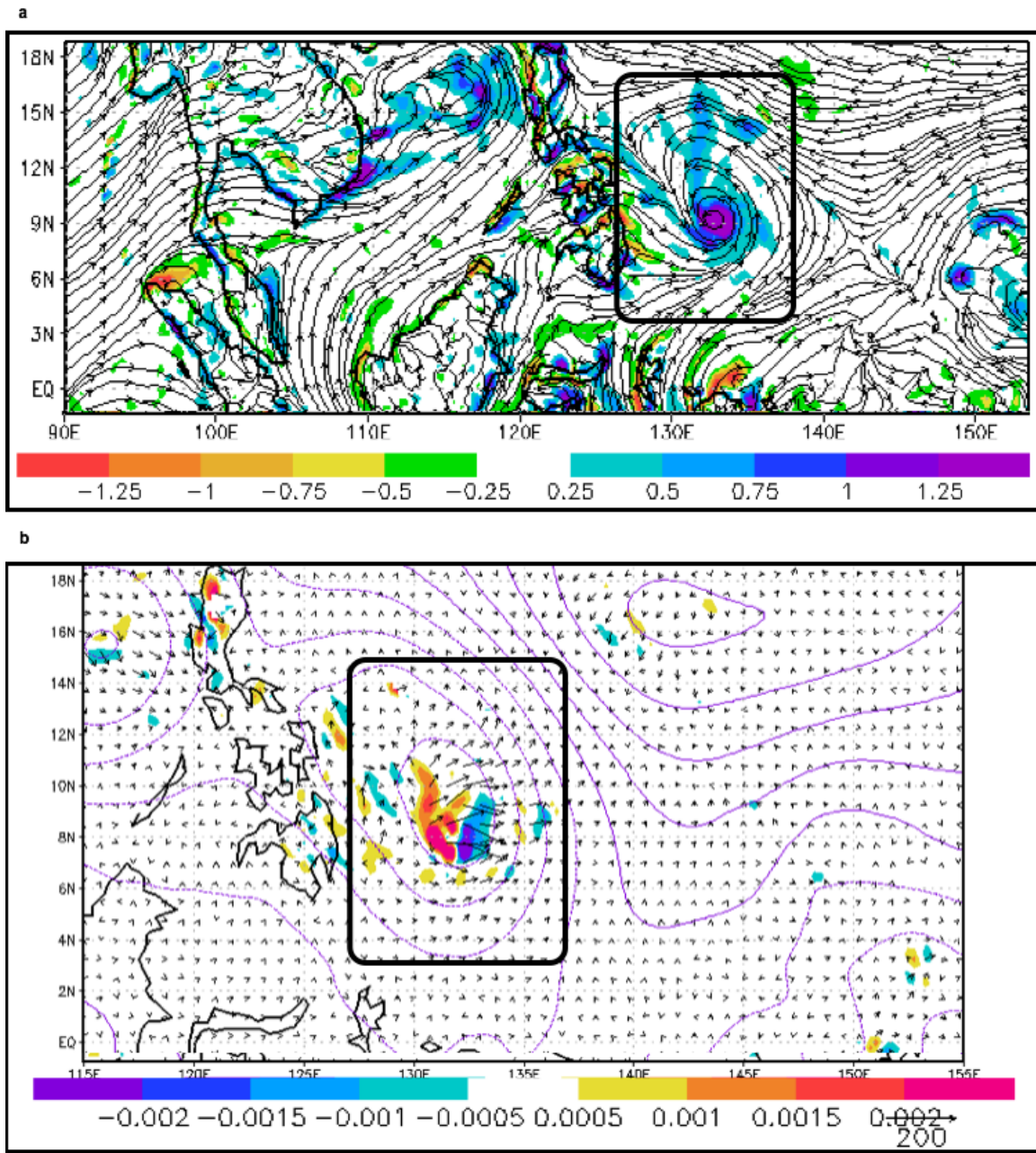


Figure 43. As in Figure 20 except at 1200 UTC 14 July with (a) streamlines and relative vorticity for a circular pre-TY Molave monsoon depression. (b) Corresponding wave-activity flux distribution.

At 1800 UTC 14 July (Figure 44a), the JTWC issued a TCFA for the pre-TY Molave monsoon depression. The circulation center cited in the TCFA is over the southern vorticity maximum of the monsoon depression (southern vorticity maximum near 10°N , 132°E), which also corresponds to a maximum in convection in the IR image (insert in Figure 44b). Note that a new airstream C is entering the southern region of the monsoon depression, where it is interacting with the westerly flow along a confluence line. Consequently, an elongated band of cyclonic vorticity extends through the southern region. To the north of the monsoon depression and extending northward to the eastern side of the second circulation, outward-directed wave-activity flux vectors are contributing to flux divergence (Figure 44b) and thus vorticity amplification is not expected in the vorticity lobes in those regions. Only a small wave-activity flux convergence is associated with the central vorticity maximum in the pre-TY Molave monsoon depression.

The new focus is on the second smaller circulation with the vorticity maximum to the north (near 14°N , 129°E), which also has a maximum of convection in the IR imagery. Beginning at 1200 UTC 14 July (Figure 43b), wave-activity flux convergence has been occurring along the southeasterly trades in association with the outward-directed wave-activity flux vectors from the eastern side of the monsoon depression being opposed by wave-activity flux vectors toward the southwest from a small circulation near 17°N , 142°E . Although not well displayed in Figure 44b due to scaling of the vectors, this wave-activity flux convergence has continued from the two sets of opposing wave-activity flux vectors, which is leading to vorticity amplification to the northwest of the monsoon depression.

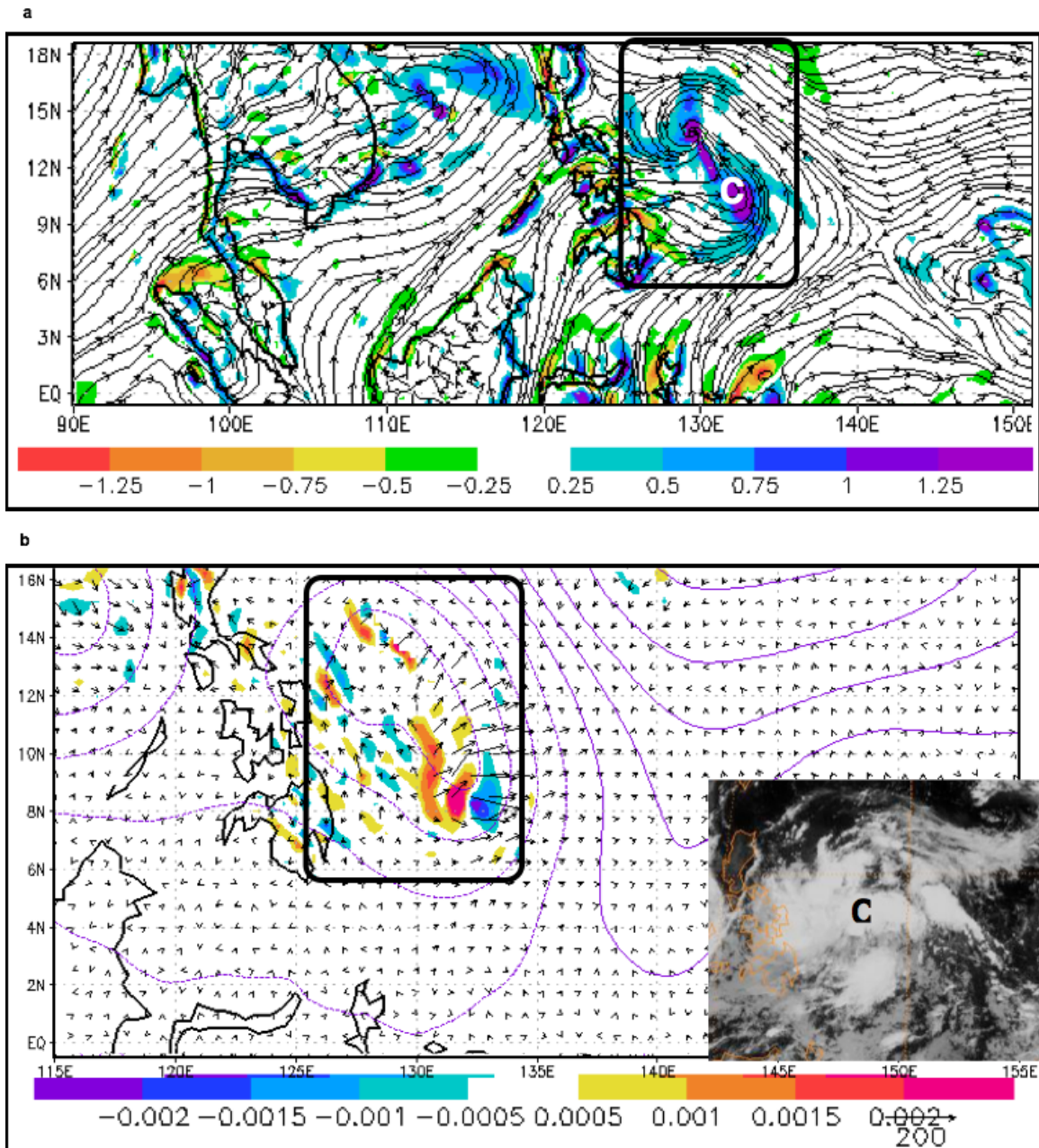


Figure 44. As in Figure 20 except at 1800 UTC 14 July with (a) streamlines and relative vorticity for the pre-TY Molave monsoon depression. C indicates the center based on the JTWC TCFA issued at this time. (b) Corresponding wave-activity flux distribution and IR satellite image annotated with the center as defined by the TCFA.

At 0000 UTC 15 July (Figure 45a), the northern vorticity maximum in the 1800 UTC 14 July analysis (Figure 44a) has become the dominate feature, and this circulation will become the pre-TY Molave pre-tropical cyclone seedling as indicated in the convective pattern (inset Figure 45b). Indeed, the center of the circulation in the ECMWF analysis, and in IR imagery (inset Figure 45b) has shifted to the north (near 14°N, 129°E) as the pre-tropical cyclone seedling continues to transition. This vorticity amplification is attributed to the large wave-activity flux convergence between the wave-activity fluxes toward the northeast from the monsoon depression wave dispersion being opposed by wave-activity fluxes toward the southwest from the small circulation farther to the northeast (Figure 45b). Note that the largest region of wave-activity flux convergence is near 13.5°N, 133.5°E. During the past 12 hours, this small circulation has weakened – presumably owing to wave-dispersion effects. Similarly, the outward-directed wave-activity flux to the east has resulted in the decrease of the central vorticity maximum in the monsoon depression.

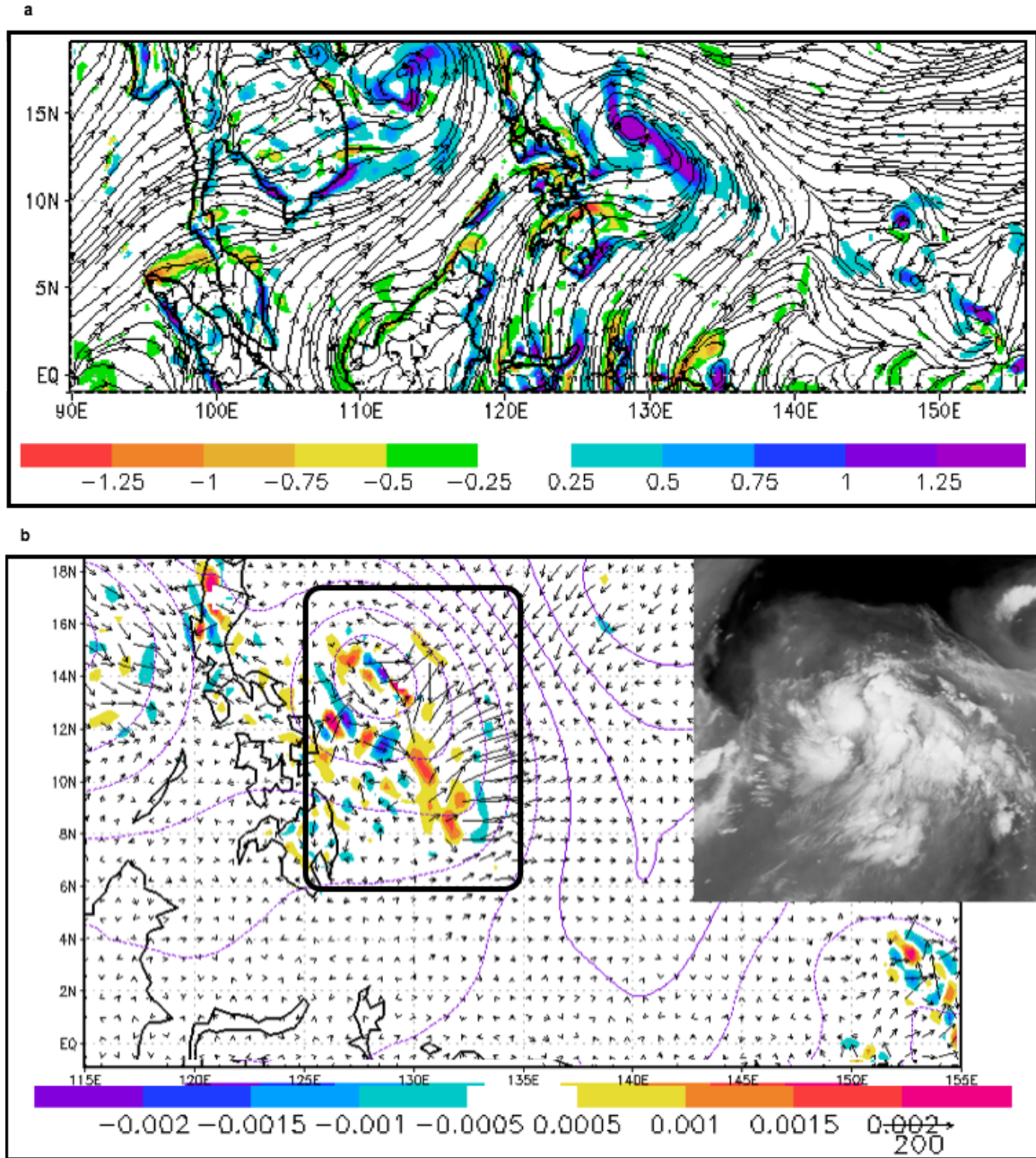


Figure 45. As in Figure 20 except at 0000 UTC 15 July with (a) streamlines and relative vorticity for the pre-TY Molave pre-tropical cyclone seedling. (b) Corresponding wave-activity flux distribution and IR satellite image.

Finally, at 0600 UTC 15 July (Figure 46a), which corresponds to the valid time of the first JTWC warning as TD 07W, the pre-TY Molave circulation has fully transitioned to a tropical cyclone. Note that the maximum of wave-activity flux convergence well to the northwest of the monsoon depression center in response to the broad, southeast-northwest extent of opposing wave-activity flux vectors. Thus, the amplification of a circulation well to the northwest of the center of the monsoon depression is not so much a propagation of a wave in the easterlies; rather, the apparent propagation is a result of the rapid northwestward displacement of the region of maximum wave-activity flux convergence as the two circulations interact. While the circulation labeled in the TCFA is a result of an interaction of the monsoon depression with the easterlies, it is different from the other monsoon depression transitions because it is a result of an interaction with an adjacent circulation within the easterlies. In the other cases, the easterlies directly interact via amplification of a vorticity maximum within the original monsoon depression rather than along the outer circulation of the monsoon depression.

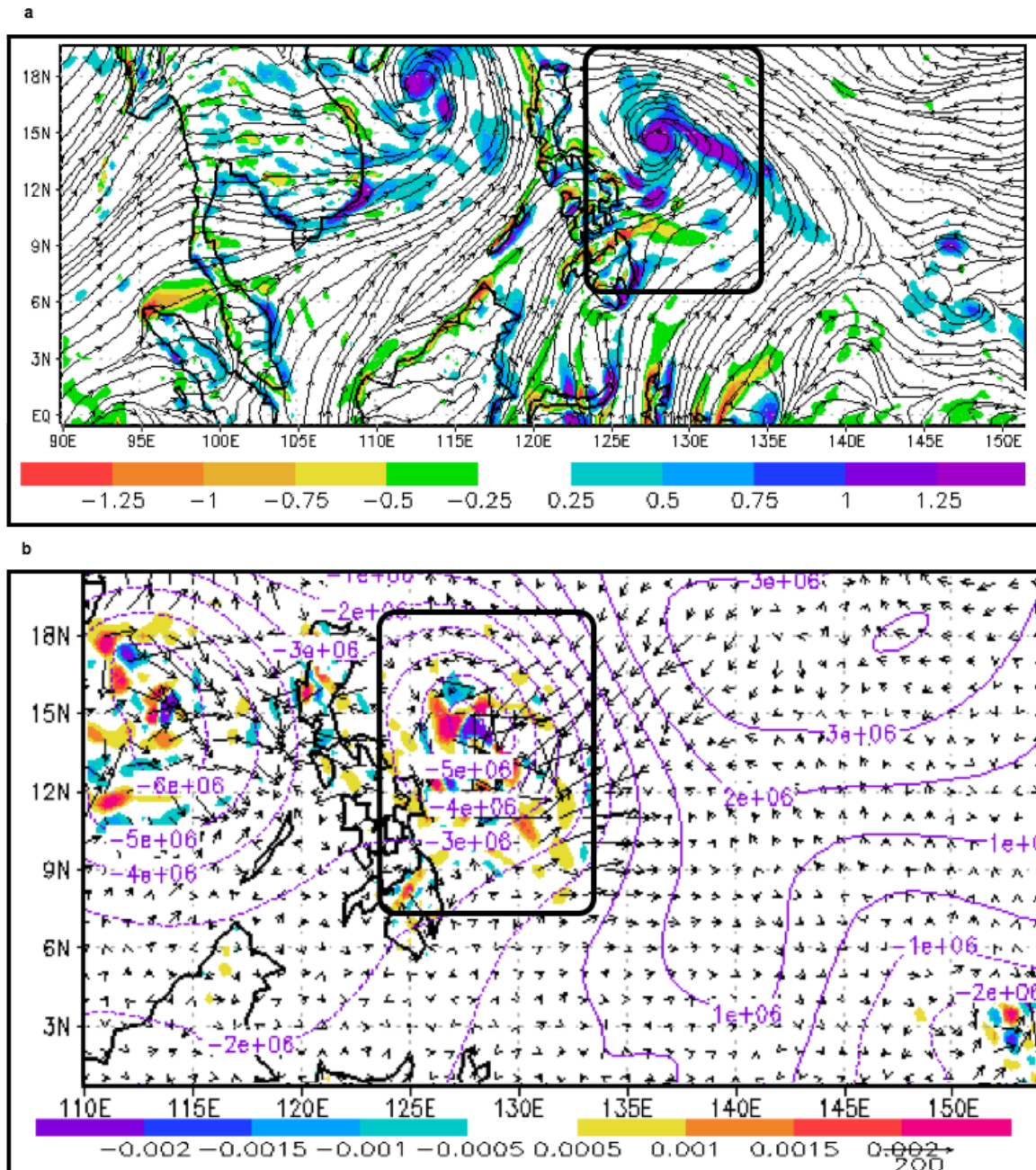


Figure 46. As in Figure 20 except at 0600 UTC 15 July with (a) streamlines and relative vorticity for the pre-TY Molave TD 07W. (b) Corresponding wave-activity flux distribution.

The pre-TY Molave monsoon depression took longer to transition (102 hours) to a tropical cyclone than did the pre-TY Man-Yi monsoon depression (42 hours). The wave-activity flux associated with the cross-equatorial flow did not persist from airstream C (or C_{SH}) into the monsoon depression, although it did persist into the southeast region. Wave-activity flux from the northwest in association with persistent confluence of trade easterlies with airstream A in the northwest quadrant of the monsoon depression also was not the primary effect. As indicated above, the amplification of the pre-TY Molave monsoon depression was a result of the rapid northwestward displacement of the region of maximum wave-activity flux convergence as a result of interaction of the monsoon depression with an adjacent circulation in the trade easterlies. Thus, the amplification of a vorticity maximum is along the outer circulation of the monsoon depression rather than within the monsoon depression.

(6) Pre-TS Soudelor (05W)

The pre-TS Soudelor monsoon depression is another example of an airstream C monsoon depression with an elliptical shape. This monsoon depression transition differs from the MD₂ case in that the primary airstream C did not persist into the region of the monsoon depression after formation at 0000 UTC 4 July. Furthermore, the transition of this monsoon depression to a pre-tropical cyclone seedling occurred north of 15°N almost six days after the monsoon depression formation. It will be demonstrated that inward-directed wave-activity flux developed around 0000 UTC 6 July from interaction of the trade easterlies with an airstream A. Prior to that time, the wave-activity flux vectors were outward-directed, and thus were not contributing to flux convergence and vorticity amplification.

This case study begins at 1200 UTC 7 July, which is several hours after inward-directed wave-activity flux resumed (Figure 47a). By this time, the monsoon depression had a broad circulation with a center near 15°N, 127°E. While a broad vorticity maximum was associated with the circulation center, a second region of cyclonic vorticity is analyzed to the east-southeast of the circulation where an airstream B was interacting with the trade easterlies. Farther north, the trade easterlies comprise the northern part of the circulation and wrap around the western quadrant. As indicated

above, inward-directed wave-activity flux from the northeast is occurring at this time (Figure 47b) along with a small inward-directed flux from the southeast. However, small outward-directed wave-activity flux toward the west will tend to inhibit spin-up of the monsoon depression circulation.

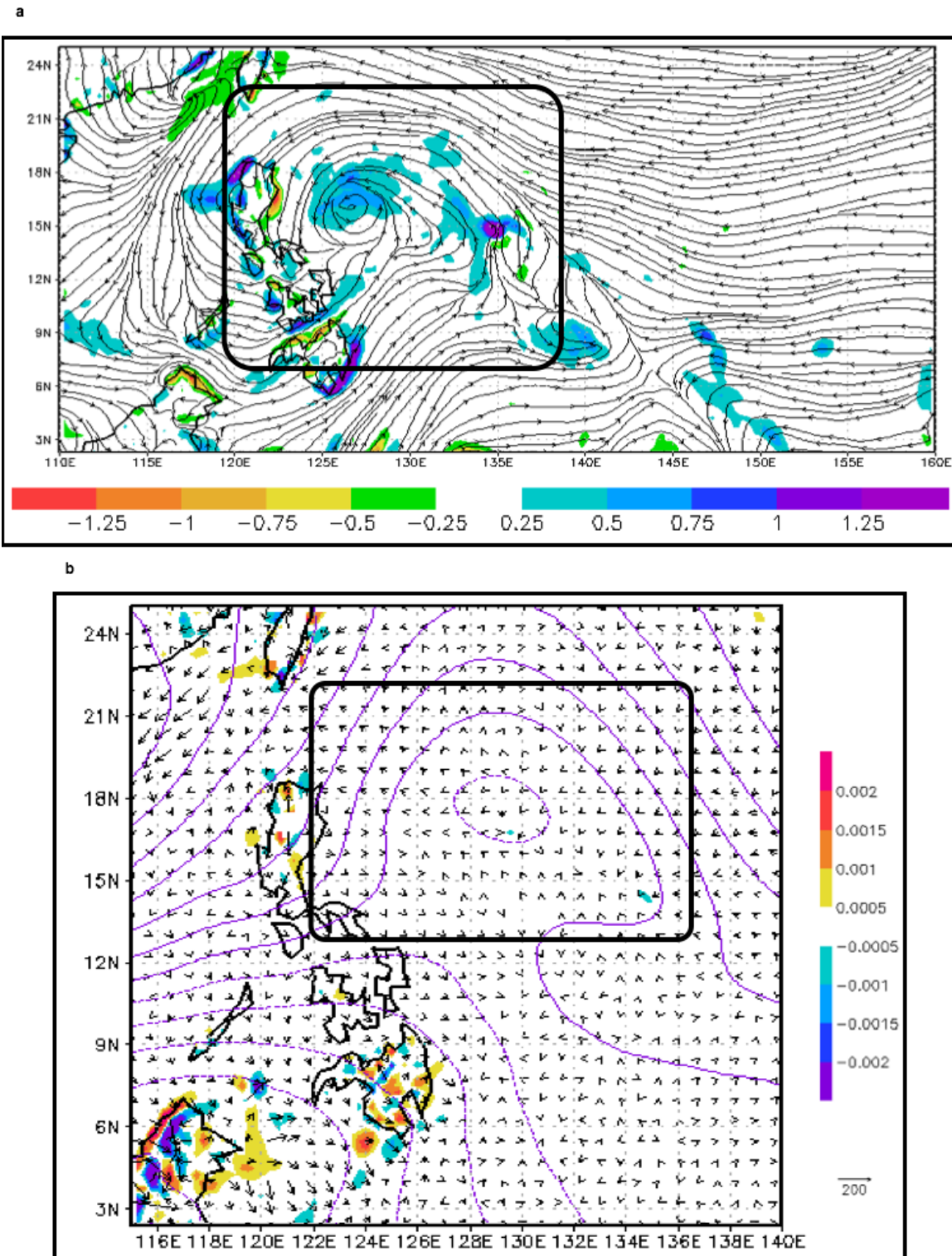


Figure 47. As in Figure 20 except at 1200 UTC 7 July with (a) streamlines and relative vorticity for the pre-TS Soudelor monsoon depression. (b) Corresponding wave-activity flux shows inward-directed flux vectors from the northeast and southeast.

At 0000 UTC 8 July, the monsoon depression is more elliptical and more compact with an eastern and a western vorticity maximum on either side of the circulation center (Figure 48a). The trade easterlies have completely wrapped around the circulation, which therefore appears to be an independent system. Inward-directed wave-activity flux is analyzed from the east and northeast (Figure 48b), which contributes to wave-activity flux convergence in the region of the eastern vorticity maximum. Even larger values of outward-directed wave-activity flux are analyzed in the northwest quadrant of the monsoon depression, which is an indication of wave dispersion. However, a region of inward-directed wave-activity flux from the west is analyzed just to the south of the outward-directed flux.

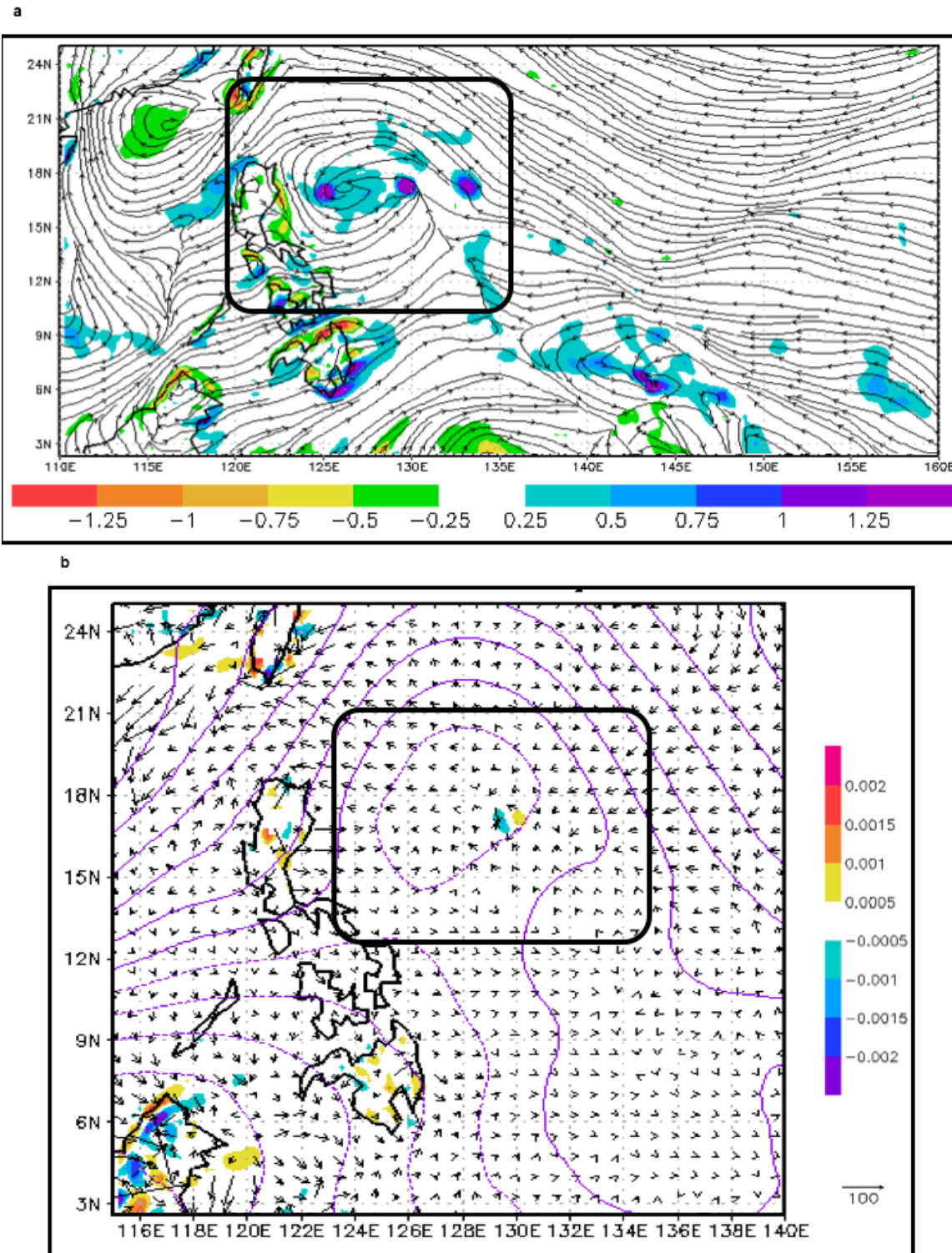


Figure 48. As in Figure 20 except at 0000 UTC 8 July with (a) streamlines and relative vorticity for the pre-TS Soudelor monsoon depression. (b) Corresponding wave-activity flux distribution.

At 1200 UTC 8 July, the ECMWF analysis has a considerably decreased size of the monsoon depression and has a vorticity maximum at the center near 16°N, 124°E (Figure 49a). Overall, the circulation appears to be losing the characteristics of a monsoon depression and becoming more like a broad tropical cyclone. The inward-directed wave-activity flux from the east and northeast has increased substantially and penetrates to the circulation center (Figure 49b). Similarly, the inward-directed wave-activity flux in the southwest quadrant has increased in magnitude and overall extent, and small inward-directed flux is detected in the southeast quadrant. Although the shading scale in Figure 49b does not indicate large amounts of convergence, this convergence can be inferred from the direction and length of the vectors entering the monsoon depression circulation from the northeast, southeast, southwest, and all of these fluxes converge in the same region as the vorticity maximum. While the outward-directed wave-activity flux continues in the northwest quadrant, the flux divergence is displaced from the circulation center.

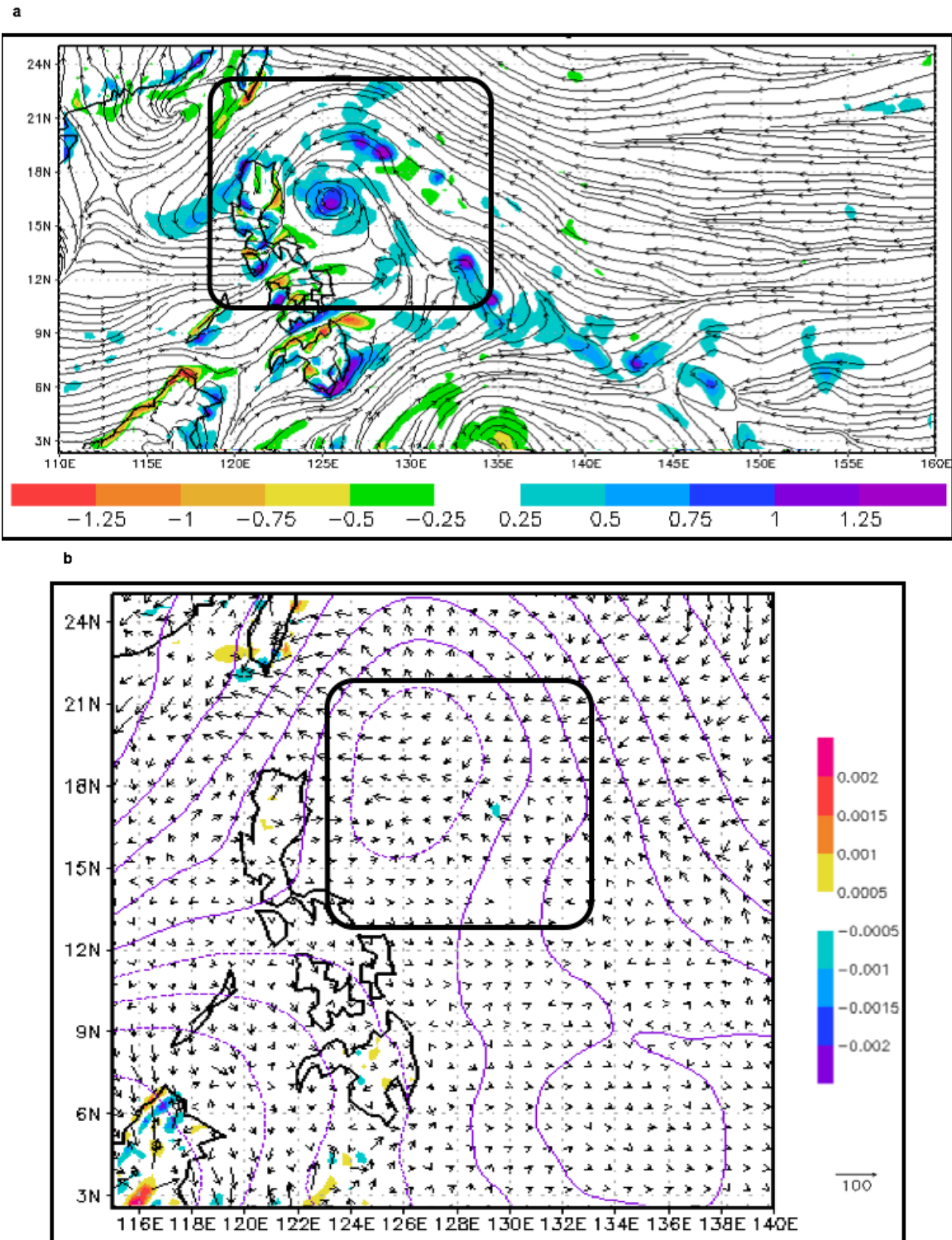


Figure 49. As in Figure 20 except at 1200 UTC 8 July with (a) streamlines and relative vorticity for the pre-TS Soudelor monsoon depression. (b) Corresponding wave-activity flux distribution.

At 0000 UTC 9 July (Figure 50a), which is just six hours prior to the JTWC issuing the TCFA at 0600 UTC 9 July, the reduction in the size of the circulation and the collocated vorticity maximum indicate the monsoon depression is becoming a pre-tropical cyclone seedling. Indeed, the pre-TS Soulelor monsoon depression would become a tropical cyclone at 1200 UTC 9 July according to the JTWC. Although the inward-directed wave-activity flux from the west has become very small, inward-directed wave-activity flux from the northeast and southeast has increased and continues to converge over the center of the circulation (Figure 50b). While the outward-directed wave-activity flux to the northwest has continued, it is offset by the inward-directed wave-activity flux into the eastern half of the circulation.

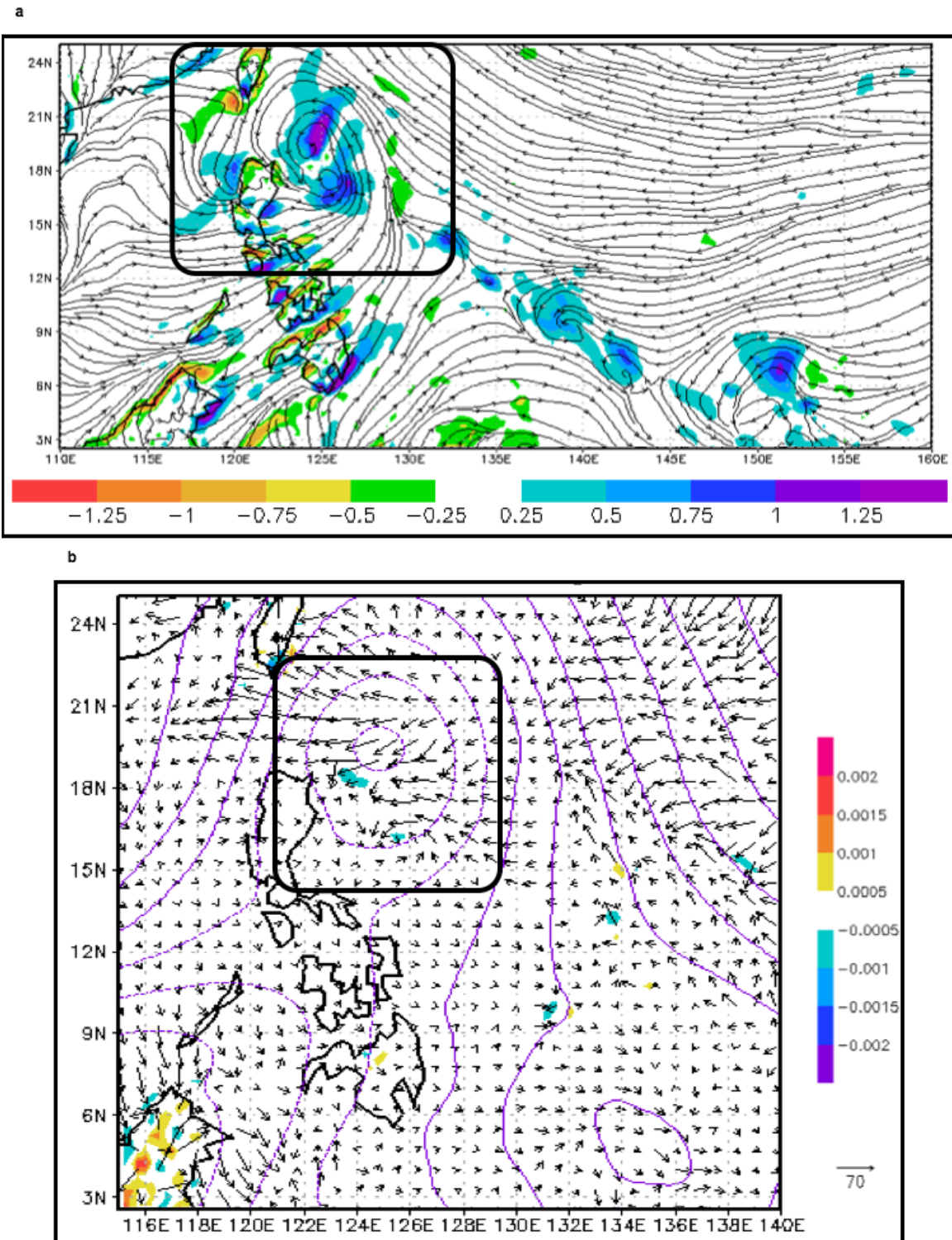


Figure 50. As in Figure 20 except at 0000 UTC 9 July with (a) streamlines and relative vorticity for the pre-TS Soudelor. (b) Corresponding wave-activity flux distribution.

In summary, there are several reasons why the same cross-equatorial airstream C that led to the formation of the pre-TS Soudelor monsoon depression was not the primary airstream in the transition, and also why the pre-TS Soudelor monsoon depression took much longer (138 hours) to transition to a tropical cyclone than did the pre-TY Man-Yi (42 hours) monsoon depression. Due to the length of time from monsoon depression formation to transition to a pre-tropical cyclone seedling, the monsoon depression was able to move northward, which removed the circulation from the original cross-equatorial airstream C. Thus, it is not surprising that the wave-activity flux associated with the cross-equatorial airstream C could not be sustained over such a large distance from the Equator. In fact, the inward-directed wave-activity flux stopped for 48 hours after formation of the monsoon depression.

As indicated in Figures 47b through 50b, the primary inward-directed wave-activity flux was from the east and northeast due to the interaction with the trade easterlies. Even the inward-directed wave-activity flux from the southeast in Figure 50b was associated with an airstream B than the original airstream C. Another unique aspect of the transition of the pre-TS Soudelor monsoon depression was the requirement to offset the large outward-directed wave-activity flux toward the northwest that was associated with wave dispersion from the large monsoon depression. Thus, the long time after monsoon depression formation for the transition to a pre-tropical cyclone seedling and resulting tropical cyclone to occur was a result of the persistence of the trade easterlies. It is uncertain whether the additional inward-directed wave-activity flux from the southeast in Figure 50b associated with airstream B was coincidental (or instrumental) in the contraction of the monsoon depression and thus the transition to a pre-tropical cyclone seedling.

(7) Pre-TY Koppu (16W)

The transition of the pre-TY Koppu (16W) monsoon depression is another example of a higher latitude (between 10° and 20°N) transition, except for an airstream B monsoon depression. This pre-TY Koppu transition case is a “hybrid” case in the sense that the airstream B did continue after the formation of the monsoon depression (0600 UTC 10 September) through the time of transition to tropical cyclone (0000 UTC 13

September). However, it is included in this second group of transitions because the contribution of the airstream B was minor compared to an airstream A and the important role of the trade easterlies in the transition of pre-TY Koppu.

Already at 0000 UTC 11 September, which is only 18 hours after monsoon depression formation, three vorticity maxima are analyzed along the central axis of the monsoon depression (Figure 51a). The original airstream B that led to the monsoon depression formation is interacting with the trade easterlies to amplify the vorticity maxima in the eastern quadrant of the circulation. However, an airstream A is flowing into the southwest quadrant of the circulation and interacting with the trade easterlies to amplify the vorticity maximum. The third vorticity maximum in the northwest quadrant of the monsoon depression circulation is associated with a wave in the trade easterlies. The largest inward-directed wave-activity flux (Figure 51b) is from the south-southwest and is contributing substantial wave-activity flux convergence (and thus amplification) over the central vorticity maximum in Figure 51a. Another region of inward-directed wave-activity flux from the northeast is contributing to amplification of the eastern-most vorticity maximum. Although it does not impact the monsoon depression circulation, there is an outward-directed wave-activity flux to the northwest over the South China Sea. There is only small outward-directed wave-activity flux to the north in association with the wave in the easterlies along the northern side of the monsoon depression.

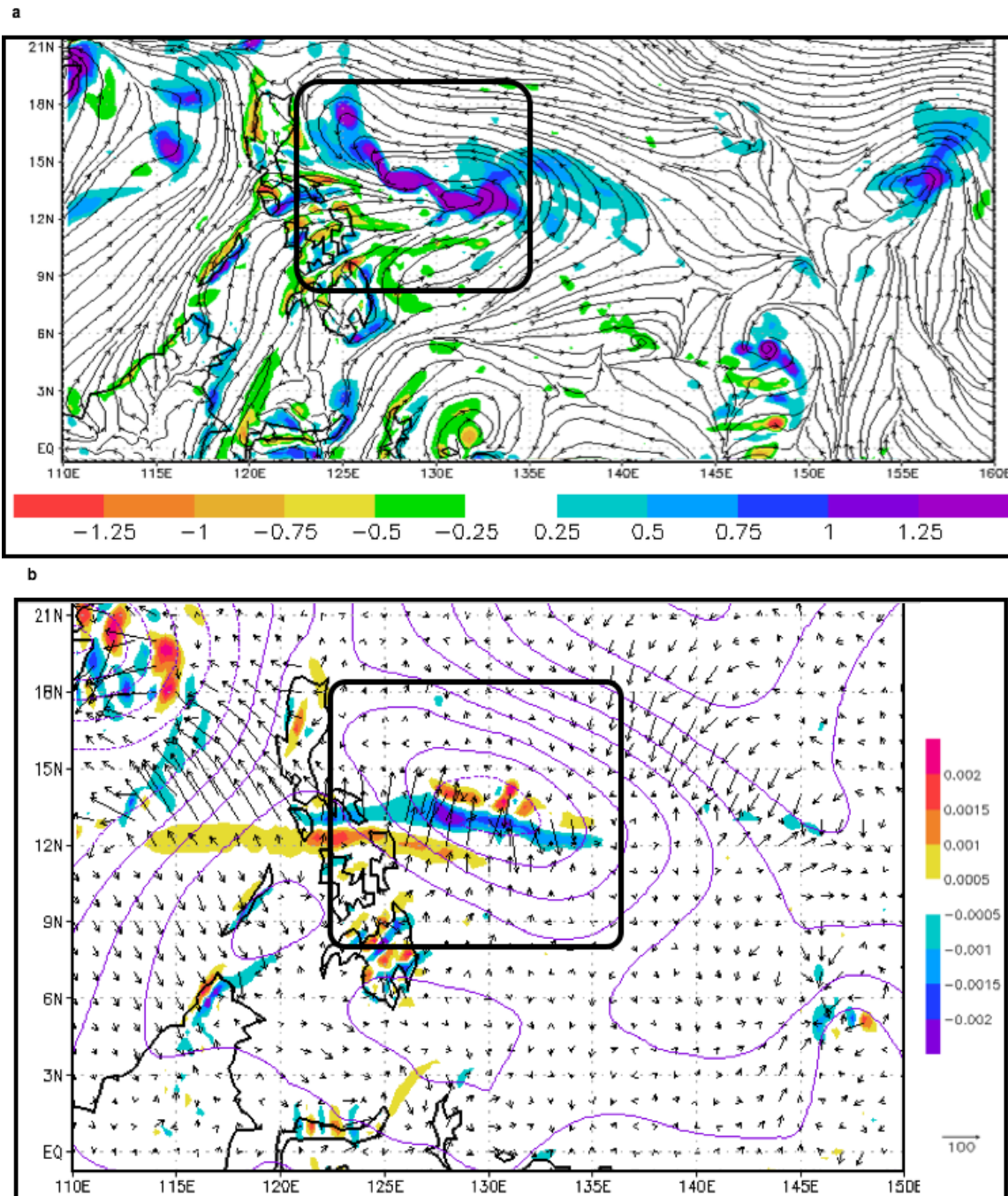


Figure 51. As in Figure 20 except at 0000 UTC 11 September with (a) streamlines and relative vorticity for the pre-TY Koppu monsoon depression. (b) Corresponding wave-activity flux distribution.

At 1200 UTC 11 September, the pre-TY Koppu monsoon depression has become more circular (Figure 52a) and has consolidated around the central vorticity maximum in Figure 51a. A broad region of cyclonic vorticity is associated with the central region of the circulation, and multiple vorticity maxima are embedded within this region. The wave-activity flux (Figure 52b) into the circulation from the northeast is now penetrating toward the center, and thus is also contributing to flux convergence and amplification of the vorticity maximum within the broad region of cyclonic vorticity in Figure 52a. The large wave-activity flux from the south is contributing to large values of wave-activity flux convergence over the central vorticity maximum. Although some outward-directed wave-activity flux is analyzed in the northwestern quadrant, it is so small relative to the inward-directed wave-activity flux that it will not act to inhibit the spin-up of the circulation (Figure 52b).

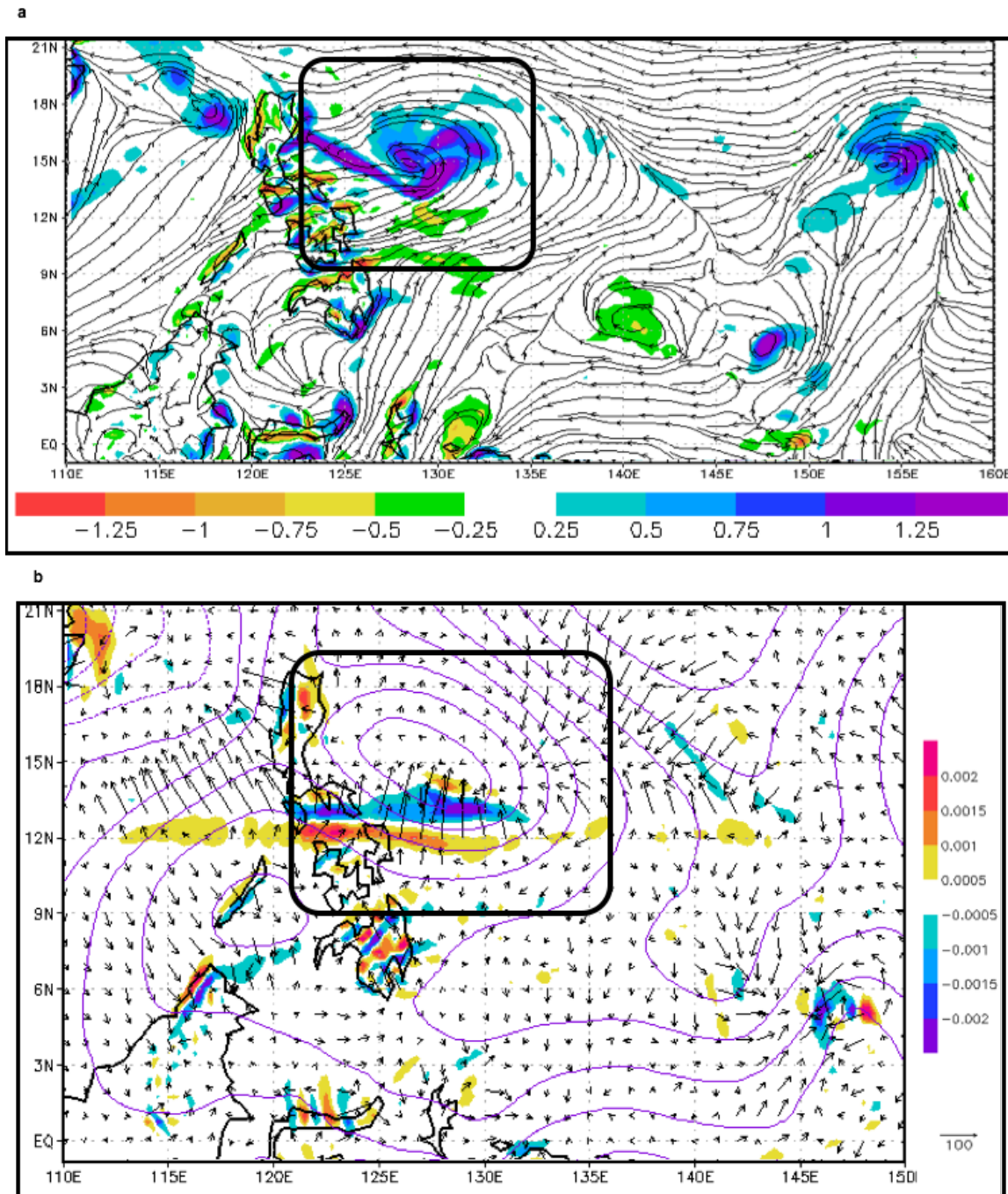


Figure 52. As in Figure 20 except at 1200 UTC 11 September with (a) streamlines and relative vorticity for the pre-TY Koppu monsoon depression. (b) Corresponding wave-activity flux distribution.

At 0000 UTC 12 September, which is only two hours before the JTWC issued a TCFA (0200 UTC 12 September), the monsoon depression is becoming a pre-tropical cyclone seedling (Figure 53a). While the characteristics of the monsoon depression circulation have become more like a tropical cyclone circulation than a monsoon depression, the first warning issued by the JTWC was not until 0000 UTC 13 September. Note that the circulation has further consolidated around the central region, but there are two vorticity bands to the north and south. Until these bands become axisymmetric about the center, the transition to a tropical cyclone will not be complete. Although outward-directed wave-activity flux is analyzed in the western quadrant, it is remote from the center and thus is not inhibiting spin-up of the vortex. Large values of inward-directed wave-activity flux are now analyzed from the southeast through the northeast quadrants (Figure 53b). Therefore, the wave-activity flux convergence is occurring over the central vorticity maximum near the center of the circulation, which is contributing to the transition to a pre-tropical cyclone seedling.

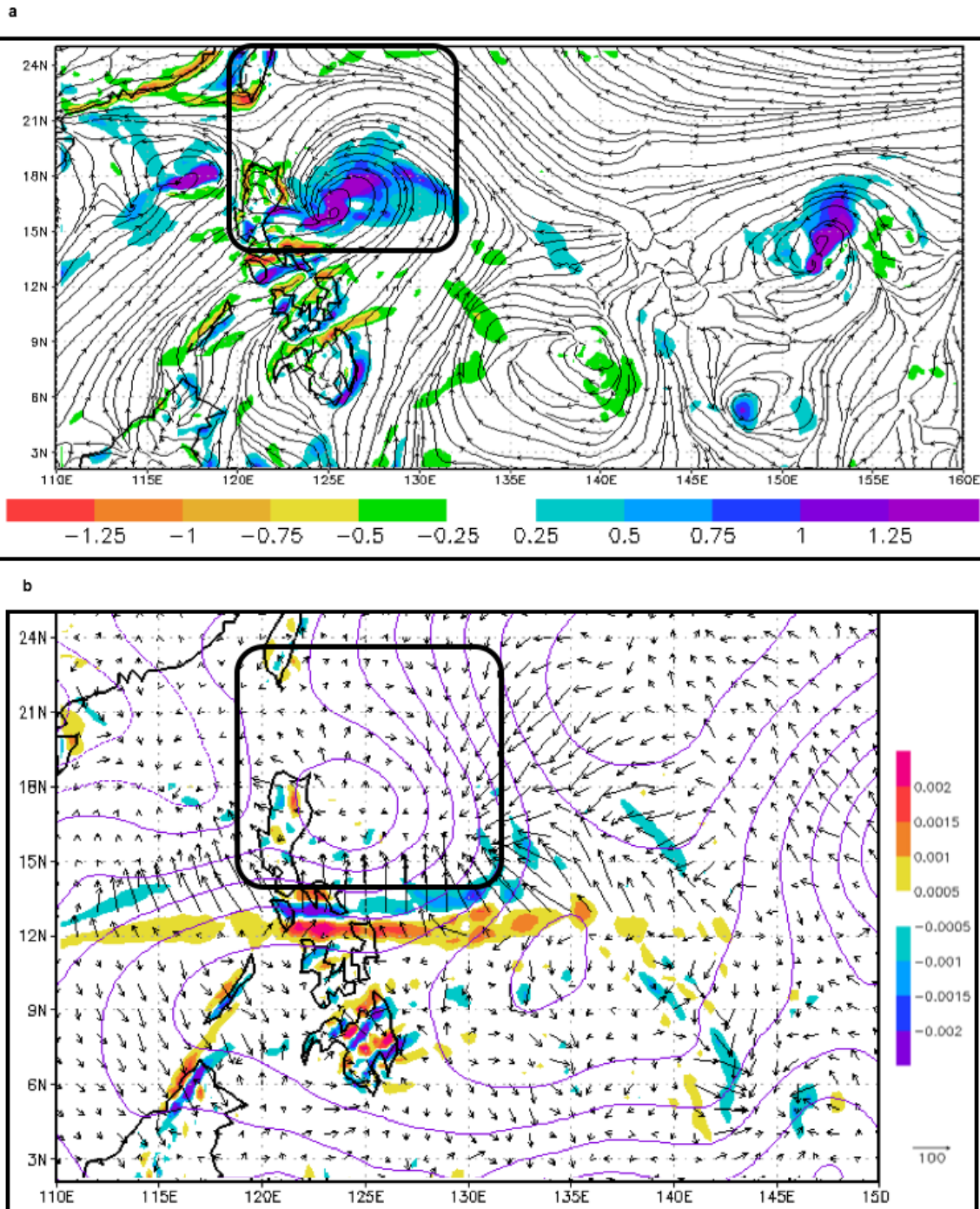


Figure 53. As in Figure 20 except at 0000 UTC 12 September with (a) streamlines and relative vorticity for the pre-TY Koppu monsoon depression. (b) Corresponding wave-activity flux distribution.

As indicated at the beginning of this pre-TY Koppu monsoon depression case study, this is a hybrid transition as the original airstream B that led to monsoon depression formation persisted, but was not the primary airstream leading to the transition. Rather, an airstream A interacting with the trade easterlies was the primary factor in the transition. Consequently, the pre-TY Koppu monsoon depression transition occurred at a higher latitude than in the pre-TY Man-Yi-based conceptual model (Figure 25), and in addition took longer to transition (66 hours) to a tropical cyclone than the pre-TY Man-Yi (42 hours). While this transition did have the persistent wave-activity fluxes from multiple directions as in the pre-TY Man-Yi case, the magnitudes of the wave-activity fluxes over a complete semicircle (Figure 53b) were noteworthy in consolidating the circulation, which thus facilitated the transition to a pre-tropical cyclone seedling.

(8) Pre-Super TY Parma (19W)

The pre-Super TY Parma (19W) monsoon depression was an airstream C_{*} monsoon depression. The transition of the pre-Super TY Parma monsoon depression transition is one where the primary interaction is an airstream A₂ interacting with the easterly trades. In contrast to the hybrid pre-TY Koppu transition, the pre-Super TY Parma transition occurred at a low latitude as the 850 hPa vorticity maximum was near 10°N. Another interesting aspect was the JTWC did not issue a TCFA for this case, and instead provided a first warning at 1800 UTC 27 September.

At 1200 UTC 25 September, which is only 24 hours after monsoon depression formation, a central vorticity maximum is analyzed near the center of the circulation and airstream A₂ (as depicted in Figure 10) is the only cross-equatorial airstream interacting with the monsoon depression (Figure 54a). Note the western and eastern vorticity maxima imbedded in the monsoon depression circulation, and the northwest-southeast oriented confluence line between airstream A₂ and the trade easterlies to the northwest. Inward-directed wave-activity fluxes from the southwest occur along the confluence line (Figure 54b), as well as in the southern quadrant. However, outward-directed wave-activity fluxes are present in the northern and southeastern quadrants that are not favorable for vortex amplification.

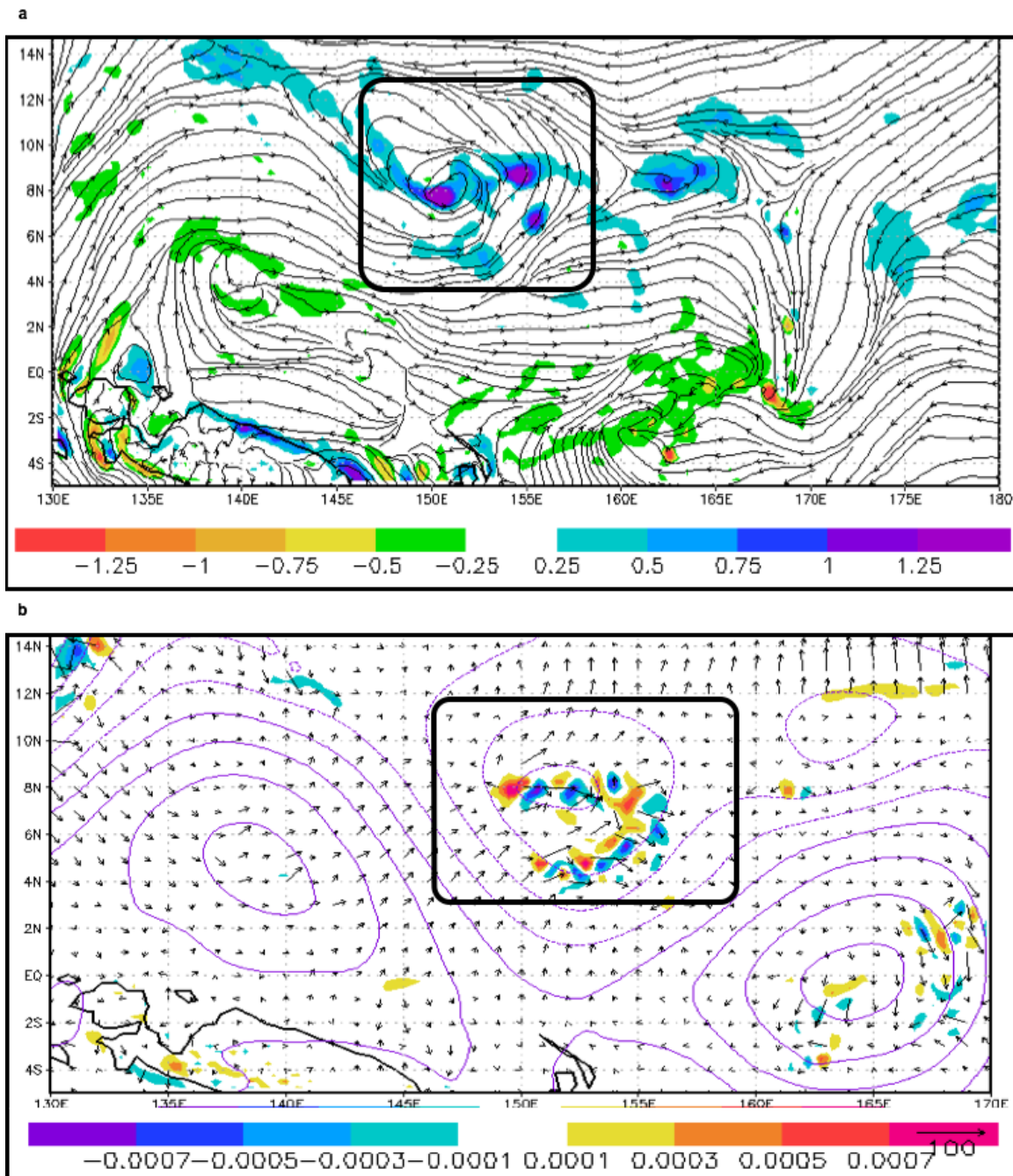


Figure 54. As in Figure 20 except at 1200 UTC 25 September with (a) streamlines and relative vorticity for the pre-Super TY Parma monsoon depression. (b) Corresponding wave-activity flux distribution.

At 0000 UTC 26 September (Figure 55a), the vorticity maximum has aligned with the circulation center, which was the western vorticity maximum of the monsoon depression in Figure 54a. The trade easterlies are continuing to interact with airstream A₂ along the confluence line to the northwest of the center. Because the airstream A₂ flows along the southern side of the circulation and does not wrap around the eastern side, the overall the circulation appears less well organized. The inward-directed wave-activity flux from the southwest continues (Figure 55b) and wave-activity flux convergence is analyzed near the area of the vorticity maximum in the western portion of the monsoon depression. However, outward-directed wave-activity flux to the north and southeast suggest negative impacts due to the resulting wave-activity flux divergence. Given both inward-directed and outward-directed wave-activity flux vectors, vortex spin-up is not as likely.

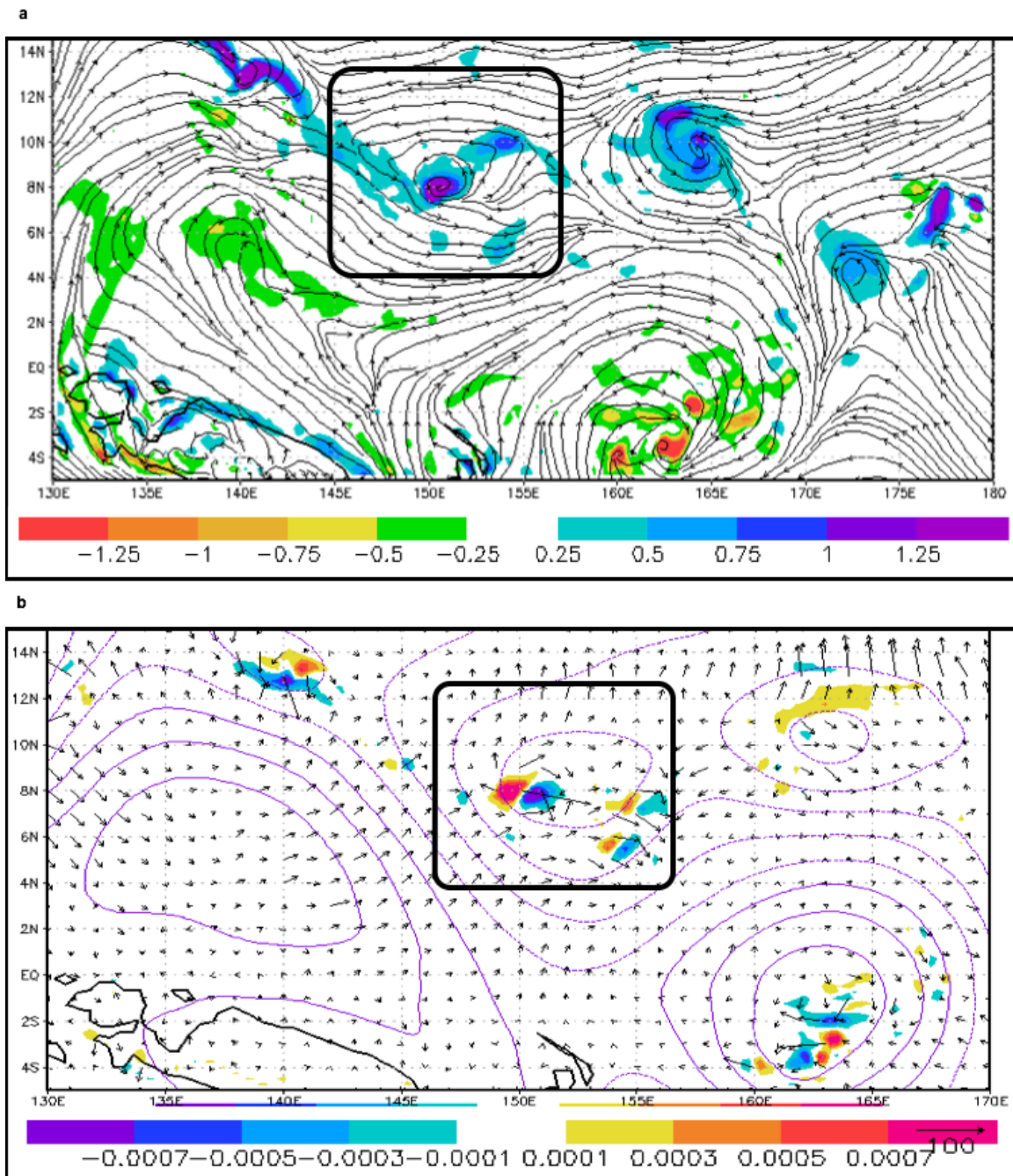


Figure 55. As in Figure 20 except at 0000 UTC 26 September with (a) streamlines and relative vorticity for the pre-Super TY Parma monsoon depression. (b) Corresponding wave-activity flux distribution.

At 1200 UTC 26 September (Figure 56a), the circulation is only slightly better organized as the trade easterlies do wrap around the western side and the central vorticity has increased. Note the pre-TD 18W circulation is starting to spin-up to the east of the monsoon depression. Inward-directed wave-activity flux from the southwest continues into the region of the vorticity maximum (Figure 56b), and the outward-directed wave-activity flux to the north and the southeast has decreased. Wave-activity flux from the east associated with pre-TD 18W has also begun, but it is not yet reaching the monsoon depression circulation. Consequently, the spin-up of the monsoon depression is only slightly more likely.

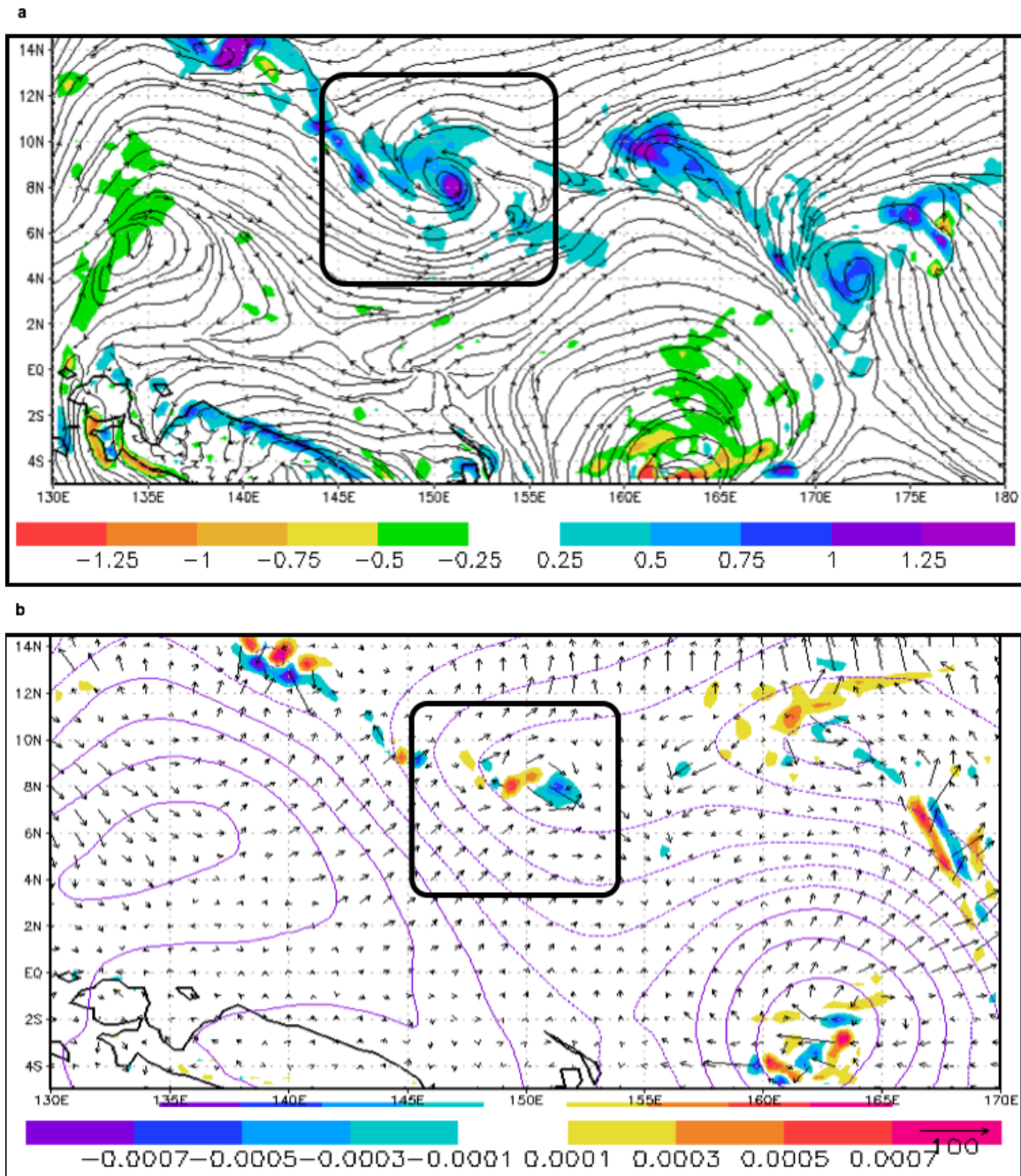


Figure 56. As in Figure 20 except at 1200 UTC 26 September with (a) streamlines and relative vorticity for the pre-Super TY Parma monsoon depression. (b) Corresponding wave-activity flux distribution.

At 0000 UTC 27 September, which is still 18 hours prior to the valid time of the first JTWC warning for this circulation, the monsoon depression has an additional vorticity maximum to the west of the circulation center (Figure 57a). While a vorticity band also extends eastward from the circulation center due to the horizontal shear between the trade easterlies and airstream A, that airstream does not wrap around the east side of the circulation as would be expected for a vortex spin-up. The areal extent of inward-directed flux vectors from the southwest has increased and only small outward-directed wave-activity flux vectors to the north remain (Figure 57b). Thus, convergence of wave-activity flux continues over the region of the western vorticity maxima. Some small wave-activity flux vectors from the pre-TD 18W to the east were also inward-directed toward the pre-Super TY Parma monsoon depression. Just as the signature of wave-activity fluxes in this pre-Super TY Parma case is less well defined than in the pre-TS Soudelor case (compare Figures 57b and 50b), the indications of a vortex spin-up from analyses such as Figure 57a (or satellite imagery) must have not been sufficient for the JTWC to issue a TCFA at this time. Instead, JTWC went directly to the first warning for the pre-Super TY Parma at 1800 UTC 27 September.

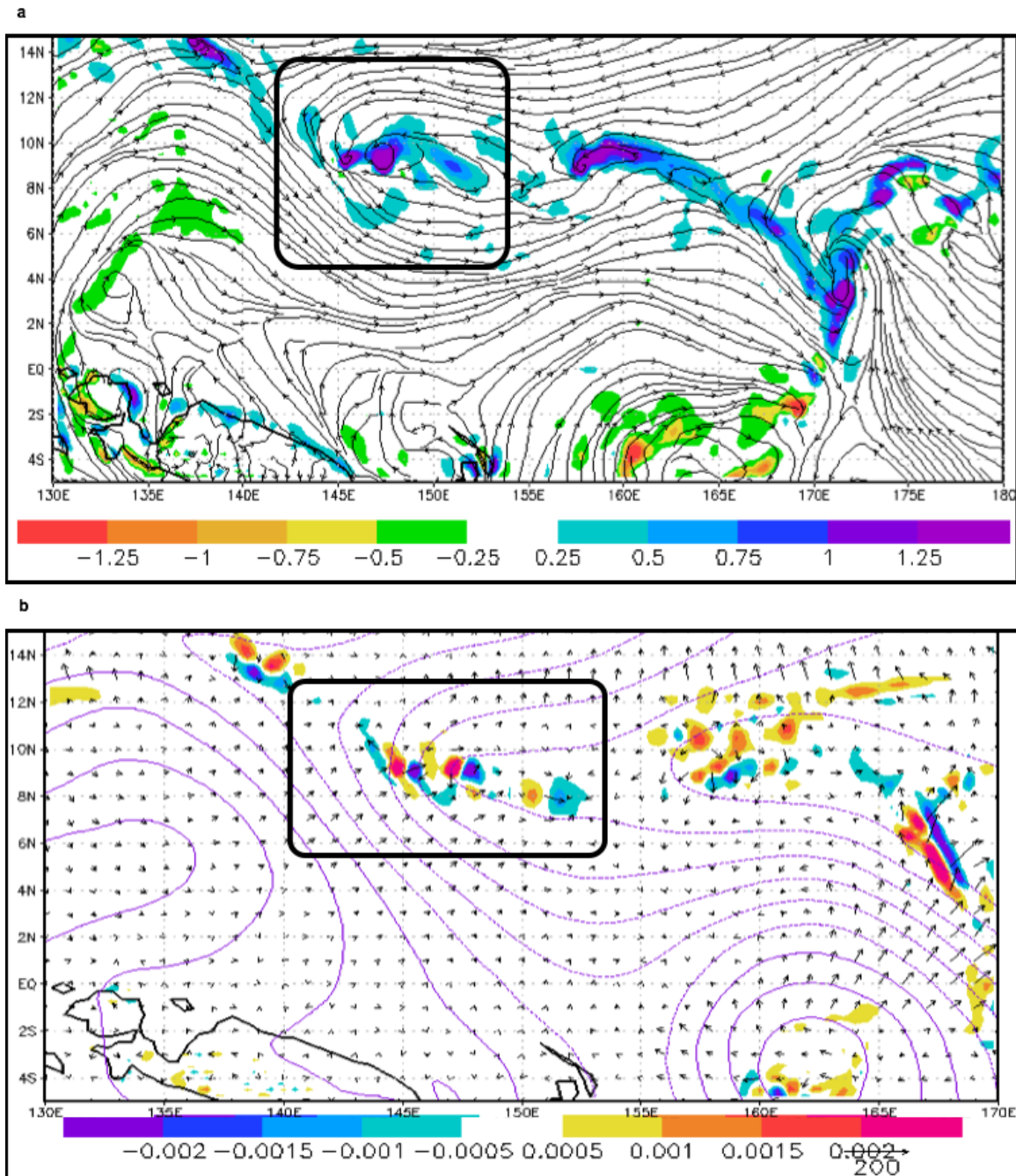


Figure 57. As in Figure 20 except at 0000 UTC 27 September with (a) streamlines and relative vorticity for the pre-Super TY Parma circulation. (b) Corresponding wave-activity flux distribution. Note that the scale for the wave-activity flux convergence is changed by a factor of three compared to Figures 55–56.

This transition of the pre-Super TY Parma monsoon depression has other important characteristics than a different primary airstream (A_2) during transition than that leading to the monsoon depression formation (C_*). This transition occurred at a low latitude (10°N) with weak equatorial westerlies (from airstream A_2) to the south and trade easterlies to the north. In this transition, the interaction of the trade easterlies with the airstream A_2 occurred along a confluence line to the northwest, and the wave-activity fluxes associated that confluence line led to an intensification of the western vorticity maximum of the monsoon depression. Somewhat surprisingly (because of the weak airstream interaction), this transition of the pre-Super TY Parma monsoon depression took the same amount of time to transition to a tropical cyclone as the pre-TY Man-Yi monsoon depression (42 hours).

(9) Pre-TY Mirinae (23W)

The transition of pre-TY Mirinae (23W) monsoon depression is second example of a hybrid transition in which the airstream C leading to the formation of the monsoon depression continued to be involved, but was not the primary airstream for the transition. In this case, the pre-TY Mirinae monsoon depression moved poleward such that the wave-activity flux from the Southern Hemisphere did not have a large role in the transition of the monsoon depression. The transition of the pre-TY Mirinae monsoon depression occurred around 12°N , and almost five days after formation.

At 1200 UTC 24 October (Figure 58a), the monsoon depression has a highly elliptical shape with a central region near 9°N , 156°E , but also a lobe to the west-southwest near 8°N , 152°E . A broad band of trade easterlies impinges on the monsoon depression from the northeast and east, and along airstream B (as depicted in Figure 10) to the south. Farther to the west (near 140°E – 145°E), airstream B and the trade easterlies form a long confluence line, and then these easterlies are deflected to the east to pass along the southern side of the monsoon depression. At this time, large values of wave-activity flux from the southwest are associated with the confluence line far to the west, and from the south in association with an airstream B that is also far from the monsoon depression (Figure 58b). However, the major wave-activity flux in this case is outward-

directed from the northern region of the monsoon depression. Consequently, wave-activity flux divergence is the largest factor, which then will inhibit the spin-up of the monsoon depression.

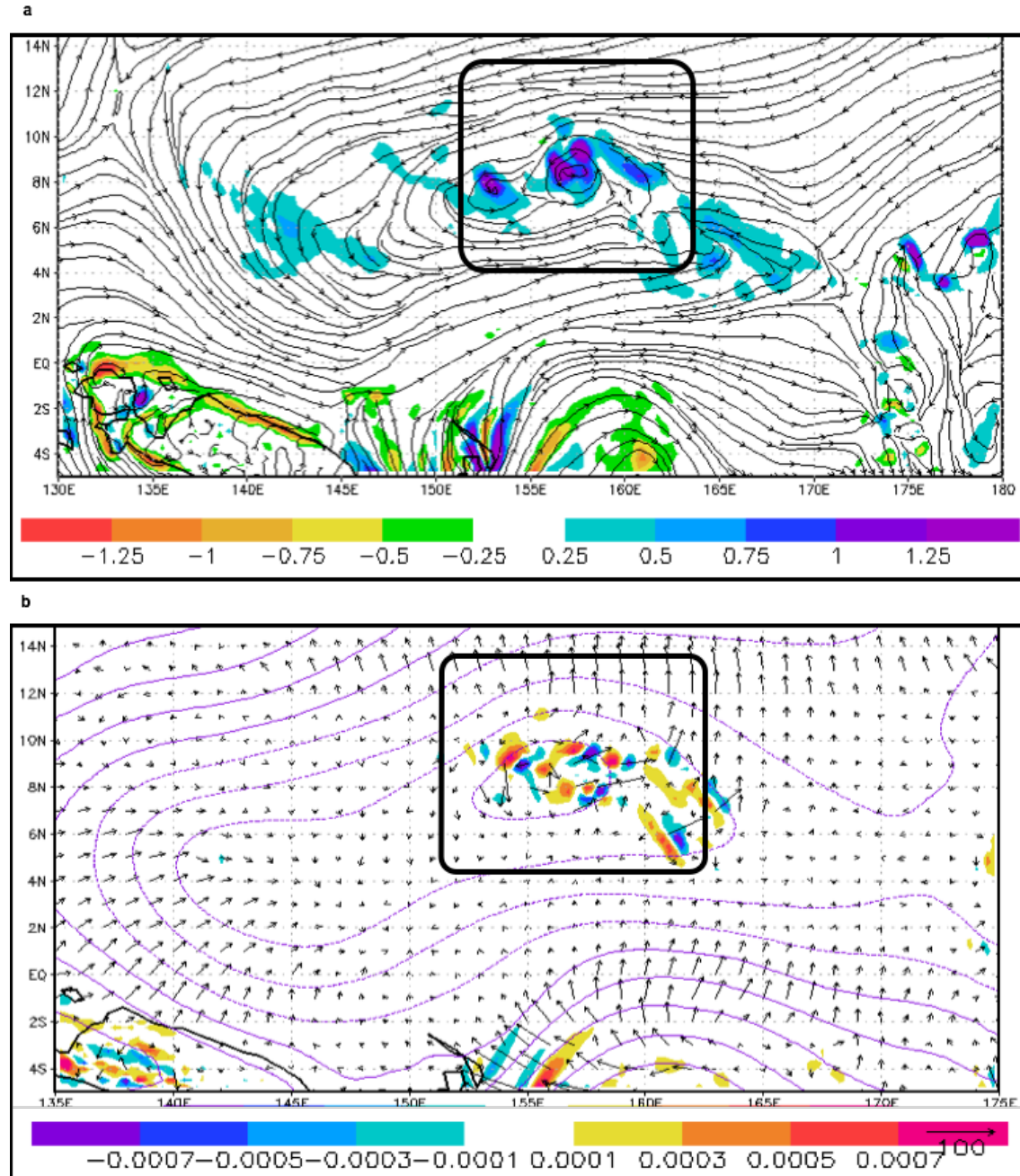


Figure 58. As in Figure 20 except at 1200 UTC 24 October with (a) streamlines and relative vorticity for the pre-TY Mirinae monsoon depression. (b) Corresponding wave-activity flux distribution.

At 0000 UTC 25 October (Figure 59a), the monsoon depression circulation has become better organized with an elliptical shape that is now oriented northeast-southwest as the outer circulation/vorticity maximum to the west has rotated to the southwest. Similarly, the large confluent region created by interaction of the trade easterlies and airstream A has also rotated cyclonically such that the associated vorticity maximum is also to the southwest of the monsoon depression, which then creates an elongated reverse-oriented monsoon trough from that vorticity maximum to the monsoon depression. Airstream B continues to be displaced equatorward by the reverse-oriented monsoon trough and is primarily in the southeast quadrant of the monsoon depression where it interacts with the easterly trades along an outer confluence line. The outer regions of large wave-activity fluxes (Figure 59b) remain the same as 12 hours previously with southwesterly fluxes associated with the confluence line, southerly fluxes from the Southern Hemisphere, and (most importantly) outward-directed fluxes all along the northern side of the monsoon depression. In the inner region of the monsoon depression, some areas with wave-activity flux convergence alternate with areas of flux divergence.

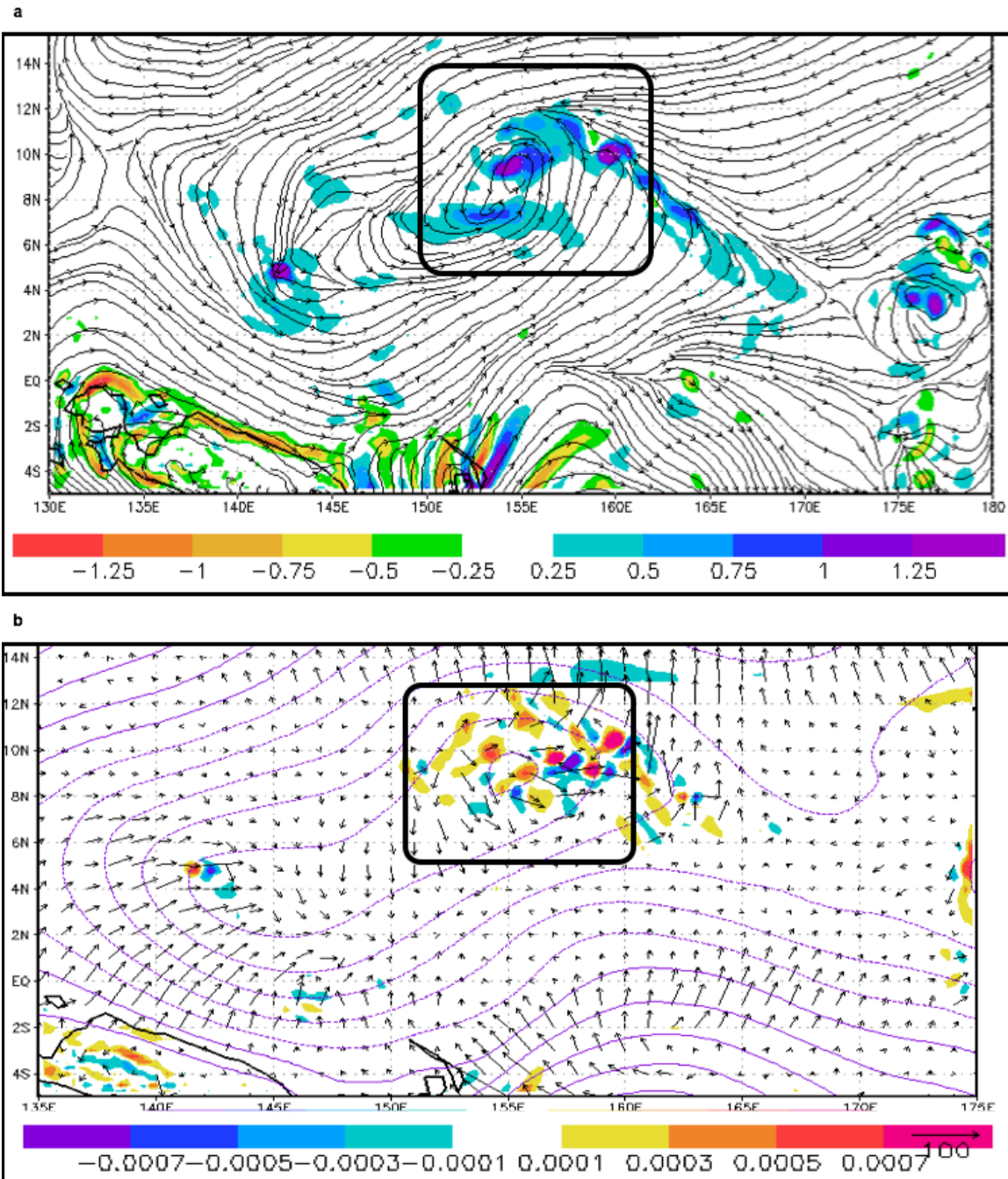


Figure 59. As in Figure 20 except at 0000 UTC 25 October with (a) streamlines and relative vorticity for the pre-TY Mirinae monsoon depression. (b) Corresponding wave-activity flux distribution.

At 1200 UTC 25 October (Figure 60a), the monsoon depression circulation is somewhat elliptical primarily due to three outer vorticity lobes with the northern vorticity maximum being largest. The weaker vorticity lobes to the southwest and the southeast are associated with confluence lines from interaction of the trade easterlies with airstream B. The outer confluence line between airstream B and the trade easterlies to the southwest of the circulation has weakened and is not influencing the circulation. The entire southern side of the monsoon depression now has outward-directed wave-activity fluxes and thus is leading to flux divergence and spin-down of the vorticity. The only regions of wave-activity flux convergence are near the northern vorticity maximum. Thus, this northern vorticity maximum will become the center of the pre-tropical cyclone seedling by 1800 UTC 25 October (not shown). While not well displayed in Figure 60a, it is concluded that this spin-up of the northern vorticity lobe is due to an interaction with the trade easterlies along the northern side of the monsoon depression, and specifically not with the original airstream C that led to the formation of the monsoon depression.

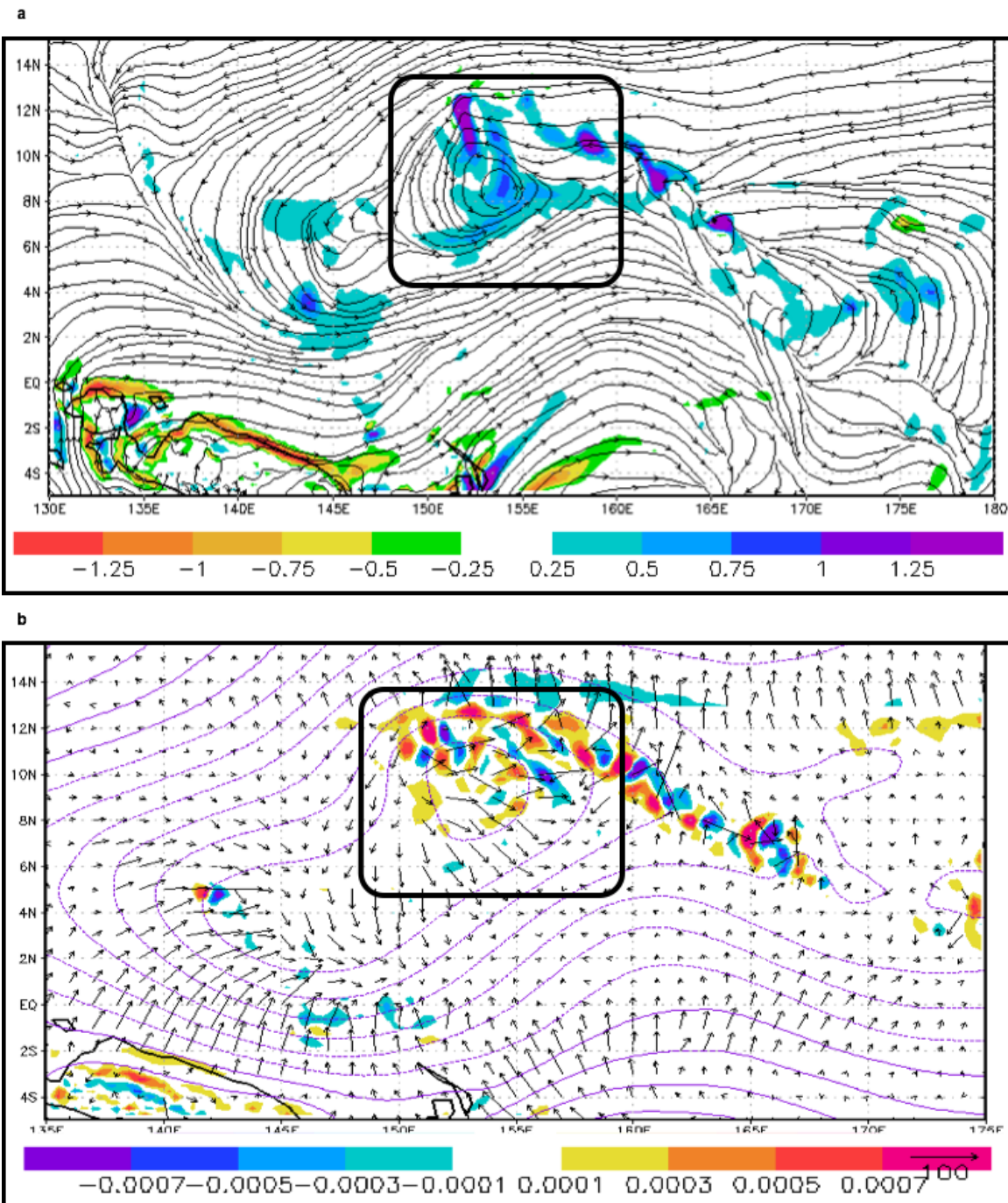


Figure 60. As in Figure 20 except at 1200 UTC 25 October with (a) streamlines and relative vorticity for the pre-TY Mirinae monsoon depression. (b) Corresponding wave-activity flux distribution.

The hybrid transition of the pre-TY Mirinae monsoon depression has some similar characteristics as the pre-Super TY Parma transition in that it occurred at a low latitude in a region with relatively weak winds. However, this transition occurred in a reverse-oriented monsoon trough (southwest–northeast rather than northwest–southeast) and the monsoon depression was the northern-most circulation. Thus, the key interaction that led to the transition to a pre-tropical cyclone seedling was with the trade easterlies in a vorticity lobe along the northern side of the monsoon depression. The long time interval (114 hours) from monsoon depression formation to transition to a pre-tropical cyclone seedling is tentatively attributed more to the timing of enhanced trade easterlies rather than a timing based on constriction or self-organization of the monsoon depression circulation.

This evolution is not well depicted in the ECMWF analyses, which may be because it occurred in a conventional data-sparse region of the equatorial Pacific Ocean. While the focus here is on dynamical (wave-activity flux) forcing leading to constriction of a circulation monsoon depression or a selective enhancement of one of the vorticity maxima within an elliptical monsoon depression, it is possible that thermodynamic factors may have an additional contribution in this low-latitude monsoon depression transition to a tropical cyclone.

c. *Summary*

The lower-tropospheric structure of the western North Pacific monsoon depressions is typically elliptical with a major/minor axis of 1100 km/ 800 km (Chapter III) with vorticity maxima at either end of the major axis, and has deep convection and gale-force winds at large radii. By contrast, a tropical cyclone has an inner-core of deep convection and strong winds at less than 100 km radius. The requirement for such a monsoon depression to spawn a tropical cyclone requires some mechanism by which the monsoon depression is constricted to a smaller size (especially if it is circular rather than elliptical in shape) or one of the two vorticity maxima is externally forced to spin-up a smaller central core of high winds.

The hypothesis in this study is that this external forcing mechanism is wave-activity flux due to interaction between an airstream and the monsoon depression circulation. No thermodynamic forcing mechanism is known that would contract the outer cloud bands of a monsoon depression to become the inner-core convection of a pre-tropical cyclone circulation. Rather, the focus here is on the presence of inward-directed wave-activity flux leading to flux convergence and therefore vorticity amplification within the broad monsoon depression circulation. The primary conclusion from these nine case studies is that each had inward-directed wave-activity flux prior to the monsoon depression undergoing a transition to a pre-tropical cyclone seedling.

The nine transitioning monsoon depressions presented in this chapter demonstrate that each transition is different, but there are general characteristics that are similar in each. Two categories of transitions have been described. In the first category are those monsoon depression transitions to a pre-tropical cyclone seedling in which the primary cross-equatorial airstream was the same for the transition as it was for the monsoon depression formation, which was the case for the conceptual model in Figure 25 based on the pre-TY Man-Yi transition described in Chapter IV.C.1. In the second category, the airstream that led to the monsoon depression formation either was not involved, or had a secondary role (hybrid cases) in the transition to a pre-tropical cyclone seedling. Consequently, another airstream or the trade easterlies had the primary role in the monsoon depression transition.

Therefore, an additional conceptual model (Figures 61a and b) is provided for this second category of a monsoon depression transitioning to a pre-tropical cyclone seedling based on Figures 43–60. These second category monsoon depressions in which the airstream that was responsible for the formation of the monsoon depression does not contribute at all to the transition to a pre-tropical cyclone seedling is illustrated in Figure 61a. In these cases it is another airstream that interacts with the trade easterlies and the resulting inward-directed wave-activity flux leads to transition to a pre-tropical cyclone seedling. Those hybrid monsoon depressions in which the airstream responsible for the formation of the monsoon depression persists, but is not the primary contributor of wave-activity flux to transition to a pre-tropical cyclone seedling, is illustrated in Figure 61b. In

these cases, the trade easterlies and/or an additional airstream interacts with the monsoon depression via a confluent region that leads to inward-directed wave-activity flux. This additional inward-directed wave-activity flux convergence over the vorticity maximum concentrates the circulation and results in the spin-up of vorticity.

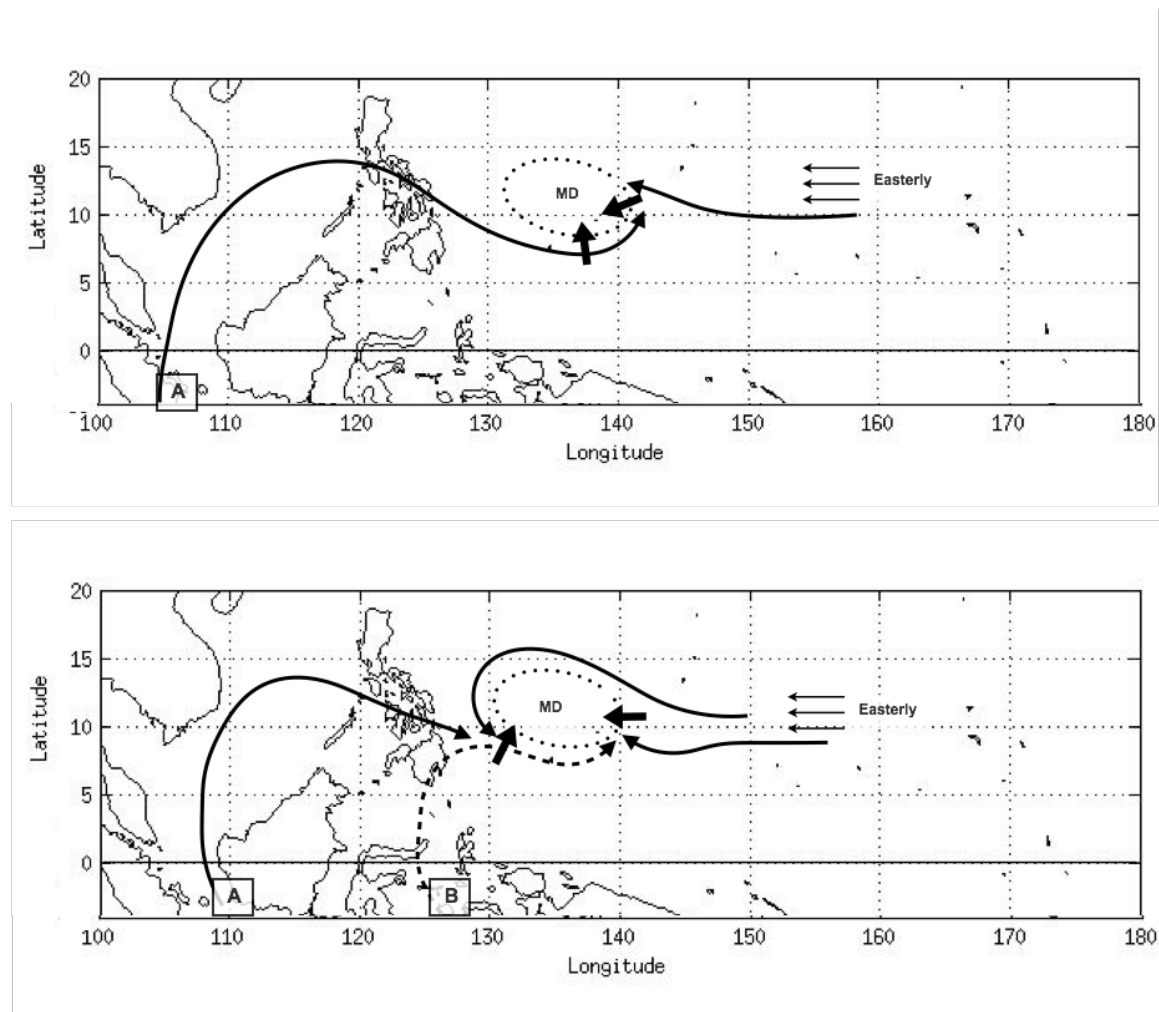


Figure 61. Idealized representations of transitioning monsoon depressions (dashed ellipse), trade easterlies (horizontal arrows), cross-equatorial airstreams (curved arrows as in Figure 6), and the primary inward-directed wave-activity flux (thick arrows) for (a) when the airstream responsible for the formation of the monsoon depression does not continue to contribute to a transition to pre-tropical cyclone seedling (e.g., airstream A as in the pre-Super TY Parma) and (b) when the airstream responsible for the formation of the monsoon depression continues (e.g., airstream B indicated by the hashed lines as in pre-TY Koppu), but it is not the primary airstream responsible for transition to pre-tropical seedling.

In the first category, persistent inward-directed wave-activity flux convergence was analyzed over one of the vorticity maxima of the monsoon depression to spin-up the monsoon depression into a pre-tropical cyclone seedling through increasing the cyclonic relative vorticity and constricting the circulation. In the second category, the primary inward-directed wave-activity flux was associated with the alternate airstream. In some of the transitions, the inward-directed wave-activity flux had to overcome wave-activity flux divergence associated with outward-directed wave-activity flux vectors due to wave dispersion effects. It was also documented that inward-directed wave-activity flux from more than one direction may be involved in the transition of the monsoon depression to a pre-tropical cyclone seedling. For example, the second source in the pre-TY Man-Yi case was a wave in the easterlies and in the pre-TY Ketsana case it was due to interaction with the trade easterlies. This second source of inward-directed wave-activity flux added to the wave-activity flux convergence over the vorticity maximum that would soon become the core of the pre-tropical cyclone seedling. In the pre-TY Mirinae case, the additional wave-activity flux convergence was near the vorticity maximum and directly contributed to the vortex spin-up.

The cases that had a short time to transition to a pre-tropical cyclone seedling had persistent wave-activity flux from the time of monsoon depression formation (e.g., MD₂ transition in Section a). Those cases with a longer time to transition generally involved the inward-directed wave-activity flux from a source other than the airstream that led to the monsoon depression formation.

3. Analysis of Non-transitioning Monsoon Depressions during 2009

In 2009, there were 25 monsoon depressions that did not transition to become pre-tropical cyclone seedlings. These cases were analyzed to evaluate whether the same wave-activity flux mechanism that contributed to monsoon depression transitions to pre-tropical cyclone seedlings were then not present. This analysis follows the same approach as for the 2007 MD₁ case in Chapter IV.C.2 that did not transition to a tropical cyclone. Specifically, MD₁ never had the wave-activity flux convergence over the vorticity maximum. Instead, the flux convergence was to the southeast of the vorticity maximum

(Figures 22b and 24b). This differs from the MD₂ case in which the wave-activity flux persisted along airstream C, and in addition to the wave-activity flux from the wave in the easterlies, that contributed to the wave-activity flux convergence over the western vorticity maximum that led to the transition to a pre-tropical cyclone seedling (Figures 22b and 24b).

A demonstration that the non-transitioning monsoon depressions during 2009 have this same absence of wave-activity flux convergence will indirectly support the hypothesis of the wave-activity flux convergence being the primary factor in the constriction of the circulation and resulting transition to a pre-tropical cyclone seedling. As in the analysis of the 2009 transitioning monsoon depressions, two primary categories of non-transitioning monsoon depressions will be described: ten cases in which the inward-directed wave-activity flux stopped shortly after formation and was never re-established (Section 3a below); and 11 cases in which the wave-activity flux persisted (or restarted) after formation of the monsoon depression that resulted in longer-lived monsoon depressions, but still did not transition to a pre-tropical cyclone seedling. Two of the four remaining monsoon depressions were very close to large tropical cyclones, so that the wave-activity flux of the monsoon depression was not discernable. Finally, bad source data prevented an accurate calculation of the wave-activity flux for the final two of the 25 non-transitioning monsoon depressions during 2009.

a. Short-Lived Wave-Activity Flux

There were 10 monsoon depressions during 2009 that had short durations (an average of three days) after the formation of the monsoon depression and did not have continued inward-directed wave-activity flux convergence (Table 5). As in the overall sample, a majority of the short-lived, non-transitioning monsoon depressions had an elliptical shape, but three of the 10 did have a circular shape that might be considered more likely to transition to a tropical cyclone (column 2, Table 5). These ten cases included at least one of all airstreams (A, B, and C [C_{*}]) (column 3, Table 5). Five of these non-transitioning monsoon depressions had an interaction with an additional airstream (column 4, Table 5), which in each case was airstream B from the west. For seven of the 10 cases, the inward-directed wave-activity flux that was involved in the

formation of the monsoon depression stopped within 6–12 hours after formation (N in column 5, Table 5), and for three cases inward-directed wave-activity flux continued after monsoon depression formation, but was significantly decreased (Y in column 5, Table 5). Incidentally, two of these three cases in which the inward-directed wave-activity flux continued also had outward-directed wave-activity flux that is not favorable for transition to a pre-tropical cyclone seedling. In only two of these 10 cases was a period of wave-activity flux convergence observed (Y in column 6, Table 5), but this did not lead to a transition to a pre-tropical cyclone seedling in the absence of inward-directed wave-activity flux (N in column 5, Table 5). In two of the 10 cases (Y in column 7), outward-directed wave-activity flux was another inhibiting factor for the spin-up of a pre-tropical cyclone seedling. The final column in Table 5 provides the durations of these 10 short-lived, non-transitioning monsoon depressions, which is attributed to the absence of persistent wave-activity flux convergence.

Table 5. Summary of the 10 non-transitioning monsoon depressions during 2009 in which the inward-directed wave-activity flux (WAF) was absent or small. The first column is the time and date that the circulation had all characteristics of a monsoon depression. The next three columns list the monsoon depression shape, the original airstream at formation, and any additional airstream that may have interacted with the monsoon depression. In column 5, the presence (Y-yes; N-no) of inward-directed wave-activity flux is indicated, and whether or not it resulted in wave-activity flux convergence is indicated in column 6. Presence of outward-directed wave-activity flux is listed in column 7. The last column is the duration (d-days) of the monsoon depression. PHI in column 6 is wave-activity flux convergence due to the interaction with the Philippines.

Time	Shape	Original Airstream	Additional Airstream	Inward-directed WAF	WAF Convergence	Outward-directed WAF	Duration (Days)
0000 UTC 14APR	E	B	N	N	Y (PHI)	N	2+
1800 UTC 7MAY	E	C _*	B	Y	N	Y	3
0000 UTC 7JUL	C	C _*	N	N	N	N	1+
1800 UTC 18JUL	E	C _*	N	Y	N	N	3+
0600 UTC 13AUG	E	C _*	N	N	Y	N	4+
1200 UTC 24AUG	C	A	N	Y	N	Y	4
0000 UTC 28AUG	C	C _*	B	N	N	N	4
0000 UTC 2SEP	E	C	B	N	N	N	2
0600 UTC 21SEP	E	C	B	N	N	N	2+
1200 UTC 5OCT	E	C	B	N	N	N	4+

b. Persistent, or Re-starting, Wave-Activity Flux

There were 11 monsoon depressions during 2009 that lasted longer (typically over five days) and experienced continued inward-directed wave-activity flux and associated convergence after the monsoon depression formed, but still did not transition to a pre-tropical cyclone seedling (Table 6). As in Table 5 and the overall sample, the majority of those monsoon depressions during 2009 had an elliptical shape, with only one that had circular shape (column 2, Table 6). These eleven cases also represented all airstreams (A, B and C [C_*]) (column 3, Table 6). Two key differences from Table 5 are than an additional airstream was involved in all but three of these 11 non-transitioning monsoon depressions during 2009 (column 4, Table 6), and consequently all 11 of these monsoon depressions had persistent inward-directed wave-activity flux (column 5, Table 6) that contributed to their longer durations (column 8, Table 6). Indeed, all but two of these 11 monsoon depressions also had outward-directed wave activity flux (column 6, Table 6), which is commonly an indicator of wave dispersion and thus is not favorable for vortex amplification. However, all 11 of these non-transitioning monsoon depressions during 2009 did not have persistent wave-activity flux convergence over the vorticity maximum (column 7, Table 6). Even though this set of monsoon depressions during 2009 interacted with another airstream and consequently had inward-directed wave-activity flux that contributed to their longer duration (column 8, Table 6), they did not have the wave-activity flux convergence that is a characteristic of the transitioning monsoon depressions in Sections 2a and 2b.

Table 6. As in Table 5, but for MD₁ during 2007 and 11 during 2009 that were non-transitioning monsoon depressions that had persistent wave-activity flux but did not result in transition to a pre-tropical cyclone seedling.

Time	Shape	Original Airstream	Additional Airstream	Inward-directed WAF	Outward-directed WAF	WAFC over vorticity maximum	Duration (Days)
1200 UTC 3JUL07 (MD1)	C	A	B	Y	Y	N	5+
1200 UTC 21APR	E	C	B	Y	Y	N	8+
0000 UTC 17MAY	E	B	N	Y	Y	N	3+
1800 UTC 22MAY	E	C _*	A, B	Y	Y	N	8+
0000 UTC 15JUN	E	C	B	Y	Y	N	2+
1800 UTC 16JUL	E	C	B	Y	Y	N	5
0000 UTC 25JUL	C	A	B	Y	Y	N	3
1200 UTC 9AUG	E	B	C	Y	Y	N	4+
1800 UTC 22AUG	E	B	N	Y	Y	N	9+
0000 UTC 29OCT	E	B	C	Y	N	N	5
1800 UTC 3NOV	E	C _*	N	Y	N	N	2
0600 UTC 17NOV	E	C	B	Y	Y	N	9+

c. Summary

Regardless of the type of non-transitioning monsoon depression, all cases had a continuation of the wave-activity flux that contributed to the formation of the monsoon depression. Those cases in which the inward-directed wave-activity flux did not continue through the subsequent six to 12 hours, or was weak, tended to be short-lived. Those cases in which the inward-directed wave-activity flux persisted, or relaxed and then returned, tended to be longer-lived circulations. Thus, the wave-activity flux convergence not only acts as the mechanism to spin-up a monsoon depression to a pre-tropical cyclone seedling, but is also as a way to sustain the monsoon depression.

The finding that the non-transitioning monsoon depressions lacked the persistent wave-activity flux convergence that was characteristic of all transitioning monsoon depressions indirectly supports the hypothesis that wave-activity flux convergence over a monsoon depression vorticity maximum is a key factor in the transition to a pre-tropical cyclone seedling. This study is also useful guidance for the forecaster in monitoring which of the western North Pacific monsoon depressions may transition to a tropical cyclone. First, the forecaster should evaluate whether the wave-activity flux associated with the cross-equatorial airstream that led to the formation of the monsoon depression is persisting and leading to wave-activity flux convergence over one of the vorticity maxima in the monsoon depression. If not (Section 3a), the monsoon depression is likely to be short-lived and thus not transition to a pre-tropical cyclone seedling. If the original airstream (and wave-activity flux) persists and/or the monsoon depression interacts with another airstream, the forecaster should continue to monitor the monsoon depression that may last five or more days. Then the key factor of persistent wave-activity flux convergence over one of the vorticity maxima in the monsoon depression must continue to be monitored because that has been demonstrated in this study to potentially lead to a transition of the monsoon depression to a pre-tropical cyclone seedling.

V. SUMMARY

The three advancements from this study are: (i) a conceptual model of monsoon depression formation in the western North Pacific has been developed (published in Beattie and Elsberry 2012); (ii) Horizontal structure of the monsoon depression has been refined (published in Beattie and Elsberry 2013); and (iii) Key indicators for transition of a monsoon depression to a tropical cyclone have been identified. This study will assist the forecasters at the JTWC in more accurately identifying which regions of deep convection are most likely to become a monsoon depression, as well as being able to recognize the indicators of transition to provide more accurate warnings of monsoon depression-related tropical cyclone formations. More accurately identifying regions of monsoon depression formation, the transition to a tropical cyclone, and the size of the monsoon depression-related tropical cyclones will also assist Department of Defense and civilian decision makers in determining whether or not they should sortie ships, evacuate coastal regions, and take other expensive and time-consuming preparations.

A. MONSOON DEPRESSION FORMATION

The analysis of the two July 2007 monsoon depressions and the 44 monsoon depressions that formed between April and December 2009 revealed the crucial role of four cross-equatorial airstreams from the Southern Hemisphere in monsoon depression formation. In the conceptual model of monsoon depression formation presented in Chapter II, a confluent region (or monsoon trough) and the cross-equatorial airstream(s) are the key elements. In order for a monsoon depression to form in a Northern Hemisphere confluent region that is typically a monsoon trough between the trade easterlies and equatorial westerlies, a Southern Hemisphere airstream (A, B, and C [C_*]) contributes by providing the wave-activity flux convergence that will help to wrap the confluent region into a large cyclonic circulation that is the monsoon depression.

This conceptual model will aid the forecasters at the JTWC in identifying regions for a potential monsoon depression formation, as the forecasters will now monitor the Southern Hemisphere for the four types of cross-equatorial flow that will interact with the

confluent region. The already favorable background environment of the confluent region (or monsoon trough) becomes more favorable as the cross-equatorial flow imports kinetic energy to the region and enhances the positive relative vorticity, which then leads to the formation of the monsoon depression circulation.

B. MONSOON DEPRESSION STRUCTURE

The original definition of a monsoon depression has been refined in this portion of the study to provide the JTWC with more accurate information to identify these circulations so they can be monitored for heavy rains and gale-force winds over broad areas, but especially for accurate warnings as they become pre-tropical cyclone seedlings. A further objective was to clarify confusion in the literature between monsoon depressions versus the larger monsoon gyres.

This study has documented that the majority (80%) of western North Pacific monsoon depressions are elliptically shaped, rather than circular, and typically have two vorticity maxima at either end of the elliptical circulation. It was documented that monsoon depressions are on average of 812 km north-south and 1098 km east-west (standard deviation of 288 and 387 km, respectively), which is almost half the size of the monsoon gyre that is on the order of 2500 km in diameter. The vertical structure was briefly studied to confirm that monsoon depressions are warm-core circulations as demonstrated by the low-level equatorial westerlies and trade easterlies reversing to become easterlies and westerlies aloft.

This portion of the study is important for the forecaster in identifying monsoon depressions and in understanding what the associated weather may be as gale warnings are possible in the outer-most regions of the circulation. It is also important for the forecaster to recognize the characteristics of the large diameter, elliptically-shaped monsoon depression with gale-force winds and how it may constrict in scale to become a larger-than-average size tropical cyclone.

C. TRANSITION TO PRE-TROPICAL CYCLONE SEEDLING

The monsoon depression provides a favorable environment for tropical cyclone formation based on the Gray (1968, 1975) necessary but not sufficient conditions for tropical cyclone formation. That is, the monsoon depressions are located in regions of sufficiently high sea-surface temperatures that provide a moist environment, the vertical wind shear is generally small, and the broad region of cyclonic vorticity is sufficient so that even the low-latitude circulations may transition to a tropical cyclone.

Seventeen (38%) of the 44 monsoon depressions during 2009 transitioned to a pre-tropical cyclone seedling. Two categories of transitioning monsoon depressions were documented. The first category of transitioning monsoon depression had the same primary airstream from the formation of the monsoon depression as described in the conceptual model in Figure 25 based on the pre-TY Man-Yi (MD_2) transition. In the second category of transitioning monsoon depressions, the cross-equatorial airstream that resulted in monsoon depression formation did not persist, and the primary inward-directed wave-activity flux was associated with an alternate airstream (conceptual model in Figure 61). This wave-activity flux from other sources than the original airstream included other cross-equatorial airstreams, regions of confluence between the circulation and the trade easterlies or another airstream, or rarely a wave in the easterlies. All of the monsoon depressions that transitioned therefore had persistent inward-directed wave-activity flux, which resulted in wave-activity flux convergence over a vorticity maximum within the monsoon depression circulation. This inward-directed wave-activity flux in some cases offset a region of outward-directed wave-activity flux, which would inhibit vortex spin-up as it removes energy from the circulation. In some other cases, multiple sources of inward-directed wave-activity flux were observed before the monsoon depression transitioned to a pre-tropical cyclone seedling. Based on these case studies, wave-activity flux convergence is regarded as a requirement for the transition of a monsoon depression to pre-tropical cyclone seedling.

Analysis of the non-transitioning monsoon depressions during 2009 confirmed the importance of persistent inward-directed wave-activity flux convergence for a transition to a pre-tropical cyclone seedling. For those short-lived monsoon depressions that did not

transition, the wave-activity flux did not persist, or decreased significantly, after the formation of the monsoon depression. For the longer-lived monsoon depressions that did not transition, the wave-activity flux did persist, but the inward-directed wave-activity flux was small and the region of wave-activity flux convergence was not associated with a maximum of vorticity within the monsoon depression. Thus, the wave-activity flux convergence not only acts as the mechanism to spin-up a monsoon depression to a pre-tropical cyclone seedling, but also as a way for the monsoon depression to persist. However, the fact that neither the short-lived or longer-lived monsoon depressions transitioned indirectly supports the hypothesis that wave-activity flux convergence is the primary factor in the scale reduction of the circulation leading to the transition to a pre-tropical cyclone seedling.

This portion of the study assists the JTWC forecasters by documenting the large-scale processes that transition the monsoon depression to a pre-tropical cyclone seedling. The forecaster should look for features such as the persistent cross-equatorial flow, confluent regions around the monsoon depression (i.e., circulation interaction with the trade easterlies or equatorial westerlies), and the continued wave-activity flux convergence over a vorticity maximum. For those monsoon depressions with persistent inward-directed wave-activity flux, the convergence must occur over a vorticity maximum and offset any divergence from outward-directed flux that may exist. Even if the original inward-directed wave-activity flux stops and then another airstream creates inward-directed wave-activity flux, the same criterion must be met: the inward-directed wave-activity flux convergence needs to converge over a vorticity maximum within the monsoon depression.

D. RELEVANCE TO THE DEPARTMENT OF DEFENSE (DOD)

Since a monsoon depression has a broad area of influence, it is important for the JTWC forecasters to understand how these circulations form, their structure, and what the characteristics of transition are to better identify and warn on the monsoon depressions. This understanding would also improve the identification of those monsoon depressions that will transition to tropical cyclone and thereby reduce the false alarm rate. Advance

indicators in the western North Pacific such as convection appearing near the center (a minimum of 12 hours prior to all 2009 TCFAs) and the scale constriction could result in earlier and more accurate TCFAs. Also, warnings would provide the Fleet with the time to re-route ships and ensure facilities are prepared for negative impacts to operations.

In order for the results of this study to translate to JTWC operations, the fields examined will have to be modified, as the JTWC does not look at wave-activity flux convergence on the watch floor. Therefore, another means to predict regions of inward-directed wave-activity flux convergence using fields the watch team regularly examines is needed. For example, knowing that confluent region in the streamline analysis between the monsoon depression and a cross-equatorial airstream will result in inward-directed wave-activity flux is an important aspect of forecasting formation and transition. A checklist would step the forecaster through the products and features that should be monitored, as they will indicate future monsoon depression formation or transition to tropical cyclone. Another example would be watching for convection to develop near the center of the monsoon depression, as this occurred 24–18 hours prior to every transition and can be easily identified on satellite imagery.

Monsoon depressions are particularly important to the safety of the Fleet as 17 (38%) of the 44 that formed in 2009 transitioned to tropical cyclones and were warned on by the JTWC. Monsoon depressions are very large (on the order of 1000 km in diameter), warm-core systems that have the potential to transition to tropical cyclones and are able to produce large amounts of precipitation with outer winds of gale force (34–40 kt). Therefore, the JTWC should consider gale warnings associated with monsoon depressions. Gale warnings on monsoon depressions, similar to those issued for tropical cyclones, would provide the warfighter to have time to prepare for the copious amounts of rain, winds, and seas associated with these circulations, which will reduce risk to personnel, facilities, and equipment and thereby save the DOD money in repairs to ships and infrastructure.

At sea, the monsoon depression-related tropical cyclones pose a risk to mariners due to the larger-than-average size, which result in high winds and seas at larger radii. As the monsoon depression-related tropical cyclone nears land, the risk due to the winds

remains, but the greater risk comes from potential flooding (e.g., TY Morakot produced over 3000 mm of rain over portions of Taiwan; Beattie and Elsberry 2013). These threats can result in significant impacts to DOD installations and operations throughout the western North Pacific.

E. FUTURE WORK

Further analysis of western North Pacific monsoon depressions is recommended to build upon these analyses based on the ECMWF analyses from the 2007 and 2009 seasons. An extended analysis with more monsoon depression formations and transitions using similar high-resolution analyses from more recent years would add to the statistical relevance of all sections, as this study examined only 46 monsoon depressions: two from July 2007 and 44 from 2009. A larger database including more recent years would increase confidence and lead to refined understanding of monsoon depressions for the benefit of forecasters.

A study focused on backward trajectories would be beneficial to understand the attributes of the cross-equatorial airstreams. Examining quantities such as velocity, moisture, vorticity and temperature are important, as they are modified along the trajectory bringing different characteristics into the monsoon depression formation and transition environments. For example, studying the velocity characteristics of the trajectories would enhance understanding of how and when the cross-equatorial airstreams begin the surge that enhances the Northern Hemisphere equatorial westerlies. A Monte Carlo simulation would help develop a model of which airstream may lead to monsoon depression formation given varying set of initial conditions.

Whereas the wave-activity flux analyses here focus on the large-scale processes, any datasets from field experiments that would aid in examination of the small-scale processes would help forecasters understand the interactions between these circulations and thereby improve early identification and warnings. Alternatively, a numerical modeling study is recommended to further examine the small-scale processes that occur during monsoon depression formation and transition to a pre-tropical cyclone seedling.

Additional research is recommended to advance understanding of the transition to a pre-tropical cyclone seedling. One recommendation is a simulation to study the character and magnitude of the inhibiting effects of the outward-directed wave-activity flux that was present in some of these monsoon depressions. Another area of research would be a sensitivity study on the magnitude of the inward-directed wave-activity flux that is sufficient to transition a monsoon depression to a pre-tropical cyclone seedling, which would shed light on why multiple sources of wave-activity flux, and the resulting convergence, are needed to reach the transition threshold.

To enhance the understanding of monsoon depression formation and evolution to pre-tropical cyclone seedling, a vorticity budget is proposed at the mesoscale, as the ECMWF analyses used here may not properly represent such small-scale processes. Of course, a special dataset from a field experiment would be required for such an analysis.

The monsoon depression provides a favorable background cyclonic vorticity environment for mesoscale convective systems (MCSs) to develop. A sensitivity study is recommended to determine the amount of latent heat required in the deep convection and stratiform clouds of the MCS to result in the radial pressure gradient enhancement that must occur during the transition of the monsoon depression to a pre-tropical cyclone seedling.

THIS PAGE INTENTIONALLY LEFT BLANK

APPENDIX. WAVE-ACTIVITY FLUX

A. WAVE-ACTIVITY FLUX DERIVATION

The formulae for the calculation of the wave-activity flux, Equations (1) and (2) from Chapter II.C. and below, used in this study are based off of the derivation presented

$$WF_x = \frac{1}{2} \frac{\left[u_b \left(v^2 - \Psi \frac{\partial v}{\partial x} \right) + v_b \left(\Psi \frac{\partial u}{\partial x} - uv \right) \right]}{|\mathbf{U}|} \quad \text{and} \quad (1)$$

$$WF_y = \frac{1}{2} \frac{\left[u_b \left(\Psi \frac{\partial u}{\partial x} - uv \right) + v_b \left(u^2 - \Psi \frac{\partial u}{\partial y} \right) \right]}{|\mathbf{U}|} \quad (2)$$

in Takaya and Nakamura (2001). Takaya and Nakamura (2001) first define a wave-activity (angular) pseudomomentum, \mathbf{M} , and then the phase-independent flux, \mathbf{W} , which is another form of equations (1) and (2). \mathbf{W} is a useful qualitative diagnostic tool to help understand the formation of atmospheric phenomena (Takaya and Nakamura 2001).

The pseudomomentum, \mathbf{M} , is analogous to linear momentum ($\bar{p} = m\bar{v}$), in that it is the force of a wave interacting with matter, or in this case a packet of air parcels interacting with the atmosphere and is defined as a combination of linear quantities A and E . $\mathbf{M} \equiv (A+E)/2$, where A is the enstrophy divided by the magnitude of the basic potential vorticity gradient and E is the energy divided by the intrinsic phase speed. Both A and E can be related to pseudomomentum. \mathbf{M} is derived from a quasi-geostrophic vorticity equation on a beta-plane, perturbations are considered and then all second order terms are neglected. The potential vorticity equation is linearized and the following assumptions are made: (i) the gradient of the mean potential vorticity is less than the enstrophy flux (analogous to kinetic energy flux); (ii) the gradient of the mean potential vorticity does not change direction; and (iii) there is a steady state basic flow. The resulting equation in pressure coordinates is from Takaya and Nakamura (1997, 2001) (equations 9a and C4

respectively), which introduces the flux, \mathbf{W} , and then defines it (Takaya and Nakamura 1997, 2001; equations 9b and C5, respectively).

$$\frac{\partial M}{\partial t} + \nabla \cdot \mathbf{W} = D_T \quad (4)$$

where D_T is a nonconservative term and can be considered the “phase-independent forcing” of \mathbf{M} (Takaya and Nakamura 2001).

$$W = \frac{1}{2|\mathbf{U}|} \begin{bmatrix} U(\psi_x'^2 - \psi_x' \psi_{xx}') + V(\psi_x' \psi_y' - \psi_x' \psi_{xy}') \\ U(\psi_x' \psi_y' - \psi_x' \psi_{xy}') + V(\psi_y'^2 - \psi_y' \psi_{yy}') \\ \frac{f_0^2}{S^2} [U(\psi_x' \psi_p' - \psi_x' \psi_{xp}') + (V(\psi_y' \psi_p' - \psi_y' \psi_{yp}')] \end{bmatrix} \quad (5)$$

\mathbf{W} becomes equations (1) and (2) as used in the Nakamura code when the following relationships are used: $u = \frac{\partial \psi}{\partial y}$ and $v = -\frac{\partial \psi}{\partial x}$. Only the zonal and meridional components are retained, the third (vertical) term in the brackets (with the Coriolis, f, and stability, S, parameters) is neglected because the Coriolis parameter is so small (or zero) in the tropical latitudinal bands over which the calculation is made. It is also neglected because the focus is on the direction of the horizontal wave-activity fluxes as they were expected to be the dominate terms in the monsoon depression formation and transition scenarios. The final term in the 2001 article (equation C5), C_{UM} , is for a propagating wave (the advancement from Takaya and Nakamura 1997 to Takaya and Nakamura 2001); this term is neglected in the program provided (H. Nakamura) as it was based on the 1997 presentation for a stationary wave.

B. PHYSICAL INTERPRETATION OF THE WAVE-ACTIVITY FLUX

Wave-activity flux is a kinetic energy-based concept. The typical application is with upper-tropospheric flows with large kinetic energy and significant regions of convergence and divergence (ageostrophic), such as extratropical transition where a perturbation of the midlatitude jet stream by the divergent, anticyclonic outflow from a tropical cyclone initiates a wave-activity flux. Due to the ageostrophic advection of kinetic energy, packets can propagate downstream through the midlatitude trough ridge

pattern and is revealed by convergence (divergence) in the wave-activity flux in advance (to the rear) of the kinetic energy packet. Cyclonic (anticyclonic) circulation enhancements may be triggered by the convergence (divergence) of the kinetic energy packets.

This applies in this study because the enhancement of the equatorial westerlies and trade easterlies by the cross-equatorial airstreams provides the surge, or perturbation of the flow, that initiates a wave-activity flux in both the monsoon depression formation and transition to pre-tropical cyclone seedling.

Monsoon depression formation starts in a confluent region of Northern Hemisphere trade easterlies and equatorial westerlies. This confluent region is a region of pre-existing vorticity that is enhanced as the cross-equatorial airstreams interact with the trade easterlies and the equatorial westerlies. This interaction results in a cross-equatorial surge in the Northern Hemisphere. Love (1985a) defines the cause of these surges as being due to a pressure rise in the Southern Hemisphere subtropics that tracks equatorward, which then leads to a rise in pressure at the Equator and the establishment of a west-east pressure gradient in the Northern Hemisphere that enhances the equatorial westerlies. In the Love (1985a) study, the enhanced equatorial westerlies resulted in tropical cyclone formation in the monsoon trough. In this study, it directly translated to monsoon depression formation in a confluent region that could be a monsoon trough.

Consequently, the regions in this study (the western North Pacific and Indian Ocean) have anomalous cross-equatorial flow from the winter (Southern) hemisphere to the summer (Northern) hemisphere during the monsoon season due to the high sea-surface temperatures and land heating in the Northern Hemisphere. That is, the background flow during this period is from the subtropical high in the Southern Hemisphere toward the monsoon (low pressure) trough in the Northern Hemisphere, which in the anomalous streamlines is often via the trade easterlies in the Southern Hemisphere to the crossing point at the Equator and then via the equatorial westerlies to the confluent region with the trade easterlies in the Northern Hemisphere. As shown in Figures 6, 10, 11, there are favored locations/channels for the cross-equatorial airstreams. Airstream A follows a path that can be attributed to summer heating of the southeast Asia

land mass that creates a low pressure region more favorable for pulling the air from the Southern Hemisphere as it is closer to the Equator. Airstream B may be attributed to summer heating of the mountainous Indonesian island chain, where it then crosses the Equator to the Northern Hemisphere monsoon trough. Airstream C (C_*) may be attributed to the convective heating at the southeastern area of the monsoon trough that is over 30° - 31°C sea-surface temperatures, and thus is an area of low pressures close to the Equator that can pull air northward from the Southern Hemisphere.

Given these background anomalous meridional and zonal airstreams in the western North Pacific summer monsoon regime relative to the global mean, there are also surges of equatorward flow in the Southern Hemisphere due to vigorous midlatitude troughs that dig deep into the subtropics and tropics, as described in Love (1985a,b). These equatorward flows then lead to cross-equatorial airstreams that penetrate into the Northern Hemisphere enhancing the equatorial westerlies, which are the identified airstreams A, B, and C (C_*) in this study that subsequently interact with, or create, the background confluent regions along the monsoon trough. Thus, the wave-activity fluxes in this study are associated with the enhanced (or anomalous) airstreams superposed on an anomalous (relative to the global mean) summer monsoon background flow.

Assuming that the pre-existing equatorial westerlies have anticyclonic shear that just balances the Coriolis parameter, the cross-equatorial airstreams A, B, and C (C_*) lead to a surge in the equatorial westerlies (or trade easterlies in the case of C (C_*)) that are inherently unstable because they will have anticyclonic shear vorticity that exceeds the small value of the Coriolis parameter near the Equator. The wave-activity flux vectors have an orientation from the anticyclonic to the cyclonic side of the equatorial westerly surge representing the kinetic energy flux necessary to reduce the maximum winds back to stable values (i.e., anticyclonic shear vorticity equal to the local Coriolis parameter). When the cross-equatorial airstreams interact with the trade easterlies they too are unstable resulting in wave-activity flux vectors toward the confluent region (toward the southwest) from the anticyclonic to cyclonic shear side of the enhanced trade easterly maximum. The process is similar for the cases in which the monsoon depression circulation is transitioning to a pre-tropical cyclone seedling. By contrast, Rossby wave

dispersion leads to an outward-directed wave-activity from large cyclonic disturbances, such as the monsoon depression, due to the beta effect.

A wave approaching a convergent region, such as the eastern end of the monsoon trough, will experience a contraction in horizontal scale (decreased zonal wavelength) that will lead to amplification of the wave. This is represented by the convergence of wave-activity flux vectors in this study. Kuo et al. (2001) demonstrated that when this wave moves northwestward along the monsoon trough, formation of a cyclonic circulation occurs (tropical cyclone in the Kuo et al. (2001) study, a monsoon depression in this study) as it is now a favorable environment for formation of a cyclonic circulation. Whereas the approaching wave has an associated wave-activity flux, the background (confluent region or monsoon trough) does not, and thus a convergence of wave-activity flux is occurring. In this study, this is similar to the monsoon depression transition to pre-tropical cyclone seedling where there is a convergent region to the northeast of the monsoon depression circulation that interacts with a wave in the easterlies. The wave-activity flux convergence enhances the monsoon depression as a favorable environment for further amplification.

THIS PAGE INTENTIONALLY LEFT BLANK

LIST OF REFERENCES

- Acker, J.G., and G. Leptoukh, 2007: Online analysis enhances use of NASA Earth science data. *Eos, Trans. AGU*, **88**, 14–17.
- Beattie, J. C., and R. L. Elsberry, 2010: Conceptual model of western North Pacific monsoon depression formation. Extended Abstract 14B.1, 29th Conf. on Hurricanes and Tropical Meteorology, Amer. Meteor. Soc., Tucson, AZ.
- , and —, 2012: Western North Pacific monsoon depression formation. *Wea. Forecasting*, **27**, 1413–1432.
- , and —, 2013: Horizontal structure of monsoon depressions in the western North Pacific at formation time. *Geophys. Res. Lett.*, **40**, 983–987, doi:10.1002/grl.50198.
- Briegel, L. M., and W. M. Frank, 1997: Large-scale influences on tropical cyclogenesis in the western North Pacific. *Mon. Wea. Rev.*, **125**, 1397–1413.
- Chen, T.-C., S.-P. Weng, N. Yamazaki, and S. Kiehne (1998): Interannual variation in the tropical cyclone formation over the western North Pacific. *Mon. Weather Rev.*, **126**, 1080–1090.
- , S.-Y. Wang, M.-C. Yen, and W. A. Gallus Jr. (2004): Role of monsoon gyre in the interannual variation of tropical cyclone formation over the western North Pacific. *Wea. Forecasting*, **19**, 776–785.
- Dickinson, M., and J. Molinari, 2002: Mixed Rossby–gravity waves and western Pacific tropical cyclogenesis. Part I: Synoptic evolution. *J. Atmos. Sci.*, **59**, 2183–2196.
- Draxler, R. R., and G. D. Rolph, cited 2011: HYSPLIT (Hybrid Single-Particle Lagrangian Integrated Trajectory) Model. NOAA/Air Resources Laboratory, College Park, MD. [Available online at <http://ready.arl.noaa.gov/HYSPLIT/php/>.]
- Elsberry, R. L., and P. A. Harr, 2008: Tropical Cyclone Structure (TCS08) field experiment: Science basis, observational platforms, and strategy. *Asia-Pac. J. Atmos. Sci.*, **44**, 209–231.
- Ferreira, R. N., and W. H. Schubert, 1997: Barotropic aspects of ITCZ breakdown. *J. Atmos. Sci.*, **54**, 261–285.
- Fiorino, M., and R. L. Elsberry, 1989: Some aspects of vortex structure related to tropical cyclone motion. *J. Atmos. Sci.*, **46**, 975–990.
- Frank, W. A., and P. E. Roundy, 2006: The role of tropical waves in tropical cyclogenesis. *Mon. Wea. Rev.*, **134**, 2397–2417.

- Fukutomi, Y., and T. Yasunari, 2005: Southerly surges on sub-monthly time scales over the eastern Indian Ocean during the Southern Hemisphere winter. *Mon. Wea. Rev.*, **133**, 1637–1654.
- Ge, X., T. Li, S. Zhang, and M. S. Peng, 2010: What caused the extremely heavy rainfall in Taiwan during Typhoon Morakot (2009)? *Atmos. Sci. Lett.*, **11**, 46–50.
- Gray, W. M., 1968: Global view of the origin of tropical disturbances and storms. *Mon. Wea. Rev.*, **96**, 669–700.
- , 1975: Tropical cyclone genesis. Dept. of Atmos. Sci. Paper No. 323, Colorado State University, 121pp. [Available from Department of Atmospheric Sciences, Colorado State University, Ft. Collins, CO 80523.]
- Guinn, T. A., and W. H. Schubert, 1993: Hurricane spiral bands. *J. Atmos. Sci.*, **50**, 3380–3403.
- Harr, P. A., and R. L. Elsberry, 1996: Structure of a mesoscale convective system embedded in Typhoon Robyn during TCM-93. *Mon. Wea. Rev.*, **124**, 634–652.
- , —, and J. C. L. Chan, 1996: Transformation of a large monsoon depression to a tropical storm during TCM-93. *Mon. Wea. Rev.*, **124**, 2625–2643.
- Haynes, P. H., and M. E. McIntyre, 1987: On the evolution of vorticity and potential vorticity in the presence of diabatic heating and frictional or other forces. *J. Atmos. Sci.*, **44**, 828–841.
- Hong, C.-C., M.-Y. Lee, H. H. Hsu, and J.-L. Kuo, 2010: Role of sub-monthly disturbance and 40–50 day ISO on the extreme rainfall event associated with Typhoon Morakot (2009) in southern Taiwan. *Geophys. Res. Lett.*, **37**, L08805, doi:10.1029/2010GL042761.
- Joint Typhoon Warning Center, 1994: Annual tropical cyclone report. JTWC, 337 pp, <http://www.usno.navy.mil/NOOC/nmfc-ph/RSS/jtwc/atcr/1994atcr.pdf>.
- , 2007: Annual tropical cyclone report. JTWC, 124 pp, <http://www.usno.navy.mil/NOOC/nmfc-ph/RSS/jtwc/atcr/2007atcr.pdf>.
- , 2009: Annual tropical cyclone report. JTWC, 109 pp, <http://www.usno.navy.mil/NOOC/nmfc-ph/RSS/jtwc/atcr/2009atcr.pdf>
- Kuo, H.-C., J.-H. Chen, R. T. Williams, and C.-P. Chang, 2001: Rossby waves in zonally opposing mean flow: Behavior in northwest Pacific summer monsoon. *J. Atmos. Sci.*, **58**, 1035–1050.

- Lander, M. A., 1994: Description of a monsoon gyre and its effects on the tropical cyclones in the western North Pacific during August 1991. *Wea. Forecasting*, **9**, 640–654.
- , 1996: Specific tropical cyclone track types and unusual tropical cyclone motion associated with reverse-oriented monsoon trough in the western North Pacific, *Wea. Forecasting*, **11**, 170–186.
- , 2004: Monsoon depressions, monsoon gyres, midget tropical cyclones, TUTT cells and high intensity after recurvature: Lessons learned from the use of Dvorak's techniques in the world's most prolific tropical-cyclone basin. Preprints, 26th Conf. on Hurricanes and Tropical Meteorology, Miami, FL, Amer. Meteor. Soc., 7A.5. [Available online at <http://ams.confex.com/ams/pdffiles/75346.pdf>.]
- Love, G., 1985a: Cross-equatorial influence of winter hemisphere subtropical cold surges. *Mon. Wea. Rev.*, **113**, 1487–1498.
- , 1985b: Cross-equatorial interactions during tropical cyclogenesis. *Mon. Wea. Rev.*, **113**, 1499–1509.
- Molinari, J., K. Lombardo, and D. Vollaro, 2007: Tropical cyclogenesis within an equatorial Rossby wave packet. *J. Atmos. Sci.*, **64**, 1301–1317.
- Nguyen, H. V., and Y.-L. Chen, 2011: High-resolution initialization and simulations of Typhoon Morakot (2009). *Mon. Wea. Rev.*, **139**, 1463–1491.
- Ritchie, E. A., and G. J. Holland, 1999: Large-scale patterns associated with tropical cyclogenesis in the western Pacific. *Mon. Wea. Rev.*, **127**, 2027–2043.
- Sheu, R.-S., and G. Liu, 1995: Atmospheric humidity variations associated with westerly wind bursts during Tropical Ocean Global Atmosphere (TOGA) Coupled Ocean Atmosphere Response Experiment (COARE). *J. Geophys. Res.*, **100** (D12), 25 759–25 768.
- Sobel, A. H., and C. S. Bretherton, 1999: Development of synoptic- scale disturbances over the summertime tropical northwest Pacific. *J. Atmos. Sci.*, **56**, 3106–3127.
- Takaya, K., and H. Nakamura, 1997: A formulation of a wave-activity flux for stationary Rossby waves on a zonally varying basic flow. *Geophys. Res. Lett.*, **24**, 2985–2988.
- , and —, 2001: A formulation of a phase-independent wave-activity flux for stationary and migratory quasigeostrophic eddies on a zonally varying basic flow. *J. Atmos. Sci.*, **58**, 608–627.

Wheeler, M., G. N. Kiladis, and P. J. Webster, 2000: Large-scale dynamical fields associated with convectively coupled equatorial waves. *J. Atmos. Sci.*, **57**, 613–640.

INITIAL DISTRIBUTION LIST

1. Defense Technical Information Center
Ft. Belvoir, Virginia
2. Dudley Knox Library
Naval Postgraduate School
Monterey, California